Atmospheric Mercury: Recent advances in theoretical, computational, experimental, observational and isotopic understanding to decipher its redox transformations in the upper and lower atmosphere and interactions with Earth surface reservoirs

Jonas O. Sommar[1], Xinyu Shi[1,2], Xueling Tang[1,2], Guangyi Sun[1], Che-Jen Lin[3] and Xinbin Feng[1,2].

[1] State Key Laboratory of Environmental Geochemistry, Institute of Geochemistry, Chinese Academy of Sciences, Guiyang 550081, China.
[2] University of Chinese Academy of Sciences, Beijing 100045, China.
[3] Department of Mechanical Engineering, University of West Florida, Pensacola, Florida, United States.

Correspondence to: Jonas O. Sommar (jonassommar@icloud.com)

List of content

Abstract 2
1 Introduction 2
2 Physical chemistry of elemental mercury 4
3 The atmospheric environment 4
3.1 Atmospheric measurements of mercury species 4
3.2 Stability of atmospheric Hg^0 6
4 Kinetics, thermodynamics and general chemistry 9
4.1 Fundamental kinetics and thermodynamic principles 8
4.2 Surface kinetics 10
4.3 Aqueous redox equilibria 10
4.4 Chemical properties of aqueous $Hg^{I,II}$ 12
4.5 Chemical equilibria data 12
4.6 The speciation of Hg^{II} in atmospheric waters 12
4.7 Chemical reactions data 16
5 Gas-phase atmospheric Hg chemistry 17
5.1 Inorganic species 17
5.1.1 Initial reactions of ground state Hg^0 17
5.1.2 Stability of $^{\bullet}Hg^{I}X$ 22
5.1.3 Bimolecular reactions of $^{\bullet}Hg^{I}X$ 23
5.1.4 Stability of $Hg^{II}XY$ 24
5.1.5 Chemical transformation of Hg in the lower stratosphere 29
5.1.6 Chemical transformation of Hg in the upper stratosphere 30
5.2 Organic species 32
5.2.1 Dimethylmercury 32
5.2.2 Monomethylmercury species 34
6. Red-ox transformations in the aqueous phase 34
6.1 Inorganic Hg species 34
6.1.1 Oxidation channels 36
6.1.2 Reduction channels 38
6.2 Organic mercury 41
7 Multi-phase transformations 42
7.1 Gas-particle partitioning and reactive gas uptake 42
7.1.1 $HgCl_2$ 42
7.1.2 Hg^0 44
7.2 Reduction of mercurial species on surfaces 45

Formatmallsdefinition: Innehåll 1: Teckensnitt:(Asian) Times New Roman, Inte Expanderad med / Kondenserad med , Ligaturer: Ingen, Radavstånd: 1,5 rader
Formatmallsdefinition: Innehåll 2: Teckensnitt:(Asian) Times New Roman, Inte Expanderad med / Kondenserad med , Ligaturer: Ingen, Avstånd Efter: 0 pt, Radavstånd: 1,5 rader
Formatmallsdefinition: Innehåll 3: Teckensnitt:(Asian) Times New Roman, Inte Expanderad med / Kondenserad med , Ligaturer: Ingen, Avstånd Efter: 0 pt, Radavstånd: 1,5 rader
Formatmallsdefinition: Innehåll 4: Teckensnitt:(Asian) Times New Roman, Inte Expanderad med / Kondenserad med , Ligaturer: Ingen, Avstånd Efter: 0 pt, Radavstånd: 1,5 rader
Formatmallsdefinition: Innehåll 5: Teckensnitt:(Asian) Times New Roman, Inte Expanderad med / Kondenserad med , Ligaturer: Ingen, Avstånd Efter: 0 pt, Radavstånd: 1,5 rader
Formatmallsdefinition: Innehåll 6: Teckensnitt:(Asian) Times New Roman, Inte Expanderad med / Kondenserad med , Ligaturer: Ingen, Avstånd Efter: 0 pt, Radavstånd: 1,5 rader
Formatmallsdefinition ... [3]
Formatmallsdefinition ... [2]
Formatmallsdefinition ... [1]
Kommenterad [JS1]: Text in blue: Changes made in resp ... [4]
Formaterat: Centrerad
tog bort: complex
tog bort: interaction
formaterade: Teckenfärg: Dekorfärg 2
tog bort: Xinyu Shi[1,2],
tog bort: Lin[1,3]
tog bort: [4]
tog bort: [1]State
Formaterat: Radavstånd: Flera 1,15 li
tog bort: [2]University
tog bort: [3]Center for Advances in Water and Air Quality, La ... [5]
tog bort: [4]Center for Excellence in Quaternary Science and ... [6]
tog bort: 16
tog bort: 16
tog bort: 16
tog bort: 21
tog bort: 22
tog bort: 28
tog bort: 29
tog bort: 31
tog bort: 31
tog bort: 33
tog bort: 33
tog bort: 33
tog bort: 35
tog bort: 37
tog bort: 40
tog bort: 41
tog bort: 41
tog bort: 41
tog bort: 43
tog bort: 44

7.3 Dark oxidation of Hg^0 accelerated by freeze-concentration effects 47
7.4 Surface-catalyzed reduction of Hg^{II} in aqueous solution 47
7.5 Field observations of photoreduction in precipitation, cloud and fog 48
8 Mercury isotope systematics and fractionation 48
8.1 Conventional mass-dependent and mass-independent fractionation 50
8.1.1 MIF Signatures as Additional Tracer 52
8.2 Isotopic characteristics of atmospheric mercury 52
8.2.1 Gaseous Hg 52
8.2.2 Aerosol-bound Hg 54
8.2.3 Hg in precipitation 55
8.2.4 Even-MIF ($\Delta^{200}Hg/\Delta^{204}Hg$) ratios in atmospheric samples 56
8.3 Isotope fractionation during gas-phase oxidation 61
8.3.1 Ground-state Hg^0 oxidation in air 61
8.3.2 Hg^0 oxidation initiated by photosensitized reactions 62
8.4 Isotope fractionation during aqueous-phase red-ox transformation 63
8.4.1 Reduction 63
8.4.2 Oxidation 65
8.5 Isotope fractionation during complexation, sorption and surface-catalyzed reduction 68
8.5.1 Processes interfacing the aqueous phase 68
8.5.2 Processes interfacing the gas phase 69
8.6 Isotopic fractionation during air-surface Hg^0 gas exchange 69
8.6.1 Mixing and fractionation modeling of Hg^0 deposition and post-depositional processes 70
8.6.2 Enclosure and related flux measurements 71
9. Future perspectives 76
9.1 Theoretical chemistry contributions & challenges
9.2 Laboratory measurement techniques & limitations
9.3 Model validation & observational gaps
Author contribution 79
Competing interests 79
Financial support 79
References 79

Abstract

Mercury is a volatile heavy element with no known biological function. It is present in trace amounts (on average, ~80 ppb) but is not geochemically well blended in the Earth's crust. As a result, it occurs in extremely high concentrations (up to a few percent) in certain locations. It is found along tectonic plate faults in deposits of sulfide ores (cinnabar), and it has been extensively mobilized during the Anthropocene. Mercury is currently one of the most targeted global pollutants, with methylmercury compounds being particularly neurotoxic. Over 5,000 tons of mercury are released into the atmosphere annually through primary emissions and secondary re-emissions. Much of the re-emitted mercury, resulting from exchanges with surface reservoirs, is related to (legacy) human activities, such as direct releases. Understanding the dynamics of the global Hg cycle is critical for assessing the impact of emission reductions under the UN Minamata Convention, which became legally binding in 2017. This review of atmospheric mercury focuses on fundamental advances in field, laboratory, and theoretical studies, including six stable Hg isotope analytical methods, which have contributed recently to a more mature understanding of the complexity of the atmospheric Hg cycle and its interactions with the Earth's surface ecosystem.

1 Introduction

Mercury (Hg) is a potent neurotoxin that, via methylmercury ($MMHg^+$) food exposure, poses a global health threat (e.g., IQ decrement and

tog bort: 46
tog bort: 46
tog bort: 47
tog bort: 47
tog bort: 49
tog bort: 51
tog bort: 51
tog bort: 51
tog bort: 53
tog bort: 54
tog bort: 55
tog bort: 59
tog bort: 59
tog bort: 60
tog bort: 61
tog bort: 61
tog bort: 65
tog bort: 65
tog bort: 66
tog bort: 66
tog bort: 67
tog bort: 68
tog bort: 73
tog bort: 76
tog bort: 76
tog bort: 76
tog bort: 76
tog bort: -
tog bort: sometimes
formaterade ... [7]
tog bort: %)
formaterade ... [8]
tog bort: internationally
tog bort: ,
tog bort: ,
formaterade ... [9]
tog bort: considered to be
tog bort: are the
tog bort: to
tog bort: the
tog bort: that
tog bort: fairly
formaterade ... [10]
formaterade ... [11]
formaterade ... [12]
formaterade ... [13]
formaterade ... [14]
tog bort: impact
formaterade ... [15]
tog bort: .
formaterade ... [16]

heart attack) (Zhang et al., 2021b). The atmosphere plays a pivotal role in the Hg biogeochemical cycle, functioning as the most important transient reservoir, a conduit for transport and transformation, and a site rich in redox chemistry. In part due to concerns about global Hg transport, the multilateral UN Environment Convention on Hg was negotiated and entered into force in 2017 with a mandate to reduce the intentional use and emissions of Hg (UNEP, 2018). Research on Hg biogeochemical cycling gained momentum after an outbreak of mass MMHg$^+$ poisoning severely affected the population of Minamata Bay, Japan, in the 1950s and 1960s through the consumption of contaminated seafood, and it became clear that MMHg$^+$ was present at chronically high levels in predatory fish in many lakes, particularly those in the boreal forest belt, through long-range transport and biomagnification (Lindqvist et al., 1991). The earliest known series of measurements of airborne elemental Hg, possibly the first systematic study of its kind, was conducted in Pacific North America during the second half of the 1960s (Williston, 1968). It was recognized as early as the 1970s that Hg circulated globally through the atmosphere (Nriagu, 1979). Somewhat later, Slemr et al. (1985) published an influential paper whose results on the distribution, speciation and budget of atmospheric Hg reproduce fairly well the qualitative features of the atmospheric Hg cycle, such as atomic vapor (Hg^0) dominating the atmospheric pool and showing an interhemispheric difference with higher concentrations in the northern hemisphere, and being relatively well mixed vertically through the troposphere with an extensive residence time (concept as a "global pollutant").

Knowledge of the physical and chemical processes that govern the dynamics of Hg in the atmosphere has developed gradually. Over time, through technological leaps (stable isotope sampling in natural probes, refined methods in the theoretical and experimental field, etc.), its full complexity began to be appreciated. In earlier research, the prevailing view was that water-phase oxidation by ozone could be the primary mechanism initiating the removal of tropospheric Hg^0 (Pleijel and Munthe, 1995; Seigneur et al., 1994). However, newer data have indicated that gaseous oxidized mercury (GOM) could also be present in the atmosphere (Xiao et al., 1997; Lindberg and Stratton, 1998), in addition to the particulate form (PBM). Specifically, the observation that Hg^0 was periodically depleted in the planetary mixing layer during the polar spring (Schroeder et al., 1998) prompted a reassessment of Hg chemistry in favor of homogeneous gas-phase chemistry (Hynes et al., 2009). The two-step gas-phase oxidation of Hg^0 initiated by Br atoms has emerged as the most important global channel for tropospheric conversion to Hg^{II} (Donohoue et al., 2006; Holmes et al., 2010). Gas-phase O_3 was previously considered an oxidizing agent for Hg^0 to Hg^{II}. Although this route was discarded, O_3 has been found to effectively oxidize intermediate Hg^I species (Gómez Martín et al., 2022). This suggests that OH- and less certain I-initiated oxidation of Hg^0, which produces less stable intermediates than Br and Cl do, may also be important for Hg turnover in parts of the troposphere and beyond (Dibble et al., 2020; Lee et al., 2024). A novel finding is that major Hg^{I,II} species, which are expected to be formed in the atmosphere upon oxidation of Hg^0, are themselves photolabile and undergo gas-phase reduction (Francés-Monerris et al., 2020; Saiz-Lopez et al., 2019). The complexity of rapid redox Hg chemistry involving multiple gas-phase oxidation states (0, +1 and +2) is further compounded by the impact of multiphase interactions, including reactive uptake and homogeneous and heterogeneous processes in condensed-phase media, on the dynamics of atmospheric Hg. An indicator of the maturation of our understanding of atmospheric Hg chemistry is the inclusion of bromine chemistry in critically evaluated datasets for use in atmospheric studies (Burkholder et al., 2019). Over the past two decades, measurements of Hg stable isotope ratios in natural samples have emerged as valuable tools for gaining insights into the atmospheric Hg cycle. One notable outcome of isotope analysis is the recognition that dry Hg^0 deposition exerts a more pronounced influence on a global scale than was previously understood, with wet and dry deposition of the atmospheric Hg^{II} fraction being of lesser importance (Jiskra et al., 2018).

Hg in the atmosphere has been the subject of reviews over the past 45 years: *topics* including *biogeochemical cycling* (Lindqvist and Rodhe, 1985; Lindqvist et al., 1991; Schroeder and Munthe, 1998; Selin, 2009; Lyman et al., 2020), *observations* (Slemr et al., 2003; Sprovieri et al., 2010; Dommergue et al., 2010; Fu et al., 2015; Steffen et al., 2015; Mao et al., 2016; Zhang et al., 2019c; Custódio et al., 2022; Bencardino et al., 2024), *isotopic observational data* (Kwon et al., 2020; Liu et al., 2024), *atmospheric measurement techniques* (Pandey et al., 2011; Huang et al., 2014; Gustin et al., 2015; Davis and Lu, 2024; Gustin et al., 2024), *anthropogenic emissions* (Carpi, 1997; Zhang et al., 2016; Cheng et al., 2023), *natural volcanism* (Edwards et al., 2021), *physical removal and air-surface exchange* (Zhang et al., 2009; Sommar et al., 2013; Zhu et al., 2016; Agnan et al., 2016; Cooke et al., 2020; Sommar et al., 2020; Zhou et al., 2021; Liu et al., 2024) with emphasis on *global change* (Obrist et al., 2018; Sonke et al., 2023), *polar atmospheric surface layer mercury depletion events* (Steffen et al., 2008), *chemical conversion in the atmosphere* (Schroeder et al., 1991; Lin and Pehkonen, 1999; Lin et al., 2011; Si and Ariya, 2018), *aqueous*

tog bort: of
formaterade ... [17]
tog bort: -
formaterade ... [18]
tog bort: the
formaterade ... [19]
tog bort: on
formaterade ... [20]
tog bort: circulates
tog bort: The knowledge
formaterade ... [21]
tog bort: there was a
formaterade ... [22]
tog bort:
formaterade ... [23]
tog bort: It used to be thought that gas
formaterade ... [24]
tog bort: However, it
formaterade ... [25]
tog bort: now
formaterade ... [26]
tog bort: more unstable
formaterade ... [27]
tog bort:
formaterade ... [28]
tog bort: multi-phase
formaterade ... [29]
tog bort:
formaterade ... [30]
tog bort: its
tog bort: data sets
formaterade ... [31]
formaterade ... [32]
tog bort: a
formaterade ... [33]
tog bort: tool
formaterade ... [34]
tog bort: dry
formaterade ... [35]
tog bort: .
formaterade ... [36]
formaterade ... [37]
tog bort: (Hynes et al., 2009;
formaterade ... [38]
flyttade (infogning) [1]
formaterade ... [39]
tog bort: Jackson, 1997; Lin
formaterade ... [40]
flyttade (infogning) [2]
formaterade ... [41]
tog bort: Bash et al., 2007; Ariya et al., 2015; Ariya et al., ... [42]
formaterade ... [43]

homogeneous and heterogeneous photoredox chemistry (Zhang, 2006; Si et al., 2022), *multi-phase atmospheric chemistry* (Ariya et al., 2015), *assessment of critical atmospheric chemical processes using state-of-the-art experimental and computational chemistry methods* (Ariya and Peterson, 2005; Ariya et al., 2008; Hynes et al., 2009), *receptor-* (Cheng et al., 2015) *and global models* (Lin et al., 2006; Lin et al., 2007; Subir et al., 2011, 2012; Amos et al., 2015; Travnikov et al., 2017). This review is based on the perspective of atmospheric scientists, with synthesis and a comprehensive account of the results of fundamental research, including field, laboratory, and theoretical studies, that have contributed to an understanding of the complexity of the atmospheric Hg cycle and its interactions with the Earth's surface ecosystem at the molecular level. This work does not address several topics related to Hg in the atmosphere. These include anthropogenic and natural emission inventories, corresponding top-down constraints and inverse modeling from atmospheric observations, accounting for long-term air data series and their temporal and spatial trends, observations of the PBM and its particle size distributions, wet deposition, future scenarios for the effects of regulatory measures (Minamata Convention), ongoing climate change and many more topics. Our goal is to provide a comprehensive review of the atmospheric chemistry of both inorganic and organic Hg in the lower and upper atmosphere, coupled with a compilation of updated, critically evaluated kinetic, thermochemical, photochemical, and isotopic fractionation data. Where appropriate, we introduce the basic concepts and fundamental aspects of Hg chemistry, including those of condensed phases. In atmospheric Hg isotope chemistry, our approach is comprehensive, encompassing a range of activities from field observations of air and Hg^0 gas exchange with natural surfaces to laboratory studies of processes that may be relevant to the atmosphere. We also highlight areas of persistent uncertainty or lack of consensus, such as measurement methods for atmospheric Hg speciation and the partitioning of Hg^{II} in atmospheric water between inorganic and organic ligands.

2 Physical chemistry of elemental mercury

Hg is the only metal that is a liquid at standard temperature and pressure (freezing point of -38.8 °C and boiling point of 356.7 °C), and its vapor is monatomic. Under these conditions, the mixing ratio of neurotoxic Hg vapor in equilibrium with metallic liquid is already at the hazardous level of approximately 1.7 ppm (Huber et al., 2006). Liquid Hg possesses properties that have given it a wide range of applications in the past despite its known toxicity, including exceptional surface tension (nearly seven times greater than that of water at 25 °C), high specific gravity, high electrical conductivity (a reference substance for measuring the SI unit Ω), low compressibility, and a constant volume of expansion in the liquid state. Hg forms solid alloys (amalgams) with most metals except iron. This property enables its application in gold panning (HgAu), dental fillings (HgAg), or as an electrode material in the chloralkali industry (NaHg). The electronic configuration of the mercury atom has filled f- and d-orbitals with a high density of 6s-valence electrons near the nucleus ($[Xe]4f^{14}5d^{10}6s^2$), which is related to a relativistic radial contraction of s- and p-orbitals as the inner electrons approach a significant fraction of the speed of light (which for a Hg 1s electron is 58%, implying a radial shrinkage of 23%; Pyykkö, 1988). It also follows that oxidation states 0 and +2 (mercuric, d^{10} metal ion) are the most stable for Hg. Nevertheless, Hg differs from other metals in its propensity to readily form a polycation in the aqueous phase, the mercurous ion, Hg_2^{2+}, which is, however, only metastable in the gaseous phase (Strömberg and Wahlgren, 1990). The solubility of Hg^0 in water is limited to 0.3 μM (Sanemasa, 1975), and the gas–water equilibrium is governed by Henry's law. The Henry's law coefficient (k_H^{cp}) for Hg^0 is 0.11 M atm^{-1} at 25 °C (Andersson et al., 2008), whereas the value is more than seven orders of magnitude greater for the $HgCl_2$ molecule at the same temperature (Sommar et al., 2000).

3 Atmospheric environment

3.1 Atmospheric measurements of mercury species

Hg is the only trace gas, other than the noble gases (Burnard, 2013), that exists as free atoms (Hg^0) in the atmosphere, making this pollutant exceptional in terms of low detection limits by optical measurement techniques. This makes it possible to measure Hg vapor emissions in real time, for example, from mining, chloralkali production and geothermal activities, as has been done in Europe for decades via light detection and ranging (LIDAR) in differential absorption mode by mobile laser systems (Svanberg, 2002). If the optical path length in the measuring cell of an instrument is sufficiently long (i.e., using multipath techniques such as cavity ring-down), then the conditions exist for continuous measurement of Hg^0 in ambient air (at the sub-ppt level, ~5×10^6 atoms cm^{-3} in the northern hemisphere) via atomic absorption spectroscopy (AAS) with Zeeman background correction (Osterwalder et al., 2020). The application of Zeeman AAS in Hg stable isotope analysis has also been described (Lu et al., 2019). As an alternative to Zeeman splitting of the Hg(6^3P) level for sensitive, selective detection of Hg^0 (Sholupov et al., 2004), sequential two-photon laser-induced fluorescence schemes

flyttade (infogning) [3]
formaterade ... [44]
flyttade upp [2]: 2014; Gustin et al.,
tog bort: 2007; Zhang et al., 2009; Gaffney and Marley,
formaterade ... [45]
flyttade upp [3]: 2006; Lin et al.,
formaterade ... [47]
flyttade upp [1]: 2015; Mao et al.,
tog bort: ;
tog bort: Lin et al.,
tog bort: 2016; Lyman et al., 2020a; Ariya and Peterson, 2 ... [48]
formaterade ... [46]
formaterade ... [49]
tog bort: fairly
formaterade ... [50]
tog bort: a reductionist
formaterade ... [51]
tog bort: down to a molecular level
formaterade ... [52]
tog bort: .
formaterade ... [53]
tog bort: account of
formaterade ... [54]
tog bort:) and the
formaterade ... [55]
tog bort: tabulations
formaterade ... [56]
tog bort: topic with
formaterade ... [57]
tog bort: that
formaterade ... [58]
tog bort: of
formaterade ... [59]
tog bort: of value
formaterade ... [60]
tog bort: ,
formaterade ... [61]
tog bort: , and several other areas
formaterade ... [62]
formaterade ... [63]
tog bort: about
formaterade ... [64]
tog bort: which
formaterade ... [65]
tog bort: 25°C
formaterade ... [66]
tog bort: the measure of
formaterade ... [67]
tog bort: -
formaterade ... [68]
tog bort: applications
formaterade ... [69]
tog bort: chlor-alkali
formaterade ... [70]
tog bort: Its
formaterade ... [71]
tog bort: with
formaterade ... [72]
tog bort:
formaterade ... [73]
tog bort: and
formaterade ... [74]
tog bort: contracts the orbital
formaterade ... [75]
tog bort: electron approaches
formaterade ... [76]
tog bort: . This shrinking cascade effect makes
formaterade ... [77]

have been used (Bauer et al., 2002; Bauer et al., 2014; Hynes et al., 2017). For initial excitation of the Hg(6^1S_0) → Hg(6^3P_1) transition at 253.7 nm, a light beam from a Hg discharge lamp or the frequency-doubled output of a dye laser pumped by the third harmonic of a Nd:YAG laser is used. As shown in **Fig. 1a**, further excitation involves the sequential excitation of different atomic transitions by two laser systems, both starting from the Hg(6^3P_1) state, followed by the detection of blue- (Hg(6^1P_1) → Hg(6^1S_0) at 184.9 nm) or redshifted (e.g., at 578.9 nm) fluorescence. The detection of Hg^0 with such a sophisticated apparatus is an exception to typical measurements, which are made via cold vapor atomic fluorescence spectroscopy (CV-AFS) after preconcentration sampling on gold (Ambrose, 2017). Smaller non-Hg^0 portions of atmospheric Hg are challenging to speciate because of their low concentrations. Instead, they are fractionated operationally based on their oxidation state (Hg^0 versus GOM) or phase state (GOM versus PBM). Since gold does not selectively trap Hg^0 but also captures other Hg species (Dumarey et al., 1985; Gačnik et al., 2024), the GOM and PBM must be individually collected upstream of the sample air to accurately measure the triad Hg^0, GOM, PBM. KCl-coated annular denuders have been utilized for fractionating ambient GOM by gas phase diffusion for over two decades. Nonetheless, upon the development of techniques to assess its accuracy in measuring ambient air regularly, the method was found to be biased in a nonsystematic manner toward lower values (Jaffe et al., 2014; Lyman et al., 2010; McClure et al., 2014). The automated KCl denuder method, with its variable efficiency, can thus

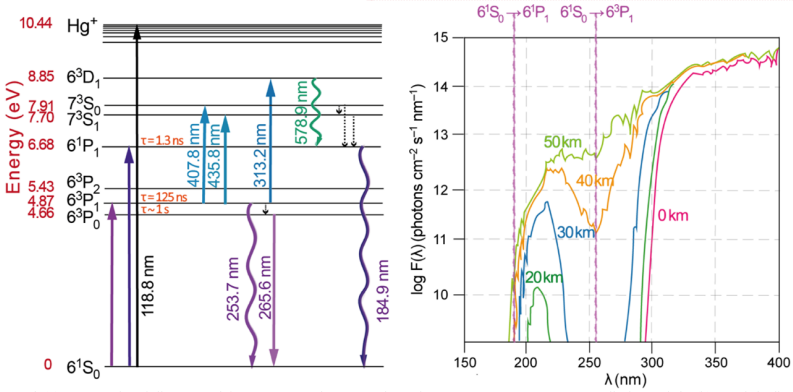

Figure 1: Left (a). Energy level diagram of the Hg atom. The wave-shaped arrows represent resonant radiation. Right (b): Actinic fluxes as a function of altitude. The wavelengths of the Hg($^1S_0$) → Hg($^3P_1$) and → Hg($^1P_1$) transitions at 253.7 and 184.9 nm, respectively, are given.

lead to serious underestimation of the GOM, whereas the refluxing mist chamber method, which is an alternative, carries the risk of cosampling the GOM with the PBM (Gustin et al., 2021). However, the KCl-covered denuder does not have full penetration of PBMs < 2.5 µm, but aerosols of a hundred nm or less are increasingly trapped by the salt surface (Ghoshdastidar et al., 2019). When compared, refluxing mist chambers yielded ambient GOM concentrations that were 3 to 4 times higher on average than those obtained with KCl-coated annular denuders (Landis et al., 2002). A decade later, the capture and retention efficiency of the KCl denuder method for GOM was evaluated, which was close to 95% in synthetic Hg^0-free air but decreased drastically to between 20% and 54% when exposed to ambient air, where ozone and humidity were found to cause severe reductive losses such as Hg^0 (McClure et al., 2014). In fact, ozone gas can heterogeneously reduce particle-bound Hg^{II} halides, as recent experiments have shown (Ai et al., 2023). In high-humidity marine applications, KCl denuder technology operates at very low efficiency; for example, He and Mason (2021) reported average losses of 80% during oceanographic expeditions in the Pacific. By determining total airborne mercury (TAM; Steffen et al., 2002; Slemr et al., 2018) and Hg^0 in air, a measure of reactive mercury (RM) is obtained as the sum of GOM + PBM by subtracting Hg^0 from TAM. In turn, Hg^0 is obtained by passing an air stream through a filter and a cation exchange membrane (CEM) in series, whereas TAM is measured as Hg^0 after a pyrolysis unit held at 800 °C converts all Hg in the sample air to elemental vapor (Lyman et al., 2020b). CEM is capable of capturing and retaining Hg^{II} quantitatively over long storage periods but has no affinity for Hg^0 (Miller et al., 2019). However, when two quantities that are usually close to each other are subtracted, the precision of the RM determination is low. Hynes et al. (2017) used two-photon laser-induced fluorescence as an online detection method for RM (by switching between ambient and pyrolyzed air as the source for the Hg^0 analyte) and concluded that the variability in ambient Hg^0 severely limits the sensitivity of dual-channel difference RM measurements. For the separation of the semivolatile GOM fraction from the PBM in ambient air, various membranes have been examined, but with recognized limitations (Dunham-Cheatham et al.,

tog bort: an
tog bort: the emission of
tog bort: .
tog bort: Detection
tog bort: the usual
tog bort: typically
tog bort: by
tog bort: The smaller
formaterade: Teckenfärg: Text 1
tog bort: due to
formaterade: Teckenfärg: Dekorfärg 2, Kondenserad med 0,2 pt
tog bort: –
tog bort: –
tog bort: The
tog bort: denuder has
tog bort: -
tog bort: regularly
tog bort: non-systematic
tog bort: towards
formaterade: Kondenserad med 0,3 pt
formaterade: Kondenserad med 0,2 pt
formaterade: Kondenserad med 0,2 pt
tog bort: KCl denuder method, with its variable efficiency, can thus …
Formaterat: Radavstånd: Flera 1,4 li
tog bort: while
tog bort: artifact formation of Hg^{II} by co-sampling
formaterade: Teckenfärg: Blå
formaterade: Teckenfärg: Blå
tog bort: ,
tog bort: dropped
tog bort: in particular
formaterade: Teckenfärg: Dekorfärg 2
tog bort:) (
tog bort: while
tog bort: °C
tog bort: CEM has the ability to
formaterade: Teckenfärg: Dekorfärg 2
tog bort: capture and retain Hg^{II}
tog bort: ,
tog bort: by subtracting
formaterade: Teckenfärg: Dekorfärg 2
tog bort: measurement
tog bort: semi-volatile
tog bort: the use of
tog bort: has
tog bort: implemented
formaterade: Teckenfärg: Dekorfärg 2
tog bort: has

2023; Gustin et al., 2023). The realization of NIST-traceable GOM calibration systems has recently progressed (Gacnik et al., 2022). Several studies have been carried out with the aim of experimentally deciphering the molecular identities (speciation) of the GOM pool in ambient air. Most methods are based on a preconcentration process of GOM on a substrate, which is then thermodesorbed in a gas stream following a programmed temperature ramp and detected as Hg^0 after pyrolysis (Gustin et al., 2015), alternatively focused on a capillary column and analyzed by different types (chemical ionization CI; electron impact ionization) of mass spectrometry (MS) (Deeds et al., 2015; Jones et al., 2016). In the former case, standards are used in the form of a number of commercially available Hg chemicals (such as $HgBr_2$, $HgCl_2$, HgO, $Hg(NO_3)_2$, and $HgSO_4$) that are assumed to be representative surrogates for GOM (Huang et al., 2017; Sexauer Gustin et al., 2016). As inferred by Khalizov et al. (2020), this speciation is indirect, as it has not been confirmed that the GOM molecules adsorbed on the substrate can be desorbed in the same chemical form as they are in air.

In contrast, studies have shown that aerosol reactions lead to the re-speciation of mercuric halides on surfaces (Mao et al., 2021; Mao and Khalizov, 2021). The authors reported that their ion-drift (ID) CI-MS system, which is sensitive enough for detection in laboratory studies, can achieve an LOD at a 1 amu resolution of (0.8–2.0) × 10^5 molecules cm^{-3} toward ambient GOM by switching to multistage atmospheric pressure ID-CI-MS. The feasibility of using proton transfer reaction mass spectrometry (PTR-MS) to study the reaction products (GOM) of Br-initiated Hg^0 oxidation has been evaluated by Dibble et al. (2014) but is not recommended because it cannot be applied in multi-stage atmospheric pressure systems (Khalizov et al., 2020). In summary, direct measurements of ambient GOM species have not yet been achieved. No method exists for chemically characterizing the GOM fraction, which is semivolatile and may contain species that are photolytically unstable. Since previous GOM measurements are considered unreliable (Lyman et al., 2020a; Slemr et al., 2016) and emerging RM data (Lyman et al., 2020b; Slemr et al., 2018; Swartzendruber et al., 2009; Gratz et al., 2015; Lyman and Jaffe, 2012) are still too sparse and spatially limited, it is not possible to draw deterministic conclusions on atmospheric Hg^{II}. Sampling methods for organic Hg (dimethylmercury; He et al., 2022 and monomethylated Hg^{II} species; Lee et al., 2003) in ambient air, as opposed to inorganic Hg species, are more unambiguous. The speciation of Hg in atmospheric waters is discussed in **Section 4.6**. Hg measurement data from air and precipitation, ground-based or aircraft (Slemr et al., 2018; Slemr et al., 2016) observations that fall outside the scope of this review, including those reported from continental (Cole et al., 2014; Cole et al., 2013; Schmolke et al., 1999; Wängberg et al., 2001; Gay et al., 2013; Fu et al., 2015) to hemispherical (Bencardino et al., 2024; Szponar et al., 2020; Slemr et al., 2020; Sprovieri et al., 2017; Sprovieri et al., 2016) monitoring networks, some of which have been in operation since before the turn of 2000 (Custódio et al., 2020), have been reviewed elsewhere (Mao et al., 2016; Lyman et al., 2020a; Howard et al., 2017; Angot et al., 2016; Kim et al., 2012; Zhang et al., 2017). In the case of the isotopic characterization of atmospheric Hg, however, we feel justified in compiling, analyzing, and discussing the considerable body of recent observations (**Section 8.2**).

3.2 Stability of atmospheric Hg^0

Hg^0 represents the primary form of atmospheric mercury in both the troposphere and stratosphere. Considering the spatial variability of Hg^0 concentrations [1], which depart from a uniform vertical distribution throughout the atmosphere (Slemr et al., 2018), a singular global atmospheric lifetime is not appropriate. A more pertinent measure is the effective lifetime of Hg^0, expressed on an annual basis and as a function of its horizontal and vertical location within the atmosphere. The observed disparity in tropospheric Hg^0 concentrations between the Northern and Southern Hemispheres of a factor of ~1.41 (Tang et al., 2025), despite anthropogenic emissions in the Northern Hemisphere being approximately 2.5 times greater than those in the Southern Hemisphere (Streets et al., 2019; Sonke et al., 2023), implies that Hg^0 has a relatively short effective lifetime in comparison to the interhemispheric air mass exchange time of approximately 1.3 years (Geller et al., 1997). As Hg^0 crosses the intertropical convergence zone, it undergoes convective uplift, enabling its transport into the stratosphere. Troposphere-to-stratosphere Hg^0 transport has been regarded as limited (100–176 Mg yr^{-1}; Lyman and Jaffe, 2012; Horowitz et al., 2017). Nevertheless, recent modeling suggests that the stratosphere is

[1] There is a widespread practice in the Hg research community to report Hg^0 air concentrations in ng m^{-3} referenced to one atmosphere (101.325 kPa) and 0 °C (STP). By that, the unit represents a mixing ratio not an absolute (mass) concentration.

tog bort:).·…. The realization of NIST-traceable GOM calibration systems has recently progressed (Gacnik et al., 2022). Several studies have been carried out with the aim of experimentally deciphering the molecular identities (speciation) of the GOM pool in ambient air. Most methods are based on a pre-concentration…reconcentration process of GOM on a substrate, which is then thermo-desorbed…hermodesorbed in a gas stream following a programmed temperature ramp and detected as Hg^0 after pyrolysis (Gustin et al., 2015), alternatively focused on a capillary column and analyzed by different types (chemical ionization CI; electron impact ionization) of mass spectrometry (MS) (Deeds et al., 2015; Jones et al., 2016). In the former case, standards are used in the form of a number of commercially available Hg chemicals (such as $HgBr_2$, $HgCl_2$, HgO, $Hg(NO_3)_2$, and $HgSO_4$) that are assumed to be a …epresentative surrogate…urrogates for GOM (Huang et al., 2017; Sexauer Gustin et al., 2016). As inferred by Khalizov et al. (2020), this speciation is indirect, as it has not been confirmed that the GOM molecule…olecules adsorbed on the substrate can be desorbed in the same chemical form as it was ... [94]

tog bort: On the contrary

tog bort: show

formaterade: Teckenfärg: Text 1

Formaterat: Avstånd Efter: 0 pt

tog bort: These…he authors also report…eported that their ion-drift (ID) CI-MS system, which is sensitive enough for detection in laboratory studies, can achieve an LOD at a 1 amu resolution of (0.8 – …2.0) x ... [95]

tog bort: towards…oward ambient GOM by switching to multi-stage…ultistage atmospheric pressure ID-CI-MS. The feasibility of using proton transfer reaction mass spectroscopy ... [96]

tog bort:),

formaterade: Teckenfärg: Blå

tog bort: with respect to its inapplicability to

formaterade: Teckenfärg: Blå

tog bort: straight-forward…method exists for chemically characterizing the GOM fraction, which is semi-volatile…emivolatile and may contain species that are photolytically unstable. Sin ... [97]

tog bort: (… He et al., 2022)…and monomethylated Hg^{II} ... [98]

tog bort: in…rom air and precipitation, ground-based or ai ... [99]

Formaterat: Avstånd Före: 9 pt, Efter: 9 pt

tog bort: Atomic vapor (

formaterade: Teckenfärg: Blå

tog bort:) dominates

formaterade ... [100]

tog bort: Hg pool, shows an interhemispheric difference ... [101]

formaterade: Teckenfärg: Blå

tog bort: the northern hemisphere (Bencardino et al., 202 ... [102]

formaterade: Teckenfärg: Blå

tog bort: (Weigelt et al., 2016). When crossing the interti ... [103]

formaterade: Teckenfärg: Blå

tog bort: In the upper troposphere of the Pacific Ocean, t ... [104]

formaterade: Teckenfärg: Blå

tog bort: augmented interhemispheric Hg exchange (Koe ... [105]

formaterade: Teckenfärg: Blå

tog bort: to the troposphere, excluding biomass burning, ... [106]

tog bort: 360 Mg (Saiz-Lopez et al., 2020). This value si ... [107]

formaterade: Teckenfärg: Blå

tog bort: previously thought. For transferring

formaterade: Teckenfärg: Blå

formaterade: Teckenfärg: Blå

crucial for biogeochemical Hg cycling, acting as the primary pathway for Hg^0 exchange between hemispheres and explaining the minor interhemispheric gradient (Saiz-Lopez et al., 2025). As posited by models developed by Shah et al. (2021) and Saiz-Lopez et al. (2025), approximately 17% of the aggregate atmospheric Hg load is situated within the stratosphere, whereas a previous study reported 12% (Horowitz et al., 2017). Given that the stratosphere's mass (9.06×10^{17} kg) constitutes approximately 18% of the total atmospheric air mass (5.13×10^{18} kg; Warneck and Williams, 2012), one might infer that the fraction of mercury present in the stratosphere is comparable to the proportion of stratospheric air relative to the entire atmosphere. However, this scaling is not supported by empirical data. Aerial measurements of Hg in the troposphere and lower stratosphere reveal a steep Hg gradient around and above the tropopause with lower Hg mixing ratios in the upper atmospheric layers (Radke et al., 2007; Talbot et al., 2007; Slemr et al., 2018) linked to a larger contribution of oxidized Hg species partitioned to aerosols (Murphy et al., 1998) from the gas phase.

With respect to the tropospheric Hg budget, there is a relative consensus that the Hg load is close to 4 Gg (Saiz-Lopez et al., 2020; 3.9 ± 1.0, Saiz-Lopez et al., 2025; 3.8, Zhang et al., 2023b; 4.0, Shah et al., 2021; 3.9, Horowitz et al. 2017), with exceptions suggesting that it is closer to 5 - 6 Gg (Holmes et al., 2010; Zhang et al., 2025) and that anthropogenic emissions, excluding biomass burning, are approximately 2.2 – 2.6 Gg yr^{-1} (Horowitz et al., 2017; Shah et al., 2021; Zhang et al., 2023b; Geyman et al., 2024; Saiz-Lopez et al., 2025), with significant reductions across developed countries in the Northern Hemisphere observed in the near term (Custódio et al., 2022; Feinberg et al., 2024). Aircraft-based observations reveal a relatively consistent mixing ratio of Hg^0 within the troposphere below the tropopause, encompassing the planetary boundary layer in regions characterized by low primary emissions (Banic et al., 2003; Talbot et al., 2007; Swartzendruber et al., 2008; Weigelt et al., 2016b; Bieser et al., 2017). This uniformity supports the adoption of a steady-state procedure (Seinfeld and Pandis, 2006), where the inverse of the Hg^0 lifetime ($\tau_{troposphere}$) is approximated by the sum of its loss rates:

$$1/\tau_{troposphere} = 1/\tau_{rxn} + 1/\tau_{ocean} + 1/\tau_{land} + 1/\tau_{wash} + 1/\tau_{stratosphere} \quad (1)$$

where the indices rxn, ocean, land, wash, and stratosphere are used to represent net oxidation, oceanic uptake, assimilation in land ecosystems, processes that lead to wet deposition and net transfer to the tropopause/stratosphere, respectively. As discussed subsequently, all the terms in equation 1 are subject to significant uncertainties. However, as is the case with many other trace gases, the chemical lifetime (τ_{rxn}) undoubtedly plays a controlling role in determining the effective lifetime of Hg^0. Representing net oxidation, τ_{rxn} encompasses the duration of the initial two-step oxidation to molecular forms and the subsequent redox cycling of the photolabile fraction of these molecules in the gas phase and aerosols prior to deposition. According to the latest redox schemes (Shah et al., 2021; Castro Pelaez et al., 2022; Saiz-Lopez et al., 2025), the extent of bidirectional Hg mass flux by atmospheric chemical conversion (oxidation and reduction, 10.4 - 13.0 vs. 6.0 - 6.9 Gg yr^{-1}, respectively) appears to be much greater than previously assumed (e.g., 8.0 vs. 3.7 Gg yr^{-1}, Holmes et al. 2010), which also holds for the bidirectional fluxes (emission and depositional uptake) that occur in the gas exchange of Hg^0 between the atmosphere and the land and ocean. Aggregate atmospheric emissions and dry deposition have been approximated at 7.4–11.2 and 2.9–6.8 Gg Hg^0 yr^{-1}, respectively (Horowitz et al., 2017; Shah et al., 2021; Sonke et al., 2023; Zhang et al., 2023b), following a tendency of researchers toward augmenting the role of re-emission of legacy Hg from the oceans (3.7–7.2 Gg Hg^0 yr^{-1}) and gross biospheric assimilation from the atmosphere (1.2–3.2 Gg Hg^0 yr^{-1}; Horowitz et al., 2017; Yuan et al., 2019; Obrist et al., 2021; Zhou and Obrist, 2021; Feinberg et al., 2022; Wang et al., 2022; Szponar et al., 2025), respectively. To transfer Hg^0 from the ocean into the atmosphere, the mass transfer rate is usually parameterized via wind speed dependencies that have been tested for CO_2 emissions. However, recent evidence (Osterwalder et al., 2021) suggests that Hg^0, which is less soluble than CO_2, behaves similarly to O_2 and N_2, where the impact of bubble-mediated transfer is greater. As a result, ocean emissions play an increased role in the global Hg budget, accounting for approximately 60% of total Hg emissions to the atmosphere due to a wind speed dependence with a cubic power exponent instead of a quadratic power exponent in model simulations (Zhang et al., 2023b). The greater gross emissions from seawater must be balanced by gross deposition of Hg^0, which is, within uncertainties, of comparable magnitude to that of Hg^{II} deposition over oceans (Jiskra et al., 2021), and much higher than previously assumed (Soerensen et al., 2010). The global net exchange of Hg^0 from the oceans has been estimated at 0.8 - 4.0 Gg Hg^0 yr^{-1} (Lamborg et al., 2002; Strode et al., 2007; Selin et al., 2008; Holmes et al., 2010; Chen et al., 2014; Horowitz et al., 2017; Shah et al., 2021), and the

flyttade (infogning) [4]
formaterade: Teckenfärg: Blå
tog bort: from the oceans into the atmosphere, the mass transfer rate is usually parameterized using wind speed dependencies that have been tested for CO_2 emissions.
formaterade: Teckenfärg: Blå
tog bort: rather
formaterade: Teckenfärg: Blå
tog bort: have
formaterade: Teckenfärg: Blå
formaterade: Teckenfärg: Blå
formaterade: Teckenfärg: Blå
tog bort: are
formaterade: Teckenfärg: Blå
tog bort: the
formaterade: Teckenfärg: Blå
formaterade: Teckenfärg: Blå
formaterade: Teckenfärg: Blå
tog bort: -
formaterade: Teckenfärg: Blå
tog bort: 2010). This also applies to the magnitude of Hg^0 dry and wet deposition (throughfall; Wang et al., 2020b) to vegetation (forests). A comprehensive overview of the understanding of the gas exchange of Hg^0 between the atmosphere and the Earth's surface has been presented elsewhere (Sommar et al., 2020).

fraction of Hg^0 emissions resulting from Hg^{II} reduction in surface waters is at an upper limit of 2.25 ± 0.89 Hg^0 Gg yr^{-1} (Tang et al., 2025). In summary, the latter terms in Equation (1) correspond to lifetimes, the spans of which are conservatively estimated to exceed one year. However, their inverses, referring to Eq. 1, when summed, can shorten $\tau_{troposphere}$ by tens of percent beyond what the tropospheric chemical lifetime of Hg^0 (τ_{rxn}) dictates, taking into account the inherent uncertainties. Currently, Hg^0 is estimated to have a $\tau_{troposphere}$ of between 3.8 and 7 months (Shah et al., 2016; Horowitz et al., 2017; Saiz-Lopez et al., 2020; Shah et al., 2021; Saiz-Lopez et al., 2025) and an average atmospheric lifetime (troposphere + stratosphere) of 8.2 months (Saiz-Lopez et al., 2025).

The sources of atmospheric Hg^{II} are twofold: primary Hg^{II} emissions from anthropogenic sources and atmospheric Hg^0 oxidation. Compared with that of Hg^0, the proportion of Hg^{II} in anthropogenic emissions in the troposphere is not well defined. One estimate suggests that 74% of cumulative anthropogenic Hg emissions into the air are Hg^0 (Streets et al., 2017). Currently, East Asia has the most emissions worldwide (Streets et al., 2019); however, compelling evidence indicates that the magnitude of total Hg air emissions in this region has already peaked (Zhang et al., 2023a) and has declined in recent years (Wu et al., 2023; Feinberg et al., 2024). Nevertheless, a shift in the contributions of distinct source categories, with cement production emerging as the predominant source since 2009 in China (Wu et al., 2016), suggests an increase in the proportion of Hg^{II} within Hg emissions (Zhang et al., 2016; Wang et al., 2024). Hg speciation profiles from anthropogenic sources may vary significantly across regions; for example, in continental Europe, the Hg^{II} contribution from coal-fired power plants may represent less than 25% (Weigelt et al., 2016a), whereas in the tropics, artisanal and small-scale gold mining represent a substantial yet largely unconstrained source of atmospheric Hg^0 (Obrist et al., 2018). On average, contemporary global models employ 60 to 65% Hg^0 speciation in current anthropogenic emissions to the atmosphere (Horowitz et al., 2017; Shah et al., 2021; Zhang et al., 2023b). There are significant differences in the estimates of the tropospheric pool of Hg^0 (~3.3–4.8 Gg), separated from Hg^{II} (0.1–1.0 Gg), within the above-mentioned constrained budgets for the total tropospheric Hg load in contemporary models. Having estimated the atmospheric load of Hg^{II} up to 20 km at ~0.36 Gg on the basis of a synthesis of RM measurements at different heights in the atmosphere (Saiz-Lopez et al., 2020), a later contribution (Saiz-Lopez et al., 2025) involving stratospheric transport and chemistry deployed a much larger tropospheric Hg^{II} pool (0.51 Gg) associated with downward transport (0.35 Gg yr^{-1}) of mostly photostable Hg^{II} from the stratosphere (Hg^{II} pool of ~0.2 Gg). The corresponding amount of (wet and dry) Hg^{II} deposited on Earth's surface is 6.92 ± 1.70 Gg yr^{-1}, which is outside the previously estimated range of 4.8--6.8 Gg yr^{-1} Hg^{II} (Strode et al., 2007; Zhang et al., 2019b; Feinberg et al., 2022; Sonke et al., 2023). The effective $\tau_{troposphere}$ of Hg^{II} is a few weeks (Horowitz et al., 2017), whereas Hg^{I} species are intermediates (lifetime << 1 s) in the Hg^0/Hg^{II} redox cycle, and their tropospheric mass is negligible (Shah et al., 2021).

Hg^0 in the planetary boundary layer can be consumed at a surprisingly high rate, leading to low concentration levels that approach complete depletion. Thus, chemical oxidation by reactive bromine species in a catalytic cycle ("bromine explosion", Toyota et al., 2014; Gao et al., 2022) can explain atomic Hg depletion events (AMDEs) during the polar spring after sunrise (Schroeder et al., 1998; Sommar et al., 2007; Nerentorp Mastromonaco et al., 2016) and those observed over the Dead Sea (Obrist et al., 2011) (**Fig. 2**). Br-controlled oxidation via the intermediate $^{\bullet}Hg^{I}Br$ is critical for the tropospheric oxidation of Hg^0, as described later in the section on gas-phase oxidation. Upon entry into the stratosphere, thermal oxidation with $Br^{\bullet}$ remains important for conversion to Hg^{II}, but with increasing altitude in the lower stratosphere, Cl chemistry plays the most important role, with OH-directed chemistry in second place at a slow net oxidation rate. With the maximum concentration of the O_3 layer (~25 km) as the dividing line, there is a strong dichotomy between the Hg chemistry in the upper and lower stratosphere. The former is UVC driven (Sun et al., 2022, the UV window > 30 km provides a substantial photon flux at λ = 253.7 nm, **Fig. 1b**), involving optically excited Hg^0 states with a strong electrophilic character. The electronic excitation of Hg^0 from the ground state (singlet, $^1S_0$) at 253.7 nm is spin-forbidden (leading to a triplet state, $^3P_1$ with a radiative lifetime of ~125 ns; **Fig. 1a**). The metastable dark Hg($^3P_0$) state cannot be produced directly from Hg($^1S_0$) by light absorption but can be produced by spin-orbit relaxation of Hg($^3P_1$) atoms involving energy transfer to surrounding (air) molecules. In N_2, the equilibrium constant between the $^3P_0$ and $^3P_1$ states at room temperature (297 K) is 1.87×10^3 (Callear and Shiundu, 1987), but in the presence of O_2, their distribution changes profoundly. Although O_2 is a slightly less effective quencher for

formaterade: Teckenfärg: Blå

tog bort: Hg^0 is estimated to have a global tropospheric lifetime of 3.8 - 7 mo. and a chemical lifetime against oxidation (to Hg^{II}) of 2.7 - 4.5 mo. (Shah et al., 2021; Horowitz et al., 2017; Zhang et al., 2023b; Shah et al., 2016; Saiz-Lopez et al., 2025), the differences between the two values being largely due to significant redox cycling in the gas phase and aerosols before deposition. Atmospheric Hg deposition persists for terrestrial ecosystems overall with a predominance of Hg^0 compared to Hg^{II} (Zhou and Obrist, 2021; Wang et al., 2020b; Feinberg et al., 2022), while the situation appears opposite for cryospheric and marine systems. The total atmospheric Hg deposition is estimated to be 4800 - 6700 Mg yr^{-1} Hg^{II} (Sonke et al., 2023; Zhang et al., 2019b; Feinberg et al., 2022) and 3600 - 6750 Mg yr^{-1} Hg^0 (Shah et al.,

flyttade upp [4]: 2021; Sonke et al., 2023; Zhang et al.,

formaterade: Teckenfärg: Blå

tog bort: 2023b). Hg in the stratosphere is estimated to account for about 20% of the total atmospheric Hg mass, with an exchange with the troposphere in the range of 176-300 Mg yr^{-1} (Shah et al., 2021; Lyman and Jaffe, 2012), where Hg is mainly removed from the stratosphere as Hg^{II} on aerosols (Murphy et al., 2006) or, to a lesser extent, as the most photostable gas-phase mercurial species (Saiz-Lopez et al., 2022 & 2025). Based on correlations between Hg^0 and N_2O in the stratosphere within 4 km above the thermal tropopause, Slemr et al. (2018) provided a lifetime estimate of 74 ± 27 yr., while Lyman and Jaffe (2012) inferred a relatively short lifetime for Hg^0 in intercepted descending air with stratospheric origin. Saiz-Lopez et al. (2022) estimate the lifetime of Hg^0 in the lower stratosphere against surface deposition of 3 – 9 years and Saiz-Lopez et al. (2025) a mean atmospheric (troposphere + stratosphere) lifetime of 8.2 mo.

tog bort: bordering on

formaterade: Teckenfärg: Dekorfärg 2

tog bort: also¶

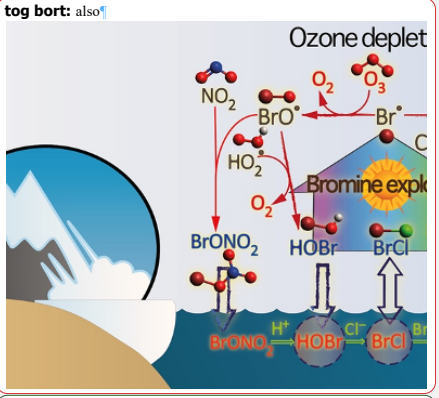

flyttade ned [5]: **Figure 2.** The chemistry behind bromine explosion events and related surface layer ozone and mercury depletion events.¶

formaterade: Teckenfärg: Dekorfärg 2

tog bort: becomes

tog bort: ¶

tog bort:)(The

tog bort: -

tog bort: ,

tog bort: ,

$Hg(^3P_0)$ than for $Hg(^3P_1)$ (Callear, 1987), their effective lifetimes in air at atmospheric pressure differ by only one order of magnitude (~1.1 ns and ~0.2 ns, respectively; Saiz-Lopez et al., 2022). In addition to physical quenching to the ground state, both $Hg(^3P_0)$ and

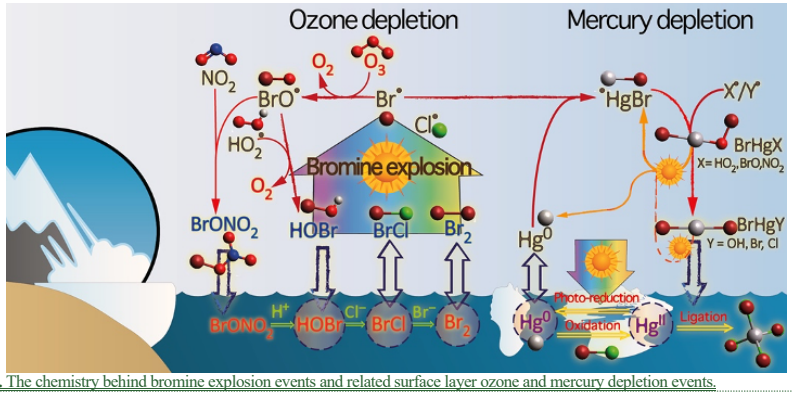

Figure 2. The chemistry behind bromine explosion events and related surface layer ozone and mercury depletion events.

$Hg(^3P_1)$ may undergo chemical oxidation to mercury oxide(s) (Callear et al., 1959), although metastable atoms are expected to be less reactive. The chemical conversion of excited Hg atoms by O_2 releases Hg^{II}, which can further react with more stable species, giving Hg^0 in the upper stratosphere a tiny lifetime against oxidation compared with that of transfer to the lower atmosphere (Saiz-Lopez et al., 2022). In the uppermost stratosphere, there appears to be access to deeper UVC (**Fig. 1b**) such that at 184.9 nm, a spin-allowed electronic transition from $Hg(^1S_0)$ to $Hg(^1P_1)$ occurs, with a light absorption cross-section nearly two orders of magnitude greater than that for the $Hg(^1S_0) \rightarrow Hg(^3P_1)$ transition (Morton, 2000). Like $Hg(^3P_1)$, the more energetic $Hg(^1P_1)$ reacts with O_2 at a rate approaching the collision frequency, but the HgO product formed in the latter case is so vibrationally hot that it promptly decays into Hg and O atoms. As a result, the chemistry of $Hg(^1P_1)$ is expected to play a minor role in the turnover of Hg in the upper stratosphere. The calculated lifetime of Hg^0 in the middle to upper stratosphere is altitude-dependent, ranging from a fraction to a few hundred hours (Saiz-Lopez et al., 2022), and is most comparable to that of Hg^0 during AMDEs. However, the underlying governing physicochemical processes are completely different.

4 Kinetics, thermodynamics and general chemistry

4.1 Fundamental kinetics and thermodynamic principles

A chemical process can be decomposed into a sequence of one or more single-step processes as elemental reactions. Elementary processes involve a transition between two atomic or molecular states, separated by a potential energy barrier, that represents the activation energy. The rate of a gas–phase reaction depends on the number of collisions between the reactants and the thermodynamics of their interactions (i.e., the change in entropy, ΔS, and enthalpy, ΔH, upon passing through the transition state), whereas for the rate of a reaction in aqueous solution, there are a number of additional factors that can influence the rate, such as solvation, ionic strength, pH, and diffusion rates. Processes that release heat as products and increase the entropy of the system favor the reaction. The balance between ΔH and ΔS is given by the Gibbs free energy equation, where T is the absolute temperature: $\Delta G = \Delta H - T\Delta S$. If the Gibbs free energy is negative, the reaction is spontaneous from a thermodynamic perspective. The index is used to distinguish the enthalpy of reaction (ΔH_R) from, e.g., the enthalpy of formation of a substance (ΔH_f). We can calculate the equilibrium constant, K, using $\ln K = -\Delta G_R/RT$ and determine the ratio of the forward and reverse rate coefficients from $K = k_f/k_r$. Examples of important types of gas-phase reactions are as follows:

Reaction order	Type	Unit
Unimolecular step	Thermal dissociation	s^{-1}
Bimolecular step	Recombination	$cm^3 molecule^{-1} s^{-1}$, $L\ mol^{-1} s^{-1}$

tog bort: ,
flyttade (infogning) [5]
tog bort: …g($^3P_1$) may undergo chemical oxidation to mercury oxide(s) (Callear et al., 1959), although metastable atoms are expected to be less reactive. It is the…he chemical conversion of excited Hg atoms by O_2 that …eleases Hg^{II}, which can further react to…ith more stable species, giving Hg^0 in the upper stratosphere a tiny lifetime against oxidation compared to…ith that of transfer to the lower atmosphere (Saiz-Lopez et al., 2022). In the uppermost stratosphere, there appears to be access to deeper UVC (**Fig. 1b**) such that at 184.9 nm allows
... [108]
tog bort: of
tog bort: mid
formaterade
... [109]
tog bort: in the range of
formaterade: Teckenfärg: Dekorfärg 2
tog bort: of up
formaterade: Teckenfärg: Dekorfärg 2
tog bort:)
formaterade: Teckenfärg: Dekorfärg 2
tog bort: , but
tog bort: thermodynamical
formaterade: Kondenserad med 0,3 pt
Formaterat: Avstånd Efter: 0 pt
formaterade
... [110]
tog bort: . The barrier
formaterade: Teckenfärg: Blå, Kondenserad med 0,3 pt
tog bort: and determines the rate at which it occurs.
formaterade
... [111]
tog bort: is determined by
formaterade: Teckenfärg: Blå, Kondenserad med 0,3 pt
tog bort: interaction
formaterade: Teckenfärg: Blå, Kondenserad med 0,3 pt
tog bort: kinetics, a rate process,
formaterade
... [112]
tog bort: that describes the energetics of
formaterade: Teckenfärg: Blå, Kondenserad med 0,4 pt
tog bort: process
formaterade
... [113]
tog bort: enthalpy (Δ
formaterade: Kondenserad med 0,3 pt
tog bort:)
formaterade: Kondenserad med 0,3 pt
tog bort: entropy (Δ
formaterade: Kondenserad med 0,3 pt
tog bort:)
formaterade: Kondenserad med 0,3 pt
tog bort: in Kelvin
formaterade: Kondenserad med 0,3 pt
tog bort: say,
formaterade: Kondenserad med 0,3 pt
tog bort: reaction
formaterade: Kondenserad med 0,3 pt

Termolecular step	Recombination assisted by a third body (M = N_2/O_2)	$cm^6 molecule^{-2} s^{-1}$, $L^2 mol^{-2} s^{-1}$

Termolecular reactions are pressure (M)-dependent at low pressures with an effective rate coefficient (k) of third order but become pressure independent at high pressures. The transition from third- to second-order behavior is known as the fall-off region. For most atmospheric reactions, we can expect that the rate coefficient is at the low-pressure limit. However, there are exceptions, which are listed in **Table 3**. While *two-body* collisions are common in the gas phase, *three-body* collisions are much less probable, and *four-body* collisions can be ignored because of their low probability. An *overall* reaction includes two or more *elementary* reactions. The temperature dependence of the rate coefficients can be fit over a relatively narrow temperature range via the empirical *Arrhenius equation*: $k(T) = A \exp(-E_a/RT)$, where E_a is the activation energy and R is the gas constant. The pre-exponential factor A, a constant in the original Arrhenius equation, is weakly temperature dependent for most reactions (varying as the square root of T according to collision theory). For a wider temperature range, the modified expression $k(T) = (T/300)^n \cdot \exp(-E_a/RT)$ provides a better fit to the experimental data. If the activation energy is high enough, there is a large endothermic barrier that prevents even a reaction with a strongly negative ΔG_R from occurring at measurable rates. In select cases, the experimental data show a negative activation energy, suggesting that the reaction proceeds by the addition of reactants to form an intermediate species with excess energy that must be dissipated before decomposing into the final products. The rate constant for termolecular reactions between small molecules in the atmosphere can usually be well approximated by a combination of three parameters k_0 (cm^6 $molecule^{-2}$ s^{-1}), k_∞ (cm^3 $molecule^{-1}$ s^{-1}) and F_C. The first two correspond to the low- and high-pressure limits, and F_C is a form factor that describes the transition region.

$$k = \frac{k_0 \cdot k_\infty \cdot [M]}{k_\infty + k_0 \cdot [M]} F_C^{\left(1 + \left[\log(k_0 \cdot [M]/k_\infty)\right]^2\right)^{-1}} \quad (2)$$

The temperature dependence of k is expressed by parameterizing k_0 and k_∞ as a function of temperature with the following expression:

$$k_0^T = k_0^{300} (T/300)^{-n} \text{ and } k_\infty^T = k_\infty^{300} (T/300)^{-m} \quad (3)$$

4.2 Surface kinetics

Atmospheric aerosols have a high surface-to-volume ratio that concentrates most of their constituents at the surface. Furthermore, the influence of surface chemistry increases with decreasing particle size. Gas-to-particle reactions, among other heterogeneous reactions, begin with adsorption, which links molecules from the gas phase to the surface of a solid or liquid. This process can be physical, with low adsorption energy (*physisorption*, van der Waals forces) or chemical (*chemisorption*) when chemical bonding occurs as molecules approach the surface, overcome the activation energy barrier, and become reactive when the adsorbent reacts with sites on the surface. Importantly, gases and solutes adsorbed at an interface frequently exhibit physicochemical properties that diverge from their bulk properties, including reactivity and spectral shifts. Surface reaction kinetics are often expressed by the uptake probability (γ), which represents the fraction of gas collisions with a substrate surface that yield uptake or reactions. The net uptake of gas γ_{net} is quantified in terms of conductances (Γ), which are normalized to the rate of gas surface collisions:

$$\gamma_{net}^{-1} = \Gamma_g^{-1} + \alpha^{-1} + (\Gamma_{rxn} + \Gamma_{sol})^{-1} \quad (4)$$

where Γ_g, Γ_{rxn}, and Γ_{sol} represent the processes of gas-phase diffusion to the surface, solubility, and reaction in the bulk liquid phase, respectively, and α represents the (reversible) mass accommodation ("sticking") across the gas–particle interface. In addition to α, these processes are related to the diffusion constants in gas (D_g) and liquid (D_l) phases, Henry's law coefficient (k_H^{cp}), and the rate constant of the first-order reaction in the condensed phase bulk (Finlayson-Pitts and Pitts, 2000). For solids, bulk diffusion is generally too slow to allow bulk solubilities or bulk kinetics to control uptake. To justify the use of the formulation of additive kinetic conductances (**Eq. 4**) to solve the continuity equation and thus to be sufficient in laboratory studies to measure the net loss of a gas over a condensed phase of known volume and surface area, it is preferable to conduct experiments at low pressure. These experiments are typically performed in a tube reactor (radius r) with fast laminar flow (FF) conditions. To vary the reaction time, a moving injector is employed to change the exposed surface length in this technique. The net flux of the gas X into the condensed phase (J_x) can in this case be expressed as **Eq. 5**:

tog bort:)
tog bort: ,
tog bort: becomes
tog bort:
tog bort:
tog bort: -
formaterade: Teckenfärg: Dekorfärg 2
formaterade: Teckenfärg: Dekorfärg 2
tog bort: 1
tog bort: by
formaterade: Kondenserad med 0,2 pt
tog bort: G^0
tog bort: describing
tog bort: 1
formaterade: Kondenserad med 0,2 pt
tog bort:
tog bort: 2
formaterade: Kondenserad med 0,2 pt
tog bort: possess
formaterade: Kondenserad med 0,2 pt
tog bort: , which enables
formaterade: Teckenfärg: Dekorfärg 2, Kondenserad med 0,2 pt
formaterade: Kondenserad med 0,2 pt
tog bort: being concentrated
formaterade: Kondenserad med 0,2 pt
tog bort: is enhanced
formaterade: Kondenserad med 0,2 pt
tog bort: -
formaterade: Kondenserad med 0,2 pt
tog bort:),
tog bort:),
formaterade: Kondenserad med 0,2 pt
formaterade: Kondenserad med 0,2 pt
tog bort: and
formaterade: Kondenserad med 0,2 pt
tog bort: It is crucial to recognize that
formaterade: Kondenserad med 0,2 pt
tog bort: reaction
formaterade: Kondenserad med 0,2 pt
tog bort: 3
tog bort: -
formaterade: Kondenserad med 0,2 pt
formaterade: Kondenserad med 0,2 pt
tog bort: k_H),
tog bort: (
tog bort:
tog bort:)
tog bort: 3
tog bort: (FF).
tog bort: 4

$$J_X = \frac{2 \cdot k_{obs}}{r} \left([X]_{g,\infty} - \frac{[X]_{surf}}{k_H^{cp}} \right) \quad (5)$$

where k_{obs} is the experimentally observed first-order rate coefficient and where the indices g, ∞ and surf represent the gas bulk and surface, respectively. In turn, k_{obs} is approximately related to γ_{net} as shown in **Eq. 6**:

$$k_{obs} = r^{-1} \left(\frac{r}{3.66 \cdot D_g} + \frac{2\gamma_{net}}{\upsilon_X} \right)^{-1} \quad (6)$$

where D_g is the diffusivity of the gas and where υ_X is its mean thermal velocity. The value of γ_{net} changes as the surface is covered by molecules and depends on the concentrations of the reactants and the reaction time. The initial phase is denoted by γ_{net}^0, whereas the steady-state phase is denoted by γ_{net}^∞. The calculated γ_{net} can be employed to estimate the lifetime of gas X (τ_X) with respect to the reactive uptake on particles. The following formula has been applied to the uptake of aerosols with a polydisperse distribution (Mao et al., 2021; Sander, 1999; Schwartz, 1986):

$$\tau_X = \left[\sum 4\pi r^2 \left(\frac{\Delta N}{\Delta \log r} \right) \Delta \log r \left(\frac{r}{D_g} + \frac{4}{\gamma_{net} \cdot \upsilon_X} \right) \right]^{-1} \quad (7)$$

The uptake of the only Hg^{II} species studied thus far, $HgCl_2$, follows a Hinshelwood–Langmuir mechanism (Mao et al., 2021), where $HgCl_2(g)$ must first be adsorbed to a site (‖) on the surface and then react as a surface complex with a reactive center (e.g., anions) R on the surface, forming a product released from ‖, which becomes vacant again:

$$HgCl_2(g) \overset{K=k_{ads}/k_{des}}{\Longleftrightarrow} \text{‖–}HgCl_2 \overset{R}{\rightarrow} \text{product(s)} + \text{‖} \quad (8)$$

where K in the above equation is referred to as the Langmuir constant. Deposition velocities and partitioning coefficients constitute an empirical framework for parameterizing heterogeneous atmospheric processes. A coefficient for absorptive partitioning of compound X onto existing aerosols, K_{gp}, was proposed as Pankow (2007):

$$K_{gp} = \frac{[X]_p / PM}{[X]_g} \quad (9)$$

where the index gp represents gas–particle partitioning; $[X]_p$ and $[X]_g$ represent the mass concentrations of compound X in the gas phase and particle phase, respectively, in a unit volume of air; and PM represents the total mass concentration of the particles.

4.3 Aqueous redox equilibria

The Gibbs free energy change (ΔG) presented previously is related to the electrode potential (E) as the equation:

$$\Delta G = -nFE \quad (10)$$

where n is the number of moles of electrons transferred in the reaction and F is the Faraday constant (96485 C mol^{-1}). The standard potentials for the mercury-mercurous-mercuric free cation couples are as follows:

$Hg_2^{2+}(aq) + 2\,e^- \rightleftarrows 2\,Hg^0(aq)$ $E^0 = 0.789$ V (Rxn 1)

$2\,Hg^{2+}(aq) + 2\,e^- \rightleftarrows Hg_2^{2+}(aq)$ $E^0 = 0.908$ V (Rxn 2)

$Hg^{2+}(aq) + 2\,e^- \rightleftarrows Hg^0(aq)$ $E^0 = 0.854$ V (Rxn 3)

These positive potentials indicate that the reduction of Hg^{2+}/Hg_2^{2+} to Hg is favored under standard conditions. It is also evident that Hg^0 can be oxidized to $Hg_2^{2+}(aq)$ rather than to $Hg^{2+}(aq)$ only by agents with potentials ranging from –0.79 to –0.85 V. None of the common oxidizing agents meet this narrow potential range. Therefore, in excess of the oxidizing agent, Hg^0 is completely oxidized to $Hg^{2+}(aq)$. Only when the excess Hg^0 exceeds 50% does oxidation lead to $Hg_2^{2+}(aq)$. Ligation and hydrolysis have a major impact on standard potentials, including those listed in **Rxn 1–3**. For example, $Hg(OH)_2 + 2\,e^- \rightleftarrows Hg^0 + 2\,HO^-$, analogous to **Rxn 3**, has an E^0 value of 0.206 V.

tog bort: $([X]_{g,\infty} - \frac{[X]_{surf}}{H})$
tog bort: 4
tog bort: ,∞… ∞ and surf represent the gas bulk and surf… [114]
formaterade … [115]
tog bort: 5
tog bort: 5
formaterade … [116]
formaterade … [117]
formaterade … [118]
tog bort: while
formaterade … [119]
tog bort:
formaterade … [120]
formaterade … [121]
tog bort: the
formaterade … [122]
tog bort: on
formaterade … [123]
tog bort: 6
tog bort: so…hus far, $HgCl_2$, follows a Hinselwood- … [124]
formaterade … [125]
tog bort: Pankow, 2007
formaterade … [126]
tog bort: can…then react as a surface complex with a re… [127]
tog bort: 7
tog bort: are…onstitute an older…empirical framework f… [128]
tog bort: 8
formaterade … [129]
tog bort: is the
formaterade … [130]
tog bort: -
formaterade … [131]
tog bort: ,
formaterade … [132]
tog bort: are
formaterade … [133]
tog bort: ,
formaterade … [134]
tog bort: is
formaterade … [135]
Formaterat … [136]
tog bort: by
formaterade … [137]
tog bort: formula
tog bort: 9
Formaterad tabell … [138]
tog bort: potential indicates
formaterade … [139]
tog bort: potential
tog bort: of …g^0 exceeds 50% does the …xidation leads … [140]
formaterade … [141]
tog bort: –
formaterade … [142]

4.4 Chemical properties of aqueous $Hg^{I,II}$

The Hg^{2+} aqua ion, $[Hg(H_2O)_6]^{2+}$, exists only in distinctly acidic aqueous solutions containing a weakly coordinating anion (e.g., ClO_4^-). It readily undergoes hydrolysis at pH > 1 (log β_{10} $[Hg(OH)]^+$ = 10.3, Powell et al., 2005). Owing to its size and stable electron configuration, Hg^{2+}(aq) can be easily polarized by ligands and, therefore, has the potential to form strong covalent bonds. This property allows Hg^{2+}(aq) to interact with organic C to readily form Hg–C bonds through mercury–hydrogen substitution (*mercuration*), addition (*oxy-* and *amino-mercuration, etc.),* and decarboxylation reactions. An example is aniline, which forms a covalent complex with Hg^{2+} readily in aqueous solution at room temperature:

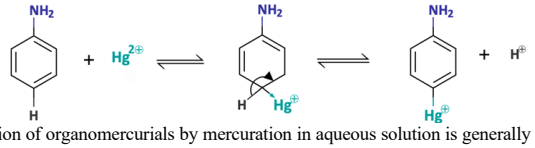

(Rxn 4)

The formation of organomercurials by mercuration in aqueous solution is generally slow because of the reduced electrophilicity of Hg^{2+} caused by hydrolysis of the metal center. However, the presence of a polar solvent has little influence on other processes of organomercurial formation, such as decarboxylation. Therefore, abiotic Hg methylation can occur in aqueous solutions with the assistance of, e.g., light carboxylic acids (Deacon et al., 1986). In the case of keto-enolic organic compounds such as acetylacetone (R = H) and malonate (R = OH), the mercuric ion can, in principle, adopt a C-bond, an O-bond or a chelate structure:

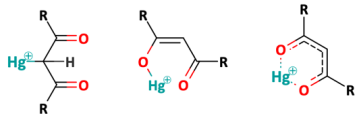

Highly toxic CH_3Hg^+ ($MMHg^+$) species are by far the most abundant organic Hg in the environment and are formed from inorganic Hg^{II}, mainly by the action of Fe^{III} and SO_4^{2-} reducing bacteria. In addition to monomethylation, permethylation can also occur anaerobically (Sommar et al., 1999). $(CH_3)_2Hg$ (DMHg) is detected mainly in deep-sea waters, but by upwelling waters (Conaway et al., 2009), it may reach the mixed layer, where gas exchange with the atmosphere can occur. DMHg has also been detected in landfills (Lindberg et al., 2005; Feldmann et al., 1994), sewage gas (Sommar et al., 1999), flood plains (Wallschläger et al., 1995) and rice paddies (Wang et al., 2019c). The binding affinity of Hg^{2+} to ligands is often qualitatively rationalized by Lewis acid–base theory, with the message that mercurials (type B metals) prefer soft ligands such as heavier halides and hydrochalcogenides (e.g., I^- and SH^-, respectively) to hard ones (e.g., OH^- and F^-). In fact, Hg^{2+} is the softest metal ion that acts as a Lewis acid. The preference for low coordination numbers (≤ 4, typically linear two-coordinate) in Hg^{II} complexes is related to the fact that relativistic effects come into play for the heaviest elements (Tossell and Vaughan, 1981). The interactions between Hg^{2+}(aq) and inorganic ligands (**Table 1**) and low-molecular-weight organics (**Table 2**) are given as stability constants. The tables show that Hg^{2+} also binds strongly to nitrogenous bases. Interactions with inorganic compounds, such as ammonia, are extensive and complex (Breitinger and Brodersen, 1970). For organic nitrogen ligands, there is a parallel between the basicity of the ligand and the stability of the Hg-ligand complex (e.g., guanidine). Heterocyclic nitrogen compounds, such as histidine, also form strong complexes with mercuric ions. The hard–soft acid–base principle applies only to highly polar solvents, such as aqueous solutions, as a result of solvation (hydrolysis) effects (Riccardi et al., 2013). In the gaseous phase, an inverse relationship prevails (Riccardi et al., 2013) and can be illustrated by the fact that gaseous $Hg(OH)_2$ is a stable molecule, whereas in aqueous solution, Hg^{2+} and 2 OH^- can form the intermediate molecule $Hg(OH)_2$ (Yang et al., 2020b), which eliminates H_2O and precipitates solid HgO. Therefore, solid $Hg(OH)_2$ is not known (Wang and Andrews, 2005). Furthermore, in the aqueous phase, the univalent state (mercurous species) is represented by the metal-metal bound ion Hg_2^{2+}(aq), which is ordinarily stable. Like Hg^{2+}(aq), Hg_2^{2+}(aq) is a soft Lewis acid.

Hg-ligand complexation is ubiquitous in the environment. This process involves a significant energy shift due to solvation effects, which results in a reduction in the number of solvating water molecules and an increase in the interaction between ligands/anions in the complexes and water. Unlike the dimer cation, the discrete $Hg^{\bullet+}$ cation is paramagnetic and was detected for the first time via

formaterade ... [143]
formaterade ... [144]
formaterade ... [145]
tog bort: K ($[Hg(OH)]^+$
formaterade ... [146]
formaterade ... [147]
formaterade ... [149]
formaterade ... [148]
tog bort: readily
formaterade ... [150]
formaterade ... [151]
tog bort: Depending on
formaterade ... [152]
tog bort: -
formaterade ... [153]
tog bort: form
formaterade ... [154]
tog bort: due to
tog bort: center's hydrolysis
tog bort: solution
tog bort: Besides
tog bort:
tog bort: via
tog bort: landfill
tog bort:) and
tog bort: Lewis'
tog bort: -
tog bort: metal
tog bort: .
tog bort: .
tog bort: of all
tog bort: ions acting
tog bort: Lewis's acids.
tog bort: coordination
tog bort: interaction
tog bort:
tog bort:
tog bort: The interaction
tog bort: ones
tog bort: is
tog bort: .
tog bort: the
tog bort: ion
tog bort: -
tog bort: -
tog bort: in
tog bort: solution,
tog bort:) that
Formaterat ... [155]
tog bort: result
tog bort: As opposed to
tog bort: using

electron spin resonance (Symons and Yandell, 1971). Free $Hg^{\bullet+}$ is a highly potent reducing agent with a one-electron reduction potential, $E^0(Hg^{2+}/Hg^{\bullet+})$, estimated to be well below -2.0 V (Gårdfeldt and Jonsson, 2003). However, hydrolyzed or ligated forms are less reactive (Gårdfeldt and Jonsson, 2003; Kozin and Hansen, 2013). The dissociation $Hg_2^{2+}(aq) \rightleftarrows 2\ Hg^{\bullet+}(aq)$ is considerably less significant than the disproportionation $Hg_2^{2+}(aq) \rightleftarrows Hg^0(aq) + Hg^{2+}(aq)$, with a conservative upper bound for the ratio $[Hg^{\bullet+}]/[Hg_2^{2+}]$ of 10^{-7} (Moser and Voigt, 1957). Free cation acidity decreases in the order of Hg^{2+} (pK 3.4), Hg_2^{2+} (pK 4.9) and $Hg^{\bullet+}$ (pK 5.1). $Hg_2^{2+}(aq) \rightleftarrows Hg^0(aq) + Hg^{2+}(aq)$ has an equilibrium constant of 5.5×10^{-9} M (Moser and Voigt, 1957), which indicates that a solution of initially only Hg_2^{2+} in pure water will contain only a single percent Hg^{2+} in the absence of ligands that form complexes with Hg^{2+}. However, in the presence of ligands that form complexes with Hg^{2+}, disproportionation is rapid, and Hg_2^{2+} is consumed. The same applies when $Hg^0(aq)$ is removed from the solution, e.g., by a gas stream. Hg_2^{2+} can be a major speciation component in heavily polluted waters (Fang et al., 2024) but is insignificant in the atmosphere.

4.5. Chemical equilibria data

For a general complex equilibrium with Hg^{2+} and the ligand L, $Hg^{2+} + q\ L + r\ H_2O \rightleftarrows [HgL_q(OH)_r]^{(2-r)+} + r\ H^+$, a stability constant β_{qr} is defined as $[\{HgL_q(OH)_r\}^{(2-r)+}][H^+]^r/([Hg^{2+}][L]^q)$. When the complex is not hydrolyzed, β_{qr} is reduced to $\beta_q = [\{HgL_q\}^{2+}]/([Hg^{2+}][L]^q)$. For the equilibrium obtained by adding a ligand (L) to a metal complex in a stepwise manner, K_q is used, which is related to β_q by $\prod_{i=1}^{q} K_q$. **Tables 1** and **2** present the equilibrium constants for Hg^{2+} associated with a range of inorganic and organic natural ligands, respectively, without being comprehensive. Quantitative details are available through the open-access AQUAMER database and web server dedicated to Hg, which provides direct speciation results by combining web-based interfaces with a speciation calculator, thermodynamic constant databases, and a computational chemistry toolbox for input to other software to estimate missing constants. (Lian et al., 2020).

4.6 Speciation of Hg^{II} in atmospheric waters

Hg^{II} speciation in atmospheric waters such as clouds and fog is governed by interactions with inorganic nucleophiles, low-molecular-weight organics (LMWO), and high-molecular-weight dissolved organic matter (DOM). The identified LMWOs typically make up a smaller mass fraction of the DOM in ambient cloud and fog droplets. Despite its limited abundance (0.5–3% in freshwater), sulfurized DOM exerts control over Hg cycling in terrestrial aquatic systems by forming predominantly strong HgL (logK ~21.9–23.6) and HgL_2 (logK ~30.1–31.6) complexes (Dong et al., 2011), where L represents functional groups with reduced sulfur. Although sulfur-containing DOM (with the elemental compositions of CHSO and CHNSO) is also relatively ubiquitous in atmospheric organic matter (AOM), sulfur is present mainly in hexavalent form, with reduced sulfur being rare (Zhao et al., 2013; Bianco et al., 2018; Jiang et al., 2022). In contrast to sub-zero valence S, which is not relevant in this context, conjugate bases of strong oxo acids that are common in AOM, such as organic nitrates and sulfates, form only weak complexes with Hg^{II}. Therefore, the application of speciation by equilibrium modeling on a geospherical basis to assess the atmospheric interaction between atmospheric DOM and Hg^{II}, as in some studies (Li et al., 2018; Zhen et al., 2023), is questionable. Bittrich et al. (2011) used pH, a confined set of inorganic ions (NH_4^+, NO_3^-, SO_4^{2-} and Cl^-), and LMWO acids to observe dissolved Hg^{II} in a study of cloud and fog water. Strongly dependent on pH, at < 5, even moderate Cl^- levels can control speciation ($HgCl_2$), whereas in more alkaline waters (e.g., influenced by NH_3), speciation is represented by $Hg(OH)_2$, $Hg(OH)Cl$, and to some extent $[Hg(NH_3)_2]^{2+}$. A more realistic approach is to include DOM in speciation. In this regard, Yang et al. employed Hg^{II} complexation with fulvic acids under conditions of binding to mainly O-donors (1:2 complexes with $\log\beta_{20}$ = 5.6, Haitzer et al., 2002) as surrogates for AOM interaction, which, when applied, was found to dominate in the Hg^{II} speciation of rainwater samples in rural and urban France (Yang et al., 2019). Studies of cloud water in eastern China revealed a marked change in acidity and other chemical compositions in the post-2008 period, where Hg^{II}, although the concentration was unchanged over time, in the former acidic environment was mainly bound by DOM (~79%) (Li et al., 2018), and in the latter more neutral environment, was more homogeneously distributed in addition to DOM among hydrolyzed and halide (X = Cl, Br)-bound species ($Hg(OH)_2$, HOHgX, and HgX_2; Zhen et al., 2023). In conclusion, until the complexation of Hg^{II} with AOM is well understood, there is considerable uncertainty regarding the partitioning of aquatic Hg^{II} between stable and reduction-labile complexes in the photic atmosphere.

tog bort: The free
tog bort: x
tog bort:),… but is insignificant in the atmosphere. … [156]
formaterade … [157]
formaterade … [158]
formaterade: Teckenfärg: Blå, Kondenserad med 0,2 pt
tog bort: $[M_pL_q(OH)_r][H^+]^r/([M]^p[L]^q)$.
formaterade … [159]
formaterade … [160]
formaterade … [161]
tog bort: $[ML_q]/([M][L]^q)$
formaterade … [162]
formaterade: Kondenserad med 0,2 pt
tog bort: purporting to be
tog bort: The reader's attention should also be drawn to
formaterade: Kondenserad med 0,2 pt
formaterade: Kondenserad med 0,2 pt
tog bort: to
formaterade: Kondenserad med 0,2 pt
tog bort: constants
formaterade: Kondenserad med 0,2 pt
Formaterat: Radavstånd: Flera 1,15 li
tog bort: The speciation
Formaterat: Radavstånd: Flera 1,45 li
tog bort: interaction…nteractions with inorganic nucleophiles, low -molecular …weight organics (LMWO), and high …molecular -weight dissolved organic matter (DOM). Identified…he identified LMWOs typically make up a smaller mass fraction of the DOM in ambient cloud and fog droplets. Despite its limited abundance (0.5 - –3% in freshwater), sulfurized DOM exerts control over Hg cycling in terrestrial aquatic systems by forming predominantly strong HgL (logK ~21.9 – …23.6) and HgL_2 (logK ~30.1–31.6) complexes (Dong et al., 2011), where L represents functional groups w… [163]
formaterade … [164]
tog bort: a …are occurrence…(Zhao et al., 2013; Bianco … [165]
formaterade: Teckenfärg: Blå
tog bort: thus
formaterade: Teckenfärg: Blå
tog bort: universal…elevant in this context, conjugate ba… [166]
tog bort: speciate observations of
tog bort: ….., influenced by NH_3)…, speciation is … [167]
tog bort: the
formaterade: Teckenfärg: Blå
tog bort: logK
formaterade: Teckenfärg: Blå
tog bort: . It
formaterade: Teckenfärg: Blå
tog bort: show…evealed a remarkable…arked change in … [168]
formaterade: Teckenfärg: Blå
tog bort: it is clear that as long as
formaterade: Teckenfärg: Blå
tog bort: less constrained
formaterade: Teckenfärg: Blå

Table 1. Hg^{2+} – inorganic ligand complexes. Omitted in the table are, e.g., interactions with reduced sulfur (HS–, R–S–), which can be found in, e.g., Skyllberg (2011).

Ligand/ion		$\log \beta_{10}$ / pKa_1	$\log \beta_{20}$ / pKa_2	$\log \beta_{30}$	$\log \beta_{40}$	$\log \beta_{11}$	Reference
Elemental mercury	Hg^0	8.46					Hietanen and Sillén, 1956
Hydroxide	HO^-	10.3	21.4				Powell et al., 2005
Fluoride	F^-	1.6					Martell and Smith, 1976
		3.17					
Chloride	Cl^-	7.3	14.0	14.9	15.5	18.0	Powell et al., 2005
		< 0					
Bromide	Br^-	9.0	17.1	19.4	21.0		Martell and Smith, 1976
		< 0					
Iodide	I^-	12.87	23.82	27.6	29.8		Martell and Smith, 1976
		<0					
Ammonia/amide	NH_3/$–NH_2$	8.8	17.4	18.4	19.1		Martell and Smith, 1976
		9.25					
Carbonate	CO_3^{2-}	10.7	14.5/15.7			5.47[2]	Puigdomenech, 2013
		6.35	10.33				
Cyanide	$C{\equiv}N^-$	17.0	32.8	36.3	39.0		Martell and Smith, 1976
		9.21					
Thiocyanate	$N{\equiv}CS^-$	9.08	17.3	20.0	21.8		Martell and Smith, 1976
		0.9					
Selenocyanate	$N{\equiv}CSe^-$	—	—	26.4	28.9		Martell and Smith, 1976
		—	—				
Sulfite	SO_3^{2-}	13.3	24.1	26.0			Martell and Smith, 1976; van Loon et al., 2001
		1.81	6.97				
Selenite	SeO_3^{2-}		12.5				Martell and Smith, 1976
		2.35	7.94				
Sulfate	SO_4^{2-}	1.34	2.4				Martell and Smith, 1976
		< 0	1.99				
Thiosulfate	$S_2O_3^{2-}$		29.23	30.6			Martell and Smith, 1976
		1.6					
Selenosulfate	$SeSO_3^{2-}$		36.8				Martell and Smith, 1976
Selenide	Se^{2-}	51.2[3]	61.0[4]			52.8[5]	Foti et al., 2009
		3.89	15.0				
Nitrate	NO_3^-	0.11					Martell and Smith, 1976
		< 0					

Table 2. Hg^{2+} –organic ligand complexes.

Ligand/ion	Structure formula	$\log \beta_{10}$ / pKa_1	$\log \beta_{20}$ / pKa_2	$\log \beta_{30}$	$\log \beta_{40}$	$\log \beta_{11}$	Reference
Oxalate		9.66/10.5					Bartels-Rausch et al., 2011; Martell and Smith, 1982
		1.25	4.27				
Formate		3.66/3.55	7.10/7.35				Martell and Smith, 1982
		3.55	—				
Acetate		3.74/4.3	7.01/8.7				Martell and Smith, 1982
		4.5	—				
Pivalate		5.92					Martell and Smith, 1977
		5.03	—				
Monochloroacetate		2.95.	5.61				Martell and Smith, 1977
		2.87	—				
Trichloroacetate		3.08					Martell and Smith, 1977
		0.66	—				
Glycolate		3.6	7.05				Martell and Smith, 1982
		3.83					
Mercaptoacetate		34.2	42.6			36.3	Cardiano et al., 2011

[2] $Hg^{2+} + HCO_3^- \rightleftarrows (HgHCO_3)^+$
[3] $Hg^{2+} + HO^- + HSe^- \rightleftarrows HgSe$
[4] $Hg^{2+} + 2\,HO^- + 2\,HSe^- \rightleftarrows HgSe_2^{2-}$
[5] $Hg^{2+} + HO^- + 2\,HS^- \rightleftarrows HgHS_2^-$

tog bort: is
Formaterat ... [170]
tog bort: –) that
formaterade ... [169]
formaterade ... [171]
formaterade ... [172]
tog bort: .
formaterade ... [173]
formaterade ... [174]
formaterade ... [175]
formaterade ... [176]
formaterade ... [177]
formaterade ... [178]
formaterade ... [179]
formaterade ... [180]
formaterade ... [181]
formaterade ... [182]
formaterade ... [183]
formaterade ... [184]
formaterade ... [185]
formaterade ... [186]
formaterade ... [188]
formaterade ... [189]
formaterade ... [187]
formaterade ... [190]
formaterade ... [191]
formaterade ... [192]
formaterade ... [193]
formaterade ... [194]
formaterade ... [195]
formaterade ... [196]
formaterade ... [197]
Formaterat ... [198]
formaterade ... [199]
formaterade ... [200]
formaterade ... [201]
formaterade ... [202]
tog bort:
tog bort:
formaterade ... [203]
tog bort:
formaterade ... [204]
tog bort:
formaterade ... [205]
tog bort:
formaterade ... [206]
tog bort:
formaterade ... [207]
tog bort:
Formaterat ... [208]
formaterade ... [209]
formaterade ... [210]
formaterade ... [211]
formaterade ... [212]
formaterade ... [213]
formaterade ... [214]

		3.43	10.1				
Metoxyacetate		3.54	6.91				Martell and Smith, 1982
		3.57					
Acetylacetonate		12.9	20.1				van der Linden and Beers, 1975
		9.00					
Phtalate		4.9					Martell and Smith, 1977
		2.7	4.9				
D-tartarate		5.4				15.5	Kornev and Kardapol'tsev, 2008
		2.8	3.9				
Thiomalate		9.94	18.07				Martell and Smith, 1977
		3.3	4.6				
Iminodiacetate	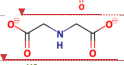	13.1	20.2				van der Linden and Beers, 1975
		2.65					
Dimercaprol (BAL)		25.7	34.3				Martell and Smith, 1982
		8.76	10.78				
Citrate		4.1	6.1	11.1	15.0	17.8	van der Linden and Beers, 1975; Kornev and Kardapol'tsev, 2008
		3.0	4.1				
Ascorbate	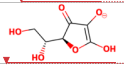	4.2	8.7				Kleszczewska, 1999
		4.1					
Urea		2.1					Martell and Smith, 1977
Thiourea		11.4	21.7	24.6	26.4		Martell and Smith, 1982
Selenourea			24.0	30.2	32.9		Martell and Smith, 1977
Semicarbazide			11.6	15.2			Martell and Smith, 1977
		3.53					
Thio-semicarbazide			22.4	24.8	25.8		Martell and Smith, 1977
		1.6					
Seleno-semicarbazide			26.9	30.4	32.4		Martell and Smith, 1977
		0.8					
Guanidine			24.5				Martell and Smith, 1982
		13.5					
Ethylenediamine (en)		13.85	23.3			10.2	Martell and Smith, 1982
		9.79	16.82				
Alanine		12.4	19.6				van der Linden and Beers, 1974
		2.50	9.80				
Arginine	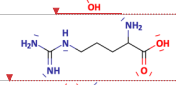	11.5	18.8				van der Linden and Beers, 1974
		2.19	9.21				
Asparagine	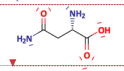	11.4	18.6				van der Linden and Beers, 1974
		2.14	8.85				
Glycine		12.2	19.2	18.82	31.42	6.98	van der Linden and Beers, 1974
		2.44	9.68				
Glutamine	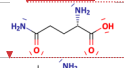	11.5	18.7				van der Linden and Beers, 1974
		2.27	9.16				
Leucine		11.9	19.5				van der Linden and Beers, 1974
		2.37	9.62				
Iso-leucine		12.4	19.6				van der Linden and Beers, 1974
		2.40	9.66				
Phenylalanine		12.4	19.6				

tog bort:

tog bort:

tog bort:

tog bort:

tog bort:

tog bort:

tog bort:

tog bort:

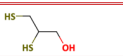

tog bort:

tog bort: (Cit^{3-})

tog bort:

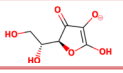

tog bort:

tog bort:

tog bort:

tog bort:

tog bort:

tog bort:

tog bort:

tog bort:

tog bort:

tog bort:

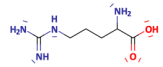

tog bort:

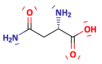

tog bort:

tog bort: (Gly)

tog bort:

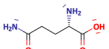

tog bort:

tog bort:

	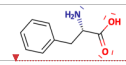	2.21	9.18				van der Linden and Beers, 1974
Proline	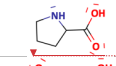	12.2	20.1				van der Linden and Beers, 1974
		2.04	10.52				
Serine	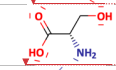	11.7	19.1				van der Linden and Beers, 1974
		2.21	9.13				
Threonine	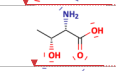	11.7	18.7				van der Linden and Beers, 1974
		2.24	8.86				
Tryptophan	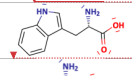	13.9	21.4				van der Linden and Beers, 1974
		2.39	9.43				
Valine	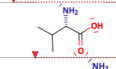	11.7	18.7				van der Linden and Beers, 1974
		2.38	9.59				
Lysine	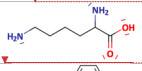	11.3	18.7				van der Linden and Beers, 1974
		2.18	9.18	10.72			
Tyrosine	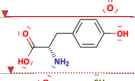	12.3	19.5				van der Linden and Beers, 1974
		2.34	9.11	10.16			
Cysteine	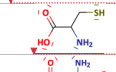		39.4				van der Linden and Beers, 1974
		1.96	8.48	10.55			
Aspartic acid	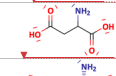	14.86	19.15		33.1	7.4	van der Linden and Beers, 1975; Kornev and Kardapol'tsev, 2008
		1.94	3.70	9.62			
Glutamic acid	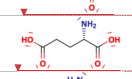	12.8	19.2				van der Linden and Beers, 1974
		2.39	4.21	9.54			
Histidine	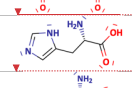	15.75	20.48		34.4	7.4	Martell and Smith, 1982
		1.79	6.00	9.16			
Methionine	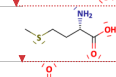	12.8	19.5				van der Linden and Beers, 1974
		2.26	9.13				
Succinic acid Succinate (suc^{2-})	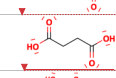	9.46	14.22			3.3	Martell and Smith, 1982
		5.20	9.17				
1,2,3,4-butane tetracarboxylic acid (btc^{4-})	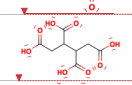	11.61	17.14		21.5	4.8	Martell and Smith, 1982
		6.42	11.67				
1,2,3,4,5,6-benzene hexacarboxylic acid (mlt^{6-})	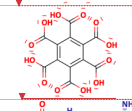	18.4	22.6		25.6	14.3	Martell and Smith, 1982
		6.55	12.11				
Glutathione (H_2GsH)	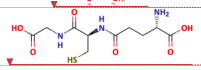	26.0	33.4			32.4	Smith et al., 2004
		2.12	3.53	8.66	9.12		
Penicillamine		18.9	25.0				Strand et al., 1983
		1.8	7.83				

4.7 Chemical reaction data

The subsequent two principal sections address the chemical redox reactions in the gaseous phase (**Section 5**) and in the aqueous phase (**Section 6**). **Table 3** summarizes the gas-phase reactions, along with the rate coefficients considered most accurate and the corresponding reaction enthalpies. The reaction numbers are designated with the prefix G (G1, G2, etc.). The aqueous-phase reaction numbers are designated with prefix W and are listed in **Table 4** with the corresponding rate coefficients. Notably, several chemical reactions that are not labeled with G or W and are not assigned to **Tables 3** and **4** appear in the text. This is particularly the case for heterogeneous (multiphase) processes (**Section 7**), such as reactive uptake and reduction on surfaces, which consequently have no prefix and follow sequential numbering throughout the document.

tog bort: 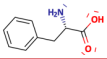
tog bort:
tog bort:
tog bort:
tog bort: 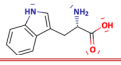
tog bort:
tog bort: 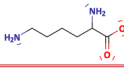
tog bort: 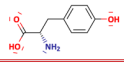
tog bort:
tog bort:
tog bort: 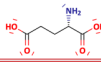
tog bort: 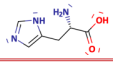
tog bort: 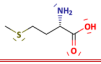
tog bort: 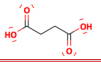
tog bort: 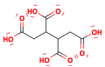
tog bort: 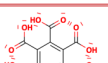
tog bort: 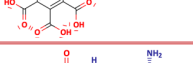
tog bort:
tog bort:
tog bort: ¶
tog bort: reactions
formaterade: Kondenserad med 0,1 pt
tog bort:), respectively.
formaterade ... [215]
tog bort: corresponding
formaterade ... [216]
tog bort:
formaterade: Kondenserad med 0,1 pt
tog bort: the
formaterade ... [217]
tog bort: It should also be noted that
formaterade: Kondenserad med 0,1 pt
tog bort: appear in the text
formaterade: Kondenserad med 0,1 pt
tog bort: .
formaterade: Kondenserad med 0,1 pt
tog bort: multi-phase
formaterade: Kondenserad med 0,1 pt
tog bort: the
formaterade: Kondenserad med 0,1 pt

5 Gas-phase atmospheric Hg chemistry

5.1 Inorganic species

5.1.1 Initial reactions of ground-state Hg^0

The homogeneous gas-phase oxidation of Hg^0 in the electronic ground state is limited to a few reactive species produced photolytically. In the atmosphere, multi-step reactions involving both Hg^I and Hg^{II} species are crucial for Hg transformation. Atmospheric oxidation of Hg^0 occurs largely in the gas phase, whereas the rates of aqueous phase reactions in deliquescent aerosols are relatively slower on a unit air volume basis and are inherently limited by the low water solubility of Hg^0. The oxidation of Hg^0 vapor by closed-shell molecules, such as halogenation chemistry with reference to the gas phase, has been studied in the laboratory at various temperatures (Hall, 1992; Qu et al., 2009; Chi et al., 2009; Ariya et al., 2002; Sumner et al., 2005; Raofie and Ariya, 2004; Raofie et al., 2008; Wilcox, 2009) since Ogg et al. (1936). Direct oxidation by free halogens (X_2) via the insertion reaction $Hg + X_2 \rightarrow XHg^{II}X$ is highly exothermic but very slow under atmospheric conditions due to large energy barriers (Auzmendi-Murua et al., 2014), whereas the abstraction $Hg + X_2 \rightarrow {}^{\bullet}Hg^{I}X + X^{\bullet}$ proceeds at significant rates only at high temperatures (Niksa et al., 2001). Thus, free halogen chemistry is important for the conversion of Hg in flue gas from power generation systems (Wilcox, 2009), such as coal-fired (CFPP) systems, but not in the atmosphere. The same applies to the $Hg + NO_2$ reaction, which is barrierless and whose pathway to $Hg^{II}(ONO)_2$ shows a negative temperature dependence (Li et al., 2022c). However, reactions that are important only in combustion and flue gas cleaning systems are outside the scope of this review.

Hg + XO (X = O_2, NO_2 and Br)

Although oxidation of Hg^0 vapor by the common atmospheric oxidants O_3 (Sumner et al., 2005; Hall, 1995; Pal and Ariya, 2004b; Snider et al., 2008), $BrO^{\bullet}$ (Raofie and Ariya, 2004; Spicer et al., 2002) and $NO_3^{\bullet}$ (Sommar et al., 1997; Sumner et al., 2005) has been observed in the laboratory, the identity and phase of the product(s) are in doubt. Laboratory studies of gas-phase oxidation of ppb levels of Hg^0 (the atmospheric level is sub-ppt) have revealed product particles in the accumulation mode, suggesting that gas-to-particle conversion takes place (Raofie and Ariya, 2004; Sun et al., 2016). These data attributed to the gas phase are almost certainly compromised by complex kinetics, including reactions at the reactor wall (Hynes et al., 2009). In all cases, gas-phase oxidation pathways leading to HgO by O atom transfer are endothermic (**Rxn G5–G7, Table 3**). Furthermore, the measured pre-exponential factors for the Hg–O_3 reaction, ~ 10^{-16}–10^{-18} cm^3 $molecule^{-1}$ s^{-1} (Hall, 1995; Pal and Ariya, 2004b), are much smaller than expected for simple O atom transfer (Calvert and Lindberg, 2005). Alternative O_3 oxidation via a weakly bound (~16 kJ mol^{-1}) adduct, HgO_3, lacks exothermic dissociation pathways (i.e., $HgO + O_2$, **Rxn G5a**) and is therefore unlikely to occur in the atmosphere. However, in laboratory experiments, HgO_3 can conceivably diffuse to surfaces and be deposited as solid HgO possibly via oligomerization (Tossell, 2006). Recombination of Hg^0 with $NO_3^{\bullet}$ results in weakly bound ${}^{\bullet}Hg^{I}NO_3$ (~27 kJ mol^{-1}), which dissociates in the lower troposphere before oxidation to Hg^{II} species of the type $O_2NOHgO^{\bullet}$ or O_2NOHgY can occur (Edirappulige et al., 2024). Abstractions (e.g., $Hg + BrO^{\bullet} \rightarrow HgO + Br^{\bullet}$ or $Hg + BrO^{\bullet} \rightarrow {}^{\bullet}Hg^{I}Br + O$, **Rxn G7a & b**) are endothermic, whereas direct insertion reactions (e.g., $Hg + BrO^{\bullet} \rightarrow BrHg^{II}O^{\bullet}$, **Rxn G7c**) are exothermic (–84 kJ mol^{-1}, Shepler 2006) but affected by large barriers (170 kJ mol^{-1}) and are therefore unlikely to proceed (Balabanov and Peterson, 2003). The remaining exit channels, namely the recombination of Hg and $BrO^{\bullet}$ (**Rxn G7d**), leading to the formation of the geometric isomers of $BrHg^{II}O^{\bullet}$ (${}^{\bullet}Hg^{I}BrO$ and ${}^{\bullet}Hg^{I}OBr$), are also inconceivable, as these adducts are thought to be very weakly bound (Shepler, 2006). Stable Hg^I species of this type have been reported, suggesting that $BrO^{\bullet}$ is important during AMDEs (Raofie and Ariya, 2004). However, other field (Wang et al., 2019a) and model (Xie et al., 2008; Ahmed et al., 2023) studies have shown that the synchronous disappearance of Hg^0 and O_3 during AMDEs can best

Formaterat ... [218]
Formaterat ... [219]
tog bort:
formaterade ... [223]
tog bort: formed by the action of actinic light
formaterade ... [220]
Formaterat ... [221]
formaterade ... [222]
tog bort: of atmospheric importance
formaterade ... [224]
tog bort: transformations.
formaterade ... [225]
tog bort: Oxidation
formaterade ... [226]
tog bort: the
formaterade ... [227]
tog bort: of great importance
formaterade ... [228]
tog bort: the
formaterade ... [229]
tog bort: the
formaterade ... [230]
tog bort: type
formaterade ... [231]
tog bort: only
formaterade ... [232]
Formaterat ... [233]
formaterade ... [234]
Formaterat ... [235]
formaterade ... [236]
formaterade ... [237]
tog bort: observed
formaterade ... [238]
tog bort: –
formaterade ... [239]
tog bort: experimentally
formaterade ... [240]
tog bort: –
formaterade ... [241]
tog bort: very
formaterade ... [242]
tog bort: a
formaterade ... [243]
tog bort: but
formaterade ... [244]
formaterade ... [245]
tog bort: the
formaterade ... [246]
tog bort: 2023a
formaterade ... [247]
tog bort: is
formaterade ... [248]
tog bort:)
formaterade ... [249]
tog bort: in one laboratory
formaterade ... [250]
tog bort: studies both in the
formaterade ... [251]
tog bort: in the form of models
formaterade ... [252]
tog bort: show
formaterade ... [253]

be described solely as the action of Br atoms, with an upper limit for $k_{Hg + BrO}$ of 1×10^{-15} cm^3 molecule^{-1} s^{-1}, but that the reaction product $^{\bullet}Hg^{I}Br$ (**Fig. 2**) rapidly adds BrO$^{\bullet}$, presumably mainly to $BrHg^{II}OBr$, which is 117 kJ mol^{-1} more stable than the isomer $BrHg^{II}BrO$ (Jiao and Dibble, 2017a). Despite its thermal stability, $BrHg^{II}OBr$ is rapidly photolyzed (**Figs. 2** and **4**) and therefore does not constitute a significant component of the Hg^{II} pool following an AMDE.

Table 3. Atmospheric gas-phase reactions. Except where otherwise noted in the reference column, the thermodynamic data have been compiled from the following sources of information: CRC Handbook of Chemistry and Physics (Lide, 2008), Hepler and Olofsson (1975), Chemical Kinetics and Photochemical Data for Use in Atmospheric Studies (Burkholder et al., 2019), Guzman and Bozzelli (2019), Saiz-Lopez et al. (2020; 2022), Balabanov and Peterson (2003; 2004), and Shepler (2006). The photolysis frequencies are calculated via the global annual average photon flux in the troposphere.

ID	Elementary reaction	Rate coefficient[6]	ΔH_R (kJ mol^{-1})[7]	Reference	Remarks
Initial reactions of ground state Hg^0					
G1	$Hg + Br^{\bullet} \xrightarrow{M} BrHg^{\bullet}$	$1.46 \times 10^{-32} \times (T/298)^{-1.86} \times [M]$	–69	Donohoue et al., 2006	
G2	$Hg + Cl^{\bullet} \xrightarrow{M} ClHg^{\bullet}$	$2.2 \times 10^{-33} \times \exp(680/T) \times [M]$	–104	Donohoue et al., 2005	
G3	$Hg + HO^{\bullet} \xrightarrow{M} HOHg^{\bullet}$	$3.34 \times 10^{-33} \times \exp(43/T) \times [M]$	–60 to –30	Sommar et al., 2001; Pal and Ariya, 2004a; Dibble et al., 2020; Bauer et al., 2003	
G4	$Hg \xrightarrow{h\nu} Hg(^3P_1)$		471	Saiz-Lopez et al., 2022	Only significant in the stratosphere
G5	$Hg + O_3 \xrightarrow{M} HgO + O_2$		93	Hall, 1995; Pal and Ariya, 2004b; Hynes et al., 2009	Thermodynamically unfeasible or adducts weakly bound
G6	$Hg + NO_3^{\bullet} \rightarrow HgO + NO_2$		195	Sommar et al., 1997; Spicer et al., 2002; Edirappuligee et al., 2024	
G7	$Hg + BrO^{\bullet} \rightarrow HgO + Br^{\bullet}$; $\rightarrow BrHg^{\bullet} + O$; $\xrightarrow{M} BrHgO^{\bullet}$; $\xrightarrow{M} HgBrO$		219; 166; 114; –85	Shepler, 2006; Raofie and Ariya, 2004	
G8	$Hg + ClOO^{\bullet} \rightarrow ClHg^{\bullet} + O_2$		–80	Hynes et al., 2009	
Reactions of excited state Hg^0					
G9	$Hg(^3P_1) \rightarrow Hg + h\nu$	8.4×10^6		Kramida et al., 2023	Only significant in the stratosphere
G10	$Hg(^3P_1) + N_2 \rightarrow Hg(^3P_0) + N_2$	$5.1 \times 10^{-11} \times \exp(-701/T)$	–21	Callear and Shiundu, 1987	
G11	$Hg(^3P_0) + O_2 \rightarrow Hg + O_2(^3\Sigma_u^+)$	$1.8 \times 10^{-10} \times (T/300)^{0.167}$	–27	Callear, 1987	
G12a	$Hg(^3P_1) + O_2 \rightarrow Hg + O_2(^3\Sigma_u^+)$	$1.3 \times 10^{-10} \times (T/300)^{-0.29}$	–6	Saiz-Lopez et al., 2022	
G12b	$Hg(^3P_1) + O_2 \rightarrow HgO(^3\Pi) + O$	$1.7 \times 10^{-10} \times (T/300)^{0.53}$	–48		
G13	$Hg(^3P_1) + H_2O \rightarrow HOHg^{\bullet} + H^{\bullet}$		–37		
Hg^I & Hg^{II} bromine chemistry					
G14a	$BrHg^{\bullet} \xrightarrow{M} Hg + Br^{\bullet}$	$1.6 \times 10^{-9} \times \exp(-7801/T) \times [M]$	69	Saiz-Lopez et al., 2019; Dibble et al., 2012	
G14b	$BrHg^{\bullet} \xrightarrow{h\nu} Hg + Br^{\bullet}$	4.3×10^{-2}		Shah et al., 2021	
G15a	$BrHg^{\bullet} + Br^{\bullet} \rightarrow Hg + Br_2$	3.90×10^{-11}	–124	Balabanov et al., 2005	
G15b	$BrHg^{\bullet} + Br^{\bullet} \xrightarrow{M} HgBr_2$	$2.5 \times 10^{-10} \times (T/298)^{0.57}$	–301	Goodsite et al., 2004	
G16	$BrHg^{\bullet} + HO^{\bullet} \xrightarrow{M} HOHgBr$	$2.5 \times 10^{-10} \times (T/298)^{0.57}$	–314	Goodsite et al., 2004	
G17	$BrHg^{\bullet} + Cl^{\bullet} \xrightarrow{M} ClHgBr$	3.00×10^{-11}	–338	Shah et al., 2021	
G18	$BrHg^{\bullet} + NO \rightarrow Hg + BrNO$	$7.0^{+1.2}_{-0.9} \times 10^{-12}$	–56	Wu et al., 2022	

[6] The basics of gas phase kinetics have been introduced in Section 4.1. Unimolecular rate coefficients are in s^{-1} (photolysis frequencies refer to excitation energies at lambda >290 nm calculated according to $\int \phi(\lambda, T) \cdot \sigma(\lambda, T) \cdot F(\lambda) d\lambda$, where ϕ is the quantum yield (≤ 1), σ is the absorption cross section (cm^2 molecule^{-1}), F is the photon flux (photons cm^{-2} s^{-1}), λ is the wavelength and T is absolute temperature), bimolecular reaction rate coefficients are in cm^3 molecule^{-1} s^{-1} (expressed as a rate constant or as a coefficient with an Arrhenius or other type of temperature dependence) and three-body reactions according to **Eq. 2**, i.e., $k = \frac{k_0[M]}{1 + k_0[M]/k_\infty} F_c^{\left[1 + \left[\log_{10} k_0[M]/k_\infty\right]^2\right]^{-1}}$ are in cm^6 molecule^{-2} s^{-1} (where [M] is the number density of air molecules, k_0 (cm^3 molecule^{-1} s^{-1}) is the low-pressure limiting rate coefficient, k_∞ (cm^6 molecule^{-2} s^{-1}) is the high-pressure limiting rate coefficient. The temperature dependence of k_0 and k_∞ is expressed with **Eq. 3**.

[7] Refers to the calculated enthalpy (0 K) or to the experimental ditto (298 K).

tog bort: x
formaterade: Inte Expanderad med / Kondenserad med
tog bort:),
formaterade: Inte Expanderad med / Kondenserad med
formaterade: Kondenserad med 0,3 pt, Ligaturer: Standard
formaterade: Ligaturer: Standard
formaterade: Ligaturer: Standard
tog bort: 3.34
tog bort: Sommar et al., 2001; Pal and Ariya, 2004a; Dibble et al., 2020; Bauer et al., 2003
tog bort: HO•
tog bort: HOHg•
tog bort: 60 to –30
tog bort: 43
tog bort: Donohoue et al., 2005
tog bort: 2.2
tog bort: 104
tog bort: Cl•
tog bort: ClHg•
tog bort: 680
tog bort: Thermo-dynamically
tog bort: 2023a
tog bort: section 3.2
tog bort: J =
formaterade: Teckensnitt:Fet
tog bort: 1
tog bort: .
formaterade: Teckensnitt:Fet
tog bort: 2

G19	$BrHg^{\bullet} + O_2 \rightleftarrows BrHgOO^{\bullet}$	$1.4 \times 10^{-26} \times \exp(3650/T)$[8]	–30	Wu et al., 2022	
G20	$BrHg^{\bullet} + NO_2 \xrightarrow{M} BrHgONO$ $\longrightarrow Hg + BrNO_2$	$k_0 = (4.3 \pm 0.5) \times 10^{-30} \times (T/298)^{-(5.9\pm0.8)}$ $k_\infty = 1.2 \times 10^{-10} \times (T/298)^{-1.9}$ $F_C = 0.6$ 3.0×10^{-12}	–176 –45	Jiao and Dibble, 2017b; Wu et al., 2020	
G21	$BrHg^{\bullet} + HO_2^{\bullet} \xrightarrow{M} BrHgOOH$	$k_0 = 4.3 \times 10^{-30} \times (T/298)^{-5.9}$ $k_\infty = 6.9 \times 10^{-11} \times (T/298)^{-2.4}$ $F_C = 0.6$	–167	Jiao and Dibble, 2017b	
G22	$BrHg^{\bullet} + O_3 \longrightarrow BrHgO^{\bullet} + O_2$	$(7.5 \pm 0.6) \times 10^{-11}$	–140	Gómez Martín et al., 2022	
G23	$BrHg^{\bullet} + O \longrightarrow Hg + BrO^{\bullet}$	$(5.3 \pm 0.4) \times 10^{-11}$	–168	Gómez Martín et al., 2022	
G24	$BrHg^{II}O^{\bullet} + O \longrightarrow BrHg^{\bullet} + O_2$	$(9.1 \pm 0.6) \times 10^{-11}$	–252	Gómez Martín et al., 2022	
G25	$BrHg^{II}O^{\bullet} + O_3 \longrightarrow {}^{\bullet}Hg^{I}Br + O_2 + O_2$ $\longrightarrow BrHg^{II}OO^{\bullet} + O_2$	$< 5 \times 10^{-12}$	–143 –171	Gómez Martín et al., 2022	
G26	$BrHgO^{\bullet} + CH_4 \longrightarrow BrHgOH + CH_3^{\bullet}$	$4.1 \times 10^{-12} \times \exp(-856/T)$	–10	Lam et al., 2019a	
G27	$BrHgO^{\bullet} + CO \longrightarrow HgBr^{\bullet} + CO_2$	$6.0 \times 10^{-10} \times \exp(-550/T)$	–282	Khiri et al., 2020	
G28	$BrHgO^{\bullet} + HCHO \longrightarrow BrHgOH + CO + H^{\bullet}$	$(4.7 - 5.5) \times 10^{-11}$[9]	–109	Lam et al., 2019a	
G29	$BrHgO^{\bullet} + NO \xrightarrow{M} BrHgONO$	2.9×10^{-11}[10]	–226	Lam et al., 2019b	
G30	$BrHgO^{\bullet} + NO_2 \xrightarrow{M} BrHgONO_2$	1.7×10^{-11}[11]	–242	Lam et al., 2019a	
G31	$BrHgO^{\bullet} \xrightarrow{h\nu} 0.56\ HgO + 0.44\ Hg + Br^{\bullet} + 0.44\ O$	2.9×10^{-2}		Francés-Monerris et al., 2020	
G32	$HgBr_2 \xrightarrow{h\nu} 0.6\ BrHg^{\bullet} + 1.4\ Br^{\bullet} + 0.4\ Hg$	1.5×10^{-6}		Shah et al., 2021	
G33	$BrHgOH \xrightarrow{h\nu} 0.35\ HOHg^{\bullet} + 0.85\ Br^{\bullet} + 0.5\ Hg + 0.65\ HO^{\bullet} + 0.15\ BrHg^{\bullet}$	1.3×10^{-5}		Shah et al., 2021	
G34	$BrHgCl \xrightarrow{h\nu} 0.6\ BrHg^{\bullet} + Cl^{\bullet} + 0.4\ Br^{\bullet} + 0.4\ Hg$			Sitkiewicz et al., 2019	Only significant in the stratosphere
G35	$BrHgONO \xrightarrow{h\nu} 0.9\ BrHgO^{\bullet} + 0.1\ NO_2 + 0.9\ NO + 0.1\ BrHg^{\bullet}$	1.1×10^{-3}		Shah et al., 2021	
G36	$BrHgOOH \xrightarrow{h\nu} 0.31\ BrHgOH + 0.66\ Br^{\bullet} + 0.66\ Hg + 0.69\ HO_2^{\bullet} + 0.03\ BrHg^{\bullet}$	1.5×10^{-2}		Shah et al., 2021	
Hg^{I} & Hg^{II} chlorine chemistry					
G37a	$ClHg^{\bullet} \xrightarrow{M} Hg + Cl^{\bullet}$	$9.0 \times 10^{-11} \times \exp(-8980/T) \times [M]$	104	Khalizov et al., 2003; Donohoue et al., 2005	
G37b	$ClHg^{\bullet} \xrightarrow{h\nu} Hg + Cl^{\bullet}$	2.5×10^{-2}		Shah et al., 2021	
G38	$ClHg^{\bullet} + Br^{\bullet} \longrightarrow ClHgBr$	3.0×10^{-11}	–307	Shah et al., 2021	
G39	$ClHg^{\bullet} + Cl^{\bullet} \longrightarrow HgCl_2$	3.0×10^{-11}, $(4\pm1) \times 10^{-12}$[12]	–346	Shah et al., 2021; Taylor et al., 2005	
G40	$ClHg^{\bullet} + HO^{\bullet} \longrightarrow ClHgOH$	3.0×10^{-11}	–315	Shah et al., 2021	
G41	$ClHg^{\bullet} + NO_2 \xrightarrow{M} ClHgONO$	$k_0 = 4.3 \times 10^{-30} \times (T/298)^{-5.9}$ $k_\infty = 1.2 \times 10^{-10} \times (T/298)^{-1.9}$ $F_C = 0.6$	–165	Shah et al., 2021	
G42	$ClHg^{\bullet} + HO_2^{\bullet} \xrightarrow{M} ClHgOOH$	$k_0 = 4.3 \times 10^{-30} \times (T/298)^{-5.9}$ $k_\infty = 6.9 \times 10^{-11} \times (T/298)^{-2.4}$ $F_C = 0.6$	–183	Shah et al., 2021	
G43	$ClHg^{\bullet} + O_3 \longrightarrow ClHgO^{\bullet} + O_2$	$1.0 \times 10^{-10} \times (T/300)^{0.5}$	–151	Saiz-Lopez et al., 2022	
G44	$ClHgO^{\bullet} + CH_4 \longrightarrow ClHgOH + CH_3^{\bullet}$	$1.5 \times 10^{-11} \times \exp(-1290/T)$	–23	Shah et al., 2021	
G45	$ClHgO^{\bullet} + CO \longrightarrow ClHg^{\bullet} + CO_2$	$6.0 \times 10^{-11} \times \exp(-550/T)$	–275	(Shah et al., 2021)	
G46	$ClHgO^{\bullet} + HCl \longrightarrow HgCl_2 + HO^{\bullet}$	$7.9 \times 10^{-11} \times (T/300)^{-0.916}$	–84	Saiz-Lopez et al., 2022	
G47	$ClHgOH + HCl \longrightarrow HgCl_2 + H_2O$	$1.3 \times 10^{-12} \times (T/300)^{-1.6}$	–122	Saiz-Lopez et al., 2022	

[8] Equilibrium coefficient (unit: $cm^3\ molecule^{-1}$)

[9] Over the interval 333 K to 200 K.

[10] Estimated value from $CH_3O + NO$

[11] Estimated value from $CH_3O + NO_2$

[12] Valid for 395-573 K

formaterade: Teckenfärg: Blå

$\longrightarrow BrHgO^{\bullet} + O_2$
tog bort: $\longrightarrow BrHg^{\bullet} + O_2 + O_2$
$\longrightarrow BrHgOO^{\bullet} + O_2$

formaterade: Teckenfärg: Blå

formaterade: Teckenfärg: Blå

formaterade: Teckenfärg: Blå

tog bort: ¶
–143¶
–171

tog bort:

tog bort:

tog bort:

tog bort:

Formaterat: Radavstånd: enkelt

G48	$ClHgO^{\bullet} \xrightarrow{h\nu} 0.673\ HgO + 0.327\ Hg + Cl^{\bullet} + 0.327\ O$			Saiz-Lopez et al., 2022	Only significant in the stratosphere
G49	$HgCl_2 \xrightarrow{h\nu} 0.6\ ClHg^{\bullet} + 1.4\ Cl^{\bullet} + 0.4\ Hg$			Saiz-Lopez et al., 2022	
G50	$ClHgOH \xrightarrow{h\nu} 0.063\ HgOH + 0.969\ Cl^{\bullet} + 0.906\ Hg + 0.937\ HO^{\bullet} + 0.031\ ClHg^{\bullet}$	1.3×10^{-5}		Shah et al., 2021	
G51	$ClHgONO \xrightarrow{h\nu} 0.9\ ClHgO^{\bullet} + 0.1\ NO_2 + 0.9\ NO + 0.1\ ClHg^{\bullet}$	1.1×10^{-3}		Shah et al., 2021	
G52	$ClHgOOH \xrightarrow{h\nu} 0.31\ ClHgOH + 0.66\ Cl^{\bullet} + 0.66\ Hg + 0.69\ HO_2^{\bullet} + 0.03\ ClHg^{\bullet}$	1.5×10^{-2}		Shah et al., 2021	
Hg^{I} & Hg^{II} HO_x chemistry					
G53a	$HOHg^{\bullet} \xrightarrow{M} Hg + HO^{\bullet}$	$3.5 \times 10^{-9} \times \exp(-5269/T) \times [M]$	30 to 60	Saiz-Lopez et al., 2022	
G53b	$HOHg^{\bullet} \xrightarrow{h\nu} Hg + HO^{\bullet}$	1.6×10^{-2}		Saiz-Lopez et al., 2019	
G54	$HOHg^{\bullet} + Br \xrightarrow{M} BrHgOH$	3.0×10^{-11}	–306	Shah et al., 2021	
G55	$HOHg^{\bullet} + Cl \xrightarrow{M} ClHgOH$	3.0×10^{-11}	–273	Shah et al., 2021	
G56	$HOHg^{\bullet} + HO^{\bullet} \xrightarrow{M} Hg(OH)_2$	3.0×10^{-11}	–321	Shah et al., 2021	
G57	$HOHg^{\bullet} + NO_2 \xrightarrow{M} HOHgONO$	$k_0 = 3.69 \times 10^{-17} \times T^{-4.75}$ $k_\infty = 1.26 \times 10^{-5} \times T^{-2.04}$ $F_C = 0.6$	–189	Jiao and Dibble, 2017b	
G58	$HOHg^{\bullet} + HO_2 \xrightarrow{M} HOHgOOH$	$k_0 = 7.68 \times 10^{-19} \times T^{-4.25}$ $k_\infty = 1.24 \times 10^{-4} \times T^{-2.53}$ $F_C = 0.6$	–184	Jiao and Dibble, 2017b	
G59	$HOHg^{\bullet} + O_3 \longrightarrow HOHgO^{\bullet} + O_2$	$10^{-10} \times (T/300)^{0.17}$	–162[13]	Saiz-Lopez et al., 2022; Castro Pelaez et al., 2022	
G60	$HOHgO^{\bullet} + H_2O \longrightarrow Hg(OH)_2 + HO^{\bullet}$	$5.3 \times 10^{-12} \times \exp(-2894/T)$	–26[14]	Saiz-Lopez et al., 2022	
G61	$HOHgO^{\bullet} + HO_2 \longrightarrow Hg(OH)_2 + O_2$	$7.2 \times 10^{-11} \times (T/300)^{-0.436}$	–282	Saiz-Lopez et al., 2022	
G62	$HOHgO^{\bullet} + CH_4 \longrightarrow Hg(OH)_2 + CH_3^{\bullet}$	$4.4 \times 10^{-12} \times \exp(-1650/T)$	–40	Saiz-Lopez et al., 2022	
G63	$HOHgO^{\bullet} + CO \longrightarrow HOHg^{\bullet} + CO_2$	$6.0 \times 10^{-11} \times \exp(-550/T)$	–252	Edirappulige et al., 2023	
G64	$HOHgO^{\bullet} + HCHO \longrightarrow Hg(OH)_2 + CO + H^{\bullet}$	$\leq 4.7 \times 10^{-11}$	–109	Edirappulige et al., 2023	
G65	$HOHgO^{\bullet} + NO \xrightarrow{M} HOHgONO$	2.9×10^{-1115}	–226	Edirappulige et al., 2023	
G66	$HOHgO^{\bullet} + NO_2 \xrightarrow{M} HOHgONO_2$	1.7×10^{-1116}	–242	Edirappulige et al., 2023	
G67	$Hg(OH)_2 + HCl \longrightarrow HOHgCl + H_2O$	$1.5 \times 10^{-12} \times (T/300)^{-2.14}$	–125	Saiz-Lopez et al., 2022	
G68	$HOHgCl + HCl \longrightarrow HgCl_2 + H_2O$	$1.3 \times 10^{-12} \times (T/300)^{-2.14}$	–122	Saiz-Lopez et al., 2022	
G69	$HOHgO^{\bullet} \xrightarrow{h\nu} 0.5\ HgO + 0.5\ Hg + HO^{\bullet} + 0.5\ O$				Tentative
G70	$Hg(OH)_2 \xrightarrow{h\nu} 0.5\ HOHg^{\bullet} + 1.5\ HO^{\bullet} + 0.5\ Hg$			Saiz-Lopez et al., 2022	Only significant in the stratosphere
G71	$HOHgONO \xrightarrow{h\nu} HOHg^{\bullet} + NO_2$	1.1×10^{-3}		Shah et al., 2021	
G72a	$HgO \xrightarrow{M} Hg + O$	$8.4 \times 10^{-11} \times \exp(-3150/T) \times [M]$	27.6	Saiz-Lopez et al., 2022	
G72b	$HgO \xrightarrow{h\nu} Hg + O$	0.54		Francés-Monerris et al., 2020	
G73	$HgO + H_2O \xrightarrow{M} Hg(OH)_2$ $\rightarrow HOHg^{\bullet} + HO^{\bullet}$		–240[17] 40	Saiz-Lopez et al., 2022	
G74	$HgO + HCl \longrightarrow ClHg^{\bullet} + HO^{\bullet}$	$7.1 \times 10^{-11} \times (T/300)^{-1.6}$	–61	Saiz-Lopez et al., 2022	
G75	$HgO + O_2 \longrightarrow Hg + O_3$	$3.4 \times 10^{-13} \times \exp(-1993/T)$	–300	Saiz-Lopez et al., 2022	
Dimethylmercury chemistry					
G76	$CH_3HgCH_3 + Cl^{\bullet}$ $\longrightarrow CH_3HgCl + CH_3^{\bullet}$ $\longrightarrow CH_3HgCH_2^{\bullet} + HCl$ $\longrightarrow CH_3Hg^{\bullet} + CH_3Cl \longrightarrow CH_3^{\bullet} + Hg + CH_3Cl$	$(2.8 \pm 0.3) \times 10^{-10}$	–121 –21 –9	Niki et al., 1983b	

[13] Based on calculation on exit-channel complexes at SC-NEVPT2 level of theory

[14] Based on $\Delta_f H^0(HOHgO^{\bullet}) = 63.2$ kJ mol^{-1}

[15] Estimated value from $CH_3O + NO$

[16] Estimated value from $CH_3O + NO_2$

[17] refers to ***singlet*** $Hg(OH)_2$, but is 10 kJ mol^{-1} endothermic for formation of spin-conserving ***triplet*** $Hg(OH)_2$

formaterade: Kondenserad med 0,5 pt
tog bort: 2023b
formaterade: Kondenserad med 0,5 pt
formaterade: Kondenserad med 0,5 pt
tog bort: 2023b
formaterade: Kondenserad med 0,5 pt
formaterade: Kondenserad med 0,5 pt
tog bort:
tog bort: 2023b
formaterade: Kondenserad med 0,5 pt
formaterade: Kondenserad med 0,5 pt
tog bort:
tog bort: 2023b
formaterade: Kondenserad med 0,5 pt
formaterade: Kondenserad med 0,2 pt
formaterade: Kondenserad med 0,2 pt
tog bort: G69
tog bort: G70
tog bort: G71a
tog bort: G71b
tog bort: G72
tog bort: G73
tog bort: G74
tog bort: G75

G77	$CH_3HgCH_3 + HO^\bullet$	$\rightarrow CH_3HgOH + CH_3^\bullet$ $\rightarrow CH_3HgCH_2^\bullet + H_2O$ $\rightarrow CH_3Hg^\bullet + CH_3OH \rightarrow CH_3^\bullet + Hg + CH_3OH$	$(2.0\pm0.2) \times 10^{-11}$	-39[18] -88 -177	Niki et al., 1983a
G78	$CH_3HgCH_3 + NO_3^\bullet$	$\rightarrow CH_3HgONO_2 + CH_3^\bullet \rightarrow HgO + 2\,CH_3^\bullet + NO_2$ $\rightarrow CH_3HgCH_2^\bullet + HNO_3$ $\rightarrow CH_3Hg^\bullet + CH_3OH \rightarrow CH_3^\bullet + Hg + CH_3OH$	$3.2 \times 10^{-11} \times \exp((-1760 \pm 400)/T)$	-93 -98 -100	Sommar et al., 1996; Sommar et al., 1997

Hg + X$^\bullet$ (X = Br, Cl, OH and I)

In addition to bromine atoms (Br$^\bullet$), hydroxyl radicals (HO$^\bullet$) and, to a lesser extent, chlorine (Cl$^\bullet$) and possibly iodine (I$^\bullet$) atoms have been proposed to initiate the global gas-phase oxidation of Hg^0 in the ground state in the atmosphere:

$$Hg + X^\bullet \xrightarrow{M} {}^\bullet Hg^{I}X \qquad \text{(Rxn G1 – G3)}$$

The reaction rates for X = Cl (**Rxn G2**, Donohoue et al., 2005; Taylor et al., 2005) and Br (**Rxn G1**, Donohoue et al., 2006) have been determined via pulsed laser photolysis-laser induced fluorescence (PLP-LIF) for a range of pressures and temperatures. The reaction is apparently termolecular, i.e., it shows a linear dependence on pressure (M), a slightly negative temperature dependence, and a significant difference in deactivation efficiency, with N_2 and He as third bodies (Donohoue et al., 2005). There are also several experimental static studies of halogen atom reactions carried out at 1-atm pressure, which, with the exception of the studies by Horne et al. (1968) and Greig et al. (1970), have used the relative rate (RR) technique at room temperature (Ariya et al., 2002; Spicer et al., 2002; Sun et al., 2016; Guérette, 2011). The Hg + X$^\bullet$ rate expression determined by Donohoue et al. over 0.26–0.79 atm and 243–293 K by the preferred PLP-LIF technique gives rate coefficients of 5.4×10^{-13} (Donohoue et al., 2005) and 3.6×10^{-13} (Donohoue et al., 2006) cm^3 molecule^{-1} s^{-1} at 298 K and 1 atm pressure in air for the Cl$^\bullet$- and Br$^\bullet$- reactions, respectively. Although the rate constant of the chlorine atom reaction is 50% greater than that of the bromine atom reaction, the significance of the former is small in the remote troposphere, considering the low concentration of chlorine atoms. Notably, a significant increase in the apparent recombination rate coefficient of Hg + Cl$^\bullet$ was observed in the presence of air. This result has been rationalized on the basis that secondarily formed ClO_x species may also react rapidly with Hg^0 (Donohoue, 2008). A plausible candidate is Hg + ClO_2 → ${}^\bullet Hg^{I}Cl$ + O_2 (**Rxn G8**), which is exothermic (ΔH_R = –80 kJ mol^{-1}), but the channel has not been investigated further. Computational studies (Shepler et al., 2007; Goodsite et al., 2004; Goodsite et al., 2012) reported a slightly larger rate constant (~10^{-12} cm^3 molecule^{-1} s^{-1}) for the Hg + Br$^\bullet$ reaction than the absolute PLP-LIF determination at STP. On the other hand, experimental RR studies generally yield rate constants that exceed the limit obtained from theoretical calculations, suggesting complex kinetics, including reactions at the reactor wall.

The reaction with X = OH (**Rxn G3**) was studied with PLP-LIF using an excess of Hg^0 over $^\bullet$OH (generated from the photolysis of HNO_3 at 266 nm) without evidence of a reaction, resulting in an upper rate limit of (<) 1.2×10^{-13} cm^3 molecule^{-1} s^{-1} (Bauer et al., 2003). The rate constant of Hg + $^\bullet$OH → products determined by Sommar et al. (2001) relative to cyclohexane + $^\bullet$OH → products of 8.7×10^{-14} cm^3 molecule^{-1} s^{-1} falls below this limit at 295 K and 1 atm air, as does the temperature-resolved kinetic RR study of Pal and Ariya (2004a) extrapolated to 295 K (~1×10^{-13} cm^3 molecule^{-1} s^{-1}). External re-analysis of Pal and Ariya (Calvert and Lindberg, 2005) and Sommar et al. (Dibble et al., 2020) data via kinetic modeling revealed that ${}^\bullet Hg^{I}OH$ under experimental conditions exclusively reacts with NO_2 (${}^\bullet Hg^{I}OH + NO_2 \rightarrow HOHg^{II}ONO$, **Rxn G57**) rather than dissociating. The temporal resolution in the PLP-LIF study also allowed a lower-bound estimate of the equilibrium constant $K_{\bullet HgOH} = [{}^\bullet HgOH]/([Hg][HO^\bullet])$ of 5×10^{-16} cm^3 molecule^{-1} (Bauer et al., 2003). This equilibrium constant has been estimated via computational studies. Recently, high-level quantum chemical calculations (Dibble et al., 2020) performed at 200–320 K yielded a $K_{\bullet HgOH}$ of ~7×10^{-16} cm^3 molecule^{-1} at 298 K, corresponding to a k_{13} of 9.5×10^{-14} cm^3 molecule^{-1} s^{-1} at 1 atm. In contrast, Saiz-Lopez et al. (2022) reported that $K_{\bullet HgOH}$ was more than an order of magnitude smaller (~5×10^{-17} cm^3 molecule^{-1}) at the corresponding temperature.

The kinetics of the reaction between Hg^0 and iodine atoms (by photolysis of CH_2I_2/CF_3I) were studied in an early work by monitoring ${}^\bullet Hg^{I}I$ by absorption spectroscopy at 403–438 K (Greig et al., 1971) and in a later study by following the Hg^0 loss by MS at 296 K (Raofie et al., 2008). In the first study, sufficiently high ${}^\bullet Hg^{I}I$ densities could not be generated to gauge a reaction, for which the rate constant was lower than that of the competing $I^\bullet + I^\bullet \xrightarrow{M} I_2$ reaction of ~1×10^{-13} cm^3 molecule^{-1} s^{-1}. The latter study lacks

[18] Assuming $\Delta_f H^0(CH_3HgCl) = \Delta_f H^0(CH_3HgOH)$

tog bort: G76
tog bort: G77
Formaterat: Radavstånd: Flera 1,15 li
tog bort: Besides
tog bort: globally
formaterade ... [254]
tog bort: rate
tog bort: has…ave been determined by…ia pulsed laser photolysis-laser …induced fluorescence (PLP-LIF) for a range of pressures and temperatures. The reaction is apparently termolecular, i.e…., it shows a linear dependence on pressure (M), a slightly negative temperature dependence, and a significant difference in deactivation efficiency, with N_2 and He as third bodies (Donohoue et al., 2005). There are also several experimental static studies of the …alogen atom reactions carried out at 1-atm pressure, which, with the exception of the studies by Horne et al. (1968) and Greig et al. (1970), have used the relative rate (RR) technique at room temperature (Ariya et al., 2002; Spicer et al., 2002; Sun et al., 2016; Guérette, 2011). The Hg + X$^\bullet$ rate expression determined absolutely …y Donohoue et al. over 0.26 – …0.79 atm and 243 – …293 K by the preferred PLP-LIF technique gives a …ate coefficient ... [255]
tog bort: -
tog bort: at STP …0% greater than that of the bromine atom reaction, the significance of the former is small in the remote troposphere, taking into account…onsidering the low concentration chlorine atoms. It should also be added that…otably, a significant increase in the apparent recombination rate coefficient of Hg + Cl$^\bullet$ was observed in the presence of air. This result has been rationalized on the basis that secondarily formed ClO_x species may also react rapidly with Hg^0 (Donohoue, 2008). A plausible candidate is Hg + ClO_2 → ${}^\bullet Hg^{I}Cl$ + O_2 (**Rxn G8**), which is exothermic (ΔH_R = –80 kJ mol^{-1}), but the channel has not been investigated further. Byun et al. (2010) studied the Hg + ClO_x gas phase system experimentally at 130 °C. Their results in favor of a rapid reaction between Hg + ClO$^\bullet$ → products at 1.1×10^{-11} cm^3 molecule $^{-1}$ s^{-1} are surprising, but they also report Hg + Cl$^\bullet$ → products at 1.2×10^{-10} cm^3 molecule^{-1} s^{-1} and Hg + Cl_2 → products at 4.3×10^{-15} cm^3 molecule^{-1} s^{-1}, which may indicate that the results are strongly affected by surface reactions. Computational studies (Shepler et al., 2007; Goodsite et al., 2004; Goodsite et al., 2012) gave ... [256]
tog bort: the …xperimental RR studies generally give…ield rate constants that exceed the limit obtained from theoretical calculations, suggesting complex kinetics, including reactions at the reac ... [257]
tog bort: for…f a reaction, giving ... [258]
tog bort: the …al and Ariya (Calvert and Lindberg, 2005) and Sommar et al. (Dibble et al., 2020) data using…ia kinetic modeling has shown…evealed that the fate of ... [259]
tog bort: their …xperimental conditions is …xclusively r ... [260]
tog bort: G59…57) rather than dissociation…issociating. The time…emporal resolution in the PLP-LIF study also allowe ... [261]
tog bort: also …een modeled by…stimated via computational studies. A recent one using…ecently, high-level quantum chemical calculations (Dibble et al., 2020),… performed at 200 – …320 K yields… ... [262]
tog bort: arrive at a
formaterade: Kondenserad med 0,2 pt
tog bort: was
formaterade: Kondenserad med 0,2 pt
tog bort: –
formaterade: Kondenserad med 0,2 pt
tog bort:),
formaterade: Kondenserad med 0,2 pt
tog bort: is
formaterade ... [263]
formaterade ... [264]

conclusive results on the Hg + $I^{\bullet} \xrightarrow{M} {}^{\bullet}Hg^{I}I$ reaction but provides a limit on the rate constant for the reaction of Hg with molecular iodine vapor ($\leq 1.3 \times 10^{-19}$ cm^3 $molecule^{-1}$ s^{-1}), a reaction that lacks any atmospheric significance. A rate coefficient of 4.0×10^{-13} $(T/298)^{-2.38}$ cm^3 $molecule^{-1}$ s^{-1} was calculated for the Hg + $I^{\bullet} \xrightarrow{M} {}^{\bullet}Hg^{I}I$ reaction at 1 atm N_2 and T between 180 and 400 K via Rice-Ramsperger-Kassel-Markus (RRKM) theory based on the calculated binding energy (46 kJ mol^{-1}) and molecular properties of ${}^{\bullet}HgI(^2\sum)$ (Goodsite et al., 2004).

5.1.2 Stability of $^{\bullet}Hg^{I}X$

The first step (termolecular reactions G1–G3), which is exothermic, produces Hg^{I} radical intermediates ($^{\bullet}Hg^{I}X$), which can revert to Hg^0 both thermally and photolytically:

$$ {}^{\bullet}Hg^{I}X \underset{h\nu}{\overset{\Delta}{\rightarrow}} Hg + X^{\bullet} \qquad \text{(Rxn G14a,b/G37a,b/G53a,b)} $$

Photolytic and thermal dissociation

The first excited electronic state of $^{\bullet}Hg^{I}X$ (designated $A^2\Pi$ for halogenated radicals) is exclusively repulsive, resulting in dissociation with visible light for wavelengths exceeding ~460 nm, where the absorption maxima are predicted at ~480, ~575, ~650, and ~690 nm for $^{\bullet}Hg^{I}OH$, $^{\bullet}Hg^{I}Cl$, $^{\bullet}Hg^{I}Br$, and $^{\bullet}Hg^{I}I$, respectively (Saiz-Lopez et al., 2019; **Fig. 3**). While the bond strengths of Hg–Cl and Hg–Br are well defined in relative terms (89.5–98.0 kJ mol^{-1}, Tellinghuisen et al., 1982; Shepler et al., 2005; Saiz-Lopez et al., 2022; Cremer et al., 2008 and 60.2–68.1 kJ mol^{-1}, Goodsite et al., 2004; Shepler et al., 2005; Cremer et al., 2008; Tellinghuisen and Ashmore, 1983, respectively), there is significant variation in the estimates of the bond strengths of $^{\bullet}Hg^{I}I$ and $^{\bullet}Hg^{I}OH$, ranging from ~33 to 46 kJ mol^{-1} (Goodsite et al., 2004; Shepler et al., 2005; Cremer et al., 2008; Jordan et al., 1993; Salter et al., 1986) and ~23 to 55 kJ mol^{-1} (Dibble et al., 2020; Tossell, 2003; Goodsite et al., 2012; Guzman and Bozzelli, 2019; Cremer et al., 2008), respectively. Therefore, the stability of $^{\bullet}Hg^{I}OH$ and $^{\bullet}Hg^{I}I$ is uncertain, and it is debatable whether their thermal lifetimes in the atmosphere are long enough for these radicals to be further oxidized to mercuric species to any significant degree. The question has been raised recently since it was experimentally established that $^{\bullet}Hg^{I}Br$ is kinetically oxidized by O_3 without a reaction barrier (**Rxn G22**), which was also theoretically established to be true at least for $^{\bullet}Hg^{I}Cl$ and $^{\bullet}Hg^{I}OH$ (**Rxn G43 & G59**, respectively, **Section 5.1.3**). A study using RRKM theory suggested that the recombination rate coefficients of Hg with $I^{\bullet}$ and $HO^{\bullet}$ are similar in the free troposphere, while the thermal dissociation of $^{\bullet}Hg^{I}I$ gradually exceeds that of $^{\bullet}Hg^{I}OH$ at lower temperatures (Goodsite et al., 2004). $^{\bullet}Hg^{I}I$ is the $^{\bullet}Hg^{I}X$ species with the shortest photolytic lifetime in the troposphere globally (~17 s), according to computational chemistry theory (Saiz-Lopez et al., 2019). Recently, Dibble et al. estimated the HO–Hg binding energy to be 46 kJ mol^{-1} using high-level quantum chemical calculations (Dibble et al., 2020). Compared with a global photolytic lifetime of just over one minute (Shah et al., 2021), the thermal lifetime of $^{\bullet}Hg^{I}OH$ in the lower troposphere is significantly shorter (according to data from Dibble et al., 2020 ~10 ms at the surface up to approximately ten seconds at the tropopause). For the lighter mercurous halides (excluding $^{\bullet}Hg^{I}I$), the relationship is reversed with respect to the importance of photolytic versus thermal dissociation. The lifetimes of the former channel are ~20 and ~40 s for $^{\bullet}Hg^{I}Br$ and $^{\bullet}Hg^{I}Cl$, respectively, while the thermal decay is slower for $^{\bullet}Hg^{I}Br$ above the planetary boundary layer and $^{\bullet}Hg^{I}Cl$ is much less thermally unstable.

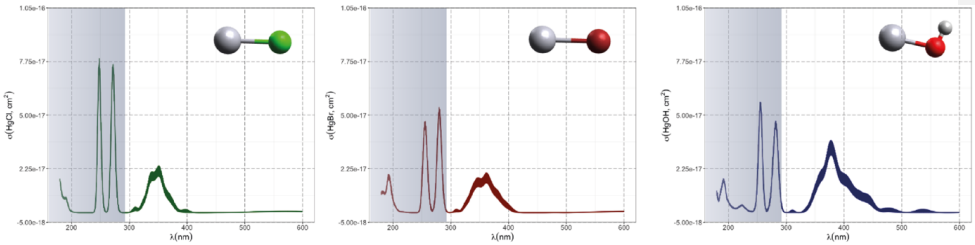

Figure 3. Computed absorption spectra of the atmospherically important mercurous chloride, bromide, and hydroxyl radicals. Wavelengths accessible in the troposphere are to the right of the colored area. Data from Saiz-Lopez et al. (2019).

formaterade: Kondenserad med 0,2 pt
formaterade: Kondenserad med 0,2 pt
formaterade: Kondenserad med 0,2 pt
formaterade: Kondenserad med 0,2 pt
formaterade: Kondenserad med 0,2 pt
formaterade: Kondenserad med 0,2 pt
formaterade: Kondenserad med 0,2 pt
formaterade: Kondenserad med 0,2 pt
tog bort: using
formaterade: Kondenserad med 0,2 pt
formaterade: Kondenserad med 0,2 pt
formaterade: Kondenserad med 0,2 pt
tog bort: ,
tog bort: a
formaterade: Kondenserad med 0,2 pt
formaterade: Teckenfärg: Dekorfärg 2, Kondenserad med 0,2 pt
formaterade: Kondenserad med 0,2 pt
formaterade: Teckenfärg: Anpassad färg(RGB(31;56;100))
tog bort: –
formaterade: Teckenfärg: Anpassad färg(RGB(31;56;100))
tog bort: Photo-
tog bort: -
tog bort: –
tog bort: –
tog bort:
tog bort: G44
tog bort: suggests
tog bort: to
tog bort: about
tog bort: i.e.,
tog bort: lifetime
tog bort: is globally

5.1.3 Bimolecular reactions of •Hg^{I}X

In addition to thermal and photolytic decomposition, the fate of •Hg^{I}X in the atmosphere is controlled by further oxidation to thermally stable mercuric species molecules. Experimental studies of the specific bimolecular reaction kinetics of •Hg^{I}X are limited to X = Br and Cl (**Rxn G15 & G39**). Taylor et al. (2005) studied the reactions of •Hg^{I}Cl with Cl_2, HCl and Cl• at temperatures characteristic of post-combustion conditions. The observed reaction with free chlorine to form $HgCl_2$ was rapid (1.2×10^{-11} cm^3 molecule^{-1} s^{-1}) and temperature independent. Jiao and Dibble (2017b) used computational chemistry to determine the rate constant and product yield for reactions of •Hg^{I}Br with abundant atmospheric NO_2 (**Rxn G20**) and HOO (**Rxn G21**) radicals. Analogous to the experimental •Hg^{I}Cl study, these reactions were calculated to be rapid, with the rate constant for oxidation by NO_2 being approximately twice that for oxidation by HOO•. This theoretical study indicated that the •Hg^{I}Br + NO_2 reaction occurs along two competing channels (**Rxn G20a, b**), one proceeding via oxidative addition resulting in BrHg^{II}ONO, and the other operating via reductive displacement resulting in Hg^0 + $BrNO_2$. The dichotomy occurs because •Hg^{I}Br ($^2\Sigma^+$) possesses a delocalized electron that spreads more equivalent spin density over the molecule (•Hg^{I}Br ↔ Hg^{I}Br•), whereas the spin density of the HgOH (^{1}A') radical is most localized on the Hg atom. A reaction with another radical center occurs for •Hg^{I}OH when the reactant is oriented toward Hg, leading to addition, while for HgBr, reductive displacement is also possible when the collision involves the Br atom (Castro Pelaez et al., 2022). The existence of a branching ratio was also confirmed by an experimental study of the •Hg^{I}Br + NO_2 reaction by Wu et al. (2020) using PLP-LIF, who reported that the computed rate coefficients for both reduction and oxidation were greatly overestimated. This study deduced that the importance of the reductive channel increases slowly with increasing altitude from the ground level to the tropopause but is only ~10% as fast as the oxidation reaction. Wu et al. (2022) also experimentally studied the interaction between NO and •Hg^{I}Br, leading to Hg^0 + BrNO. •Hg^{I}Br + O_2 → BrHg^{II}OO• (**Rxn G19**) is slightly exothermic, while that leading to Hg^0 + BrOO• is less feasible due to endothermicity. The •Hg^{I}Br + O_2 reaction is thus described by •Hg^{I}Br + O_2 ⇄ BrHg^{II}OO•, with an equilibrium constant that decreases with increasing temperature (Wu et al., 2022). To the extent that BrHg^{II}OO• can be attributed significance, it is a reservoir for •Hg^{I}Br at low temperatures, with an upper limit of ~50% stored at 220 K. Wu et al. (2022) argued that BrHg^{II}OO• behaves like a peroxyl radical (HOO•/ROO•) in reactions with atmospheric radicals. Recently, Saiz-Lopez et al. (2020) implied missing oxidation pathways to better reconcile their GEOS-Chem global atmospheric chemistry model simulations with field observations. Suggested by Shepler (2006) and later Lam (2019) as a potential pathway of Hg^{I} oxidation, the Saiz-Lopez group has carried out theoretical (Saiz-Lopez et al., 2020) and experimental (Gómez Martín et al., 2022) investigations of the system •Hg^{I}Br + O_3. In addition, Castro Palaez et al. (2022) carried out theoretical calculations for rate constants and product yields, including •Hg^{I}OH + O_3. •Hg^{I}X + O_3 → XHg^{II}O• + O_2 (**Rxn G22, G43 and G59**) is highly exothermic (172 kJ mol^{-1} for X = Br), proceeds without a substantial activation barrier and is currently considered to be important for the atmospheric oxidation of •Hg^{I}X, with XHg^{II}O• as a key intermediate. As a radical, XHg^{II}O• is relatively thermally stable with strong Hg–O bond (333 and 294 kJ mol^{-1} for X = Cl & Br, respectively; Balabanov and Peterson, 2003). Gómez Martin et al. (2022) determined the rate coefficient of the •Hg^{I}Br + O_3 reaction at 295 K via a PLP-LIF system. To generate •Hg^{I}Br (photolysis of $HgBr_2$ at 248 nm by a KrF excimer laser), the introduced O_3 would inevitably be photolyzed to some extent before it could react with •Hg^{I}Br. This led to complications due to the following potential chemistry:

$$\text{•Hg}^{I}\text{Br} + O_3 \rightarrow \text{BrHg}^{II}\text{O•} + O_2 \quad \text{(Rxn G22)}$$

$$\text{•Hg}^{I}\text{Br} + O(^3P) \rightarrow \begin{cases} \text{BrHg}^{II}\text{O•} \\ Hg^0 + \text{BrO•} \end{cases} \quad \text{(Rxn G23)}$$

$$\text{BrHg}^{II}\text{O•} + O(^3P) \rightarrow \text{•Hg}^{I}\text{Br} + O_2 \quad \text{(Rxn G24)}$$

$$\text{BrHg}^{II}\text{O•} + O_3 \rightarrow \begin{cases} \text{•Hg}^{I}\text{Br} + O_2 + O_2 \\ \text{BrHg}^{II}\text{OO•} + O_2 \end{cases} \quad \text{(Rxn G25)}$$

By performing experiments at different KrF laser energies and ozone concentrations and by numerical modeling of the data, Gómez Martin et al. isolated k(•HgBr + O_3), k(•HgBr + O) and k(BrHgO• + O) as 7.5, 5.3 and 9.1 (all × 10^{-11} cm^3 molecule^{-1} s^{-1}),

formaterade ... [265]
tog bort: reaction
formaterade ... [266]
tog bort: determined
formaterade ... [267]
tog bort: the
formaterade ... [268]
tog bort: using computational chemistry.
formaterade ... [269]
tog bort: by
formaterade ... [270]
tog bort: another
formaterade ... [271]
tog bort: by
tog bort: depending on the fact that
formaterade ... [272]
formaterade ... [273]
tog bort: Reaction
formaterade ... [274]
tog bort: towards
formaterade ... [275]
tog bort: found
formaterade ... [276]
tog bort: have
formaterade ... [277]
formaterade ... [278]
tog bort: dramatically
formaterade ... [279]
tog bort: och
formaterade ... [280]
tog bort: -
formaterade ... [281]
tog bort: -
formaterade ... [282]
tog bort: have
formaterade ... [283]
tog bort: G22a
formaterade ... [284]
tog bort:) and
formaterade ... [285]
tog bort: of great importance
formaterade ... [286]
tog bort: Being
formaterade ... [287]
tog bort: a
formaterade ... [288]
tog bort: -
formaterade ... [289]
tog bort: ,
formaterade ... [290]
tog bort: using
formaterade ... [291]
tog bort: it was inevitable that
formaterade ... [292]
tog bort: G22a
tog bort: the
tog bort:

respectively. They presented an upper limit for $BrHg^{II}O^{\bullet} + O_3$ ($k < 5 \times 10^{-12}$ cm^3 molecule^{-1} s^{-1}), which was considered infeasible by theoretical calculations due to steric hindrance. Instead of leading primarily to $BrHg^{II}O^{\bullet}$ as is the case for the $^{\bullet}Hg^{I}Br + O_3$ reaction, $^{\bullet}Hg^{I}Br + O$ results in reductive elimination ($Hg^0 + BrO^{\bullet}$) for all collision geometries. Hg^0 is also produced in the rapid reaction between $BrHg^{II}O^{\bullet} + O$. In the lower atmosphere (≤ 25 km), the content of free O atoms is low, and therefore, its role as an oxidant is minor (Calvert et al., 2015). The energetic $O(^1D)$, formed primarily by photolysis of O_3 by UV light (< 340 nm), is rapidly consumed through two competitive channels: deactivation to $O(^3P)$ by collision with air molecules or reaction with the ubiquitous water vapor to form OH radicals. $O(^3P)$, also formed by the photolysis of NO_2 (< 430 nm), reacts rapidly and thermally with O_2 in the atmosphere to form ozone (Calvert et al., 2015). Importantly, $k(^{\bullet}HgBr + O_3)$ is more than twice as fast as $k(^{\bullet}HgBr + NO_2)$ when the experimental results are extrapolated to the atmospheric surface layer (1 atm, 295 K). The combination of a high $k(^{\bullet}HgBr + O_3)$ and the abundance of ozone relative to other radicals, such as NO_2 and HOO, suggests that $^{\bullet}Hg^{I}Br + O_3$ is predominant in the conversion of Hg^I to Hg^{II} in the atmosphere. The experimentally determined $k(^{\bullet}HgBr + O_3)$ is close to the upper limit of 1×10^{-10} cm^3 molecule^{-1} s^{-1} estimated by Saiz-Lopez et al. (2020), which excludes steric effects. For an updated chemical mechanism in the global atmospheric model GEOS-Chem, Shah et al. (2021) used a conservative rate constant of 3×10^{-11} cm^3 molecule^{-1} s^{-1} for the oxidation of $^{\bullet}Hg^{I}X$ with O_3 (X = Cl, Br and OH). By postulating $k(^{\bullet}HgOH + O_3) = k(^{\bullet}HgBr + O_3)$, simulations by Shah et al. (2021) revealed that the OH-initiated pathway accounts for one-third of global Hg^{II} production. In contrast, by not including $^{\bullet}Hg^{I}OH + O_3$ in their model, Dibble et al. (2020) reported that the OH-initiated channel is largely irrelevant, with only some regional significance in areas with high levels of photochemical smog. More recently, Castro Pelaez et al. (2022) compared $^{\bullet}Hg^{I}Br + O_3$ and $^{\bullet}Hg^{I}OH + O_3$ systems via computational chemistry and reported that the former has a slight tendency (≤ 0.1%) to undergo reductive elimination ($Hg + BrO^{\bullet} + O_2$) rather than oxidation ($BrHg^{II}O^{\bullet} + O_2$) when the orientation of the terminal oxygen in ozone is toward the Br atom. There was no such tendency for $^{\bullet}Hg^{I}OH + O_3$. It was also found that $k(^{\bullet}HgBr + O_3)$ and $k(^{\bullet}HgOH + O_3)$ are likely similar at 298 K in the range of (6.6 - 8.5) × 10^{-11} cm^3 molecule^{-1} s^{-1}. The positive covariation of O_3 and $^{\bullet}OH$, as opposed to $^{\bullet}Br$ and O_3 (O_3 titrates $^{\bullet}Br$, **Fig. 2**), suggests precedence for OH-initiated Hg oxidation in air with secondary pollutants (Rutter et al., 2012). Field observations of GOM in urban air may suggest radical-initiated $Hg^0 \rightarrow Hg^{II}$ gas-phase transformation, which is claimed to be completed by certain radicals (Peleg et al., 2015; Hong et al., 2016; Edirappulige et al., 2024). An interesting case is urban Jerusalem, where episodes of elevated daytime and nighttime gaseous Hg^{II} levels covary with O_3 (max 250 μg m^{-3}) and NO_3 (430 ng m^{-3}), respectively (Peleg et al., 2015). To the east of the city lies the Dead Sea basin, where effective bromine-controlled oxidation of Hg^0 has been observed (Tas et al., 2012). Finally, the reactivity of $^{\bullet}Hg^{I}X$ toward volatile hydrocarbons is low, as $^{\bullet}Hg^{I}X$ does not abstract a hydrogen atom from an alkane (e.g., from CH_4), nor does it significantly add to a double bond of an alkene (e.g., to $CH_2{=}CH_2$) (Dibble and Schwid, 2016).

5.1.4 Stability of $Hg^{II}XY$

Photoreduction and stoichiometric yields

Although atmospheric Hg^{II} species are generally more stable than Hg^I species, are, many Hg^{II} molecules are still labile, and the atmospheric pool contains mercuric species with different thermal and photolytic stabilities. Most of the atmospherically relevant gas-phase species have well-defined absorption bands in deep UV, in some cases extending into the UV-B and UV-A regions. Early theoretical studies (Strömberg et al., 1989; Strömberg et al., 1991), when knowledge of the atmospheric chemistry of Hg was rudimentary, indicated that the photoreduction of $HgCl_2$ and $Hg(CN)_2$ in actinic light at the Earth's surface was negligible, while that of $Hg(OH)_2$ and $Hg(SH)_2$ was extremely slow. The UV absorption spectra of mercuric halides are increasingly red-shifted as the halogen becomes heavier. $HgCl_2$ vapor absorbs only radiation below 240 nm (**Fig. 8a**), $HgBr_2$ absorbs mainly deep UV light with a tiny tail (< 10^{-19} cm^2 molecule^{-1}, **Fig. 8c**) into UV-B, while HgI_2 has significant absorption in the entire UV region (Maya, 1977; Sitkiewicz et al., 2019). However, binary compounds such as $HgBr_2$ or $HgCl_2$ do not completely dominate the atmospheric $Hg^{II}(g)$ speciation. Mixed compounds such as $BrHg^{II}Y$ molecules (Y= ONO, OOH, OH, OCl, OBr, etc.) and $XHg^{II}O$ radicals (X = Br, OH) are also predicted to be important. Saiz-Lopez et al. (2018) computed the absorption spectra of mixed compounds and found that abundant $BrHg^{II}Y$ molecules absorb in UV-B. The rapidly photolyzed Hg^{II} species

tog bort: , however,…was considered obsolete…nfeasibl … [293]
tog bort: It is important to note that
tog bort: of ultimate significance
tog bort: showed…evealed that the OH-initiated pathway … [294]
tog bort: found…eported that the OH-initiated channel to … [295]
formaterade … [296]
tog bort: .,
formaterade … [297]
tog bort: by…ia computational chemistry and found … [298]
tog bort: towards…oward the Br atom. There is … [299]
tog bort: to be …imilar with a computational value for th … [300]
tog bort: the
formaterade … [301]
tog bort: speciated Hg
tog bort: speculate
formaterade … [302]
formaterade … [303]
tog bort:).… Edirappulige et al., 2024). An interesting ca … [304]
tog bort: in discussing
formaterade … [305]
tog bort: , it can be concluded that it is low viz-á-viz
formaterade … [306]
tog bort: organic compounds in that the species neither ab … [307]
formaterade … [308]
tog bort: .
formaterade … [309]
tog bort:)
formaterade … [310]
tog bort: adds
formaterade … [311]
tog bort: bonds (C = C
formaterade … [312]
Formaterat … [313]
tog bort: Atmospheric
formaterade … [314]
tog bort: . Not all
formaterade … [315]
tog bort: stable, but
formaterade … [316]
tog bort: stability…tabilities. Most of the atmospherically … [317]
tog bort: is
tog bort: is
formaterade … [318]
tog bort: for…f mercuric halides become … [319]
tog bort: in the
formaterade … [320]
tog bort:
formaterade … [321]
tog bort: a
formaterade … [322]
tog bort: •
formaterade … [323]

identified include BrHgONO (**Rxn G35**), BrHgOOH (**Rxn G36**) and BrHgOBr (with lifetimes of a few min to less than a second, **Fig. 4a-c**), with BrHgOH being comparatively long-lived (> 1 day, **Fig. 4d**) in terms of photodissociation. In their modeling study, $HgCl_2$ and $Hg(OH)_2$ were estimated to be photolytically stable in the troposphere by Shah et al. (2021), while the photolysis frequency of $HgBr_2$ was calculated to be just over an order of magnitude lower than that of BrHgOH (1.2×10^{-6} and 1.3×10^{-5} s^{-1}, respectively).

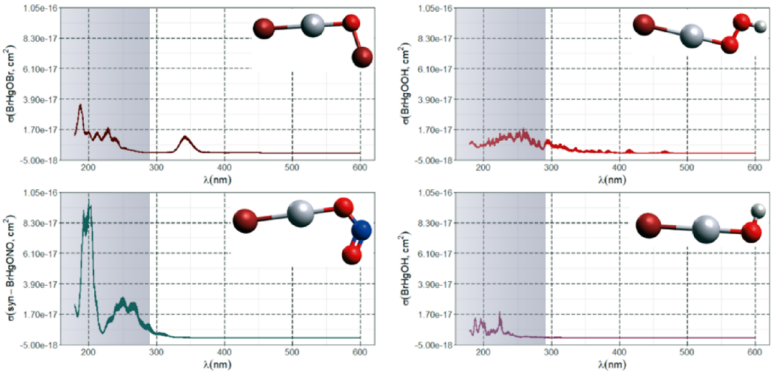

Figure 4. Computed absorption spectra of the atmospherically important (a) BrHgOBr, (b) BrHgOOH, (c) syn-BrHgONO and (d) BrHgOH. Wavelengths accessible in the troposphere are to the right of the colored area (Francés-Monerris et al., 2020).

The photodissociation mechanism (quantum and product yield) of $BrHg^{II}Y$ has been studied using computer-aided calculations based on 2D potential energy surfaces, with the result that photodynamics lead to different channels in which the Hg-containing products can exhibit +II, +I and 0 oxidation states (Francés-Monerris et al., 2020; Lam et al., 2019b). Photolysis of $BrHg^{II}ONO$ results in the formation of NO and $BrHg^{II}O^{\bullet}$ in 90% of cases, while the remainder reverts to $^{\bullet}Hg^{I}Br$ and NO_2 (Francés-Monerris et al., 2020). Consistently, a large dominance of the photoproducts $BrHg^{II}O^{\bullet}$ + NO was predicted by the calculations of Lam et al. (2019b), in contrast to an early work by Saiz-Lopéz et al. (2018) that favored $^{\bullet}Hg^{I}Br$ and Hg^0 formation. During the photolysis of $BrHg^{II}OOH$, the Hg–Br, Hg–O and O–O bonds can be broken, resulting in three main exit channels:

$$BrHg^{II}OOH \xrightarrow{h\nu} \begin{matrix} Hg + Br + {}^{\bullet}OOH\ (66\%) \\ BrHg^{II}O^{\bullet} + {}^{\bullet}OH\ (31\%) \\ {}^{\bullet}Hg^{I}Br + O\sim O\text{–}H\ (\leq 3\%) \end{matrix} \qquad \text{(Rxn G36)}$$

Thus, the photodissociation of $BrHg^{II}OOH$ produces Hg^0, $^{\bullet}Hg^{I}Br$ and $BrHg^{II}O^{\bullet}$ to varying degrees (Francés-Monerris et al., 2020). In the case of $BrHg^{II}OH$, the photolytic formation of $BrHg^{II}O^{\bullet}$ is negligible, while in half of the cases (49%), reduction to elemental Hg occurs, and in the other half, $^{\bullet}Hg^{I}Br$ or $^{\bullet}Hg^{I}OH$ is formed, with the former being predominant (~70%) (Francés-Monerris et al., 2020). The photolysis of $BrHg^{II}ONO$ and $BrHg^{II}OOH$ thus results in significant yields of $BrHg^{II}O^{\bullet}$, the radical form of Hg^{II} described above as the major product of the rapid reaction between $^{\bullet}Hg^{I}Br$ and O_3. In this series of reported compositional chemical results, the only $YHg^{II}O^{\bullet}$ species that has been experimentally characterized is the fluorine analog that is formed along with $FOHg^{II}F$ when excited Hg atoms react with OF_2 (Andrews et al., 2012). Although $FHg^{II}O^{\bullet}$ has no atmospheric significance, its experimentally determined properties are important benchmarks for other homologs in the series. $YHg^{II}O^{\bullet}$ has two strong bonds (the dissociation energy for YHg-O is ~250 kJ mol^{-1}) and is thermally stable in the gas phase. However, $YHg^{II}O^{\bullet}$ is photolabile under UV–VIS light (cf. **Fig. 5b**) and decomposes photolytically along two channels. The calculated branching ratios for both Y = Cl and Br favor the formation of HgO (67% and 56%, respectively, Saiz-Lopez et al., 2022) over splitting into atoms, as shown below:

$$YHg^{II}O^{\bullet} \xrightarrow{h\nu} \begin{matrix} HgO + Y^{\bullet}\ (56\%) \\ Hg + O + Y^{\bullet}\ (44\%) \end{matrix} \qquad \text{(Rxn G31 \& G48)}$$

For $HOHg^{II}O^{\bullet}$, there are no stoichiometric calculations for the photoproducts. The main product generated, HgO with a $^3\Pi_1$ ground state, as a monomer in the gas phase (Sun et al., 2022), possesses a weak Hg–O bond of disputed magnitude (15–30 kJ mol^{-1}, Tossell, 2006; Balabanov and Peterson, 2003; Cremer et al., 2008; Filatov and Cremer, 2004; Shepler and Peterson, 2003; Peterson et al., 2007), which

tog bort: .
formaterade: Kondenserad med 0,4 pt
formaterade: Kondenserad med 0,4 pt
tog bort:) in their modeling study,
formaterade: Kondenserad med 0,4 pt
tog bort: assisted theoretical
Formaterat: Avstånd Efter: 0 pt
formaterade: Teckenfärg: Blå
formaterade: Teckenfärg: Blå
tog bort: leads
tog bort: , forms NO_2
tog bort: favors
tog bort: -
tog bort: -
tog bort: $\xrightarrow{h\nu}$ Hg + Br + $^{\bullet}$OOH (66%); $BrHg^{II}O^{\bullet}$ + $^{\bullet}$OH (31%); $^{\bullet}Hg^{I}Br$ + O~O–H (2%)
tog bort: Photolysis
tog bort: it should be noted that
tog bort: as a benchmark
tog bort: in
tog bort: -
tog bort: 5
tog bort: decompose
tog bort: ratio
tog bort: is in
tog bort: of
tog bort: a
formaterade: Kondenserad med 0,3 pt
Formaterat: Avstånd Efter: 0 pt
formaterade: Teckensnitt:Symbol, Kondenserad med 0,3 pt
formaterade: Kondenserad med 0,3 pt
tog bort: -
formaterade: Kondenserad med 0,3 pt
tog bort:
formaterade: Kondenserad med 0,3 pt

is only ≤ 10% as strong as in $YHg^{II}O^{\bullet}$. HgO can be reduced to Hg^0 by reaction with O_2 and by thermal and photo-dissociation:

$$HgO \xrightarrow{M} Hg + O \quad \text{(Rxn G71a)}$$

$$HgO \xrightarrow{h\nu} Hg + O \quad \text{(Rxn G71b)}$$

$$HgO + O_2 \rightarrow Hg + O_3 \quad \text{(Rxn G74)}$$

The $HgO + O_2$ reaction is exothermic but is subject to a barrier, which, using transition state theory, results in a rate coefficient of 3.4×10^{-13} exp (−1993/T) cm^3 $molecule^{-1}$ s^{-1} (Saiz-Lopez et al., 2022). The enthalpy of thermal decay of HgO is only weakly endothermic and therefore favored by high temperature, with a dependence of 8.4×10^{-11} exp (−3150/T) cm^3 $molecule^{-1}$ s^{-1}, as calculated by RRKM theory (Saiz-Lopez et al., 2022). In addition, HgO is more photolabile than $^{\bullet}Hg^{I}OH$ is, with a calculated global annual mean J(HgO) of 0.54 s^{-1} for the troposphere (Saiz-Lopez et al., 2018, absorption spectrum in **Fig. 5a**). These suggest that gas-phase HgO in the troposphere is highly unstable. Although the decay slows at lower temperatures and pressures as the reaction is collisionally activated, the thermal lifetime is still only about 1 ms at 250 K and 0.1 atm. Analogous to the photolysis of Hg^{I} compounds, the quantum yield for the photo-dissociation of Hg^{II} compounds is assumed to be unity.

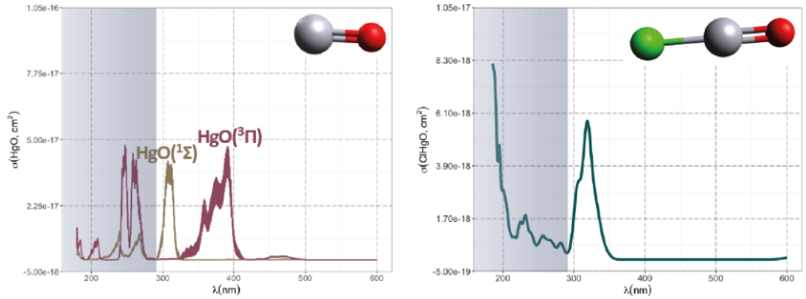

Figure 5. Computed absorption spectra of (a) HgO (lowlying $^3\Pi$ and $^1\Sigma$ states) and (b) ClHgO radical (Saiz-Lopez et al., 2018; Saiz-Lopez et al., 2022). Wavelengths accessible in the troposphere are to the right of the colored area.

Thermochemistry of $YHg^{II}O^{\bullet}$

Experimental data on the kinetics and mechanisms of the atmospheric chemistry of $YHg^{II}O^{\bullet}$ are scarce (the reaction $BrHg^{II}O^{\bullet} + O_3$ to $^{\bullet}Hg^{I}Br$ and O_2 has been described above, Gómez Martín et al., 2022). Initially, the focus of computer simulations was on the Br analog and its reactions. Later, the scope was expanded to include the thermochemistry of the OH and Cl analogs, which will be recapitulated below. Dibble and colleagues (Lam et al., 2019b; Khiri et al., 2020; Lam et al., 2019a) concluded that the bimolecular reaction with CH_4 is of primary importance for the disappearance of $BrHg^{II}O^{\bullet}$: $BrHg^{II}O^{\bullet} + CH_4 \rightarrow BrHg^{II}OH + {}^{\bullet}CH_3$ (**Rxn G26**). Unlike $^{\bullet}Hg^{I}X$, $BrHg^{II}O^{\bullet}$ readily abstracts hydrogen atoms from saturated hydrocarbons and overcomes a modest energy barrier with a rate expression of $4.1 \times 10^{-12} \times \exp(-856/T)$ cm^3 $molecule^{-1}$ s^{-1} for $BrHg^{II}O^{\bullet} + CH_4$. Computational modeling suggested that $BrHg^{II}O^{\bullet}$ mimics the OH radical in terms of reaction selectivity. In addition to $BrHg^{II}O^{\bullet}$ abstract H from aliphatic hydrocarbons, it adds to the unsaturated bonds of olefins (such as the biogenic isoprene), NO (**Rxn G29**) and NO_2 (**Rxn G30**) and interacts with CO (**Rxn G27**). The addition of NO produces $BrHg^{II}ONO$, which is susceptible to photolytic decomposition to predominantly $BrHg^{II}O^{\bullet}$, whereas the addition of NO_2 promptly produces peroxynitrites of the $BrHg^{II}OONO$ type, which are likely isomerized to $BrHg^{II}ONO_2$. Whether bromomercuric nitrate is photolabile in the troposphere is not yet known. Another source of $BrHg^{II}OH$ is the reaction of $BrHg^{II}O^{\bullet}$ with aldehydes (e.g. HCHO, **Rxn G28**). The pathway for the $BrHg^{II}O^{\bullet}$ + HCHO reaction bifurcates into two processes leading to different products (Khiri et al., 2020). The dominant reaction is H-abstraction, leading to $BrHg^{II}OH$ and a formyl radical. The alternative route involves the addition of the oxygen atom in $BrHg^{II}O^{\bullet}$ to the carbon center in HCHO to form a methoxy radical, which eliminates a hydrogen atom unimolecularly or in the presence of O_2 to form a formate salt ($BrHg^{II}OCHO$). Secondary chemistry initiated by O_2 after the addition of $BrHg^{II}O^{\bullet}$ to a carbon double bond (such as in ethene) also involves alkoxy radicals formed after titration of the primary peroxyl radical formed by NO. The atmospheric fate of these mercuric alkoxy and alkyl peroxyl radicals (with one Hg–O bond) is similar to the general characteristics

tog bort: -
formaterade: Kondenserad med 0,3 pt
Formaterat: Avstånd Efter: 3 pt
tog bort: <object>…The HgO + O2 reaction is exothermic but is subject to a barrier, which, using transition state theory, giv… [324]
tog bort: Taken together, this information indicates
formaterade … [325]
tog bort: in the troposphere, but that
formaterade: Teckenfärg: Blå, Inte Expanderad med / Kondenserad med
tog bort: extended at cryogenic conditions (T <
formaterade: Teckenfärg: Blå, Inte Expanderad med / Kondenserad med
tog bort:) in the
formaterade: Kondenserad med 0,1 pt
Formaterat: Avstånd Efter: 6 pt
tog bort: low lying
formaterade: Kondenserad med 0,1 pt
tog bort: stratosphere where HgO has more abundant sources than that controlled by Hg^{II} radical species photolysis (see below). Analogous to the photolysis of Hg^{I} compounds, the quantum yield for the photo-dissociation of Hg^{II} compounds is assumed to be at unity.¶
formaterade: Kondenserad med 0,3 pt
tog bort: marginal
formaterade: Kondenserad med 0,3 pt
tog bort: The computational calculations
formaterade … [326]
tog bort: $BrHg^{II}O^{\bullet}$.
formaterade … [327]
tog bort: have
formaterade … [328]
tog bort: , overcoming
formaterade … [329]
tog bort: suggests
formaterade: Kondenserad med 0,3 pt
tog bort: that
tog bort: abstracts
formaterade: Kondenserad med 0,3 pt
formaterade … [330]
tog bort: while
formaterade … [331]
tog bort: to be
formaterade: Kondenserad med 0,3 pt
tog bort: .
formaterade … [332]
tog bort: primarily formed
formaterade … [333]

of organic oxidation in the atmosphere described in detail elsewhere (Finlayson-Pitts and Pitts, 2000). However, apart from the CH_4 reaction, the interaction between $BrHg^{II}O^{\bullet}$ and VOCs is considered limited in the atmosphere.

Analogous to $^{\bullet}OH + CO$, the reaction between $BrHg^{II}O^{\bullet}$ and CO is not a simple bimolecular reaction. However, the intermediate BrHgOCO is much less stable than HOCO with respect to the release of CO_2. The very weakly bound BrHgOCO promptly dissociates in $^{\bullet}Hg^{I}Br + CO_2$ (Khiri et al., 2020). The above reaction is highly exothermic (> 280 kJ mol^{-1}); therefore, the product $^{\bullet}Hg^{I}Br$ can be chemically activated to the extent that it increasingly decomposes into atoms. The importance of this Hg reduction channel has been identified as difficult to constrain theoretically, as the shape of the potential energy surface is unfavorable for the application of standard kinetic simulation methods. Nevertheless, by using an inverse Laplace transformation method, Khiri et al. (2020) calculated the range for the rate coefficient at two temperatures: $(9.4 - 52) \times 10^{-12}$ cm^3 $molecule^{-1}$ s^{-1} at 298 K and $(3.8–29) \times 10^{-12}$ cm^3 $molecule^{-1}$ s^{-1} at 220 K. These data are the basis for the current inclusion of the $YBr^{II}O^{\bullet} + CO \rightarrow {}^{\bullet}Hg^{I}Y + CO_2$ reaction in chemical models (Shah et al., 2021; Saiz-Lopez et al., 2022), with an average expression of $6.0 \times 10^{-11} \times \exp(-550/T)$ cm^3 $molecule^{-1}$ s^{-1}. With this numerical characterization, the $YHg^{II}O^{\bullet} + CO$ reaction becomes profoundly important when implemented in simulations, as it largely counteracts the effect of the $^{\bullet}Hg^{I}X + O_3$ reaction, thereby extending the predicted lifetime of Hg^0 in the troposphere. However, other candidates have emerged that, like CH_4, may react with $HOHg^{II}O^{\bullet}$ to form the stable $Hg(OH)_2$ molecule, namely, water vapor. The reaction $HOHg^{II}O^{\bullet} + H_2O \rightarrow Hg(OH)_2 + {}^{\bullet}OH$ (**Rxn G60**) is nearly thermoneutral due to the stability of $Hg(OH)_2$ ($\Delta H_f = -226$ kJ mol^{-1}; Wang and Andrews, 2005) and Saiz-Lopes et al. (2022) give a temperature-dependent rate constant expression of $5.3 \times 10^{-12} \times \exp(-2894/T)$ cm^3 $molecule^{-1}$ s^{-1} without further details. Since both the calculated $HOHg^{II}O^{\bullet} + H_2O$ rate coefficient and the $H_2O(g)$ mixing ratio vary considerably across the troposphere, the $HOHg^{II}O^{\bullet}$ loss due to this channel may largely exceed or fall below the more monotonic rate of hydrogen abstraction by $HOHg^{II}O^{\bullet}$ from CH_4, depending on the circumstances. The fate of $HOHg^{II}O^{\bullet}$ is thus influenced by several exit channels (Edirappulige et al., 2023), none of which have been investigated experimentally. Particularly, the uncertainty of the CO and H_2O reactions makes it difficult to determine the importance of OH-initiated oxidation to the atmospheric Hg^{II} pool.

Can mercury species nucleate in the atmosphere?

While Hg^0 vapor has been observed to nucleate homogeneously in laboratory experiments conducted under high pressures (Martens et al., 1987), neither Hg^0 atoms nor GOM species, which are molecular rather than ionic entities, have a vapor pressure that is sufficiently low and a concentration that is sufficiently high in the atmosphere to nucleate new particles by simple condensation (Murphy et al., 1998). However, the concerted action of a foreign gas-phase precursor (e.g., amines, highly oxygenated organics, sulfuric, nitric, and iodic acids, etc.; Lehtipalo et al., 2025; He et al., 2021) or heterogeneous condensation on pre-existing nuclei of subcritical or critical size may result in the transfer of GOM species to aerosols (Ariya et al., 2015). Measurements of individual aerosol particles have shown that a significant portion of the aerosols present in the lowest kilometers of the stratosphere contain small yet measurable amounts of Hg^{II}. Interestingly, Hg^{II} is empirically correlated with bromine and iodine in these organic-sulfate-type particles and has the highest relative concentrations in the stratosphere near the tropopause. However, Hg^{II} is rarely observed in the relatively pure sulfuric acid particles characteristic of the main stratospheric aerosol (Junge) layer (Murphy et al., 2006). While bromine and iodine aerosols are also observed throughout the troposphere, no Hg can be detected in these aerosols, indicating that the Hg^{II} products can evaporate rapidly into GOM species (Murphy et al., 2014). Both Br and I, with oceans as the primary sources, are injected into the stratosphere, where they account for most of the ozone depletion caused by halogens (Koenig et al., 2020). It is challenging to determine whether there is a causal mechanistic relationship and, if so, what can explain the observed correlation between aerosol Hg, Br, and I. Nevertheless, a plethora of clues can be utilized to assemble a coherent narrative. First, the combination of $Br^{\bullet}$ (**Rxn G14a**) and O_3 (**Rxn G22**) constitutes a significant oxidation pathway for Hg^0 to Hg^{II}. However, as mentioned above, there is no firm evidence that this reaction pathway is relevant when $I^{\bullet}$ is a substitute for $Br^{\bullet}$. Second, the gas phase system $I^{\bullet} + O_3 + H_2O$ has been identified as a substantial precursor of particle nucleation (as iodine oxoacids) and growth that is highly important within marine (Sipilä et al., 2016) and stratospheric (Koenig et al., 2020) environments. Third, the condensed phases Br^- and I^- act as robust complexing ligands (**Table 1**) for the GOM to partition into the aerosol, thereby impeding its recycling back to the gas phase. Presumably, the fundamentals are similar for a particle formation event observed in the context of the polar spring partial AMDE

tog bort: By analogy with
formaterade: Kondenserad med 0,3 pt
tog bort:), and
formaterade: Kondenserad med 0,3 pt
tog bort: in
formaterade: Kondenserad med 0,3 pt
tog bort: reaction
formaterade: Kondenserad med 0,3 pt
formaterade: Kondenserad med 0,3 pt
tog bort:)
formaterade: Kondenserad med 0,3 pt
tog bort: the averaged
formaterade: Kondenserad med 0,3 pt
tog bort: directly
tog bort: very
formaterade: Kondenserad med 0,3 pt
formaterade: Teckenfärg: Dekorfärg 2, Kondenserad med 0,3 pt
formaterade: Kondenserad med 0,3 pt
formaterade: Kondenserad med 0,3 pt
tog bort: ,
formaterade: Kondenserad med 0,3 pt
tog bort: the
formaterade: Kondenserad med 0,3 pt
tog bort:
formaterade: Kondenserad med 0,3 pt
tog bort: 2023b
formaterade: Kondenserad med 0,3 pt
tog bort: and especially
formaterade: Kondenserad med 0,3 pt
tog bort: reaction
tog bort: the
formaterade: Kondenserad med 0,3 pt
formaterade: Kondenserad med 0,3 pt
tog bort: **Gas to nucleation**¶ **Oxidized Hg**
formaterade: Teckensnitt:9,5 pt, Teckenfärg: Blå
tog bort: **have properties that make them suitable for nucleation processes, such as being ionic solids at equilibrium under atmospheric conditions, which makes them improbable to evaporate from nucleating clusters (Ariya et al., 2015). They can condense, either**
Formaterat: Avstånd Efter: 0 pt
formaterade: Teckenfärg: Blå, Kondenserad med 0,4 pt
formaterade: Teckenfärg: Blå, Kondenserad med 0,4 pt
tog bort: onto
formaterade: Teckenfärg: Blå, Kondenserad med 0,4 pt
tog bort: . A
formaterade: Teckenfärg: Blå, Kondenserad med 0,3 pt
tog bort: associated with
formaterade: Teckenfärg: Blå, Kondenserad med 0,3 pt

in East Antarctic pack ice by Humphries et al. (2015), where the formation of 3 nm particles lags the phase of gaseous Hg^0 loss in the air mass. Observations over a decade in the Canadian high Arctic region clearly show that PBM transmitted by KCl-coated denuders dominated Hg^{II} fractionation over the GOM during the early period of AMDEs, where the highest frequencies of depleted Hg^0 occurred between –45 and –40 °C, whereas during the late period of higher temperatures and lower particulate concentrations (AMDEs then occurred most frequently between –25 and –20 °C), Hg^{II} fractionation shifted to a clear dominance of the GOM (Steffen et al., 2014). The KCl-denuder technique used cannot selectively separate nano- to submicron-sized mercuric halide clusters completely from GOM (Ghoshdastidar and Ariya, 2019), which, along with the other nonsystematic bias of the method previously mentioned, makes separation into Hg^{II} fractions tentative. The measurement methodology deficiencies make establishing empirical gas–particle partitioning schemes highly uncertain (Amos et al., 2012; Rutter and Schauer, 2007b, a). This complicates the assumption and verification of model parameterization, which relies on accurate atmospheric concentration measurements. For example, the release of Hg^{II} from aerosols into the gas phase is assumed to be entirely in the form of the tropospherically stable $HgCl_2$ molecule (Shah et al., 2021). Coupling an oxidized Hg vapor source or a reactor where oxidized Hg is formed by gas-phase oxidation of Hg^0 to particle characterization instruments (such as scanning mobility or optical particle sizers) provides conclusive evidence that mercuric halide molecules readily form clusters that undergo particle growth (Ghoshdastidar and Ariya, 2019). In experimental studies of the vapor-phase oxidation of volatile Hg forms Hg^0 and $(CH_3)_2Hg$, aerosol-phase products have been detected (Raofie et al., 2008; Raofie and Ariya, 2004; Sun et al., 2016; Niki et al., 1983a; Niki et al., 1983b). For example, using a scanning mobility particle sizer, Sun et al. (2016) found that well below the saturation pressure of HgX_2, reaction products from X (Cl and Br)-initiated Hg^0 vapor oxidation began to generate particles that grew from the Aitken nuclei range (few tens of nm) into the accumulation range (> 100 nm) over the course of a few hours (**Fig. 6**). **Fig. 7** summarizes the main elements of the Hg gas phase chemistry in the troposphere.

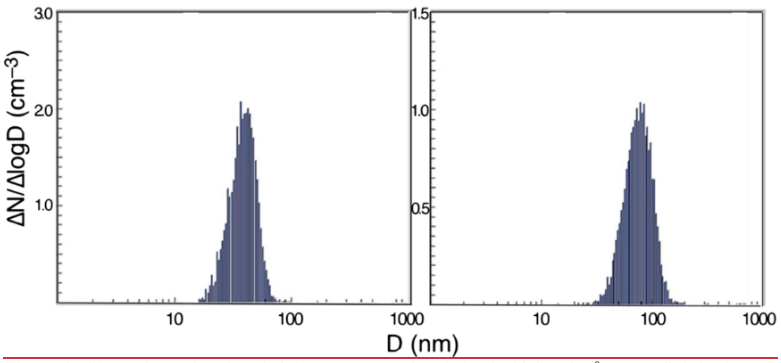

Figure 6. Particle growth of the reaction products from the halogen atom (X = Cl, Br) induced oxidation of Hg^0 vapor studied after the same degree of Hg^0 conversion (~75%, 5–8 ppb) but at different reaction times a and b (~45 min, Hg^0 + Br and ~4 h, Hg^0 + Cl, respectively). Adopted from Sun et al. (2016).

tog bort: has been observed
tog bort: the
formaterade: Teckenfärg: Blå, Kondenserad med 0,3 pt
tog bort: ,
formaterade: Teckenfärg: Blå, Kondenserad med 0,3 pt
formaterade: Teckenfärg: Blå, Kondenserad med 0,3 pt
tog bort: 3 nm particle
formaterade ... [334]
tog bort: (Humphries et al., 2015).
formaterade ... [335]
tog bort: High
formaterade: Kondenserad med 0,3 pt
tog bort: dominate
formaterade ... [336]
tog bort: occur
formaterade: Kondenserad med 0,3 pt
tog bort: °C, while
formaterade: Kondenserad med 0,3 pt
tog bort: occur
formaterade: Kondenserad med 0,3 pt
tog bort: °C) the
formaterade: Kondenserad med 0,3 pt
tog bort: has
formaterade ... [337]
tog bort: the
formaterade: Kondenserad med 0,3 pt
tog bort: it highly uncertain to establish
formaterade: Kondenserad med 0,3 pt
tog bort: -
formaterade ... [338]
tog bort: assuming that
formaterade ... [339]
tog bort:
formaterade: Kondenserad med 0,3 pt
tog bort: the
formaterade ... [340]
formaterade ... [341]
tog bort: (yield of HgX_2 > Hg_2X_2)
formaterade: Kondenserad med 0,4 pt
tog bort:). Induced
formaterade: Kondenserad med 0,4 pt
tog bort: –
formaterade ... [342]

5.1.5 Chemical transformation of Hg in the lower stratosphere

In the lower stratosphere, chlorine atoms and hydroxyl radicals initiate most of the oxidation of Hg^0. This is because the concentrations of these species increase with altitude, and the channels in which they are contained produce more photostable products, such as $Hg(OH)_2$ and $HgCl_2$ (**Fig. 8a, b**). The prediction of these model calculations that Hg^0 converts to long-lived (photostable) oxidized forms and thus leads to a higher RM/TAM ratio is supported by hundreds of profile measurements made with an Airbus 340-600 passenger aircraft in intercontinental traffic as an upper troposphere-lowermost stratosphere observatory (Slemr et al., 2018). In addition to the frequently observed higher RM/Hg^0 ratios, a steep decrease in the Hg^0 mixing ratio occurs when crossing the tropopause. In the stratosphere, the latter ratio decreases to 0.25–0.7 ng m^{-3} (STP), measured up to an altitude of 4 km (Slemr et al., 2018). The results of both studies above show a more than tenfold increase in the lifetime of Hg^0 in the lower stratosphere compared with that in the troposphere. The chemical lifetime of Hg^0 increases and approaches 10 years as the concentration in the lower stratosphere bound by the ozone layer increases. (Saiz-Lopes et al, 2025).

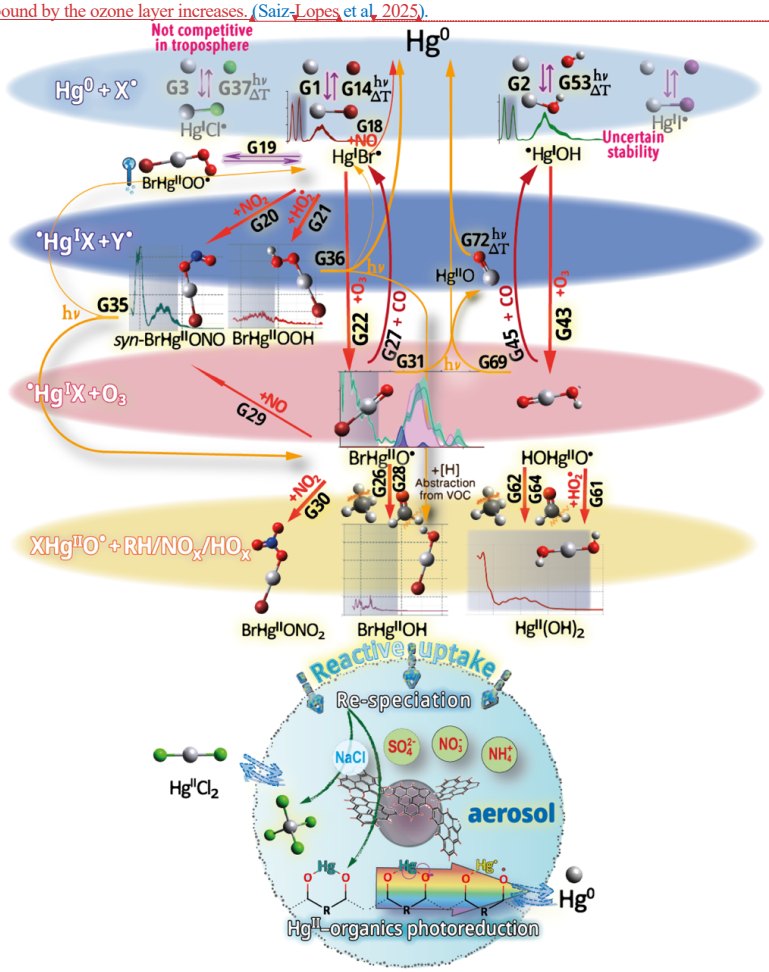

Figure 7. Outline of tropospheric gas-phase Hg chemistry. The reactions of the type Hg + XO• (X = O_2, Br and NO_2) directly leading to mercuric species are, for the (varying) reasons given in the text, impossible processes in the homogeneous gas phase. In the troposphere, gas-phase oxidation of Hg^0 in termolecular reactions is initiated by a few radicals in which Br atoms and, with some uncertainty, OH radicals have the

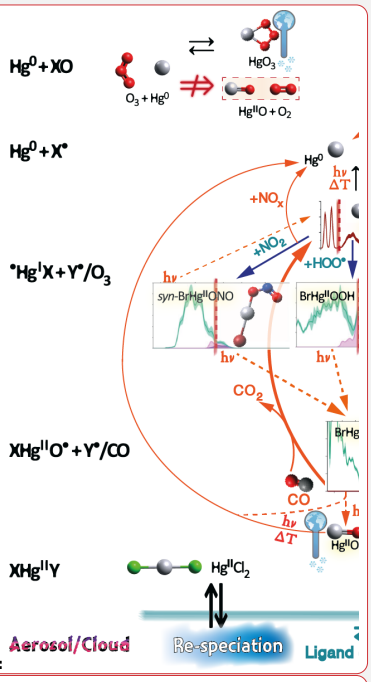

tog bort: 5.1.5 Lower stratospheric conditions¶
formaterade: Kondenserad med 0,2 pt
tog bort: the
formaterade: Kondenserad med 0,2 pt
tog bort: atom
formaterade ... [343]
tog bort: However, the increasing photon flux as one moves up through the ozone layer increases the photolysis rate
formaterade: Teckenfärg: Blå, Kondenserad med 0,2 pt
tog bort: $Hg(OH)_2$ and $HgCl_2$, so
formaterade ... [344]
tog bort: above the ozone maximum extends
formaterade ... [345]
tog bort: Lopez
formaterade: Teckenfärg: Blå, Kondenserad med 0,2 pt
tog bort: ., 2022
formaterade: Teckenfärg: Blå, Kondenserad med 0,2 pt
tog bort:
formaterade ... [346]
tog bort: Reactions
formaterade: Kondenserad med 0,1 pt
tog bort:
formaterade: Kondenserad med 0,1 pt
tog bort: of
formaterade ... [347]

greatest importance, leading to the formation of thermally and photolytically labile mercurous radical species (i.e., $^{\bullet}Hg^{I}Br$ and $^{\bullet}Hg^{I}OH$). These Hg^{I} species are further oxidized to Hg^{II} not only by ozone but also by radicals (in descending order of abundance), such as NO_3 > HO_2 > BrO ~ OH. NO cannot efficiently oxidize Hg^{I} to Hg^{II} but instead induces thermal reduction, e.g., $^{\bullet}Hg^{I}Br + NO \rightarrow Hg + BrNO$. As O_3 is a closed shell species, it directly oxidizes $^{\bullet}Hg^{I}Br$/$^{\bullet}Hg^{I}OH$ to mercuric radical species $YHg^{II}O^{\bullet}$; for example, $HOO^{\bullet}$ and $BrO^{\bullet}$ are added to linear mercuric molecules (e.g., $BrHg^{II}OOH$) that are photolytically labile while those resulting from, e.g., NO_2, $^{\bullet}OH$ and $Br^{\bullet}$ are more photostable. The photolysis of many of the major thermally more stable Hg^{II} species, such as syn-$BrHg^{II}ONO$, $BrHg^{II}OOH$ and $BrHg^{II}OH$, leads to several species-specific photoproducts (potentially Hg^0, Hg^{I} species or $YHg^{II}O^{\bullet}$) with various yields (**Table 3**). The remarkably thermally stable YHgO radical exhibits versatile thermochemistry, such as abstracting hydrogen from VOCs, adding to double bonds and being reduced by CO. Some of its bimolecular reactions, such as with CH_4, directly form fairly stable Hg^{II} compounds such as $Hg(OH)_2$, and $BrHg^{II}OH$. When these encounter hydrometeors, they dissolve and are re-speciated by rapid equilibration with major aqueous ligands. This leads to the formation of strong complexes, e.g., by Cl^- to chloromercurates $HgCl_2$, $HgCl_3^-$ and $HgCl_4^{2-}$. Thus, molecular $HgCl_2$ is released into the gas phase when the particle dries. $HgCl_2$ is completely photostable and is enriched in the troposphere (a major Hg^{II} species), with dry and wet deposition as the only sink processes.

5.1.6 Chemical transformation of Hg in the upper stratosphere

The presence of UVC radiation above the ozone layer maximum opens completely new reaction pathways for redox cycling of stratospheric Hg. New insights into its conceptual stratospheric chemistry (Saiz-Lopez et al., 2022; 2025) and associated anomalous isotope fractionation (Sun et al., 2022; Fu et al., 2021) have been presented. The gas-phase oxidation of Hg^0 is rapid (10^3–10^4 times faster than in the troposphere, Saiz-Lopez et al., 2022) and is driven entirely by the oxidation of electronically excited Hg atoms by one of the major constituents of air, O_2.

$Hg^0(^3P)$ reaction with elemental oxygen

Already involved in the discovery of the element oxygen toward the end of the 18th century, the chemistry of the system of Hg + O_2 has exhibited intricate complexity. These early observations, made independently in northern and western Europe, address an important aspect of the thermochemistry of the system. A direct combination of liquid Hg and O_2 occurs just below the boiling point of Hg to form HgO, but the reaction is reversed above 400 °C. While the reaction of ground-state Hg vapor ($Hg(^1S)$) with O_2 is negligibly slow (Hall et al., 1995), deep UV light excitation of singlet to triplet Hg atoms ($Hg(^3P)$) leads to significant homogeneous reactions with O_2. In contrast, further excitation of $Hg(^1P_1)$ in blue and subsequent reaction with O_2, as discussed above, is unlikely to result in the net formation of mercury oxides. The gas-phase reactions of $Hg(^3P)$ have been studied in the laboratory since 1922 (Cario and Franck, 1922). In particular, O_2/air has been used as a route for ozone synthesis since the mid-1920s (Dickinson and Sherrill, 1926). While larger quantities of ozone are produced by Hg photochemistry (photo-sensitization), the elemental vapor is oxidized more slowly, resulting in the deposition of a yellow–brown film of solid HgO on the reactor walls downstream of the irradiation zone (Volman, 1953). However, the $Hg(^3P) + O_2$ mechanism is unclear because of the controversy regarding the molecular intermediates, and whether there is a direct route from $Hg(^3P)$ to gaseous HgO or oxidation starting from the $Hg(^1S)$ state remains undetermined (Callear et al., 1959; Volman, 1953; Hippler et al., 1978; Morand and Nief, 1968). The dark homogeneous reaction $Hg(^1S) + O_3 \rightarrow HgO + O$, supported by early researchers (Callear et al., 1959; Volman, 1953; Pertel and Gunning, 1959) as driving the oxidation in the photochemical experiments, can now be rejected for the reasons discussed above in **Section 5.1.1**. Considering more recent results (Wang and Andrews, 2005; Hall, 1995), e.g., those obtained by refined computational chemistry, the following mechanism seems to be the most plausible:

$$Hg(^1S_0) + h\nu\ (\lambda{=}253.7\ nm) \rightarrow Hg(^3P_1) \quad \text{(Rxn G4)}$$

$$Hg(^3P_1) \rightarrow Hg(^1S_0) + h\nu\ (\lambda{=}253.7\ nm) \quad \text{(Rxn G9)}$$

$$Hg(^3P_1) + N_2 \rightarrow Hg(^3P_0) + N_2 \quad \text{(Rxn G10)}$$

$$Hg(^3P_1) + O_2 \xrightarrow{M} HgO_2^* \xrightarrow{M} OHgO \begin{cases} \rightarrow Hg(^1S_0) + O_2(^3\Sigma_u^+) \\ \rightarrow HgO(^3\Pi) + O(^3P) \end{cases} \quad \text{(Rxn G12a,b)}$$

$$Hg(^3P_0) + O_2 \rightarrow Hg(^1S_0) + O_2(^3\Sigma_u^+) \quad \text{(Rxn G11)}$$

$$O_2(^3\Sigma_u^+) + O_2 \rightarrow O_3 + O(^3P) \quad \text{(Rxn 5)}$$

$$O_2 + O(^3P) \rightarrow O_3 \quad \text{(Rxn 6)}$$

Photoexcitation (**Rxn G4**) has been discussed, but its reverse (**Rxn G9**), i.e., the spontaneous emission of a photon that brings $Hg(^3P_1)$ to the ground state, is spin-forbidden, and the radiative lifetime is relatively long (0.12 µs corresponding to $k_9 = 8.4 \times 10^6\ s^{-1}$). The quenching of $Hg(^3P)$ states (i.e., **Rxn G9 & G10 – G12a**) for several gases has been studied, with $Hg(^3P_1)$ atoms being 21.3 kJ mol^{-1} more energetic than $Hg(^3P_0)$ atoms. The two main constituents of air play different roles in the quenching process, with N_2 almost exclusively deactivating $Hg(^3P_1)$ to $Hg(^3P_0)$ with $k_{G10} = 5.1 \times 10^{-11} \exp(-701/T)\ cm^3\ molecule^{-1}\ s^{-1}$, while O_2 quenches both $Hg(^3P_1)$

formaterade ... [348]
tog bort: .
formaterade ... [349]
tog bort: the action of mainly
tog bort: , HOO,
tog bort: ,
formaterade ... [350]
tog bort: abundant inorganic
formaterade ... [351]
formaterade ... [352]
formaterade ... [353]
tog bort: etc. It should be noted that NO_x (NO and to a l ... [354]
formaterade ... [355]
tog bort: induce
tog bort: .
formaterade ... [356]
formaterade ... [357]
tog bort: • while
formaterade ... [358]
tog bort: .
formaterade ... [359]
tog bort: .
formaterade ... [360]
tog bort: as shown
formaterade ... [361]
tog bort: and NO_2
formaterade ... [362]
tog bort: and $YHg^{II}ONO_2$.
formaterade ... [363]
tog bort: equilibrations
tog bort:
formaterade ... [364]
formaterade ... [365]
tog bort: .
formaterade ... [366]
tog bort: ⁻
formaterade ... [367]
tog bort: up
formaterade ... [368]
tog bort:)
formaterade ... [369]
formaterade ... [370]
Formaterat ... [371]
tog bort: **Reactions**
formaterade ... [372]
tog bort: **electronically excited state Hg^0**
formaterade ... [373]
tog bort: the
tog bort: …10^4 times faster than in the troposphere, Saiz ... [374]
tog bort: **molecular**
formaterade ... [375]
tog bort: towards…oward the end of the 18th century, the ... [376]
tog bort: further out …n the ... [377]
tog bort: those with …/air has been used as a route to… ... [378]
tog bort: In any case, considering
formaterade ... [379]
tog bort: O_2^*→
formaterade ... [380]
tog bort: 5)↵ ... [381]
tog bort: 6
tog bort: 7
tog bort: The photoexcitation…hotoexcitation (**Rxn G4**) ... [382]
tog bort: …….**Rxn G6…9 & G10 – G12a**) for a numbe ... [383]

and Hg($^3P_0$) directly to Hg($^1S_0$) with k_{G12a} and k_{G11} values of 1.3×10^{-10} (T/300)$^{-0.29}$ and 1.8×10^{-10} (T/300)$^{0.167}$ cm^3 molecule^{-1} s^{-1}, respectively. In the stratosphere (T = 240 K), the k_{G12a}/k_{G10} ratio is ~50, suggesting that O_2 is a much better physical quencher than N_2, which is true throughout the atmosphere. Of primary interest here, however, is the spin-conserving **Rxn G12b**, which allows the oxidation of Hg and is overall nearly thermoneutral (exothermic by ~6 kJ mol^{-1}), yielding HgO ($^3\Pi$) with low vibrational energy, as noted by Saiz-Lopez et al. (2022), which is important for increasing the lifetime of this weakly bound molecule. First tentatively identified as an intermediate in a low-temperature UVC-irradiated matrix consisting of Hg, O_2 and H_2 yielding discrete Hg(OH)$_2$ molecules (Wang and Andrews, 2005), linear OHg^{II}O as the initial product is calculated to be 275 kJ mol^{-1} lower in energy than the reactants Hg(^{3}P) + O_2 and therefore sufficiently stable over time to participate in barrier rearrangement to Hg(^{1}S) + O_2* alongside dissociation to HgO and O. Experimental data suggest that the branching ratio between **Rxn G12b** and **G12a** is low, making oxidation the minor process. Sun et al. reported a quantum yield of up to a few percent for the oxidation step in experiments using synthetic air at 46–88 kPa and 233–298 K (Sun et al., 2022). Callear et al. (1959) observed a faster reaction in air than in O_2, suggesting that Hg($^3P_0$) may also react with O_2 to form HgO, analogous to Hg($^3P_1$).

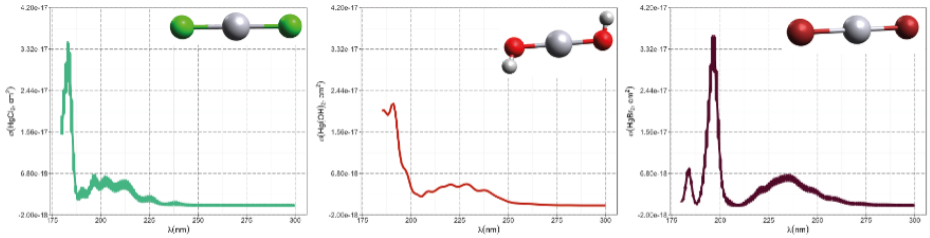

Figure 8. Computational absorption spectra of $HgCl_2$, Hg(OH)$_2$ and $HgBr_2$. Data from Saiz-Lopez et al. (2022) and Sitkiewicz et al. (2019).

Chemical turnover of HgO in the stratosphere. Formation of $HgCl_2$

The instability of the HgO molecule and its unimolecular decay to elemental Hg was discussed earlier. Produced in greater quantities by rapid photosensitized but nearly thermoneutral oxidation, the initially vibrational cold stratospheric HgO is more likely to survive in the colder part of the upper stratosphere until it can react further into less unstable oxidized forms. The most abundant trace gases in this part of the stratosphere are water vapor, hydrochloric acid and ozone (Calvert et al., 2015). H_2O can oxidize Hg(^{3}P) (Gunning and Strausz, 1963; Gruss et al., 2017) and may react with HgO:

$$Hg(^3P) + H_2O \rightarrow {}^{\bullet}Hg^{I}OH + H^{\bullet} \qquad \text{(Rxn G13)}$$

$$HgO(^3\Pi) + H_2O \xrightarrow{M} Hg(OH)_2 \rightarrow {}^{\bullet}Hg^{I}OH + HO^{\bullet} \qquad \text{(Rxn G72)}$$

However, the reaction of Hg(^{3}P) + H_2O is so exothermic (~200 kJ mol^{-1}) that the product $^{\bullet}Hg^{I}OH$ can be expected to be vibrational hot and dissociate rapidly with less time for further bimolecular oxidation. A possible reaction between water vapor and HgO is strongly exothermic if the final product is singlet Hg(OH)$_2$ but weakly endothermic if the triplet form is formed instead. Nevertheless, there is currently no evidence to suggest that HgO can be converted to Hg(OH)$_2$ in a direct reaction with moisture. According to Saiz-Lopez et al. (2022), the reaction between stratospheric HgO and HCl is fast enough (close to the collision limit) to allow some Hg^{II} to be converted to $^{\bullet}Hg^{I}Cl$ rather than being reduced to elemental vapor:

$$HgO + HCl \rightarrow {}^{\bullet}Hg^{I}Cl + {}^{\bullet}OH \qquad \text{(Rxn G73, } \Delta H_R = -61 \text{ kJ mol}^{-1}\text{)}$$

As with $^{\bullet}Hg^{I}OH$ and $^{\bullet}Hg^{I}Br$, the reaction between $^{\bullet}Hg^{I}Cl$ and O_3 is barrierless and rapid, in this case $ClHg^{II}O^{\bullet}$ is produced:

$$^{\bullet}Hg^{I}Cl + O_3 \rightarrow ClHg^{II}O^{\bullet} + O_2 \qquad \text{(Rxn G43)}$$

Of the versatile tropospheric chemistry presented for $YHg^{II}O^{\bullet}$, hydrogen abstraction (**Rxn G44**) is still important in the stratosphere, and is again dominated by CH_4 (which is not photolyzed and reacts with the OH radical as the main sink). The product $ClHg^{II}OH$, like $ClHg^{II}O^{\bullet}$, is further converted by reaction with HCl to $HgCl_2$ (**Rxn G46 & G47**), which is the most thermally and photolytically stable of the Hg^{II} molecules present. The photolytic lifetime of $HgCl_2$ in the upper stratosphere is close to one hour and about twice that of Hg^0, so the oxidized Hg species dominate (of which ≥ 90% is $HgCl_2$). The Hg^{I} concentration increases rapidly above 50 km with increasing UVC photon flux, so the ratio $^{\bullet}Hg^{I}Cl/Hg^{II}Cl_2$ approaches unity at 60 km. An overview of the gas-phase Hg chemistry in the upper stratosphere is given in **Fig. 9** below.

tog bort: ratio
tog bort: ,
tog bort: less energetic
formaterade: Teckenfärg: Blå
tog bort: with
tog bort: observed
tog bort: %
tog bort: –
tog bort: –
tog bort: has been
tog bort: larger
tog bort: the
tog bort: ,
tog bort: producing
tog bort: •:
tog bort: , which
tog bort: remains the reaction
tog bort: From insignificant, the
tog bort: rises
tog bort: the
tog bort: stratospheric

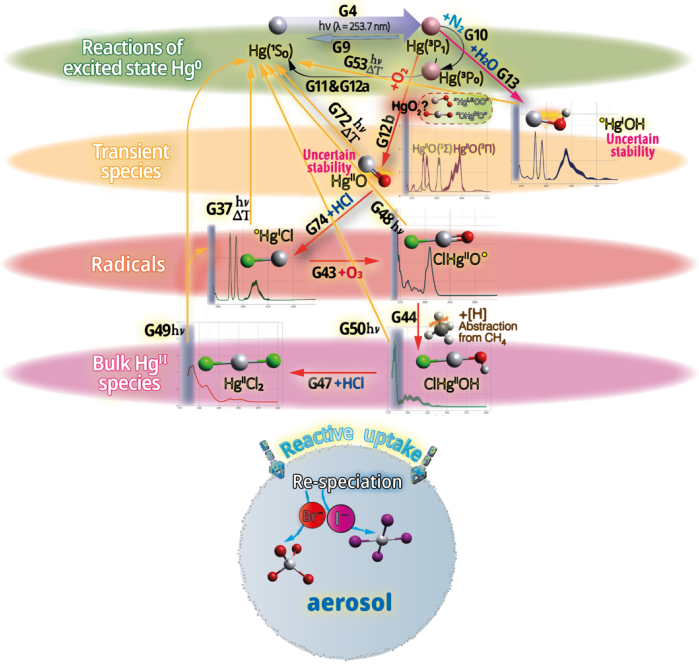

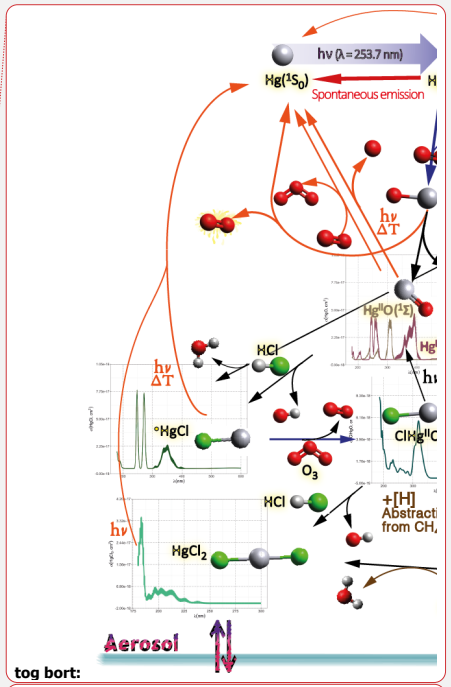

Figure 9. At approximately 35 km, the stratosphere begins to contain actinic radiation, which can electronically excite Hg (at 253.7 nm), but below it is absorbed by O_3 in the Hartley bands (with a maximum at 254 nm). Electronically excited Hg^0 reacts primarily with O_2, with one of the exit channels leading to the formation of HgO via the intermediate $OHg^{IV}O$. Before HgO can fully decompose into elements, it reacts further via secondary HCl-driven fast chemistry to $HgCl_2$, the major constituent of Hg in the mid-upper stratosphere. A 2:1 steady state between $HgCl_2$ and Hg^0 occurs because the former photo dissociates more slowly than photosensitized Hg oxidizes, both at significant rates (Saiz-Lopez et al. 2022). The reactive uptake in aerosols, followed by Hg^{II} complexation with the heavier halides, reflects the observed situation in the lower stratosphere (Murphy et al. 1998).

5.2 Organic species

5.2.1 Dimethylmercury

In addition to Hg^0, "supertoxic" DMHg is another volatile Hg species that exists in nature (Siegler et al., 1999). DMHg has a boiling point below 100 °C, a high vapor pressure and a Henry's law coefficient equivalent to that of Hg^0 (Schroeder and Munthe, 1998). Both DMHg and $MMHg^+$ species have been detected in ambient air (Lee et al., 2003; Bloom et al., 2005; Weiss-Penzias et al., 2018; Baya et al., 2015; Zhang et al., 2019a). DMHg has no known sources in the atmosphere. Its occurrence is due mainly to volatilization from surface waters, where it is transported by upwelling conditions from the deep sea, where it is formed under anoxic conditions (Conaway et al., 2009; Pongratz and Heumann, 1999). Polar sea ice harbors Hg-methylating microbes and is thought to be a source of DMHg that can be degassed as ice melts (Schartup et al., 2020). Recently, DMHg has been measured in marine air and corresponding surface water and has an air–sea gas flux that is 1/30 of the magnitude of the simultaneously measured Hg^0 flux (He et al., 2022). The atmospheric transformation of DMHg is the main source of atmospheric $MMHg^+$ species (Sommar et al., 1997). DMHg vapor does not absorb actinic light (Terenin, 1934; Terenin and Prileshajewa, 1935) and is therefore not photolyzed in the planetary boundary layer, where it is only expected to be found (Sommar et al., 1996). DMHg appears to be prone to rapid gas phase transformation and, depending on the products formed, could be an important source of atmospheric $MMHg^+$ on a regional scale. However, in addition to $MMHg^+$ species (Niki et al., 1983a; Niki et al., 1983b), inorganic Hg compounds (Thomsen and Egsgaard, 1986; Sommar et al., 1997) have also been reported as products of radical reactions with DMHg. Aware of its acute toxicity (Siegler et al., 1999), it has been more than a quarter of a century since any laboratory kinetic and reaction mechanistic studies of the atmospheric gas-phase chemistry of DMHg have been reported and, in retrospect, some comments are worth making. There are three

tog bort:
tog bort: this
formaterade ... [384]
tog bort: about
formaterade: Kondenserad med 0,3 pt
formaterade: Kondenserad med 0,3 pt
tog bort: $OHg^{II}O$
formaterade: Kondenserad med 0,3 pt
tog bort: decay
formaterade: Kondenserad med 0,3 pt
tog bort: the
formaterade ... [385]
tog bort: .
formaterade: Teckensnitt:Inte Fet, Svenska, Kondenserad med 0,2 pt
Formaterat: Avstånd Efter: 6 pt
tog bort: the …supertoxic" DMHg is another volatile Hg species that exists in nature, namely DMHg classified as a 'supertoxic' chemical…(Siegler et al., 1999). In fact, …MHg has a boiling point below 100 °C…C, a high vapor pressure and a Henry's Law ... [386]
tog bort: due …o volatilization from surface waters, where it is transported by upwelling conditions from the deep sea, where it is formed under anoxic conditions (Conaway et al., 2009; Pongratz and Heumann, 1999). Polar sea ice harbors Hg-methylating microbes and is thought to be a source of DMHg that can be degassed as ... [387]
formaterade: Teckenfärg: Dekorfärg 2
tog bort: automatically …easured in marine air and corresponding surface water and shows…as an air- ... [388]
tog bort: ,…therefore, ... [389]

thermodynamically accessible bimolecular pathways that can potentially initiate the gas phase transformation of DMHg, where X• below denotes a radical oxidant:

$$CH_3HgCH_3 + X^\bullet \longrightarrow \begin{cases} \longrightarrow CH_3HgX + CH_3^\bullet \\ \longrightarrow CH_3HgCH_2^\bullet + HX \\ \longrightarrow CH_3Hg^\bullet + CH_3X \end{cases} \qquad \text{(Rxn G76 – G78)}$$

The existence of the CH_3Hg radical formed in the latter reaction was tentatively demonstrated in a matrix isolation study (Snelson, 1970). The small dissociation energy of the methylmercury bond of the radical (Kominar and Price, 1969) together with a predicted barrierless $CH_3Hg^\bullet \rightarrow {}^\bullet CH_3 + Hg$ reaction (Kallend and Purnell, 1964) suggest rapid decomposition to metallic Hg without time, e.g., a reaction with O_2 to form a methylmercury peroxyl radical ($CH_3HgOO^\bullet$). In contrast, a composite reaction such as $CH_3HgCH_3 + X^\bullet \rightarrow {}^\bullet Hg^{I}X + 2\,CH_3^\bullet$, which directly produces inorganic Hg, is endothermic and, therefore, less plausible. In a high-pressure study of the gas phase reaction between atomic F and DMHg of low atmospheric relevance, ~10% of the reacted DMHg was reported to be converted to CH_3F via the above substitution reaction (McKeown et al., 1983). However, a static FT–IR study of the Cl-initiated gas phase reaction in the presence and absence of O_2 at atmospheric pressure revealed the importance of the displacement reaction that generates CH_3HgCl. The remaining CH_3 group is converted to CH_3Cl in N_2 as a bath gas in a chain reaction that regenerates Cl atoms, whereas the end products of the group in air can be attributed to the self-reaction of the CH_3OO radical. The reaction $CH_3HgCH_3 + {}^\bullet OH$ was studied with the same static method by photolysis of a mixture of CH_3HgCH_3, ethyl nitrite, and NO in air, which primarily followed the displacement reaction. The rate constant of $\sim 2 \times 10^{-11}$ cm^3 molecule^{-1} s^{-1} indicates that the lifetime of DMHg in the planetary boundary layer with respect to the OH channel active during the day is a few to tens of hours. In the nocturnally active DMHg + $NO_3^\bullet$ reaction, studied by fast flow discharge technique with Hg/CI–MS detection (Sommar et al., 1996) and a static long path FT–IR system (Sommar et al., 1997), both CH_3 groups contained in DMHg react. A small but significant yield of Hg^0 was detected along with a product with m/z = 78 (CH_3ONO_2) after the reaction of DMHg and $NO_3^\bullet$ under fast flow discharge conditions, indicating that substitution had occurred. In the DMHg

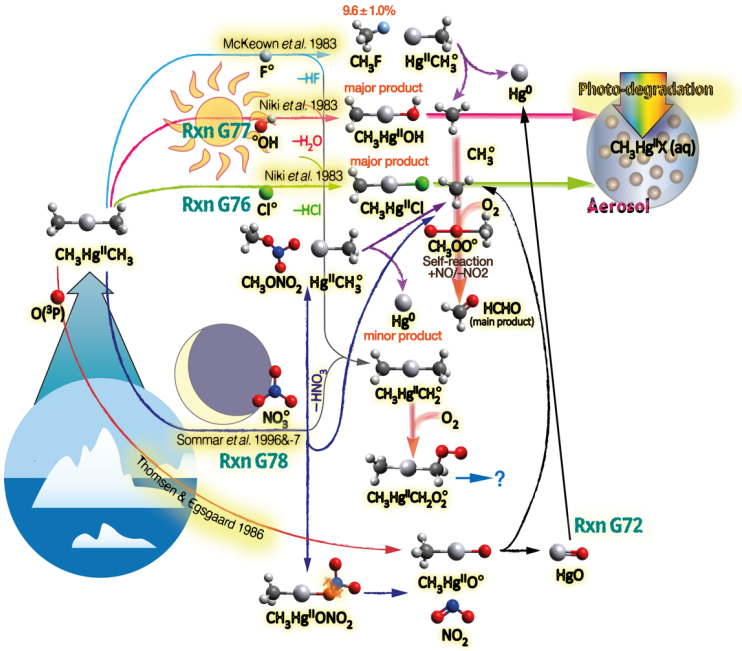

Figure 10. Schematics of the atmospheric fate of DMHg.

tog bort: can

tog bort: $\longrightarrow CH_3HgX + CH_3^\bullet$ $\longrightarrow CH_3HgCH_2^\bullet + HX$ →→→→ (Rxn G75 – G77 $\longrightarrow CH_3Hg^\bullet + CH_3X$

formaterade: Teckenfärg: Dekorfärg 2

formaterade: Kondenserad med 0,1 pt

tog bort: a

formaterade: Kondenserad med 0,1 pt

tog bort: for

formaterade: Kondenserad med 0,1 pt

tog bort: .

formaterade: Kondenserad med 0,1 pt

tog bort: $CH_3HgCH_3 + X^\bullet \rightarrow$

formaterade: Kondenserad med 0,1 pt

formaterade ... [390]

tog bort: producing

tog bort: are

formaterade: Kondenserad med 0,1 pt

formaterade: Kondenserad med 0,1 pt

tog bort: ,

formaterade: Kondenserad med 0,1 pt

tog bort: it was reported that

formaterade: Kondenserad med 0,1 pt

tog bort: is

formaterade: Kondenserad med 0,1 pt

tog bort: -

formaterade: Kondenserad med 0,1 pt

tog bort: shows

formaterade: Kondenserad med 0,1 pt

tog bort: while

formaterade: Kondenserad med 0,1 pt

tog bort: -

formaterade ... [391]

formaterade ... [392]

tog bort: also

formaterade: Kondenserad med 0,1 pt

tog bort: follows

formaterade: Kondenserad med 0,1 pt

tog bort: up

formaterade ... [393]

formaterade: Kondenserad med 0,1 pt

tog bort: by

formaterade: Kondenserad med 0,1 pt

tog bort: are accounted to

formaterade ... [394]

formaterade: Kondenserad med 0,1 pt

flyttade (infogning) [6]

formaterade: Kondenserad med 0,1 pt

tog bort: has occurred. Assessment of the stability of HgO(Shepler and Peterson, 2003) suggests that although the quantitative carbon balances for non-Hg-containing reaction products are close to unity for both the X = O (Thomsen ... [395]

+ O study, ~95% of the Hg in the converted DMHg was recovered as HgO downstream of the injector in the fast-flow experiments. In the DMHg + $NO_3^•$ batch reactor study, carbon and nitrogen mass balances ruled out the formation of $MMHg^+$ entities, and no Hg compound other than HgO could be considered an end product. Experimental evidence for the tentative intermediate $CH_3HgO^•$ (indicated in **Fig. 10**) is lacking. The rate constant of the nitrate radical reaction (**Rxn G78**) evaluated in the temperature range 258–358 K can be described by the Arrhenius expression $3.2 \times 10^{-11} \times \exp[-(1760 \pm 400)/T]$ cm^3 molecule^{-1} s^{-1}, and the reaction is fast enough to put the lifetime of DMHg during the night in the same time range as that for $^•OH$-initiated degradation during the day (Sommar et al., 1997). To summarize this section, the degradation of DMHg in the atmosphere is illustrated in **Fig. 10**.

5.2.2 Monomethylmercury species

Although experimental data are lacking, gaseous $MMHg^+$ species (e.g., MMHgCl) are expected to react with atmospheric radicals, which leads to demethylation similar to the process that occurs in the reactions of CH_3HgCH_3 and OH/Cl radicals. However, the rate constant is likely lower, and the uptake of particles is more important for the atmospheric fate of $MMHg^+$ species.

6. Red-ox transformations in the aqueous phase

6.1 Inorganic Hg species

Aqueous redox reactions of Hg^{II} complexes can include primary (intramolecular) processes involving direct electron transfer and secondary (intermolecular, usually bimolecular) reactions caused by reactive intermediates. Atmospheric aerosols serve as microreactors for redox Hg reactions (Lin and Pehkonen, 1999). Both oxidation and reduction occur in the aqueous phase. Since Hg^{2+}(aq) has a rapid ligand exchange rate, the formation of Hg^{II} hydrated complexes does not limit the redox reaction rates and can therefore be treated separately as chemical equilibria. The aqueous speciation of Hg^{II}, where pH is often a critical parameter, is important for the reaction kinetics, not least for the reduction pathways. Thus, aerobic reduction pathways in principle require the formation of specific complexes, since Hg^0 cannot be formed from Hg^{2+} by successive bimolecular (single-electron) reduction steps, since dissolved O_2 instantaneously re-oxidizes $Hg^{•+}$:

$$XHg^• + O_2 \rightleftarrows {}^•OOHgX \rightleftarrows HgX^+ + O_2^{•-} \qquad \text{(Rxn W11)}$$

The overall forward rate constant for **Rxn W11** is at the diffusion limit (k~10^9 M^{-1} s^{-1}, Nazhat and Asmus, 1973). In contrast, Hg^0 can be formed by fragmentation of a ligand bound to Hg^{II} (reductive elimination, van Loon et al., 2000). Such photo- or thermolabile Hg^{II} complexes are characterized by low-energy ligand-to-metal charge transfer (LMCT) excited states, which tend to induce internal redox processes leading to oxidation of a ligand and reduction of the mercuric ion. There is evidence that Hg^{2+} complexes can undergo both one-electron and two-electron LMCT. An example is mercuric oxalate, where 2e-LMCT is photoinduced and occurs as part of a concerted series of electron rearrangements (heterolytic cleavage of σ-bonds in the complex), resulting in the oxalate ligand being eliminated as two molecules of CO_2 and the oxidation state of the metal ion decreasing by two units. This mechanism occurs without any detectable intermediates such as free radicals:

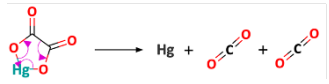

(Rxn W16a)

As described in **Sections 8.1 & 8.4**, 1e- and 2e-LMCT reactions produce isotopic effects, the specific fractionation of which can be used to identify the reaction mechanism. In addition to the quenching of triplet complex states, the presence of dissolved O_2 leads to the scavenging of radicals such as $Hg^{•+}$ produced by the 1e-LMCT mechanism, resulting in reoxidation to Hg^{2+} (**Rxn W11**, Zhao et al., 2021). As previously noted (Pehkonen and Lin, 1998), in certain laboratory experiments, such as reduction experiments, sufficiently elevated Hg concentrations are employed such that the Hg^0 formed exceeds its solubility, thereby existing predominantly in a colloidal form. **Table 4** below outlines the potentially significant redox reactions occurring in the aqueous phase, which are then elaborated upon in the subsequent text.

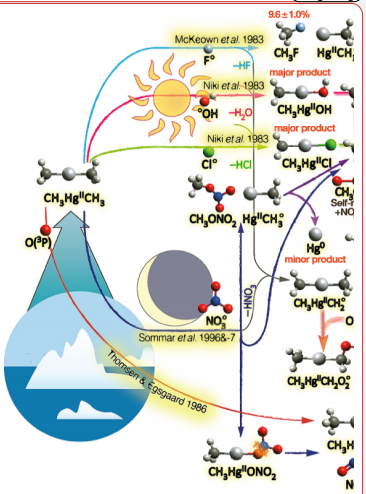

flyttade upp [6]: Figure 10. Schematics of the atmospheric

formaterade: Kondenserad med 0,1 pt
tog bort:
formaterade ... [396]
Formaterat: Avstånd Efter: 9 pt
formaterade ... [397]
tog bort: as
formaterade ... [398]
tog bort: G77
formaterade: Kondenserad med 0,1 pt
tog bort: 'and
formaterade ... [399]
tog bort:
formaterade: Kondenserad med 0,1 pt
tog bort: has been
formaterade ... [400]
tog bort:
tog bort: destiny of DMHg. The fate of HgO indicated is uncertain.¶
tog bort: there is a lack of …xperimental data are lacking ... [401]
Formaterat: Avstånd Före: 8 pt, Efter: 8 pt
Formaterat ... [402]
formaterade: Inte Expanderad med / Kondenserad med
Formaterat: Avstånd Efter: 6 pt
formaterade: Inte Expanderad med / Kondenserad med
tog bort: the
formaterade: Inte Expanderad med / Kondenserad med
tog bort: ,
formaterade: Inte Expanderad med / Kondenserad med
tog bort: of great importance
tog bort: it appears that
formaterade: Inte Expanderad med / Kondenserad med
formaterade: Inte Expanderad med / Kondenserad med
tog bort: reoxidizes
formaterade ... [403]
formaterade: Inte Expanderad med / Kondenserad med
Formaterat: Avstånd Före: 6 pt, Radavstånd: 1,5 rader
Formaterat: Avstånd Efter: 0 pt, Radavstånd: Flera 1,15 li
Formaterat: Ingen kontroll av enstaka rader
tog bort: Section
tog bort: has been
tog bort: as
formaterade: Engelska (USA)

Table 4. Aqueous-phase redox chemistry

ID	Reaction type	Reactant	Co-reactant	Reaction mechanism		Technique/ Comments	Rate coefficient (M^{-1} s^{-1})[19]	References
W1	Oxidation, bimolecular	Hg^0 (aq)	Ozone (O_3)	$Hg^0 + O_3 \xrightarrow{H^+} Hg^{2+} + OH^- + O_2$	pH 5.2–6.2	Relative rate[20]	$(4.7 \pm 2.2) \times 10^7$	Munthe, 1992
W2			Hydroxyl radical ($^{\bullet}OH$)	$Hg^0 + HO^{\bullet} \rightarrow HOHg^{\bullet} \xrightarrow{H^+,\ O_2} Hg^{2+} + O_2^{\bullet-}$	pH 5.6 – 5.9	Steady-state[21]	2.0×10^9	Lin & Pehkonen, 1997
					pH 7.9	Relative rate[22]	$(2.4 \pm 0.3) \times 10^9$	Gårdfeldt et al., 2001
W3			Carbonate radical ($CO_3^{\bullet-}$)	$Hg^0 + CO_3^{\bullet-} \rightarrow$ products	pH 8	Relative rate[23]		He et al., 2014
W4			Hypochloric acid (HOCl)	$Hg^0 + HOCl \rightarrow Hg^{2+} + Cl^- + HO^-$	pH 6.5 – 8.4	Steady-state concentration of reactant by hydrolysis of the precursor NH_2Cl	$(2.1 \pm 0.1) \times 10^6$	Lin & Pehkonen, 1998b
			Hypochlorite (ClO^-)	$Hg^0 + ClO^- \xrightarrow{H^+} Hg^{2+} + Cl^- + HO^-$	pH 6.5 – 8.4		$(2.0 \pm 0.1) \times 10^6$	
W5			Hypobromic acid (HOBr)	$Hg^0 + HOBr \rightarrow Hg^{2+} + Br^- + HO^-$	pH 6.7 – 6.8	Steady state disproportionation of Br_2	0.28 ± 0.02	Wang & Pehkonen, 2004
			Hypobromite (BrO^-)	$Hg^0 + BrO^- \xrightarrow{H^+} Hg^{2+} + Br^- + HO^-$	pH 11.7 – 11.8		0.27 ± 0.04	
			Bromine (Br_2)	$Hg^0 + Br_2 \rightarrow Hg^{2+} + 2\ Br^-$	pH 2.0 – 2.1		0.20 ± 0.03	
W6			Peracids (peracetic and perbenzoic acid)	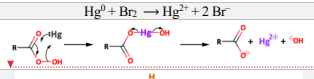		Screening study		Wigfield & Perkins, 1985a
W7	Oxidation, complexation		2–mercapto propionic acid		pH 7, anoxic	Absolute	0.61	Zheng et al., 2013
W8	Comprop., bimolecular		Mercuric ion (Hg^{2+})	$Hg^0 + Hg^{2+} \rightarrow Hg_2^{2+}$	pH 3 – 4	e^-_{aq} (pulse radiolysis)	5.9×10^8	Buxton et al., 1995
W9	Dimerization, bimolecular	$Hg^{\bullet+}$ (aq)	Mercurous ion radical ($Hg^{\bullet+}$)	$2\ Hg^{\bullet+} \rightarrow Hg_2^{2+}$			$\geq 10^9$	
W10	Disprop., bimolecular			$2\ Hg^{\bullet+} \rightarrow Hg^{2+} + Hg^0$	pH 3.15		2.6×10^9	
W11	Oxidation, bimolecular		Oxygen (O_2)	$XHg^{\bullet} + O_2 \rightleftarrows {}^{\bullet}OOHgX \rightleftarrows HgX^+ + O_2^{\bullet-}$			$(1 - 4) \times 10^9$ [24]	Jungbluth et al., 1976
W12			p–benzoquinone		pH 5.0 – 5.5		$(1 - 4) \times 10^9$	
W13	Reduction, 2e–LMCT, thermal	Hg^{II} (aq)	Sulfite (SO_3^{2-})	$Hg^{2+} + SO_3^{2-} \rightleftarrows HgSO_3 \rightarrow Hg^0 S^{VI}O_3 \rightarrow Hg^0 + S(VI)$	pH 3.0 – 4.8	Absolute[25]	$0.6\ s^{-1}$	Munthe et al., 1991
					280 –307 K	Absolute[26]	$T \cdot \exp\left[\frac{(31.971 \cdot T - 12595)}{T}\right]$	van Loon et al., 2000
					pH 3, 298 K		$0.0106 \pm 0.0009\ s^{-1}$	Feinberg et al., 2015
W14	Reduction, bimolecular		Carbon dioxide anion radical ($CO_2^{\bullet-}$)	$HgCl_2 + CO_2^{\bullet-} \rightarrow ClHg^{\bullet} + CO_2 + Cl^-$	pH 1 – 2, anoxic	Relative rate[27]	1.8×10^8	Berkovic et al., 2010
W15			Superoxide anion radical ($O_2^{\bullet-}$)	$HgCl_2 + O_2^{\bullet-} \rightarrow ClHg_2^{\bullet+} + O_2 + Cl^-$	pH 6	Relative rate[28]	5×10^3	Gårdfeldt & Jonsson, 2003
			Hydroperoxy radical ($HO_2^{\bullet}$)	$C_2O_4^{\bullet-} \rightarrow CO_2 + CO_2^{\bullet-}$, $CO_2^{\bullet-} + O_2 \rightarrow CO_2 + O_2^{\bullet-}$, $H^+ + O_2^{\bullet-} \rightleftarrows HO_2^{\bullet}$, $Hg^{2+} + HO_2^{\bullet} \rightarrow$ products	pH 3.9	Absolute[29]	1.7×10^4	Pehkonen and Lin, 1998
W16	Reduction, 2e⁻ and 1e⁻ LMCT, photolytic		Oxalate	$Hg^{2+} + C_2O_4^{2-} \rightleftarrows HgC_2O_4 \xrightarrow{h\nu} Hg^0 + 2\ CO_2$	pH 3 – 6, anoxic	Absolute[30]	15.7 ± 2.8 [31]	Zhao et al., 2021
				$HgC_2O_4 \xrightarrow{h\nu} Hg^{\bullet+} + C_2O_4^{\bullet-}$, $Hg^{2+} + C_2O_4^{\bullet-} \rightarrow Hg^{\bullet+} + 2\ CO_2$, $Hg^{\bullet+} + C_2O_4^{2-} \rightarrow Hg^0 + C_2O_4^{\bullet-}$	pH 3, anoxic		$(1.2 \pm 0.2) \times 10^4$ [32]	Si & Ariya, 2008
			Malonate (R = CH_2), Succinate (R = C_2H_4)	$Hg^{2+} + R(COO)_2^{2-} \rightleftarrows Hg(OOC)_2R \xrightarrow{h\nu} Hg^0 + CO_2 + HORCOOH - H_2O$, $Hg(OOC)_2R \xrightarrow{h\nu} Hg^{\bullet+} + {}^{\bullet}OOCRCOO^-$,	pH 3, anoxic		$(4.9 \pm 0.8) \times 10^3$, $(2.8 \pm 0.5) \times 10^3$	Si & Ariya, 2008

[19] Unless otherwise stated.
[20] with SO_3^{2-} as reference.
[21] using C_6H_6 as •OH scavenger. NO_3^- photolysis as •OH source.
[22] with CH_3Hg^+ as reference. NO_3^- photolysis as •OH source.
[23] The loss of Hg^0(aq) was followed, but neither $^{\bullet}OH$ nor $CO_3^{\bullet-}$, which co-occur in the solution, were quantified. NO_3^- photolysis as •OH source, •OH reaction with carbonate anion as a source of $CO_3^{\bullet-}$
[24] Concerns various mercurous halide and pseudohalide radicals $^{\bullet}HgX$ (X = Cl, Br, I, SCN and CN)
[25] Followed by decay of $[Hg(SO_3)_2]^{2-}$ absorption (λ = 230 nm)
[26] Followed by the formation of Hg_2^{2+} (λ = 236 nm)
[27] Methyl viologen as reference. $S_2O_6^{2-}$ photolysis in the presence of HCOOH.
[28] Methyl viologen as reference. Reduction of O_2 by e^-_{aq} (pulse radiolysis). Determination of K = 2.5 for W11/W16 and using W11 for calculating W16.
[29] Dithizone colorimetric quantification of Hg^{II} decay. $HO_2^{\bullet}$ produced by $C_2O_4^{\bullet-}$ photolysis with air bubbling. $[HO_2^{\bullet}]$ estimated from production of H_2O_2.
[30] After analytically determining the initial Hg^{II} concentration, the reduction process was studied by measuring the production of Hg^0 by CV-AFS.
[31] The oxalate ion ($C_2O_4^{2-}$) was identified as the sole reducing agent (complexing ligand), hence $k = k_{obs}/[C_2O_4^{2-}]$.
[32] Based on the total concentration, the second-order rate coefficient is expressed as $k = k_{obs}/([H_2C_2O_4] + [HC_2O_4] + [C_2O_4^{2-}])$.

tog bort:
tog bort:
tog bort:
tog bort:
tog bort:
tog bort:
tog bort:
tog bort:
tog bort:
formaterade: Teckensnitt:Times New Roman
formaterade: Teckensnitt:Times New Roman
formaterade: Teckensnitt:Times New Roman
formaterade: Teckensnitt:Times New Roman
formaterade: Teckensnitt:Times New Roman
formaterade: Teckensnitt:Times New Roman
formaterade: Teckensnitt:Times New Roman
formaterade: Teckensnitt:Times New Roman
formaterade: Teckensnitt:Times New Roman
formaterade: Teckensnitt:Times New Roman
formaterade: Teckensnitt:Times New Roman
formaterade: Teckensnitt:Times New Roman
formaterade: Teckensnitt:Times New Roman
formaterade: Teckensnitt:Fet
tog bort:
tog bort:
formaterade: Teckensnitt:Symbol
tog bort: of
formaterade: Teckensnitt:Symbol
formaterade: Inte Expanderad med / Kondenserad med
tog bort: WO8/WR4
formaterade: Inte Expanderad med / Kondenserad med
tog bort: WO8
formaterade: Inte Expanderad med / Kondenserad med
tog bort: WR4
formaterade: Inte Expanderad med / Kondenserad med
formaterade: Inte Expanderad med / Kondenserad med
formaterade: Inte Expanderad med / Kondenserad med
formaterade: Teckensnitt:Times New Roman
formaterade: Teckensnitt:Times New Roman
formaterade: Teckensnitt:Times New Roman
formaterade: Teckensnitt:Times New Roman
formaterade: Teckensnitt:Times New Roman
formaterade: Teckensnitt:Times New Roman
formaterade: Teckensnitt:Times New Roman
tog bort:

				$Hg^{\bullet+} + R(COO)_2^{2-} \rightarrow Hg^0 + {}^{\bullet}OOCRCOO^-$				
	Reduction, thermal	$Hg^{II}(aq)$	Ascorbate (H_2asc, $Hasc^-$) (enolic acids)	$HOHg(Hasc) \rightarrow Hg^0 + H_2O$ + dehydroascorbate	pH 4 – 5.5		$2.8 \times 10^{-3}\ s^{-1}$	
	Reduction, photolytic		Salicylic acid	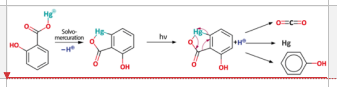	pH 4.3		$1.0 \times 10^{-4}\ s^{-1}$	This work
			p-aminobenzoic acid p-hydroxybenzoic acid	See Rxn 7	pH 4.9 pH 5.6		$3.1 \times 10^{-4}\ s^{-1}$ $1.1 \times 10^{-5}\ s^{-1}$	
W17	1e⁻LMCT, followed by bimolecular reduction, photolytic		Anthraquinone–2,6–disulfonate (AQDS)	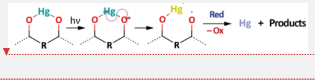	UVB, pH 3.4	Absolute[33]	$(9.9 \pm 2.7) \times 10^{-4}\ s^{-1}$	Zhao et al., 2021
W18	Reduction, photolytic		1–alkanethiols	$Hg(RS)_2 \xrightarrow{h\nu} Hg^0 + RS–SR$	UV–VIS, pH 7	Absolute	$(2.0 \pm 0.2) \times 10^{-7}\ s^{-1}$ ($R = C_3H_7$) $(1.4 \pm 0.1) \times 10^{-7}\ s^{-1}$ ($R = C_4H_9$) $(8.3 \pm 0.5) \times 10^{-8}\ s^{-1}$ ($R = C_5H_{11}$)	Si & Ariya, 2011
	Reduction etc. Photolytic		Thioglycolic acid	$Hg(O(=O)CCH_2S) \xrightarrow{h\nu} Hg^0 + \text{products}$ $\xrightarrow{h\nu} HgS + \text{products}$	UV–VIS, pH 4		$(2.3 \pm 0.4) \times 10^{-5}\ s^{-1}$	Si & Ariya, 2015

6.1.1 Oxidation channels

The mass transfer (diffusion) of gas-phase Hg^0 into typical size regimes of aerosols (radius of 0.1–10 μm) does not limit the rate of aqueous Hg^0 oxidation. The concentration of dissolved Hg^0 in a droplet is at a steady state governed by Henry's law (Lin and Pehkonen, 1998a).

Elemental mercury

Inorganic oxidants

Rxn W1. Ozone (O_3)

The presence of O_3 in atmospheric water is due mainly to the scavenging of gaseous O_3 ($k_H^{cp} = 0.013$ M atm^{-1} at 298 K). An early study of the oxidation of Hg^0 by O_3 in the aqueous phase was carried out by Iverfeldt and Lindqvist (1986) using a flow system in which 70–200 ppb O_3 was introduced. Their results suggested a conversion rate of 1–4% h^{-1} when applied to atmospheric conditions. Munthe and coworkers (McElroy and Munthe, 1991; Munthe, 1992) studied the ozone reaction with the mercurous cation in an acidic solution (pH = 1 - 3) in a stopped-flow system and with elemental Hg using the relative rate technique (sulfite as a reference compound, pH 5.2 - 6.2) and obtained pH-independent rate constants of $(9.2 \pm 0.9) \times 10^6$ and $(4.7 \pm 2.2) \times 10^7$ M^{-1} s^{-1}, respectively.

Rxn W2. Hydroxyl radical ($^{\bullet}OH$)

The OH radical in atmospheric water can come from the air ($k_H^{cp} = 30$ M atm^{-1}) or from aqueous phase production via pathways including photolysis of H_2O_2, HONO, O_3 and NO_3^- (Finlayson-Pitts and Pitts, 2000). The reaction rate of $Hg^0 + {}^{\bullet}OH$ in the aqueous phase was determined by Lin and Pehkonen (1997) using a steady-state technique with the photolysis of NO_3^- as the $^{\bullet}OH$ source and C_6H_6 as the $^{\bullet}OH$ scavenger to 2.0×10^9 M^{-1} s^{-1} at pH 5.6–5.9. Like the first step ($Hg^0 + {}^{\bullet}OH \rightarrow {}^{\bullet}Hg^{I}OH$), the second step, which is mediated by dissolved O_2 (**Rxn W11**), is near the diffusion limit. Gårdfeldt et al. (2001) subsequently studied the same reaction at pH 7.9 but with the reaction between CH_3Hg^+ and $^{\bullet}OH$ as a reference but with similar results (2.4×10^9 M^{-1} s^{-1}).

Rxn W3. Carbonate radical ($CO_3^{\bullet-}$)

In water, the carbonate system (HCO_3^- and CO_3^{2-}) can react with OH radicals to form strongly oxidizing carbonate radicals ($CO_3^{\bullet-}$) in fast reactions (8.5×10^6 and 3.9×10^8 M^{-1} s^{-1}, respectively). In a comparative study, He et al. (2014) studied the disappearance of Hg^0 in aqueous solutions where NO_3^- was photolyzed via UV–VIS in the absence and presence of CO_3^{2-} at pH = 8. When both NO_3^- (0.23 mM) and CO_3^{2-} (2.75 mM) were present in the irradiated solutions (electron paramagnetic resonance spin trapping analysis detected the presence of $^{\bullet}OH$ and $CO_3^{\bullet-}$), the rate of oxidation of Hg^0(aq) (1.44 h^{-1}) was 8 times faster than that observed when only NO_3^- (which

[33] AQDS is not the reductant rather photohydroxylated reduced AQDS forms.

tog bort: 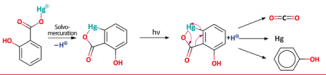

tog bort: 8

formaterade: Teckenfärg: Dekorfärg 2

tog bort: 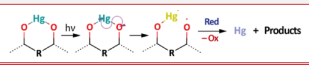

tog bort: 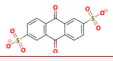

formaterade: Kondenserad med 0,4 pt

tog bort: –

formaterade: Kondenserad med 0,4 pt

tog bort: the

formaterade: Kondenserad med 0,4 pt

tog bort: Law

formaterade: Kondenserad med 0,4 pt

tog bort: from

tog bort: Henry's constant

tog bort: flowing

tog bort: -

tog bort: -

tog bort: co-worker (Mcelroy

tog bort: equilibrium at

tog bort: –

tog bort: reaction 6)

tog bort: later

tog bort: ,

tog bort: ,

tog bort: the

tog bort: radical

tog bort: in

tog bort: -

produces •OH) was irradiated. The carbonate radical is a single-electron oxidant and reacts according to $Hg^0 + CO_3^{\bullet-} \rightarrow Hg^{\bullet+} + CO_3^{2-}$. In addition to identifying the carbonate radical as an effective oxidant of Hg^0 dissolved in water alongside the hydroxyl radical, this study investigated the role of $^1\Delta_g$ O_2 (singlet oxygen) as an oxidant for Hg^0(aq). However, the latter species, an excited state of O_2, does not initiate any measurable oxidation. Notably, the absolute rate constant for $Hg^0 + CO_3^{\bullet-}$ remains to be determined.

Rxn W4. Aqueous chlorine ($HOCl/ClO^-$)

Aqueous chlorine is formed mainly by the scavenging of gaseous Cl_2 ($k_H^{cp} = 7.61 \times 10^{-2}$ M atm^{-1} at 298 K) into the aqueous phase and the oxidation of chloride ions by •OH. Once incorporated into the aqueous phase, it dissociates to form $HOCl/OCl^-$ ($pK_a = 7.5$) and Cl^-, the former being the primary oxidant and increasing the solubility of total chlorine. It is a nocturnal oxidant, as both Cl_2 and HOCl are readily photolyzed by solar radiation. The prospects for Hg^0 oxidation by aqueous chlorine were investigated by Kobayashi (1987) and Munthe and McElroy (1992). In the former, rapid dissolution of Hg was reported when a gas stream containing Hg^0 was passed through a solution containing dissolved chlorine (HClO), while in the latter, Hg_2^{2+}(aq) was used as a proxy for Hg^0, whose oxidation was observed to be "relatively fast" in a solution containing HClO. A detailed kinetic study (Lin and Pehkonen, 1998b) of the reaction between Hg^0 and $HClO/ClO^-$ was carried out using a steady-state method with chloramine as a reservoir of free hypochlorous acid formed by hydrolysis: $NH_2Cl + H_2O \rightarrow NH_3 + HClO$. The turnover of Hg^0 was studied in the pH range of 6.5 - 8.5 around the pK_a (HClO) to investigate the influence of HClO (aq) and ClO^- (aq), which were found to be closely equivalent according to the rate constants for $Hg^0 + HClO$ and $Hg^0 + ClO^-$ of $(2.09 \pm 0.06) \times 10^6$ and $(1.99 \pm 0.06) \times 10^6$ M^{-1} s^{-1}, respectively. The products of both reactions (2 electrons are transferred) are chloride and hydroxide anions with a stoichiometry of 1:1 together with a mercuric cation, which rapidly forms a strong complex ($\log\beta_{11} = 18.0$).

Rxn W5. Aqueous bromine ($HOBr/BrO^-/Br_2$)

Bromine has a higher k_H^{cp} (0.725 atm M^{-1}) than chlorine does, but the disproportionation of Br_2 to $HBrO/BrO^-$ ($pK_a = 8.7$) and Br^- is slow, and the equilibrium is shifted in favor of Br_2. In contrast, Br^{+1} is formed by the action of O_3 on bromide ions and exists in the presence of Cl^- largely as BrCl (Liu and Margerum, 2001). Aqueous bromine (Br_2, HOBr) oxidizes Hg^0 only slowly (0.2–0.3 M^{-1} s^{-1}, Wang and Pehkonen, 2004). However, BrCl is likely important, as it is used as an oxidant for Hg in current analytical methods, although the kinetics have not been investigated.

Organic oxidants

Rxn W6. Peroxides

H_2O_2 cannot oxidize Hg^0 (aq) (Kobayashi, 1987) but participates in the metal-catalyzed oxidation of Hg^0, as in Fenton's system. Fenton's reagent itself, $Fe^{2+} + H_2O_2$, produces OH radicals, for which Hg^0, Fe^{2+} and H_2O_2 compete for oxidation. The latter reaction, $H_2O_2 + •OH$, produces the HO_2 radical, which propagates a chain reaction (Fenton's reaction) supported by Fe^{3+} acting as a catalyst to decompose H_2O_2 to O_2 and H_2O, during which a stable concentration of Fe^{2+} is produced as a source of •OH. Hg^0 oxidation is most pronounced when the ferrous part of the Fenton reaction dominates over the ferric part, corresponding to a higher concentration of OH radicals (Liu, 2011). The -OOH functional group in organic hydroperoxides, like that in hydrogen peroxide, lacks the ability to oxidize Hg^0, whereas that in peroxocarboxylic acids (peracetic and perbenzoic acid) seems to possess it, tentatively forming a mercuric carboxylate by a cyclic mechanism (Wigfield and Perkins, 1985b; Wigfield and Perkins, 1985a).

Rxn W7. Thiocarboxylic acids

Thiol compounds, as substituted carboxylic acids, including cysteine and glutathione, can oxidize Hg^0(aq) both thermally under anoxic conditions (Gu et al., 2011). For example, Zheng et al. (2013) reported that 2-sulphanylpropanoic acid in greater excess (1000:1) oxidized Hg^0 at a rate of 2.18 ± 0.13 h^{-1}. The presence of an electron acceptor (such as a quinone) further increased the reaction rate. The reaction mechanism has been described as oxidative complexation. Hg^0, which is polarizable, interacts with a thiol group, leading to ligand-induced oxidative complexation in which hydrogen participates in charge transfer (Cohen-Atiya and Mandler, 2003).

Mercurous radical species ($•Hg^IX$)

Inorganic oxidants

tog bort: :
tog bort: .
tog bort: the
tog bort: also
tog bort: It should also be noted that
tog bort: formed
tog bort: Henry's constant =
tog bort: the
tog bort: ion
tog bort:
tog bort: oxidants
tog bort: Henry's constant
tog bort: –
tog bort: itself
tog bort:),
tog bort: the
tog bort: The
tog bort: are in competition
formaterade: Kondenserad med 0,3 pt
formaterade: Kondenserad med 0,3 pt
tog bort: observed
formaterade: Kondenserad med 0,3 pt
tog bort: quinones
formaterade: Kondenserad med 0,3 pt
tog bort: enhanced
formaterade: Kondenserad med 0,3 pt
tog bort: the
formaterade: Kondenserad med 0,3 pt

Rxn W11. Oxygen (O_2)

The reaction between $Hg^{\bullet+}$ and O_2 has been studied for a variety of ligands and over a range of pH values well into the alkaline range using pulse radiolysis ~~with a homogeneous kinetic result~~ (Nazhat and Asmus, 1973; Jungbluth et al., 1976; Fujita et al., 1975; Fujita et al., 1973; Liu et al., 1983; Pikaev et al., 1975). Mercurous species are formed by the reduction of corresponding mercuric species by the action of solvated electrons and H atoms derived from H_2O radiolysis: $HgX_2 + e^-_{aq} \rightarrow {}^{\bullet}Hg^{I}X + X^-$ and $HgX_2 + H^{\bullet} \rightarrow {}^{\bullet}Hg^{I}X + H^+ + X^-$. All types of ${}^{\bullet}Hg^{I}X$ species react rapidly ($\geq 1 \times 10^9$ M^{-1} s^{-1}) with O_2 (aq): $Hg^{\bullet+} + O_2 \rightleftarrows {}^{\bullet}OOHg^+ \rightleftarrows Hg^{2+} + O_2^{\bullet-}$, where the equilibrium is very strongly shifted to the right. In one case (X = CN, Jungbluth et al., 1976) the reaction takes place without the clear formation of a peroxyl radical intermediate. In an air-saturated solution (~0.2 mM O_2), the lifetime of ${}^{\bullet}Hg^{I}X$ is about 1 µs (Jungbluth et al., 1976).

Organic oxidants

Rxn W12. Quinones

Both $Hg^{\bullet+}$ and $^{\bullet}OOHg^+$ are rapidly oxidized by benzoquinone ($\gtrsim 10^9$ and $\lesssim 10^9$ M^{-1} s^{-1}, Jungbluth et al., 1976), which accepts an electron to form a semiquinone anion. Lalonde et al. (2001) observed that Hg^0 is oxidized (~0.6 h^{-1}) in UVB-irradiated aqueous solutions containing both benzoquinone (32 nM) and chloride ions (0.5 M) without being able to fix the mechanism.

6.1.2 Reduction channels

Mercuric compounds (Hg^{II})

Inorganic reductants

Rxn W13. Sulfite (SO_3^{2-})

SO_2 dissolves in water (K_H^{cp} = 1.36 M atm^{-1}) to form the weak acid H_2SO_3 (aq), which can be deprotonated to HSO_3^- and SO_3^{2-}. The oxidation of sulfite to sulfate is rapid in the atmosphere and takes a few hours under typical oxygenated conditions in atmospheric droplets. SO_3^{2-} is a soft ligand that forms strong complexes with Hg^{2+} (**Table 1**), such as $HgSO_3$ and $[Hg(SO_3)_2]^{2-}$, the latter completely dominating under natural conditions where the sulfite content greatly exceeds that of Hg^{2+}. The reduction of aqueous Hg^{II} by the sulfite system was first investigated by Munthe et al. (1991). $[Hg(SO_3)_2]^{2-}$ is stable, whereas $HgSO_3$ decomposes readily to Hg^0 and sulfate with firstorder rate constants of $<10^{-4}$ s^{-1} and 0.6 s^{-1}, respectively. Scott and co-workers (van Loon et al., 2001, 2000) carried out a thorough re-examination and confirmed that the bis-sulfite complex is thermally stable but that the reduction of $HgSO_3$, which is strongly temperature dependent (k approximately quadruples with each 10 °C increase in temperature) and weakly pH dependent, is more than 50 times slower than that reported by Munthe et al. (0.011 vs. 0.6 s^{-1} at 25 °C). The reaction mechanism is intramolecular with 2e-LMCT and heterolytic cleavage of the Hg–S bond: $Hg^{2+} + SO_3^{2-} \rightarrow Hg^{II}S^{IV}O_3 \rightarrow Hg^0S^{VI}O_3 \xrightarrow{H_2O} Hg^0 + SO_4^{2-}$.

Rxn W14. Carbon dioxide anion radical ($CO_2^{\bullet-}$)

The carbon dioxide radical ($CO_2^{\bullet-}$) can be formed in nature by the oxidation of carboxylic acids (see above under oxalic acid). It is strongly reducing and occurs in anaerobic environments. Berkovic et al. (2010) studied the $CO_2^{\bullet-}$–mediated reduction of Hg^{2+} at low pH by laser flash photolysis of a dilute mixture of $HgCl_2$, formic acid and sodium peroxydisulfate at 266 nm. The one-electron reaction $Hg^{2+} + CO_2^{\bullet-} \rightarrow Hg^{\bullet+} + CO_2$ is exothermic, with a rate constant of 1.8×10^8 M^{-1} s^{-1}. The $Hg^{\bullet+}$ formed can only be further reduced to Hg^0 in the absence of O_2.

Rxn W15. Superoxide anion/hydroperoxy radical ($O_2^{\bullet-}$/$HO_2^{\bullet}$)

$HO_2^{\bullet}/O_2^{\bullet-}$ (pK_a 5.5) is a one-electron reductant of Hg^{2+} to $Hg^{\bullet+}$. Gårdfeldt and Jonsson (2003) determined the one-electron reduction potential for the pair $HgCl_2/{}^{\bullet}HgCl$ vs. NHE at $[Cl^-]$ = 0.05 M to be –0.47 V, which, together with that for $O_2/O_2^{\bullet-}$ vs. NHE of –0.155 V, gives an equilibrium constant for $HgCl_2 + O_2^{\bullet-} \rightleftarrows {}^{\bullet}HgCl + O_2 + Cl^-$ of 5×10^{-6} at the aforementioned $[Cl^-]$. Given that the rate constant for the reaction ${}^{\bullet}Hg^{I}Cl + O_2$ is ~10^9 M^{-1} s^{-1} (**Rxn W11**), the bimolecular rate constant between $HgCl_2$ and $O_2^{\bullet-}$ can be estimated to be 5×10^3 M^{-1} s^{-1}. Pehkonen and Lin (1998) studied the photoreduction of mercuric ions to Hg^0 with nitrate or chloride as counterions in the presence of formic, acetic or oxalic acid at neutral (7.0) and acidic (3.9) pH values in aerated solutions. Only in the presence of oxalic acid does significant photoreduction occur, and as in the later studies by Zhao

formaterade: Genomstruken
tog bort: x
tog bort: ,
tog bort:)
tog bort:),
tog bort: Henry's constant
tog bort: Oxidation
tog bort: , taking
tog bort: first order
tog bort: not
formaterade: Teckenfärg: Blå
tog bort: unstable,
formaterade: Teckenfärg: Blå
tog bort: 25°C
tog bort: -
formaterade: Teckensnitt:9,5 pt
formaterade: Teckensnitt:9,5 pt
formaterade: Teckensnitt:9,5 pt
formaterade: Teckensnitt:9,5 pt
formaterade: Teckensnitt:9,5 pt
formaterade: Teckensnitt:9,5 pt
formaterade: Teckensnitt:9,5 pt
formaterade: Teckensnitt:9,5 pt
formaterade: Teckensnitt:9,5 pt
formaterade: Teckensnitt:9,5 pt
tog bort: x
tog bort: x
tog bort: carried out a study of
tog bort: ion
tog bort: counterion
tog bort: a
tog bort: ,

et al. (2021) and Si and Ariya (2008), an increase in the reaction rate is observed with increasing ratios of oxalic acid to Hg^{II}. The reduction is also suppressed in the presence of Cl^-. Photoreduction results in an exponential increase in H_2O_2 formation, which is due to the presence of hydroperoxyl radicals in solution ($2\ HO_2^\bullet \rightarrow H_2O_2 + O_2$). In retrospect (see above), this follows from the homolytic decomposition of $Hg(\eta^2\text{-}C_2O_4)$ into radicals in an aerated solution ($CO_2^{\bullet-} + O_2 \rightarrow O_2^{\bullet-} + CO_2$) and does not necessarily mean that $HO_2^\bullet/O_2^{\bullet-}$ can reduce Hg^{II} to Hg^0.

Organic reductants

In the atmospheric environment, Hg^{II} complexation by DOM plays a pivotal role in the redox chemistry of Hg (Åkerblom et al., 2015). The chemical-reducing effect of DOM (humic substances) on Hg^{II} has been recognized for nearly 50 years (Alberts et al., 1974). These heterogeneous macromolecular ligands contain not only building blocks that can form complexes with Hg^{II} but also redox-active aromatic chromophores that can photolytically convert Hg. The fractions of DOM contributing to Hg^{II} photoreduction include fulvic- and flavin-like fractions that contain more quinone and flavin moieties than usual (Yang et al., 2020a). Furthermore, DOM contains several functional groups that can reduce complex-bound mercuric ions to Hg^0 by a 2e-LMCT reaction (**Table 5**).

Table 5. Main functional groups of DOM that can (photo)reduce ligated Hg^{2+}.

Binding atom	Ligand oxidation process
Oxygen (O)	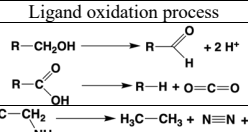
Nitrogen (N)	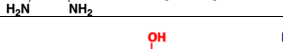
Sulfur (S)	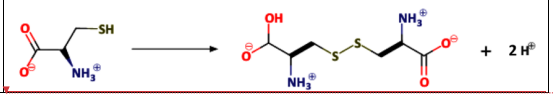

Rxn W16. Organic acids

The low-molecular-weight organic acids present in the atmosphere can reduce Hg^{II} to Hg^0 in the presence of O_2. These include dicarboxylic acids, ortho-substituted aromatic carboxylic acids, and enolic acids. Since 1880 (Eder, 1880), the salt of the lightest dicarboxylic acid, oxalate, has been known to reduce Hg^{II} in daylight. Oxalic acid is formed from, e.g., ethylene or acetylene, by atmospheric oxidation over several reaction cycles (chemical aging, Warneck, 2003). Mercuric ions form a complex with oxalate in a 1:1 ratio ($Hg(\eta^2\text{-}C_2O_4)$), characterized by $\log \beta_{10} = 9.66$, which is most photolabile under UVB irradiation. Si and Ariya (2008) studied the kinetics and products of the photoreduction of Hg^{II} in a series of experiments with different concentrations of the lightest dicarboxylic acids, C_2–C_4, at an initial pH of 3.0 and a temperature of 296 ± 2 K, while the kinetic, product and isotopic study of Zhao et al. (2021) involved the system Hg^{II} + oxalic acid with ClO_4^- as a counterion in the pH range of 2.7–6.3 and a small temperature range of 295–303 K. The pH-resolved experiments show that in the $C_2O_4^{2-}$, $HC_2O_4^-$, $H_2C_2O_4$ – system, only the oxalate ion reduces Hg^{2+} with a $k_{Hg^{2+}+C_2O_4^{2-}}$ of 15.7 ± 2.8 $M^{-1}\ s^{-1}$ at 295 ± 1 K. Si and Ariya reported a much larger bimolecular rate constant between Hg^{2+} and the total oxalic acid concentration of $1.2 \times 10^4\ M^{-1}\ s^{-1}$ at pH 3.0. The magnitude is surprisingly large and is comparable to the rate constant between Hg^{2+} and HO_2/O_2^- radicals (see below). When this higher rate constant, which is based on the total oxalic acid concentration, is implemented in regional air quality models, the impact is significant (Bash et al., 2014). However, with respect to the reaction mechanism, there is more consensus that it follows a branched route. $Hg(\eta^2\text{-}C_2O_4)$ undergoes photolysis followed by partial reductive elimination in one step (insensitive to the presence of O_2): $Hg(\eta^2\text{-}C_2O_4) \xrightarrow{h\nu} Hg^0 + 2\ CO_2$ and, in part, homolysis of a Hg–O bond, which initiates a chain reaction: $Hg(\eta^2\text{-}C_2O_4) \xrightarrow{hv} Hg^{\bullet+} + C_2O_4^{\bullet-}$. Hg^0 should form from the reaction of $Hg^{\bullet+}$ with the bulk ligand $C_2O_4^{2-}$, where $Hg^{\bullet+}$ is reformed from the reaction between bulk Hg^{2+} and the oxalyl ($C_2O_4^{\bullet-}$) or carbon dioxide anion ($CO_2^{\bullet-}$) radical. The reduction to Hg^0 in the chain reaction is inhibited by O_2, which reacts rapidly with both $C_2O_4^{\bullet-}$ and $CO_2^{\bullet-}$ and re-oxidizes $Hg^{\bullet+}$ to Hg^{2+}. Like dicarboxylic acids, aqueous solutions of aromatic ortho- and para-substituted carboxylic acids exposed to UVB can oxidize Hg^{2+} to Hg^0 via elimination of CO_2, and $Hg^{2+} \rightarrow Hg^0$ photoreduction is attenuated but not completely

tog bort: It is also observed that the
tog bort: natural organic matter (NOM)
tog bort: dissolved NOM
tog bort: for
formaterade: Teckenfärg: Dekorfärg 2
tog bort: ,
tog bort: NOM
tog bort: the
tog bort: ,
tog bort: NOM
tog bort: NOM
tog bort: 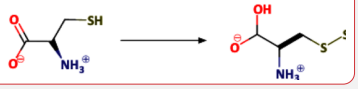
tog bort: Low
Formaterat: Radavstånd: exakt 18 pt
tog bort: It has been known since
tog bort:) that
formaterade: Upphöjd
tog bort: can
tog bort: ion forms
formaterade: Teckenfärg: Dekorfärg 2
tog bort: β
tog bort: –
tog bort: –
tog bort: strongly divergent
formaterade: Teckenfärg: Blå
tog bort: x
tog bort: on
tog bort: routes
tog bort: which is
tog bort: partly by
tog bort: an
tog bort: Reduction
tog bort: also
formaterade: Teckenfärg: Dekorfärg 2
tog bort: As with
tog bort: by
tog bort: the

inhibited by the presence of dissolved O_2 and competing counterions. Previously, He et al. (2012) studied the aqueous photoreduction of Hg^{2+} coupled with a series of aromatic carboxylic acid derivatives in the absence of O_2 at pH 4.3 and suggested that the reaction proceeded via a radical mechanism. However, studies of the same reactants in our laboratory (unpublished results, shown in **Table 4**) have shown that Hg^0 is formed even in the presence of dissolved O_2, suggesting the existence of an additional non-radical reduction pathway. We propose that this channel requires solvo-mercuration to an arylmercurial intermediate followed by photolytically induced 2e-LMCT as part of a concerted series of electron rearrangements, including cleavage of a Hg-C bond yielding Hg^0, CO_2 and a decarboxylated aromatic as end products. Taking p-aminobenzoic acid as an example:

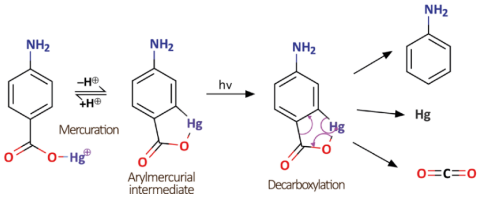

(Rxn 7)

Photo-reduction has also been observed in the presence of dissolved O_2 when Hg^{2+} is bound mainly to the amino acid serine (HSer), similar to $HgSer_2$ (Motta et al., 2020b), which can be explained as the result of reductive elimination with CO_2 and 2-aminoethanol as byproducts in addition to Hg^0 and involves an intermediate with a photolabile Hg–C bond (Zhao et al., 2021). In cysteine-mediated photoreduction (Motta et al., 2020b; Zheng and Hintelmann, 2010b), the ligand is converted from a thiol to a disulfide (**Table 5**). Ascorbic acid, as a representative enolic acid, can readily reduce inorganic divalent Hg in aqueous solutions to Hg^0. Studies in our laboratory have shown that the reaction is thermal and not affected by actinic light. When ascorbic acid is in excess (>10:1) relative to Hg^{2+}, the reaction rate is not significantly affected by increasing ascorbic acid concentration. The reaction rate is highest in the pH range where the hydrogen ascorbate ion ($HAsc^-$) is dominant and the hydrolysis of Hg^{2+} is not complete, i.e., typical pH values for atmospheric hydrometeors (≤ 5.5). Presumably, $HgOH^+$ (aq) forms a reactive complex with $HAsc^-$, $Hg(HAsc)^+$, which is labile to the elimination of water in a heterolytic process, forming Hg^0 and dehydroascorbate as the final products. Enols act as atmospheric intermediates, and it is unclear whether they are present in high concentrations, which makes them interesting reducing agents for atmospheric Hg^{2+}. In any case, $k_{Hg^{2+}+HAsc^-}$ is relatively high (~0.17 min^{-1}, **Rxn W16c**, **Table 4**).

Rxn W17. Hydroquinones and polyphenols

The quinonic (Zheng et al., 2012) and fulvic (Yang et al., 2020a) units in DOM act as key red-ox centers. How this happens at the molecular level is being investigated by studying model compounds that contain redox-active groups but lack other functional groups (Zhao et al., 2021). The simplest quinone forms a red-ox pair with the corresponding hydroquinone in the half-reaction:

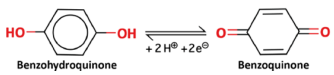

$E^0 = -0.699$ V (Rxn 8)

Combined with the half-reaction in **Rxn 3**, this gives a $\Delta E^0 > 0$ for $Hg^{2+} + C_6H_4(OH)_2 \rightarrow Hg^0 + C_6H_4(=O)_2 + 2\ H^+$, i.e., thermodynamically feasible. Relatively slow reduction of Hg^{2+} to Hg^0 by hydroquinone occurs in the dark in a dilute aqueous solution $(8.2 \pm 2.4) \times 10^{-5}\ s^{-1}$). These results are consistent with a reaction mechanism involving a hydroxyphenoxymercuric complex or via *ipso*-mercuration followed by electron shuttling and elimination of Hg^0 and H_2O:

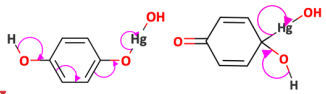

(Rxn 9)

The aqueous photochemistry of quinones is complicated and can involve both ground and excited state reactions as well as free radicals (Görner, 2019). With respect to the interaction of benzoquinone with Hg under actinic light, one study revealed significant oxidation (~0.6 h^{-1}) of Hg^0 in Cl^--enriched water (see above, Lalonde et al., 2001), whereas another study reported photoreduction of $Hg^{II} \rightarrow Hg^0$ of about the same magnitude (~0.8 h^{-1}) under anaerobic conditions and in the absence of strongly complexing inorganic ligands (Zhao

tog bort: proceeds by
tog bort: show
tog bort: 8
tog bort: bound
tog bort:) as
tog bort: by-products besides
tog bort: involving
tog bort: -
tog bort: the
tog bort: of the
tog bort: acids
tog bort: solution
tog bort: show
tog bort: product
tog bort: doubtful
tog bort: that would make
tog bort: as
tog bort: W16b
tog bort: NOM
tog bort: the
tog bort: group
formaterade: Teckenfärg: Dekorfärg 2
tog bort: 9
formaterade: Teckenfärg: Dekorfärg 2
tog bort: .
tog bort: The
tog bort:
Formaterat: Avstånd Efter: 0 pt
formaterade: Teckenfärg: Dekorfärg 2
tog bort: 10
formaterade: Teckenfärg: Dekorfärg 2
tog bort: Concerning
tog bort: shows a
tog bort: -
tog bort: shows a

et al., 2021). An anthraquinone (AQ) derivative (AQ-2,6-disulfonate) is an effective electron shuttle that facilitates electron transfer from metal-reducing bacteria (MRB) to Hg^{II} (Lee et al., 2018), as well as from Hg^0 (aq) to organic thiols (R-SH) during oxidative complexation to form $Hg(SR)_2$ (Zheng et al., 2013). Zheng et al. (2013) reported that AQDS(aq) alone is unable to oxidize Hg^0 or reduce Hg^{II} under dark and anaerobic conditions. AQDS-assisted biotic Hg^{II} reduction by the MRB *Shewanella oneidensis* MR-1 is associated with negative charge scavenging, which temporarily increases the content of reduced AQDS species, such as AQH_2DS and semiquinone radicals (Lee et al., 2018). The reduced species AQH_2DS alone is a potent reductant of Hg^{II} in the dark. On the other hand, Hg^{II} is efficiently reduced to Hg^0 in a UVB-irradiated aqueous solution containing dissolved AQDS (~10^{-3} M^{-1} s^{-1}). The reactive species is tentatively photohydrated AQDS ($AQH_2(OH)DS$), which interacts with Hg^{II} by forming a photolabile bidentate O–coordinated mercuric complex. In conjunction with a strong isotope effect (**Section 8.4**), the photoreaction is likely to occur via a paramagnetic intermediate (a mercurous semiquinone biradical complex). The reaction rate decreases to ~0.2 h^{-1} in the presence of dissolved O_2 (Zhao et al., 2021). Hg^{II} interacts with ortho-QH_2 moieties such as those in the natural polyphenols of humic substances and tannins (Jerzykiewicz, 2013). A direct reaction yields redox-active Hg^{I} complexes with ligands of semiquinone radical character that may eventually decompose into Hg^0 (Jerzykiewicz et al., 2015). Reaction kinetic and mechanistic studies that are more applicable to the environment are not available.

Rxn W18. Thiols

Hg^{2+} and CH_3Hg^+ bind extremely strongly to heavier hydrochalcogenide groups (such as RSH and RSeH) and other corresponding groups of reduced chalcogenides, such as sulfides and disulfides (Skyllberg, 2011). Most relevant, both inorganic (e.g., H_2S, CS_2) and organic (CH_3SH, CH_3SCH_3) low-molecular-weight reduced sulfur compounds have short lifetimes (Warneck, 1988) and therefore have no effect on aqueous Hg speciation. It is questionable whether reduced sulfur/thiol groups associated with macromolecular organic compounds in aerosols influence internal Hg speciation. The photoreduction of divalent Hg by lighter aliphatic thiols is slow (< 10^{-7} s^{-1}, Si and Ariya, 2011), whereas that by thioglycolic thiols is slightly faster (2.3 × 10^{-5} s^{-1}, Si and Ariya, 2015) but hardly significant in the atmosphere.

6.2 Organic mercury

6.2.1 Demethylation channels

Biogenically produced organo-Hg in the environment is almost exclusively methylated Hg, although there are few reports of the presence of ethyl Hg (Wu et al., 2023b), which must be derived from a natural source. However, only methylated Hg has been detected in air. As mentioned above, DMHg is a major source of $MMHg^+$ compounds in the atmosphere through gas-phase degradation. Gaseous $MMHg^+$ species (Lee et al., 2003) can potentially react homogeneously to inorganic Hg, but as $MMHg^+$ species are only semi-volatile and have a high k_H^{cp}, they are more likely to be rapidly absorbed on aerosols. $MMHg^+$ species have been detected in cloud water (Li et al., 2018; Weiss-Penzias et al., 2018), fog water (Weiss-Penzias et al., 2012), rainwater (Conaway et al., 2010; Won et al., 2019) and snow (St Louis et al., 2007). Photolytic demethylation of dissolved DMHg occurs in pure water (Chen et al., 2024) incubated with sunlight ($CH_3HgCH_3 \xrightarrow{hv,\ +H^+} CH_3Hg^+ + CH_4$, ~0.32 ± 0.07 d^{-1}, West et al., 2022). Acidolytic demethylation of DMHg to $MMHg^+$ species is of very minor importance and occurs only at low pH (Maguire and Anand, 1976; Wolfe et al., 1973). A theoretical study of $CH_3HgOH_2^+$ and CH_3HgOH, which dominate the speciation of $MMHg^+$ in natural waters without significant levels of Cl^-- and reduced sulfur ligands, including DOM, indicated that $CH_3HgOH_2^+$ can be excited to the triplet state by sunlight and that this state dissociates into CH_3 and Hg^I radicals (Tossell, 1998). An room-temperature study of the photo-degradation of CH_3HgOH (aq) when irradiated by a Xe lamp with filter blocking wavelengths < 290 nm reported a rate constant of (2.2 ± 0.2) × 10^{-4} s^{-1} (Gårdfeldt et al., 2003). Rapid indirect demethylation of $MMHg^+$ species by a bimolecular process with the OH radical occurs at the limit of what diffusion allows (9.83 ± 0.66) × 10^9 M^{-1} s^{-1}, Chen et al., 2003). In natural water, select reactive oxygen species, such as singlet oxygen (see above, Suda et al., 1993; Zhang and Hsu-Kim, 2010), have been suggested to cause Hg^{II} demethylation, but their reactivity has not been directly quantified. Instead, its presence has been suggested based on the results of added scavenger/promoter tests, some of which may yield misleading results for some water compositions (Han et al., 2017). Chen et al. (2003) concluded that OH-initiated demethylation is comparable to the rates of $MMHg^+$ photodegradation reported in situ in natural waters. These researchers reported that, in addition to inorganic Hg^{II},

tog bort:) interacting
tog bort: may
tog bort: strong
formaterade: Kondenserad med 0,2 pt
formaterade: Kondenserad med 0,2 pt
tog bort: , etc.
tog bort: .
formaterade: Kondenserad med 0,2 pt
formaterade: Kondenserad med 0,2 pt
tog bort:),
formaterade: Kondenserad med 0,2 pt
tog bort:
formaterade: Kondenserad med 0,2 pt
tog bort:
formaterade: Kondenserad med 0,2 pt
tog bort: Photo-reduction
formaterade: Kondenserad med 0,2 pt
tog bort: while
formaterade: Kondenserad med 0,2 pt
formaterade: Kondenserad med 0,2 pt
tog bort: x
formaterade: Kondenserad med 0,2 pt
tog bort:),
formaterade: Kondenserad med 0,2 pt
tog bort:
formaterade: Kondenserad med 0,2 pt
formaterade: Kondenserad med 0,2 pt
tog bort: a
formaterade: Kondenserad med 0,2 pt
tog bort: have
formaterade: Kondenserad med 0,2 pt
tog bort: Henry's constant,
tog bort: rain water
tog bort: only
tog bort: NOM, indicates
tog bort: ,
tog bort: experimental
tog bort:
tog bort: a
tog bort: gave
tog bort: waters
formaterade: Teckenfärg: Dekorfärg 2
tog bort: give
tog bort: found

Hg^0 was a by-product of OH-initiated degradation in an O_2-saturated system, presumably by homolytic substitution.

6.2.2 Methylation channels

The paucity of empirical data renders the budgets of tropospheric $MMHg^+$ species highly uncertain. A recent estimate of the $MMHg^+$ pool size is 5.5 Mg, associated with a lifetime of 1.9 d, of which one of the major sources is inferred to be in-cloud methylation (Wu et al., 2024b). The potential for atmospheric biotic methylation is considered limited, despite the presence of pathogens and bacteria in aerosols and hydrometeors, because Hg-methylating microbes (possessing two important methylation genes, hgcA and hgcB, Parks et al., 2013) usually thrive in anaerobic environments, in contrast to the distinctly oxic environment of atmospheric waters. However, many unknowns about the potential for Hg^{II} methylation under oxic conditions need to be resolved (Sonke et al., 2023). There have been extensive studies on the abiotic methylation of Hg^{2+} (Ullrich et al., 2001). Methylating agents that are important for $MMHg^+$ formation in the atmosphere are oxygenated hydrocarbons containing a methyl group (Yin et al., 2012; Hammerschmidt et al., 2007). Some of them have properties that allow competitive photochemical reduction and methylation of Hg^{2+} (Yin et al., 2012). Earlier studies have investigated photochemical Hg^{2+} methylation by deep UV irradiation (Yin et al., 2012; Akagi et al., 1974; Hayashi et al., 1977), making it impossible to generalize these results to the lower atmosphere. The formation of $MMHg^+$ species was observed in the dark in dilute Hg^{II} solutions (1 nM) containing an excess of acetic acid (100:1 M/M), with an apparent first-order rate constant of $5.4 \times 10^{-6}\ s^{-1}$ in artificial rainwater (pH 4.9 Gårdfeldt et al., 2003). When the system is exposed to sunlight, photo-demethylation occurs, which counteracts $MMHg^+$ formation mediated by acetic acid/acetate, and within hours, the $MMHg^+$ concentration reaches a steady state (~2.5% of inorganic Hg^{II}). Hammerschmidt et al. (2007) noted that the average ratio of $MMHg^+$ to reactive Hg^{II} measured in North American continental precipitation (2.5 ± 0.6%) agrees with the findings of the above laboratory study. Methylation takes place intramolecularly in the acetato-mercuric complexes present in solution concerted with decarboxylation (Gårdfeldt et al., 2003; Yin et al., 2012; Akagi et al., 1974): $[Hg(CH_3COO)_n]^{2-n} \rightarrow CH_3Hg^+ + CO_2 + (n-1)\ CH_3COO^-$.

7 Multi-phase transformations

Multiphase transformations address dynamics and chemistry at interfaces and media, such as aerosol particles and cloud droplets, which interact heterogeneously with gases and solute species. Despite a wealth of studies addressing the multiphase chemical or physical transformation of Hg under processes such as those under simulated post-combustion conditions, which undoubtedly pertain to interactions with certain environmental surfaces, the findings offer limited insight into the surface and heterogeneous atmospheric Hg chemistry. The subsequent chapter addresses the studies that have been identified as contributing meaningfully to the advancement of understanding in this domain.

7.1 Gas–particle partitioning and reactive gas uptake

The behaviors of gaseous Hg^0 atoms and Hg^{II} molecules in interacting with the atmospheric condensed phase differ. The dominant Hg^0 pool has limited water solubility, and the uptake of Hg^0 vapor to aerosol surfaces is low, to the limited extent that it has been investigated. Gas phase Hg^{II} molecules, "GOM", have k_H^{cp} several orders of magnitude greater than that of Hg^0, favoring the liquid phase. The heterogeneous processes that allow GOM to be adsorbed reversibly or irreversibly, modified by ligand exchange, or dissociated to Hg^0 by reduction on surfaces are key parameters that need to be characterized to appropriately parameterize chemical transport models.

7.1.1 $HgCl_2$

Understanding the transformation from GOM to PBM through gas phase processes (condensation, **Section 5.1.4**) and aerosol surface interaction (**Section 4.2**) is crucial for parameterizing deposition. Since the separation of GOM from PBM with current methods is tentative, the accuracy of studies of Hg^{II} distribution between the gas and condensed phases, performed by preconcentration in laboratory experiments with nebulized aerosols (Rutter and Schauer, 2007b, a) and in the field (Amos et al., 2012), is retrospectively ambiguous. Fitting observational data to an equilibrium GOM + $PM_{2.5} \overset{1/T}{\Leftrightarrow}$ PBM according to a van't Hoff-type relationship $\log_{10}(K_{gp}^{-1}) = a + b/T$ is used in models to calculate the volatilization of GOM from atmospheric aerosols, where K_{gp} (**Eq. 9**) is weighted by the inverse of the mass concentration of fine particulate matter ($PM_{2.5}$; Shah et al., 2021). The partitioning expression does not consider that the interaction between

tog bort: budget
tog bort:
tog bort: have been discussed as
tog bort: in deep UV
tog bort: Formation
formaterade: Kondenserad med 0,4 pt
tog bort:)
formaterade: Kondenserad med 0,4 pt
tog bort: ,
tog bort: enters
tog bort: have pointed out
tog bort: is in agreement
tog bort: The methylation
tog bort: $[Hg(CH_3COO)_n]^{2-n}$
tog bort: deal with the
formaterade: Teckenfärg: Dekorfärg 2
tog bort: various
Formaterat: Avstånd Efter: 6 pt
tog bort: interacting
tog bort: Although there is a significant amount of literature
formaterade: Teckenfärg: Blå
tog bort: field (Ariya et al., 2015; Subir et al., 2011, 2012), it is mostly irrelevant to the atmosphere
formaterade: Teckenfärg: Blå
tog bort: -
tog bort: behavior
tog bort: differs
tog bort: is of
tog bort: is low
tog bort: Henry's coefficients
tog bort: Heterogeneous
tog bort: keep
tog bort: ,
Formaterat: Avstånd Efter: 6 pt
tog bort: 3
tog bort: phase
tog bort: aerosol
tog bort:
tog bort: 8
tog bort: here
tog bort: ,

GOM and a surface is significantly influenced by the composition of the surface layer. $HgCl_2$(g) partitions among particles consisting of typical alkali metal salts such as chlorides, nitrates, and sulfates (Mao et al., 2021; Malcolm et al., 2009). To compensate, global Hg models treat the uptake of GOM onto sea salt particles separately as an irreversible first-order process parameterized by wind speed and humidity. The equilibrium studies conducted at atmospheric pressure do not provide insights into the dynamics of the system, as the experiments are limited by mass transport, which negates the possibility of obtaining quantitative information on reactive uptake. As an alternative (Liu et al., 2022), partition coefficients have been calculated for individual GOM species based on theoretical predictions of both adsorption and absorption (Wu et al., 2024a). The reactive uptake of $HgCl_2$(g) on surfaces representative of inorganic and organic primary and secondary atmospheric aerosols has recently been studied via the fast flow technique coupled with an ion drift chemical ionization mass spectrometer (ID-CI-MS). The reported data (Mao et al., 2021; Khalizov and Mao, 2023) are summarized in **Table 6**.

Table 6. Reactive uptake of $HgCl_2$(g) on surfaces

Chemical	Structural formula[34]	γ_{net}[35]		Surface coverage (θ, %)	Lifetime (τ, days)
		γ^0_{net},	γ^∞_{net}		
Inorganic aerosol surrogates					
Na_2SO_4		3.1×10^{-2}	1.7×10^{-3}	98	0.1
NaCl		2.2×10^{-2}	1.9×10^{-3}	65	0.1
$(NH_4)_2SO_4$		1.4×10^{-2}	7.0×10^{-4}	5.6	0.2
NH_4NO_3		3.6×10^{-3}	3.3×10^{-4}	0.3	0.7
Primary organic aerosol (POA) surrogates					
Levoglucosan		1.1×10^{-2}	2.9×10^{-4}	9.6	0.2
Pyrene		2.1×10^{-3}	5.0×10^{-4}	1.3	1.2
Perylene		3.0×10^{-3}	5.2×10^{-4}	3.8	0.8
Soot	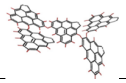	8.9×10^{-5}		0.1	20.2
Secondary organic aerosol (SOA) surrogates					
Citric acid (H_3cit) NaH_2cit Na_2Hcit Na_3cit	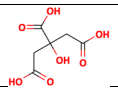	$< 1 \times 10^{-5}$ 6.9×10^{-5} 2.4×10^{-3} 8.4×10^{-3}	$< 1 \times 10^{-5}$ 5.0×10^{-5} 2.3×10^{-4} 6.6×10^{-4}	< 0.02 < 0.02 1.2 7.5	> 242 35 1.0 0.3
Pimelic acid (H_2pim) NaHpim Na_2pim	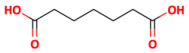	1.1×10^{-3} 2.2×10^{-3} 8.2×10^{-3}	1.8×10^{-4} 3.1×10^{-4} 8.0×10^{-4}	1.0 1.4 11.6	2.2 1.1 0.3
Succinic acid (H_2suc) NaHsuc Na_2suc	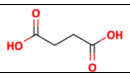	9.3×10^{-4} 2.0×10^{-3} 8.3×10^{-3}	1.0×10^{-4} 3.6×10^{-4} 6.6×10^{-4}	0.02 0.7 6.2	2.6 1.2 0.3
Dioctyl sebacate	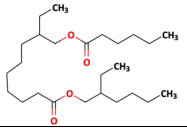	2.6×10^{-2}	7.1×10^{-3}	153	0.1

The data in **Table 6** are for dry surfaces, where γ^0_{net} is the initial uptake coefficient, which is relevant throughout the lifetime of the aerosol, as the surface coverage by atmospheric $HgCl_2$ remains unchanged and low. In the presence of sea salt aerosols (>0.6 μm, initially at pH 8) that dominate in marine air, where NaCl represents >95% of its mass, the lifetime of $HgCl_2$ (g) is expected to be between 4 and 20 h depending on aerosol loading (Mao et al., 2021). When the relative humidity exceeds ~75%, a hygroscopic sea salt droplet is formed as the salt deliquesces, and a highly mobile surface phase in which Hg^{II} is equilibrated in ionic form as $HgCl_4^{2-}$ may contribute to more rapid GOM loss in marine air (Holmes et al., 2009). Ammonium salts such as nitrates and sulfates are

[34] For soot, a clichéd structure is used that does not claim to be accurate.
[35] Calculated by Eq. 5

tog bort: has a high partitioning for
tog bort: the basis of
formaterade: Teckenfärg: Dekorfärg 2
tog bort: using
tog bort: to
tog bort: ,
tog bort:
Formaterat: Radavstånd: Flera 1,15 li
Formaterad tabell
Formaterad tabell
tog bort:
tog bort:
tog bort:
Formaterad tabell
tog bort: the
formaterade: Teckenfärg: Dekorfärg 2
tog bort: a
tog bort:

primarily found in secondary particles, typically in urban and agricultural-rural air. Although $HgCl_2$ uptake is lower here, its lifetime is comparable because of the higher particle number and the large surface area they generally represent. These semi-volatile ammonium salts do not occur in isolation but coexist with oxygenated organics formed through photochemical activity, resulting in the formation of secondary aerosols, which constitute the primary fraction of the atmospheric burden of organic aerosols (OA, Jimenez et al., 2009). The acidity of secondary organic aerosols (SOAs), a dominant component of $PM_{2.5}$, affects $HgCl_2$ uptake by controlling the acid–base equilibria of characteristic chemical species such as aliphatic dicarboxylic acids, aromatic polycarboxylic acids, and other oxygenated multi-functional organics in aerosols. For the diprotic acids in **Table 6**, the reactivity becomes noticeable only after the first deprotonation step at pH 4.5 - 5.5. For the triprotic citric acid, activation occurs after the second step at pH 6.5. The adsorption of $HgCl_2$ on primary organic aerosol (POA) surfaces is significant in the presence of levoglucosan, an anhydrosugar, which is a fingerprint of fire activity. Nevertheless, the interaction between $HgCl_2$ and polyaromatic hydrocarbons (PAHs) derived from carbonaceous fuel combustion is more constrained, occurring between the electrophile $HgCl_2$ and the π electrons delocalized over the aromatic fused ring skeleton. The observed adsorption on fresh soot, which is porous and graphitic with a high specific surface area, is more than one order of magnitude lower than that for the minor type of PAH studied (pyrene, perylene). If morphology affects uptake, so does the state of the surface phase, as a diester of sebacic acid (a close homolog of pimelic acid), octyl sebacate, a lubricant, is more reactive to $HgCl_2$ than the microcrystalline pimelic acid film is. The adsorption of $HgCl_2$ on mineral surfaces (dust aerosols) represented by iron (hydr)oxides has not been studied experimentally, but calculations indicate a partition coefficient (K_{gp}) for α-Fe_2O_3 that exceeds that for NaCl by three orders of magnitude (Tacey et al., 2018b). The studies listed in **Table 6** were performed without observing redox chemistry (i.e., no Hg^0 was detected to be emitted from the $HgCl_2$-exposed surfaces when heated to 120 °C), but a combined study using FF-ID-CIMS and Raman spectroscopy revealed that exchange reactions between gaseous mercuric compounds are catalyzed by surfaces such that $HgCl_2$ and $HgBr_2$ molecules in the presence of a deactivated surface produce mixed BrHgCl molecules (Mao and Khalizov, 2021), which are also volatile. Owing to rapid exchange reactions, the prospect of accurately speciating GOMs by pre-concentration on filters and cation exchange membranes, as discussed previously (**Section 3.1**), is unlikely.

7.1.2 Hg^0

A challenge in studying gas-phase- or liquid-phase-initiated reactions is the potential for side reactions and phase changes to occur during experiments. Thus, a portion of the loss of gas-phase Hg^0 in laboratory experiments designed to study homogeneous oxidation (e.g., by O_3, Snider et al., 2008; $NO_3^{\bullet}$, Sommar et al.,1997, etc.) has been linked to a heterogeneous rate component (k_{surf}) occurring on new surfaces that form during experiments (product clusters undergoing particle growth in free suspension, **Section 5.1.4**) and/or on initially deactivated existing surfaces (reactor walls) that begin to catalyze Hg^0 surface oxidation as deposits form (Sommar et al., 1997; Medhekar et al., 1979). For example, in a series of spherical reactors with varying surface-to-volume ratios (S/V), Pal and Ariya (2004b) reported the loss of Hg^0 by reacting with excess O_3 in N_2 as follows:

$$-d[Hg^0]/dt = \left\{k_{gas} + \frac{S}{V}\cdot k_{surf}\right\}\cdot[Hg^0]\cdot[O_3] = k_{net}\cdot[Hg^0]\cdot[O_3] \qquad (11)$$

where k_{gas} (cm^3 $molecule^{-1}$ s^{-1}) is the gas-phase reaction rate, S/V (cm^{-1}), k_{surf} (cm^4 $molecule^{-1}$ s^{-1}) is the surface rate loss, and $[O_3]$ (molecules cm^{-3}) is the gas-phase O_3 concentration. In the S/V range of 0.28–0.93 cm^{-1}, k_{net} increased by 30% simultaneously with the formation of particles (Snider et al., 2008) during the experiments, which started homogeneously. Using a fluorocarbon film smog chamber (9 m^3, S/V = 0.03 cm^{-1}), Rutter et al. (2012) studied the influence of SOA (yielding an ~100-fold increase in the surface area of the system) and secondarily formed $^{\bullet}OH$ (at ambient level due to added scavenger) generated from an irradiated mixture of O_3 and various biogenic and anthropogenic VOCs (at a level ~one order of magnitude greater than ambient) on the oxidation of Hg atoms (at a level ~two orders of magnitude greater than ambient). Neither Rutter et al. nor subsequent researchers (Lyman et al., 2022) have been able to identify evidence that interactions with photochemical smog particles significantly contribute to the oxidation of Hg^0. Nevertheless, few studies concerning Hg^0 uptake have been conducted with a sufficiently rigorous standard, employing techniques used in specific studies of heterogeneous processes to produce a kinetic formalism that can be related to

tog bort: comparative due to
tog bort: seeding
tog bort: SOA
tog bort: -
tog bort: the aerosol. Of
formaterade: Teckenfärg: Dekorfärg 2
tog bort: it
tog bort: of the
tog bort: type
tog bort: PAHs of the
tog bort: homologue
tog bort: microcrystaline
tog bort: being
tog bort: up
tog bort: shows
tog bort: ,
tog bort: the
tog bort: molecule
tog bort: is
tog bort: Due
tog bort: the
tog bort: GOM
tog bort: 4
tog bort:
tog bort: .
tog bort: of
tog bort: observed
tog bort: reaction
tog bort: an
tog bort: of
tog bort: following
tog bort: 10
tog bort: -
tog bort: a
tog bort: higher
tog bort: order
tog bort: higher
tog bort: interaction
tog bort: contributes
tog bort: to
tog bort: the
tog bort: ,

atmospheric models. These studies, which were conducted with a coated-wall laminar flow tube reactor, focused on the light- and moisture-dependent uptake of Hg^0 (detected by CV-AFS), which may be photocatalytic, on the major metal oxides (TiO_2, Fe_2O_3, FeOOH, and Al_2O_3) present in mineral dust aerosols (Kurien et al., 2017; Lee et al., 2022). The first three metal oxides have semiconductor properties with band gaps that allow photoexcitation in the UVA (≤ 395 nm) and visible (≤590 nm) regions, while Al_2O_3, the second most abundant mineral oxide in the Earth's crust after SiO_2, is an insulator but has some thermal conductivity. It has been established for over half a century that Hg^0 vapor in the presence of O_2 over an irradiated TiO_2 surface is consumed by reactive uptake (Kaluza and Boehm, 1971) via the following tentative mechanism:

$$TiO_2 \xrightarrow{h\nu} e^-_{CB} + h^+_{VB}$$
$$e^-_{CB} + O_2\,(ads) \rightarrow O_2^{\bullet-}\,(ads)$$
$$h^+_{VB} + H_2O|OH^-\,(ads) \rightarrow HO^{\bullet}\,(ads) + (H^+(ads))$$
$$Hg^0\,(ads) + HO^{\bullet}\,(ads) \rightarrow {}^{\bullet}Hg^{I}OH\,(ads) \qquad \text{(Rxn 10a-g)}$$
$${}^{\bullet}Hg^{I}OH\,(ads) + O_2\,(ads) \rightarrow HgO\,(ads) + HO_2^{\bullet}\,(ads)$$
$$HO^{\bullet}\,(ads) + HO_2^{\bullet}\,(ads) \rightarrow H_2O\,(ads) + O_2\,(ads)$$
$$HO_2^{\bullet}\,(ads) + O_2^{\bullet-}\,(ads) \xrightarrow{H^+} H_2O_2\,(ads) + O_2\,(ads)$$

When excited by light of a wavelength shorter than the band gap energy, the generation of electron–hole pairs (e^-_{CB}, h^+_{VB}) occurs in the conduction and valence bands (**Rxn 10a**). The electrons and holes transported to the particle surface initiate redox chemistry by reacting with H_2O and O_2 molecules to form reactive oxygen species (ROS, **Rxn 10b, c**). The oxidation potential of h^+_{VB} exceeds +2.27 eV in the TiO_2, Fe_2O_3 and FeOOH cases, which is sufficient to generate hydroxyl radicals from surface water (**Rxn 11c**) that can oxidize adsorbed Hg^0 (**Rxn 10d**). The reported uptake coefficients are in the range of $<10^{-10}$ to $>10^{-4}$ (based on the Brunauer–Emmett–Teller surface area), with relative reactivities of $Fe_2O_3 \lesssim FeOOH < Al_2O_3 < TiO_2$, where γ^{∞}_{net} without irradiation is below the detection limit. The uptake of Hg^0 on iron (hydr)oxides is less than 10^{-8} under both UV and visible light and is inhibited by humidity, as is the case for Al_2O_3, which shows measurable uptake under UV irradiation ($\gamma^{\infty}_{net} = 1.2 \times 10^{-8}$). The photo-initiated uptake of Hg^0 on TiO_2 is significant, especially under UV light at low humidity ($\gamma^{\infty}_{net} > 3 \times 10^{-5}$, diffusion-controlled limit). However, as with Al_2O_3, it shows reversibility (desorption of Hg^0) in the presence of water vapor during darkness (Lee et al., 2022), whereas Hg^0 exhibits almost irreversible binding to iron (hydr)oxides at the temperatures studied (< 150 °C, Kurien et al., 2017). Based on limited published data, only under conditions of low humidity and very high mineral dust aerosol loading can the uptake of Hg^0 be considered to have any effect on the atmospheric cycling of Hg^0. Notably, there are no corresponding experimental data for $HgCl_2$ uptake on mineral dust surrogates.

The uptake of Hg^0 on ice, which involves the migration of radioactive Hg isotopes into ice spheres in a packed bed flow tube exposed to a strong temperature gradient, can be described as reversible adsorption without significant solvation. The observations were in accordance with a Langmuir isotherm, where the adsorption equilibrium can be described thermodynamically by Bartels-Rausch et al. (2008):

$$-RT\ln K = \Delta H^0_{ads} - T\Delta S^0_{ads} = -28000 + 38 \cdot T \qquad (12)$$

where K is the Langmuir absorption constant (**Eq. 8**), R is the gas constant, T is the absolute temperature, and ΔH^0_{ads} and ΔS^0_{ads} are the enthalpy and entropy of adsorption, respectively. Compared with k^{cc}_{H} for Hg^0 (0.18 at 5 °C), the Langmuir adsorption coefficient on ice, which is expressed in a dimensionless way, is much smaller even at temperatures lower than the freezing point of the metal (2.2×10^{-5} at 220 K), which is most relevant for polar regions and the upper troposphere. Therefore, in both atmospheric and polar environments, the uptake of $Hg^0(g)$ on ice surfaces is negligible.

7.2 Reduction of mercurial species on surfaces

Computational chemistry studies report that the adsorption of mercuric halides on dry salt- or mineral-like surfaces reduces the energy required for reduction to Hg^0 (Tacey et al., 2016) and that the reduction of $HgCl_2$ and $HgBr_2$ to Hg^0 on iron oxide aerosols requires the presence of actinic light (Tacey et al., 2018a). Breaking the first Hg–X bond is possible either thermally or photolytically, while the

tog bort: concern
tog bort:
tog bort:) that
formaterade: Teckenfärg: Dekorfärg 2
tog bort: 11a
formaterade: Teckenfärg: Dekorfärg 2
tog bort: -
tog bort: ,
tog bort: 12a). Electrons
tog bort: 11b
tog bort: 11d
tog bort: BET
formaterade: Teckenfärg: Blå
tog bort: the
tog bort: the
tog bort: ,
tog bort: was
tog bort: in
tog bort: while
tog bort: 150°C
formaterade: Teckenfärg: Dekorfärg 2
tog bort: the
tog bort: discussed as having
tog bort: It is worth noting that
tog bort: is
tog bort: studied by
tog bort: by
tog bort: 11
tog bort: 7
tog bort: to the Henry's law equilibrium
tog bort: °C
tog bort: both
tog bort: its
tog bort: x
tog bort: the
tog bort: environment,
tog bort:),

second requires photons with $\lambda \leq 461$ nm. To release Hg^0 from the surface, an excitation energy of 2.59 eV ($\lambda \leq 479$ nm) is required in a photoinduced charge transfer process between the surface and the adsorbate.

The photoreduction of particle-bound Hg^{II} has been the subject of experimental investigations (Tong et al., 2013; Tong et al., 2014). In these experiments, aerosol surrogates doped with $HgCl_2$ were generated and dried in laboratory air and subsequently captured on filters, which were then exposed to light with three spectral options in a flow-through reactor. Photoreduction of NaCl aerosols occurs under actinic light (both UV and visible light, with approximately 2.5% and 2.0% of Hg^{II} reduced, respectively, during a 30-minute exposure, normalized per 100 W m^{-2} irradiation). However, the presence of iron species (mainly Fe^{III} rather than Fe^{II}) has been observed to exert some inhibitory effects (Tong et al., 2013). In contrast, photoreduction on carbon-based synthetic aerosols has been demonstrated to be more significant but also more variable. For example, Hg^{II} on adipic acid aerosols is reduced by 8% (per same time unit and normalization as above), while on levoglucosan, it is less than 2% (Tong et al., 2014). Notably, however, these experiments were carried out without O_2 in the carrier gas stream.

The reduction of Hg^{II} in ice in the presence of organics has been studied in an ice-coated flow tube at atmospheric pressure under irradiation with light between 300 nm and 420 nm (Bartels-Rausch et al., 2011). O_2-free ice matrices containing 60 nM Hg were doped with a stoichiometric excess (up to 50:1 M/M) of either benzophenone (a strong photosensitizer), oxalic acid-oxalate (forming photolabile Hg^{II} complexes), or humic acid (ditto photolabile complexes), which, upon irradiation, accelerated the release of Hg^0, which was most rapid in the presence of benzophenone at high pH. The presence of O_2 (20% in the gas stream), the introduction of sea ice-like conditions, or a large drop in temperature (from 270 to 250 K) or pH (to 4) resulted in diminished photoreduction. The mechanism by which Hg^{II} reduction is sensitized by benzophenone is challenging to ascertain. One potential mechanism involves the dissociation of an excited state of the major species, $Hg(OH)_2$, which has been reported to be photolabile as a solute in water (Xiao et al., 1994). A controlled laboratory study of light-irradiated natural snow samples at a temperature of -10 °C revealed that the release of Hg^0 follows first-order kinetics with a coefficient between 0.18 and 0.25 h^{-1}, corresponding to a natural lifetime of 4–5.6 h (Dommergue et al., 2007). However, no monitoring of Hg^{II} in the condensed phase has been conducted. Given that light does not penetrate the entire snowpack, it can be assumed that a Hg^{II} gradient toward depletion at the top is established.

Brominated mercurials that are present in the Arctic environment during AMDE may play a role in light-induced Hg re-emission from the cryosphere to the atmosphere (cf. **Fig. 2**). A computational study (Carmona-García et al., 2025) suggested that compared with $HgBr_2$ in the gas phase, $HgBr_2$ in solution has an increased absorption cross section for wavelengths longer than 290 nm, whereas bromomercurate anions ($Hg^{II}Br_3^-$ and $Hg^{II}Br_4^{2-}$) have a comparatively greater absorption in actinic light. The low-energy excited states of $HgBr_2$, $Hg^{II}Br_3^-$, and $Hg^{II}Br_4^{2-}$ in solution are characterized by electronic transitions in which the electron density is mainly transferred from the Br atoms to the Hg atom, indicating a significant photoreductive character upon light absorption, leading to the generation of Hg^I species ($^\bullet Hg^IBr$, $^\bullet Hg^IBr_2^-$ and $^\bullet Hg^IBr_3^{2-}$) and a bromine atom. The photoreductive character is also recognized for the aforementioned Hg^I species in their electonically excited states, which plausibly dissociate via an LMCT mechanism with Hg^0 as the product. The predicted peak photolysis constants for the polar spring (March, ~80°N) are 3.9×10^{-6}, 3.8×10^{-4} and 7.9×10^{-5} s^{-1} for $HgBr_2$, $HgBr_3^-$ and $HgBr_4^{2-}$, respectively.

For pure heterogeneous reduction, there is experimental evidence that SO_2(g) can reduce HgO(s) at room temperature via $Hg^I_2SO_4$ (Zacharewski and Cherniak, 1987) to Hg^0, HgS and $HgSO_4$ as stable products (Scott et al., 2003), and that O_3(g) in the presence of actinic light can reduce $HgCl_2$/$HgBr_2$(s) to mercurous species (Ai et al., 2023, which may tentatively undergo Hg^0/Hg^{II} disproportionation). In the latter exploratory study, single-particle reactors, 10–50 µm in size, synthesized from mercuric halides in single-walled carbon nanotubes were prepared to levitate during the experiments via optical tweezers. The turnover of HgX_2 by breaking a Hg–X bond was measured by time- and position-resolved Raman spectroscopy, which also showed that the decomposed X atom was bound to the carbon material (X = Cl, Br). Heterogeneous reactions of this type, i.e.,

$\xrightarrow{h\nu}$ (Rxn 11)

tog bort: investigation
Formaterat ... [404]
tog bort: aerosolized
formaterade ... [405]
tog bort: ,
tog bort: ,
tog bort: on
tog bort: in
tog bort: in
tog bort: exhibits a comparatively 8% reduction
tog bort: It should be noted
tog bort: that
formaterade ... [406]
tog bort: with a maximum rate constant
tog bort: ~5 × 10^4 M^{-1} s^{-1} observed for
formaterade ... [407]
formaterade ... [408]
tog bort: the
tog bort: –
tog bort: was
tog bort: towards
Formaterat ... [409]
tog bort:
tog bort: , 2024) suggests
tog bort:
tog bort: compared to $HgBr_2$ in the gas phase, while the
tog bort: even higher
tog bort: end
tog bort: Predicted
tog bort: °N
tog bort: x
tog bort: x
tog bort: x
formaterade ... [410]
tog bort:),
formaterade ... [411]
tog bort: a
formaterade ... [412]
tog bort: nanotube,
formaterade ... [413]
tog bort: and made
formaterade ... [414]
tog bort: using
formaterade ... [415]
tog bort: means
formaterade ... [416]
tog bort: an
formaterade ... [417]
formaterade ... [418]
tog bort: 12
formaterade ... [419]

$$XO^{\bullet} + O(^3P) \rightarrow X^{\bullet} + O_2$$

$$2\ {}^{\bullet}Hg^{I}X\ (s) \rightarrow Hg_2X_2\ (s) \rightleftarrows Hg^0\ (ads) + HgX_2\ (s)$$

may explain why KCl-coated denuders do not work as a robust quantitative method for measuring GOM in ambient air (Lyman et al., 2010). Since the gas-phase reaction $HgX_2 + O/O_3 \rightarrow {}^{\bullet}Hg^{I}X + XO^{\bullet}$ (+ O_2) is endothermic (≥ 66 kJ mol^{-1}) and therefore unlikely, the results of a steady-state study (Tong et al., 2021) claiming gas-phase photoreduction of HgX_2 in the presence of O_3 and light can instead be attributed to the above-mentioned heterogeneous reactions. Additionally, voltammetry can provide valuable insights into the redox chemistry of mercury. Hg^0 is frequently employed as the working electrode and has a high overpotential for the reduction of H_3O^+ to H_2. This enables the utilization of standard potentials as negative as -1 V in acidic solutions and -2 V in basic solutions. The surface of the hanging mercury drop electrode (HMDE) can be readily renewed by extruding a new drop. In a study by Giannakopoulos et al. (2012), the interfacial adsorption mechanism of gallic acid onto HMDE was investigated, and a series of easily reducible Hg^{II} complexes with mono-, di-, or tridentate gallic acid ligation were identified.

7.3 Dark oxidation of Hg^0 accelerated by freeze-concentration effects

Slow oxidation of dissolved Hg^0 by O_2 occurs in aquatic systems in the presence of Cl^- ions (Amyot et al., 2005; Wang et al., 2023). However, upon freezing, most of the solutes are separated from the forming ice phase and concentrated in the remaining liquid at a significantly reduced pH (Bartels-Rausch et al., 2011). In experimental mimics of the micro-pockets of solutions that occur in ice, experiments in the presence of O_2, H_2O_2, and HONO each result in significant Hg^0 oxidation. It has been postulated that protonated forms, $HO\text{-}OH_2^+$ and $ONOH_2^+$, are responsible for oxidation processes, which can be classified as strongly exothermic on the basis of the provided thermodynamic data (O'Concubhair et al., 2012). Moreover, neither dilute H_2O_2 (aq) nor HONO (aq) will oxidize Hg^0 (aq) to any significant extent at room temperature (Kobayashi, 1987).

7.4 Surface-catalyzed reduction of Hg^{II} in aqueous solution

In the presence of a solid phase of ferric (hydr)oxide and dissolved di- or monocarboxylic acids under oxic conditions, the reduction of Hg^{II} in aqueous solution to Hg^0 occurs upon UV irradiation (Lin and Pehkonen, 1997). The systems studied for the photoreduction of Hg^{II} are goethite (α-FeOOH) + oxalate/formate, hematite (α-Fe_2O_3) + oxalate, and maghemite (γ-Fe_2O_3) + oxalate. The experiments with filtered Xe light were conducted with 10 µM $HgCl_2$, 1 mM organic acid, and 0.1 g L^{-1} ferric hydr(oxide) suspension, with a starting pH of 3.9. During some of the experiments, the pH increased substantially, resulting in the dominance of oxalate over hydrogen oxalate. Unlike oxalate, formate alone is not capable of reducing Hg^{II} to Hg^0 under actinic light. It requires irradiation in the deep UV by processes such as (Leonori and Sturgeon, 2019):

$$Hg^{2+} + 2\ HCOO^- \rightleftarrows Hg(OOCH)_2 \xrightarrow{h\nu} Hg^0 + 2\ CO_2 + H_2 \qquad \text{(Rxn 12)}$$

$$Hg^{2+} + HCOO^- \rightleftarrows Hg^{II}(OOCH)^+ \xrightarrow{h\nu} Hg^{\bullet+} + HCO_2^{\bullet} \text{ and } Hg^{\bullet+} + HCOO^- \rightarrow Hg^0 + HCO_2^{\bullet}$$

One study described Hg^{II} reduction mediated by the carbon dioxide radical anion ($CO_2^{\bullet-}$) generated from formic acid via photo-sensitization by visible light-excited naphthoquinone (Berkovic et al., 2012). Iron(III) complexes with formate and oxalate are photolabile under UVA and visible, where a fast 1e–LMCT step generates Fe^{2+} and eventually $CO_2^{\bullet-}$, which initiates a chain process (Mangiante et al., 2017; Baxendale and Bridge, 1955):

$$\equiv Fe^{III}\text{–}OH + HC_2O_4^- | HCOO^- \rightleftarrows \equiv Fe^{III}\text{–}C_2O_4^- | OOCH + H_2O$$

$$\equiv Fe^{III}\text{–}C_2O_4 | OOCH \xrightarrow{h\nu} \equiv Fe^{II} + C_2O_4^{\bullet-} | HCO_2^{\bullet}$$

$$\equiv Fe^{II} \rightleftarrows \equiv + Fe^{2+} \text{ and } HCO_2^{\bullet} \rightleftarrows H^+ + CO_2^{\bullet-}$$

$$C_2O_4^{\bullet-} \rightarrow CO_2 + CO_2^{\bullet-},\ CO_2^{\bullet-} + O_2 \rightarrow CO_2 + O_2^{\bullet-} \text{ and } H^+ + O_2^{\bullet-} \rightleftarrows HO_2^{\bullet} \rightarrow \tfrac{1}{2}\ O_2 + \tfrac{1}{2}\ H_2O_2 \qquad \text{(Rxn 13)}$$

$$Fe^{2+} + H_2O_2 \rightarrow Fe^{III} + HO^- + HO^{\bullet}$$

$$Hg^{II} + CO_2^{\bullet-} | Fe^{2+} | \equiv Fe^{II} \rightarrow Hg^{I} + CO_2 | Fe^{III} | \equiv Fe^{III},\ Hg^{I} + CO_2^{\bullet-} | Fe^{2+} | \equiv Fe^{II} \rightarrow Hg^0 + CO_2 | Fe^{III} | \equiv Fe^{III} \text{ (red.)}$$

$$2\ Hg^{I} \rightleftarrows Hg^0 + Hg^{II} \text{ (disprop.)}$$

$$Hg^{0/I} + HO^{\bullet} \rightarrow Hg^{I/II} + HO^-,\ Fe^{2+} + HO^{\bullet} \rightarrow Fe^{III} + HO^- \text{ and } H_2O_2 + HO^{\bullet} \rightarrow HO_2^{\bullet} + H_2O \text{ (ox.)}$$

The oxic reaction system described by **Rxn 13** reaction formulas contains a number of ROS with different designations, such as strongly reducing $CO_2^{\bullet-}$ and strongly oxidizing $HO^{\bullet}$, as extreme cases. One subsystem is Fenton's reagent (**Section 6.1.1**, **Rxn W6**), which

tog bort:
formaterade ... [420]
formaterade ... [422]
Formaterat ... [421]
tog bort: a
formaterade ... [423]
tog bort: ¶
formaterade ... [424]
tog bort: , exhibiting
formaterade ... [425]
formaterade ... [426]
tog bort: solution
formaterade ... [427]
tog bort: the
formaterade ... [430]
tog bort: based
formaterade ... [428]
formaterade ... [429]
formaterade ... [431]
tog bort: O'concubhair
formaterade ... [432]
tog bort: It should be added that
formaterade ... [433]
formaterade ... [434]
tog bort: Systems
formaterade ... [435]
tog bort: that show
formaterade ... [436]
tog bort: in
formaterade ... [437]
formaterade ... [438]
tog bort: 13
formaterade ... [439]
tog bort:
formaterade ... [440]
tog bort: describes
formaterade ... [441]
formaterade ... [442]
tog bort: in the
formaterade ... [443]
tog bort: into the
formaterade ... [444]
tog bort:
formaterade ... [445]
tog bort: that
formaterade ... [446]
formaterade ... [447]
tog bort: 14
formaterade ... [448]
formaterade ... [449]
tog bort: 14
formaterade ... [450]
tog bort: the
formaterade ... [451]
formaterade ... [452]
tog bort: the
formaterade ... [453]
formaterade ... [454]
tog bort: the
formaterade ... [455]

produces $HO^{\bullet}$, for which each of the $Hg^{0/I}$, Fe^{2+}, and H_2O_2 competes to be oxidized. Except for the heterolytic photolysis of $Hg(\eta^2\text{-}C_2O_4)$, which produces Hg^0 from Hg^{II} in a single step (**Section 6.1.2**, **Rxn W16**), the remaining redox steps involving metals are of the single-electron type. The reduction of Hg^{II} occurs via reactions with $HCO_2^{\bullet}/CO_2^{\bullet-}$ nucleophiles (**Section 6.1.2**, **Rxn W14**), which are both homogeneous and heterogeneous with dissolved and adsorbed ferrous species, respectively. A second-order homogeneous reaction coefficient of ~120–313 M^{-1} s^{-1} has been determined in the near-neutral pH range, with $Hg(OH)_2$ and $FeOH^+$ identified as the reactive species in solution (Amirbahman et al., 2013; Schwab et al., 2023). Under anoxic conditions, the rate of Hg^0 production derived from surface-catalyzed reduction on hematite and goethite has been described by the expression $k_{het}[\equiv Fe^{II}][Hg(OH)_2]$, with k_{het} values of ~89 and ~78 M^{-1} s^{-1}, respectively (Amirbahman et al., 2013). In an O_2-saturated, non-bubbled solution, a photo-stationary state between Hg^{II} and Hg^0 occurs, indicating that the reduction pathways (**Rxn J3, red.**) are gradually balanced by oxidation pathways (**Rxn J3, ox.**, Ababneh et al., 2006). In the absence of Hg^0 removal, solubility limitations are easily exceeded during experiments (Lin and Pehkonen, 1997; Ababneh et al., 2006), resulting in the precipitation of colloidal Hg^0. The removal of dissolved Hg^0 by sorption on hydrous iron oxides, which is relevant here, is also documented (Richard et al., 2016). In the presence of competing anions, such as chloride, the rate of reduction decreases, in part owing to the formation of metastable, poorly soluble dimeric mercurous salts that compete with the disproportionation of Hg^I to Hg^0 and Hg^{II} (Pasakarnis et al., 2013).

7.5 Field observations of photoreduction in precipitation, clouds and fog

In precipitation and clouds, a strong correlation between Hg and total organic carbon was observed (Li et al., 2018; Åkerblom et al., 2015), suggesting that Hg-organics complexes are also important in aerosols. Authentic rain samples, where Hg-organics complexes dominate, present photoreduction rates ranging from 0.02–0.2 h^{-1} (Yang et al., 2019; Saiz-Lopez et al., 2019; Fu et al., 2021). There have been a handful of measurements of Hg in cloud water (Li et al., 2018; Weiss-Penzias et al., 2018; Malcolm et al., 2003; Gerson et al., 2017; Huang et al., 2016a), but thus far, only a few studies on the photoreduction rate in this category of water exist (Li et al., 2018; Zhen et al., 2023; Gao et al., 2023). Photolysis rates in cloud water samples of 0.07–0.21 h^{-1} measured in situ under actinic light and in the laboratory under UV (> 290 nm) light are consistent with those observed in precipitation. Whether the photoreduction rates observed in rain or cloud water are representative of atmospheric aerosols is questionable. Hg^{II} in snowfall or freshly fallen snow has been reported to be labile for photoreduction (Steffen et al., 2008; Faïn et al., 2013). In temperate urban and pristine rural snow, within 24 h, approximately 50% (Lalonde et al., 2003; Lalonde et al., 2002) and, within 48 h, up to 90% (Poulain et al., 2004) of the newly deposited Hg can be effectively recycled back to the atmosphere. The reduction is reportedly strong even under cloudy conditions and is not limited by light (Faïn et al., 2013). In general, less than 5% of the Hg content of a snowpack is in the elemental form (Hg^0), which is concentrated stratigraphically in the first few centimeters. Nevertheless, if the rates are implemented as a mean value (~0.07 h^{-1}), determining the lifetime of atmospheric Hg against wet deposition, then the model-estimated wet deposition underestimates the observations by an average of 25% globally. Current global chemistry and transport models (GMOS-Chem) consider photoreduction on particles with the pool of Hg^{II} complexed with organic ligands as the reactant (Shah et al., 2021).

8 Mercury isotope systematics and fractionation

Natural Hg contains seven stable isotopes with mass numbers of 196, 198, 199, 200, 201, 202 and 204. In the 1920s, significant separation of Hg into its isotopes was achieved through vaporization in a vacuum (Harkins and Mulliken, 1921; Mulliken, 1923; Brønsted and De Hevesy, 1921), a process that is conducted on a preparative scale through electromagnetic (Love, 1973) and photochemical (Vyazovetskii, 2012) methods. When the feed flow is in the form of DMHg, total gram quantities of highly enriched Hg isotopes can be obtained through cascade centrifugation (Babaev et al., 2010). The longest-lived radioisotope is ^{194}Hg at 444 y. Since it does not occur naturally, it cannot be used in the dating typical of ^{14}C. Two additional unstable isotopes (^{197}Hg and ^{203}Hg, with half-lives of 64.1 h and 46.6 d, respectively) are valuable for instrumental neutron activation analysis and radiolabeled Hg compounds because of their decay by emission of readily detectable γ rays. It was not until after the turn of the century, 80 years later, with the development of high-precision analytical instruments such as multi-collector inductively coupled plasma–mass spectrometry (MC–ICP–MS), that it became possible

formaterade ... [456]
formaterade ... [457]
tog bort: by reaction
tog bort: the
formaterade ... [461]
tog bort: and
formaterade ... [458]
formaterade ... [459]
formaterade ... [460]
formaterade ... [462]
tog bort: homogeneously
formaterade ... [463]
tog bort: heterogeneously
formaterade ... [464]
tog bort: to
formaterade ... [465]
tog bort:
formaterade ... [466]
tog bort: In
formaterade ... [467]
tog bort: the
formaterade ... [468]
tog bort: 14
formaterade ... [469]
tog bort: the
formaterade ... [470]
tog bort: 14
formaterade ... [471]
tog bort: due
formaterade ... [472]
tog bort: cloud
Formaterat ... [473]
tog bort: show…resent photoreduction rates in the range ... [474]
tog bort: so…hus far there seems to be… only a few stud ... [475]
Formaterat ... [476]
formaterade ... [477]
Formaterat ... [478]
tog bort: the
formaterade ... [479]
tog bort: a
formaterade ... [480]
tog bort: a
formaterade ... [481]
tog bort: life
formaterade ... [482]
tog bort: of value in
formaterade ... [483]
tog bort: radio-labeled
formaterade ... [484]
tog bort: , due to
formaterade ... [485]
tog bort: γ rays
formaterade ... [486]
tog bort:
formaterade ... [487]
tog bort: -
formaterade ... [488]
tog bort: -
formaterade ... [489]

to measure differences in the naturally stable Hg isotopic compositions in the environment (Jackson, 2001; Lauretta et al., 2001). Natural processes, including redox reactions, complexation, sorption, precipitation, dissolution, evaporation, diffusion, and biological processes can alter the isotopic composition, i.e., cause stable isotope fractionation (cf. **Fig. 17**). Stable isotope analyses can, therefore, provide a previously untapped source of valuable information on the sources and biogeochemical cycling of natural and anthropogenic Hg. Isotopic fractionation refers to the division of a sample into two (or more) parts with different ratios of "heavy" and "light" isotopes than the original ratio. In isotopic jargon, if one part contains more heavy isotopes, it is said to be "enriched," while the other part is said to be "depleted". Hg has extremely large isotopic variation in nature, which, when normalized by the relative mass difference between isotopes, approaches that of traditional light element isotopes (Wiederhold, 2015). However, the overlapping signals from different fractionation processes can be a major challenge in deciphering natural isotopic signatures when tracing sources. It is important to determine the Hg stable isotope fractionation for *individual* key processes, which can be accomplished, inter alia, through controlled laboratory and field experiments. Stable isotope variations are reported as relative values compared with a reference standard (NIST SRM 3133 Hg solution, Blum and Bergquist, 2007):

$$\delta^{xxx}Hg = 1000\cdot\left[\left(^{xxx}Hg/^{198}Hg\right)_{sample}/\left(^{xxx}Hg/^{198}Hg\right)_{NIST3133} - 1\right] \quad (13)$$

where $^{xxx}Hg/^{198}Hg$ ($R^{xxx/198}$) is the ratio of the isotopes with mass numbers xxx and 198. The prevailing practice of expressing isotope ratios relative to the lightest stable isotope for each element is not applicable to Hg because of the rarity of ^{196}Hg (0.15% occurrence). The standard unit for δ values is per mill (‰). $\delta^{202}Hg$ expresses the total mass-dependent fraction (TMDF, containing contributions from conventional mass-dependent fractionation; hereafter, MDF and nuclear field shift (NFS) are described in **Section 8. 1**), while the isotope anomalies caused by mass-independent fractionation, MIF are expressed by capital deltas, Δ is defined as the difference between the measured δ value and that predicted from the measured $\delta^{202}Hg$ value and the scale factor for the kinetic MDF ($\beta^{xxx}_{KIE\text{-}MDF}$; see **Section 8. 1**) and is approximated for δ values < 10‰ according to:

$$\Delta^{xxx}Hg = \delta^{xxx}Hg - \beta^{xxx}_{KIE\text{-}MDF}\cdot\delta^{202}Hg \quad (14)$$

which is expressed numerically for each relevant Hg isotope:

$\Delta^{196}Hg = \delta^{196}Hg + 0.508\cdot\delta^{202}Hg$, $\Delta^{199}Hg = \delta^{199}Hg - 0.252\cdot\delta^{202}Hg$, $\Delta^{200}Hg = \delta^{200}Hg - 0.502\cdot\delta^{202}Hg$, $\Delta^{201}Hg = \delta^{201}Hg - 0.752\cdot\delta^{202}Hg$ and $\Delta^{204}Hg = \delta^{204}Hg - 1.493\cdot\delta^{202}Hg$.

The fractionation between two compounds A and B (assuming that A is a product of a reaction and that B is the remaining reactant) is expressed with the fractionation factor, α, which is defined as the ratio of the isotope ratios in the compounds:

$$\alpha^{xxx}_{A\text{-}B} = R^{xxx/198}_A/R^{xxx/198}_B = R^{xxx}_A/R^{xxx}_B = \frac{1000 + (\delta^{xxx}Hg)_A}{1000 + (\delta^{xxx}Hg)_B} \quad (15)$$

The last term is obtained by substituting **Eq. 13** into the first term of **Eq. 15**. Actual δ values are usually very close to unity. Therefore, it is usually more practical to use an enrichment factor:

$$\varepsilon^{xxx}_{A\text{-}B} = (\delta^{xxx}Hg)_A - (\delta^{xxx}Hg)_B \cong 1000\cdot(\alpha^{xxx}_{A\text{-}B} - 1) \cong 1000\cdot\ln\alpha^{xxx}_{A\text{-}B} \quad (16)$$

The last similarity is valid only for δ values less than 10‰. Substitute **Eq. 14** into **Eq. 16** and obtain:

$$\varepsilon^{xxx}_{A\text{-}B} \cong \{(\Delta^{xxx}Hg)_A - (\Delta^{xxx}Hg)_B\} + \beta^{xxx}_{KIE\text{-}MDF}\cdot[(\delta^{xxx}Hg)_A - (\delta^{xxx}Hg)_B] \quad (17)$$

Eq. 17 expresses total fractionation during the process A → B, with the first term representing the MIF enrichment factor and the second term representing the total mass-dependent enrichment factor. Thus, the enrichment factor for MIF is written as a capital epsilon:

$$E^{xxx}_{A\text{-}B} = \{(\Delta^{xxx}Hg)_A - (\Delta^{xxx}Hg)_B\} = \varepsilon^{xxx}_{A\text{-}B} - \beta^{xxx}_{KIE\text{-}MDF}\cdot\varepsilon^{202}_{A\text{-}B} \quad (18)$$

Many kinetic processes can be described as Rayleigh fractionation, which is an irreversible process in an open system involving the progressive removal of a fraction of a trace substance from a larger reservoir. It is described by the following differential equation:

tog bort: natural
formaterade ... [490]
tog bort: isotope composition
formaterade ... [491]
tog bort: can alter the isotopic composition, i.e., causing ... [492]
formaterade ... [493]
tog bort: .
formaterade ... [494]
tog bort: ”
formaterade ... [495]
tog bort: an
formaterade ... [496]
tog bort: the
formaterade ... [497]
tog bort: isotope
formaterade ... [498]
tog bort: done
formaterade ... [499]
Formaterat ... [500]
formaterade ... [501]
tog bort: $(R^{xxx/198}_{sample}/R^{xxx/198}_{NIST3133} - 1)$
tog bort: 12
Formaterat ... [502]
formaterade ... [503]
tog bort: R
formaterade ... [504]
tog bort: Parenthesized:^{196}Hg
formaterade ... [505]
tog bort: an alternative
formaterade ... [506]
tog bort: its low
formaterade ... [507]
tog bort: of only 0.15%.
formaterade ... [508]
tog bort: The
formaterade ... [509]
tog bort: factor α determines the distribution of isotopes
formaterade ... [510]
flyttade (infogning) [7]
formaterade ... [511]
formaterade ... [512]
formaterade ... [513]
formaterade ... [514]
formaterade ... [515]
formaterade ... [516]
formaterade ... [517]
tog bort: any
Formaterat ... [518]
formaterade ... [519]
tog bort: parts (
formaterade ... [520]
tog bort:)
formaterade ... [521]
tog bort: system as follows
formaterade ... [522]
tog bort: ¶ ... [523]
Formaterat ... [524]
formaterade ... [525]
Formaterat ... [526]
tog bort: $\varepsilon_{A-B} = \delta_A$
formaterade ... [527]
tog bort: $-\delta_B=-$ ... [528]
tog bort: 14
formaterade ... [529]
tog bort: only
formaterade ... [530]

$$d \ln R^{xxx} = (\alpha^{xxx} - 1) \cdot d \ln f_R \quad (19)$$

If the fractionation factor is constant, the differential equation can be integrated directly into the expression:

$$R^{xxx} / (R^{xxx})_0 = f_R^{(\alpha^{xxx}-1)} \quad (20)$$

where $(R^{xxx})_0$ is the isotope ratio of the initial reservoir (when $f_R = 1$) and where R^{xxx} is the isotope ratio of the reservoir at a given time when the fraction of initial material remaining in the reservoir is defined by f_R. The following expression is often used to evaluate the fractionation factor:

$$\ln \frac{1000 + \delta^{xxx}Hg}{1000 + (\delta^{xxx}Hg)_0} = (\alpha^{xxx}-1) \cdot \ln f_R \quad (21)$$

The process tends to enrich the heavier isotopes in the reservoir ($\alpha < 1$, normal kinetic isotope effect, KIE) rather than removing the heavier isotopes from the reservoir more rapidly ($\alpha > 1$, inverse KIE).

8.1 Conventional mass-dependent and mass-independent fractionation

The scaling factor β describes the relationship between the fractionation factors as follows:

$$\alpha^{xxx} = (\alpha^{202})^{\beta} \quad (22)$$

where β for mass-dependent equilibrium fractionation ($\beta_{EIE\text{-}MDF}$) and kinetic fractionation ($\beta_{KIE\text{-}MDF}$) are as follows (Young et al., 2002):

$$\beta_{EIE\text{-}MDF} = \frac{1/m_{198} - 1/m_{xxx}}{1/m_{198} - 1/m_{202}} \quad (23)$$

$$\beta_{KIE\text{-}MDF} = \frac{\ln(m_{198}/m_{xxx})}{\ln(m_{198}/m_{202})} \quad (24)$$

The equilibrium MDF resulting from the differences in zero-point vibrational energy (ZPE) distances and the kinetic MDF resulting from the differences in dissociation energies between the isotopologues and their respective effects can be expressed in two rules: Heavier isotopes are preferentially concentrated in compounds with the highest force constant, where the element is most rigidly bound and has greater potential energy. Conversely, compounds enriched in lighter isotopes have weaker bonds and require less energy to break, so they preferentially enter chemical reactions and are enriched in the product (Criss, 1999). Combining kinetic and equilibrium MDF makes it possible to achieve a limit of approximately 10‰ fractionation (Sun et al., 2022).

Properties of nuclei, such as nuclear size and shape or the presence of non-zero nuclear spins, may trigger isotope fractionation that does *not* follow the expected MDF relationships. The nuclear field shift (NFS, Rosenthal and Breit, 1932) is the interaction of the nuclear volume with electrons (NVE, Schauble, 2007). It is highly relevant for very heavy metals, including Hg, Tl, Pb, and U. NFS involves a shift in the ground electronic energy of an atom or molecule due to differences in nuclear size and shape between isotopes. The shift caused by an odd (neutron number) nucleus scales non-linearly between those of the even isotopes of the next highest and lowest atomic masses. The odd isotope electronic energy level is shifted toward the next lower even nucleus (odd-even staggering). Owing to its smaller size and greater surface charge density, the electronic energy of a light isotope is lower than that of a heavier isotope. The amount of shift is a product of two factors: the electron density at the nucleus and the charge, size, and shape of the nucleus and the change in the latter two between isotopes. Hg orbital electrons significantly overlap with the nucleus, whereas 5p, 5d, and 4f orbitals do not, although f electrons in inner shells have a smaller screening effect on 6s-valence electrons (Bigeleisen and Wolfsberg, 1957). The lowest energy of a system occurs when the heavier isotopes of Hg are enriched in chemical species with the fewest s-electrons in the bonding or valence orbital. The largest shifts, therefore, occur when the number of Hg 6s electrons is greatly reduced by the formation of an ionic bond (to an electronegative element), while a covalent bond has less influence. Examples of Hg species in the former category are chloro- or aqua-complexes with high coordination numbers (e.g., $[Hg(H_2O)_6]^{2+}$), while the latter includes soft ligands with typical linear bi-coordination (e.g., $Hg(SH)_2$ and $(CH_3)_2Hg$). The scale factor of nuclear volume fractionation (β_{NFS}) is defined as follows:

Formaterat ... [531]
tog bort: ln R = (α–1)
tog bort: 15
Formaterat ... [532]
Formaterat ... [533]
tog bort: $R/R_0 = f_R^{\alpha-1}$
tog bort: 16
tog bort: R_0
tog bort:), R
Formaterat ... [534]
tog bort: In the literature, the
tog bort: $\ln\frac{1000+\delta}{1000+\delta_0} = (\alpha^{xxx/198}-1)\ln f_R$
tog bort: 17
Formaterat ... [535]
tog bort: remove
tog bort: Scaling
tog bort: $\alpha_{xxx/198} = \alpha^{\beta}_{202/198}$
tog bort: 18
tog bort: 19
tog bort: β_{KIE_MDF}
tog bort: 20
tog bort: of thumb: the heavier… Heavier isotopes are ... [536]
Formaterat ... [537]
tog bort: spin
formaterade ... [538]
tog bort: first effect, called
formaterade ... [539]
tog bort:), detected in atomic spectra, results from
formaterade ... [540]
tog bort: on
tog bort: also called nuclear volume effect,
formaterade ... [542]
tog bort:) and
formaterade ... [543]
tog bort: the
formaterade ... [544]
tog bort: which besides
formaterade ... [545]
tog bort: also include, e.g.,
formaterade ... [541]
formaterade ... [546]
tog bort: is
formaterade ... [547]
tog bort: higher
formaterade ... [548]
tog bort: lower
formaterade ... [549]
tog bort: mass
formaterade ... [550]
tog bort: neutron
formaterade ... [551]
tog bort: towards
formaterade ... [552]
tog bort: Due
formaterade ... [553]
tog bort: The
formaterade ... [554]
tog bort: 6s-
formaterade ... [555]
tog bort: -,
formaterade ... [556]
tog bort: -
tog bort: -
formaterade ... [558]
tog bort: -
formaterade ... [557]
formaterade ... [559]

$$\beta_{NFS} = \frac{\langle r^2_{198}\rangle - \langle r^2_{xxx}\rangle}{\langle r^2_{198}\rangle - \langle r^2_{202}\rangle} \quad (25)$$

where $\langle r^2 \rangle$ describes the mean-square nuclear charge radii of different isotopes. Coincidentally, MDF and NFS with ^{198}Hg, ^{200}Hg and ^{202}Hg show almost identical β values, but ^{199}Hg, ^{201}Hg and ^{204}Hg and, to a lesser extent, ^{196}Hg show distinct non-mass dependent signatures due to NFS. Only a small proportion of the NFS is mass independent because it creates a deviation from MDF (Yang and Liu, 2015). The mass-dependent part of the two effects can be synergistic (increasing TMDF) or antagonistic (decreasing TMDE), with the former being dominant for Hg redox chemistry (Hintelmann and Zheng, 2011; Jiskra et al., 2012). The MDF scale is proportional to $1/T^2$, whereas the NFS scale is proportional to $1/T$ and is more prominent than MDF for the Hg red-ox reactions studied (Schauble, 2007). Among the commonly measured isotopes 198-202, a minor to moderate level of MIF has been experimentally observed in the odd isotopes 199 ($\leq$ 0.6‰) and 201 as a result of NFS. NFS has been described for equilibrium exchange reactions but has never been extended to kinetic processes. In contrast to the small magnitude observed in natural samples, the possibility has recently been suggested that nonequilibrium isotopic effects of NFS in photodissociation may give rise to a significant magnitude of MIF (Motta et al., 2020b).

The only effect that has been documented to lead to significant odd-mass number Hg MIF (odd-MIF) in present-day surface ecosystems is the magnetic isotope effect (MgIE). MgIE is a purely kinetic effect triggered by the formation of a long-lived radical pair after a primary process that causes homolysis of a Hg–ligand bond upon photolytic excitation. (**Fig. 11**). Among the stable isotopes of Hg, only ^{199}Hg and ^{201}Hg (odd mass numbers) have non-zero nuclear spin and momentum, with half-integer ($^1/_2$ and $^3/_2$, respectively) spins. MgIE arises when hyperfine coupling (HFC) acts on a spin-coherent solvent-separated radical pair after dissociation by changing the rate of intersystem crossing from singlet to triplet (S↔T) or vice versa (T↔S) in odd Hg isotopes. Radical pairing and MgIE are suppressed in mercuric complexes with strong spin–orbit coupling (containing bromine and iodine ligands), favoring spin mixing and to the ground state, while S-, Cl- and C-bonded complexes with generally weak spin–orbit coupling favor strong MgIE (Motta et al., 2020a). If the radical pair is born in the triplet state (lower panel of **Fig. 11**), HFCs are induced, enriching odd isotopes in the resulting singlet state. The singlet radical pair can then recombine to the ground state, resulting in odd isotope enrichment in the reactant, expressed as (+)MgIE. When the radical pair is in the singlet state (top panel of **Fig. 11**), the overall effect is to deplete odd isotopes in the reactant, as expressed by (–)MgIE, because mainly the odd isotopes with the majority in the triplet radical pair dissociate into free radicals. A computational study has explained why the photodissociation of monomethyl Hg species in nature is observed to yield only (+)MgIE, whereas the photolysis of inorganic mercuric complexes may yield positive or

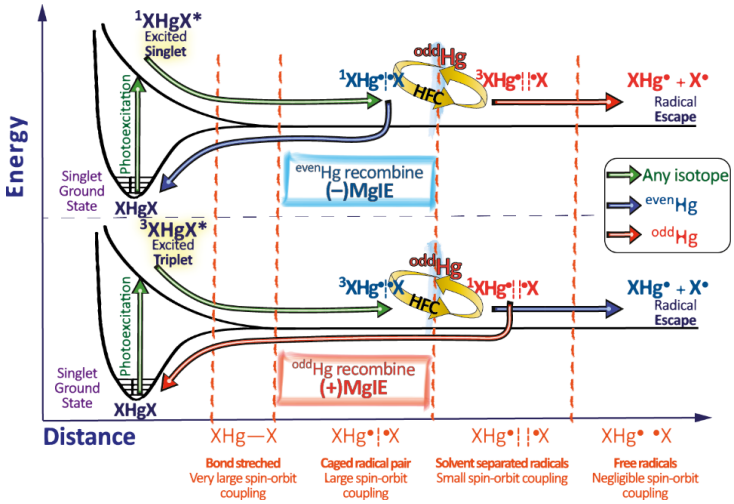

tog bort: 21
Formaterat: Radavstånd: Flera 1,15 li
Formaterat: Avstånd Efter: 6 pt
tog bort: -
tog bort: -
tog bort: total fractionation
tog bort: total fractionation),
formaterade: Teckenfärg: Dekorfärg 2
tog bort: Regular
tog bort: scales are proportionate
tog bort: NVF scales are proportionate
tog bort: regular
tog bort: isolated
formaterade: Teckenfärg: Blå
formaterade: Teckenfärg: Blå
tog bort: -
tog bort: the
tog bort: -
tog bort: return
tog bort: -
formaterade: Kondenserad med 0,3 pt
tog bort: an
formaterade: Kondenserad med 0,3 pt
tog bort: provided an explanation as to
formaterade: Kondenserad med 0,3 pt
formaterade: Kondenserad med 0,3 pt
formaterade: Kondenserad med 0,3 pt

negative MgIE, depending on the reaction conditions and the degree of complex ligation (**Section 8.4**).

Figure 11. General scheme for the photolysis of a molecule to produce a spin-correlated radical pair (RP). The singlet and triplet RPs can be interconverted by intersystem crossing. Both the singlet and triplet RPs can escape from the solvent cage. Only the singlet RP can recombine. Adopted from Turro (1983) and Motta et al. (2020a).

Thus, odd-MIF results from both the MgIE and NFS mechanisms. MgIE is most effective in viscous solvents, where a "solvent cage" environment is possible (Turro, 1983). In addition, a seemingly enigmatic even mass number Hg isotope MIF (even-MIF) has been observed in samples of atmospheric origin or deposition. However, analog atmospheric photochemical anomalous isotope fractionation is well known for the lighter (traditional) elements for which MIF (containing three or more stable isotopes), such as oxygen and sulfur, can be detected. However, understanding the underlying causes of multi-isotope anomalous fractionation is limited because investigations require detailed quantum mechanical calculations at the molecular isotope level, e.g., photodissociation. Recently, rock records have revealed significant even-MIF in the Archean atmosphere, which lacked an ozone (O_3) layer to filter UVC from actinic light, suggesting that contemporary UVC-induced atmospheric chemistry may be responsible for the coupled changes in even-MIF for both Hg and sulfur (Zerkle et al., 2020). Correlations between these entities have also been observed in marine aerosols in the Southern Hemisphere (Auyang et al., 2022).

8.1.1 MIF signatures as additional tracers

The isotopic measurement of Hg results in up to six useful isotopic signatures (δ^{202}Hg, Δ^{196}Hg, Δ^{199}Hg, Δ^{200}Hg, Δ^{201}Hg and Δ^{204}Hg). In addition, pairs of these signatures have been utilized to distinguish between fractionation mechanisms. The relationship between these signatures is typically illustrated using a three-isotope plot. To interpret the experimental results satisfactorily, specific robust linear regression methods are recommended (Stephan and Trappitsch, 2023). On the basis of early results (Bergquist and Blum, 2007), it was assumed that photoreduction of Hg^{II} to Hg^0 would result in a $\Delta^{199}Hg/\Delta^{201}Hg$ ratio of unity. Several investigated photoreactions exhibit just a ratio of 1 within the margin of error (refer to **Table 8**, **Section 8.4**). However, further data have shown that this is not always the case, as the slope depends on factors such as the complexing ligand and reaction conditions. Clearly, the odd-MIF signature for the photolysis of organomercurials is different from that stipulated for inorganic Hg. The photolytic degradation of $MMHg^+$ species results in a variation in $\Delta^{199}Hg/\Delta^{201}Hg$ ranging from 1.17 to 1.38 depending on the reaction conditions (Bergquist and Blum, 2007; Chandan et al., 2015; Rose et al., 2015; Malinovsky et al., 2010). Compared with MgIE, NFS generally results in a much weaker MIF, with greater anomalous fractionation of ^{199}Hg than of ^{201}Hg, which approaches a ratio of ~1.6. However, the NFS should be confirmed via alternative methods when the experimentally measured NFS is too limited to determine a definitive odd-MIF ratio (Motta et al., 2020b). Another commonly used parameter is $\Delta^{199}Hg/\delta^{202}Hg$, which describes the degree of odd-MIF in relation to TMDF. The even-MIF signature of Δ^{200}Hg to Δ^{204}Hg, which is negative in natural samples (air, rainfall, and fish), is discussed in **Section 8.2.4**.

8.2 Isotopic characteristics of atmospheric mercury

Fig. 13 summarizes the magnitude of the isotopic observations reported in the literature on the main fractions of Hg in the atmosphere, namely, gaseous Hg dominated by Hg^0, particle-bound Hg and Hg associated with hydrometeors (rain, snow and water from clouds and fog). Here, δ^{202}Hg, Δ^{199}Hg, and Δ^{200}Hg are used to describe TMDF, odd-MIF, and even-MIF, respectively. The number of isotopically resolved samples has increased dramatically in recent years. Readers should consult the literature regularly to stay up to date. On the other hand, this development justifies revisiting the topic, even though it has been satisfactorily addressed in the recent past (Kwon et al., 2020). Notably, the spatial distribution of available data is heavily skewed toward North America, Europe, and East Asia, and observations from large parts of the world are missing (**Fig. 13**). However, as far as marine remote regions are concerned, recent oceanographic expeditions have contributed to an increasing amount of data. Further below, the in situ and laboratory experiments performed thus far to study the gas exchange of Hg^0 between air and water, soil and foliage in terms of isotope fractionation are discussed.

8.2.1 Gaseous Hg

The following part excludes an early series of measurements where the air was not filtered prior to sampling (Rolison et al., 2013). The referenced series of measurements should be considered TAM, not total gaseous mercury (TGM). TGM significantly affects δ^{202}Hg (–3.75 to 1.52‰) and Δ^{199}Hg (–0.62 to 1.32‰) but is more limited to Δ^{200}Hg (–0.22 to 0.11‰). Analogous to Hg^{II} deposited

formaterade ... [571]
flyttade (infogning) [8]
formaterade ... [572]
tog bort: solvent
formaterade ... [574]
tog bort: a
Formaterat ... [573]
formaterade ... [575]
formaterade ... [576]
tog bort:)
formaterade ... [577]
tog bort: an
formaterade ... [578]
tog bort:) can be detected,
formaterade ... [579]
tog bort: the investigation requires
formaterade ... [580]
tog bort: for
formaterade ... [581]
tog bort: photo absorption and
formaterade ... [582]
tog bort: southern hemisphere
formaterade ... [583]
tog bort: MIF (denoted with capital delta, Δ) is ... [584]
Formaterat ... [585]
flyttade upp [8]: **Figure 11.** General scheme for the photolysis of
formaterade ... [586]
flyttade upp [7]: $\Delta^{196}Hg = \delta^{196}Hg + 0.508 \cdot \delta^{202}Hg$,
formaterade ... [590]
formaterade ... [591]
formaterade ... [592]
tog bort: The MIF enrichment factor E^{xxx}Hg for a proces ... [593]
formaterade ... [587]
formaterade ... [588]
formaterade ... [589]
tog bort: **Signatures…ignatures as Additional Tracer** ... [594]
Formaterat ... [595]
tog bort: Based on
tog bort: **4…, Section 8.4**). However, further data has ... [596]
tog bort: exhibits…esults in a variation of ... [597]
tog bort: gives rise to a …enerally results in a much weal ... [598]
Formaterat ... [599]
Formaterat ... [600]
tog bort: shown…sed to describe MDF…MDF, odd-MIF ... [601]
formaterade ... [602]
tog bort: keep…tay up to date. On the other hand, this ... [603]
Formaterat ... [604]
Formaterat ... [605]
tog bort: as total airborne Hg
formaterade ... [606]
tog bort: shows a significant spread for…ignificantly aff ... [607]

in biomass and fossil fuels such as coal (Sun et al., 2014), Hg^0 in natural gas (Washburn et al., 2018) and in smoke from spontaneous combustion in coal fields (Sun et al., 2023) has strongly negative $\delta^{202}Hg$ values. This differs from the majority of Hg^0 in ambient air, which is isotopically heavy (often with positive $\delta^{202}Hg$ values). Terrestrial background air (rural, subpolar and forest in **Fig. 13a**) has higher $\delta^{202}Hg^0$ values because it is modified by vegetation, which preferentially incorporates lighter isotopes of Hg^0 into the foliage. Foliar uptake of Hg^0 is discussed in more detail in **Section 8.6.2**. The estimate of atmospheric Hg^0 dry deposition to vegetation has recently been revised and constrained to approximately 2300 Mg yr^{-1} (Feinberg et al., 2022), and together with the large negative $\varepsilon_{foliage/air}$ of the process, the global atmospheric Hg^0 pool is estimated to have a $\delta^{202}Hg$ mean of 0.5‰, in contrast to that of Hg^0 from anthropogenic sources (global bulk mean of –0.7‰, Sun et al., 2019). Studies examining the vertical distribution of mercury (Hg^0) concentrations from near the ground to above the canopy in different forest types reveal clear gradients averaging 10% (Wang et al., 2022) and 20% (Fu et al., 2016b) of ambient Hg^0. Under stable conditions, such as during summer nights, Hg^0 levels are strongly depleted below the canopy (Fu et al., 2016b; Mao et al., 2008; Poissant et al., 2008; Lan et al., 2012; Fu et al., 2019a). Thus, isotopic measurements of above-canopy air versus in-canopy air (Wang et al., 2022; Fu et al., 2016b) and daytime air versus nighttime air in forests (Kurz et al., 2020) show statistically significant differences ($p < 0.01$) in $\delta^{202}Hg^0$. For a deciduous forest in Northeast China, Fu et al. (2019a) reported that $\delta^{202}Hg^0$ in biweekly air samples during the growing season was 0.35 to 0.99‰ higher than that during the dormant season. In a subtropical, perennial forest in southwestern China, where there is little seasonal variation in the photosynthetic activity of vegetation, the existing seasonal variation in $\delta^{202}Hg^0$ (with an amplitude of 0.4 ‰) can be attributed to the influence of long-range anthropogenic emissions, which primarily occur during the warmer seasons. However, over the last five to seven years, the air concentrations of Hg^0 have decreased significantly in the two mentioned forest reserves due to reduced regional anthropogenic emissions, as evidenced by the median value of $\delta^{202}Hg^0$ shifting from 0.42 to 0.46‰ and from 0.17 to 0.57‰. The marine $\delta^{202}Hg^0$ data ($n = 112$) are significantly lower (Wilcoxon test, $p < 0.01$) than those from the forest ($n = 113$). Coastal measurements in the Gulf of Mexico show that the marine-influenced air isotopically represents background air modified by Hg^0 emitted from the sea after being formed in surface water by photoreduction (Demers et al., 2015). Measurements in the marine boundary layer of the offshore East China Sea indicated that airborne Hg^0 is essentially a binary mixture of anthropogenic outflow from mainland China and air masses from the sea (significantly correlated $\delta^{202}Hg^0$ and $\Delta^{199}Hg^0$ vs. $C^{-1}_{Hg^0}$), with an extrapolated $\Delta^{199}Hg^0$ of –0.26‰ for the marine component. The extrapolated $\Delta^{199}Hg^0$ value agrees well with observations made in Hawaii with passive samplers (Szponar et al., 2020) as well as with the signatures of a larger number of samples from Mauna Loa (3397 m a s l) in the free troposphere (Tate et al., 2023; Yamakawa et al., 2024).

The generally negative signature of $\Delta^{199}Hg^0$ in the background air indicates that Hg^0 has been added to the pool subsequent to Hg^{II} photoreduction (of the variant that induces (+)MgIE in the reactant and complements it by depleting the product Hg^0 isotopically for odd isotopes) in oceans and aerosols. This is supported by atmospheric Hg^0 exhibiting $\Delta^{199}Hg/\Delta^{201}Hg$ slopes close to unity (Kwon et al., 2020), similar to aqueous photoreduction of inorganic Hg^{II}. However, not all photolytically controlled Hg^0 re-emissions from terrestrial ecosystems contribute to negative $\Delta^{199}Hg^0$ values in the atmosphere. An analysis of gas exchange in a subtropical beech forest revealed bidirectional fluxes of Hg^0, with uptake partially balanced by reemission of previously metabolized Hg^{II}. Photo reduction recirculates Hg^0, contradicting a retro flux of deposited Hg^0 at the leaf surface (data in **Fig. 18a**). This re-emission is isotopically distinct in that it is enriched in odd isotopes compared with ambient air (Yuan et al., 2019b), indicating that leaf photoreduction induces (–)MgIE, as reported for Hg^{II} bound to organic ligands containing sulfur or nitrogen in low oxidation states (Motta et al., 2020b; Zheng and Hintelmann, 2010b). A mass balance based on isotope measurements indicates that, compared with the uptake of Hg^0 from the air, re-emission from beech foliage gradually increases from emergence to senescence, accounting for an average of 30% (Yuan et al., 2019b). Observations from a temperate deciduous forest revealed 0.06–0.09 ‰ higher $\Delta^{199}Hg^0$ values during the growing season than in winter, suggesting that foliar Hg^0 efflux contributes to the atmospheric enrichment of odd Hg isotopes (Fu et al., 2019a).

The large spread of odd-MIF shown by Hg^0 in polar air (Araujo et al., 2022; Yu et al., 2021; Sherman et al., 2010, **Fig. 13a**) is due to the portion of the collected data that includes Hg^0 depletion events in the spring and Hg^0 enhancement during the summer, when reemissions of Hg^0 occur from the cryosphere. **Fig. 12** shows the isotopic compositions of airborne Hg fractionated into Hg^0 and Hg^{II}

tog bort: -
tog bort: upward …nd constrained to about…pproximate … [608]
tog bort: concentration
formaterade … [609]
tog bort: show
formaterade … [610]
tog bort: for
formaterade … [611]
formaterade … [612]
tog bort: , respectively.… Under stable conditions, such … [613]
tog bort: northeast…ortheast China, Fu et al. (2019a) obs … [614]
tog bort: southwest
formaterade … [615]
tog bort: with
formaterade … [616]
tog bort: the
formaterade … [617]
tog bort: related
formaterade … [618]
tog bort: transported
formaterade … [619]
tog bort: mainly
formaterade … [620]
tog bort: in
formaterade … [621]
tog bort: 5
formaterade … [622]
tog bort: 7
tog bort: been falling rapidly
tog bort: decreasing
formaterade … [623]
formaterade … [624]
formaterade … [625]
tog bort: can be seen in
formaterade … [626]
tog bort: Based on coastal
formaterade … [627]
tog bort: , Demers et al. (2015) determined
formaterade … [628]
tog bort: measured
formaterade … [629]
tog bort: ….(Demers et al., 2015). Measurements in the … [630]
tog bort: $\delta^{202}Hg^0$and
tog bort: -
formaterade … [631]
Formaterat … [632]
formaterade … [633]
tog bort: can be considered to reflect
formaterade … [634]
tog bort: after
formaterade … [635]
tog bort: in Earth's surface reservoirs interacting with th … [636]
formaterade … [637]
tog bort: in
formaterade … [638]
tog bort:).
formaterade … [639]
tog bort: photo
formaterade … [640]
tog bort: A branch-level study
formaterade … [641]
tog bort: air-foliage Hg^0
tog bort: perennial
formaterade … [642]
formaterade … [643]
tog bort: , where leaf
formaterade … [644]
tog bort: of Hg^0 from ambient air is

(RM) during the Arctic spring (at three stations) compared with the corresponding data from a background station in the Pyrenees (Fu et al., 2021). With respect to $\Delta^{199}Hg$, a dichotomy between the polar and temperate data is striking for both Hg^0 and Hg^{II} (RM), in that montane oxidized Hg is enriched in a limited range (0.14 to 0.77‰) whereas the polar Hg^{II} is depleted in a greater range (–2.15 to –0.18‰), with a complementary relationship existing for Hg^0 (–0.31 to –0.16‰ versus –0.22 to 1.32‰). This relationship could be caused by surface layer airborne Hg being strongly influenced by the oxidation of Hg^0 to Hg^{II}, which is controlled by halogen atoms during AMDEs, processes characterized by $E^{199}Hg$ values of –0.37‰ and –0.23‰ for $Cl^{\bullet}$-initiated and $Br^{\bullet}$-initiated oxidation, respectively (**Table 7**, Sun et al., 2016). In this way, the remaining reactant is driven to a higher $\Delta^{199}Hg^0$ and the molecular products assume negative $\Delta^{199}Hg^{II}$ values. However, this interpretation is not corroborated by the measured $\Delta^{199}Hg/\Delta^{201}Hg$ ratio of nearly unity in airborne Hg, which is more typically indicative of Hg^{II} photo-reduction (–MgIE) occurring in snow. It has been proposed that this process also operates in aerosols of the boundary layer, with Hg^0 reemissions providing such a strong positive imprint that the entire boundary layer of the Hg^0 pool becomes enriched in odd isotopes (Araujo et al., 2022). Isotopic measurements of $Hg^{II}(g)$ separated from $Hg^{II}(p)$ using CEM (cf. **Section 3.1**) have commenced and are anticipated to elucidate the mechanisms underlying the pronounced fractionation of odd isotopes in airborne Hg^0 and Hg^{II}. Several such datasets are currently in preparation for publication. Furthermore, Hg^0 in the Arctic during the dark period of the year and from the Antarctic Peninsula throughout the year (Yu et al., 2021) shares a consistently slightly negative $\Delta^{199}Hg^0$ with other background air (represented by montane air in **Fig. 13a**). In the late Arctic summer, minimum $\Delta^{199}Hg^0$ values (approaching –0.5 ‰) are observed uniformly without much variation from coastal stations around the Arctic Ocean, which are thought to result from photoreduction of cryospheric Hg^{II}, a substrate that has been strongly depleted of odd isotopes during months of long sunshine (Araujo et al., 2022).

$\Delta^{200}Hg^0$ is generally negative for non-fossil/anthropogenic sources, while the remainder is significantly shifted to higher values (Wilcoxon T-test, e.g., natural gas vs. arid data, $p < 0.01$). As mentioned above, even-MIF is generated exclusively by atmospheric chemical processes, which may be mainly limited to molecular $Hg^{I,II}$ photolysis processes (Sun et al., 2022), of which Hg^0 is a product. The marine and polar $\Delta^{200}Hg^0$ data have the most negative values. For example, a recently published TGM record from Mauna Loa (not shown in **Fig. 13a**) in the Pacific Ocean has $\Delta^{200}Hg$ values as low as –0.20‰ (Yamakawa et al., 2024). The polar pool as a unit significantly shifted toward lower $\Delta^{200}Hg^0$ values than did the forest pool (Wilcoxon T-test, $p < 0.05$). One can only speculate as to the reason, but it should be mentioned in the context of a halogen-rich environment that any presence of Cl-initiated Hg^0 oxidation in the gas phase will result in depletion of ^{200}Hg in the reactant pool ($E^{200}Hg \sim 0.06$‰, Sun et al., 2016). Owing to its relatively limited range, ambient $\Delta^{200}Hg^0$ and $\Delta^{204}Hg^0$ are considered conservative tracers of atmospheric Hg^0 deposition, and terrestrial surface and water $\Delta^{200}Hg$ and $\Delta^{204}Hg$ values can constrain the relative contribution of Hg^0 to Hg^{II} deposition. Throughout, a median value of -0.05‰ (IQR –0.02 to –0.08‰) of $\Delta^{200}Hg^0$ was used to calculate this contribution to atmospheric transfer to soil ($\Delta^{200}Hg^{II}$~0‰, Enrico et al., 2016; Zhou et al., 2021; Zheng et al., 2016) and oceans ($\Delta^{200}Hg$~0.04‰, Jiskra et al., 2012). The quantitative AMDEs observed in Alaska are isotopically mass balanced in that the $\Delta^{200}Hg^{II}$ in snow (-0.06‰) corresponds, within the measurement uncertainty, to that in ambient Hg^0 (–0.05‰).

8.2.2 Aerosol-bound Hg

While Hg^0 has a relatively long lifetime and $Hg^{II}(g)$ has a short lifetime, the lifetime of particle-bound Hg (PBM, Hg^{II}_p) reflects that of particles, which varies from days to months due to their size and composition. Isotopic analyses have been performed on airborne $PM_{2.5}$, PM_{10}, and TSP, as well as on particles in precipitation. Studies of urban air, regionally polluted air, and air associated with anthropogenic emissions (CFPP, traffic and waste incineration, etc.) are well represented and strongly biased toward Asia. As reviewed and discussed in Kwon et al. (2020), attempts to decipher the cause of seasonal variations in urban and industrial air are challenging in environments with a plethora of local and regional emission sources. However, primary particles from fossil fuel and biomass combustion inherit the clearly negative but highly variable $\delta^{202}Hg^{II}(p)$ and the less negative $\Delta^{199}Hg^{II}(p)$ of the material. The large range in $\Delta^{199}Hg^{II}(p)$ (–0.93 to 1.5‰) around the origin depends on $Hg^{II}(p)$ photoreduction with (+)MgIE, halogen atom-initiated Hg^0 oxidation or, more speculatively, $Hg^{II}(p)$ photoreduction with (–)MgIE, driving the data to extremes. In a series of papers, including field measurements of particle-bound isotopic Hg in regionally polluted air (Huang et al., 2016b; Huang et al., 2019; Qiu et al., 2022; Zhang et al., 2022) and laboratory experiments (Huang et al., 2021; Huang et al., 2015), Chen and colleagues have focused on the effect of (+)MgIE photoreduction, which is accelerated in the presence of a particle surface liquid layer (wet haze)

tog bort: to
formaterade ... [674]
tog bort: while
formaterade ... [675]
tog bort: (
formaterade ... [676]
tog bort: supported
formaterade ... [677]
tog bort: of close to unity
formaterade ... [678]
tog bort: a reflection
formaterade ... [679]
tog bort: the
formaterade ... [680]
tog bort: ((−)
formaterade ... [681]
tog bort: taking place
formaterade ... [682]
tog bort: the
formaterade ... [683]
tog bort: , and it
formaterade ... [684]
tog bort: giving
formaterade ... [685]
tog bort: share
formaterade ... [686]
tog bort: which
formaterade ... [687]
formaterade ... [688]
Formaterat ... [689]
tog bort: the
formaterade ... [690]
tog bort: 13
formaterade ... [691]
tog bort: down to
formaterade ... [692]
tog bort: shows a significant shift towards
formaterade ... [693]
tog bort: compared to
formaterade ... [694]
tog bort: -
formaterade ... [695]
tog bort: Due
formaterade ... [696]
tog bort: &
formaterade ... [697]
tog bort: is
formaterade ... [698]
tog bort: a
formaterade ... [699]
tog bort: tracer
formaterade ... [700]
tog bort: &
formaterade ... [701]
tog bort: in
formaterade ... [702]
tog bort: Quantitative
formaterade ... [703]
tog bort: -
formaterade ... [704]
tog bort: (-
formaterade ... [705]
Formaterat ... [706]
formaterade ... [707]
formaterade ... [708]
tog bort: In the literature, studies
formaterade ... [709]
tog bort: etc.

and water-soluble organic carbon as a reducing agent (Zhang et al., 2022). Several peripheral monitoring stations in China, primarily receptors of long-range particle transport, generally measure positive $\Delta^{199}Hg^{II}(p)$ values (Fu et al., 2019b). A strong anticorrelation between $\Delta^{199}Hg^{II}(p)$ (up to ~1.2‰, but initially at near zero) and the concentration of particle-bound Hg, rationalized as caused by photo-produced Hg^0 loss from aerosols, was observed in samples from these stations, with the major potential source area identified as northeastern China and the regions along the lower reaches of the Yangtze River to its mouth (Fu et al., 2019b). The results indicate that the globally modeled tropospheric lifetime of Hg^{II} against photoreduction in aerosols and clouds of nearly two weeks (Horowitz et al., 2017) is significantly shorter in East Asia, possibly because of a greater fraction of organic aerosols. As shown in **Fig. 13b**, there is a statistical anomaly in the PBM polar data for all reported isotopic signatures: positively shifted $\delta^{202}Hg^{II}(p)$, negatively shifted $\Delta^{199}Hg^{II}(p)$ and negatively shifted $\Delta^{200}Hg^{II}(p)$. It is represented in both Arctic (Araujo et al., 2022; Zheng et al., 2021) and Antarctic (Auyang et al., 2022; Li et al., 2020a) data in conjunction with AMDEs. In the high Arctic (~83°N), there is good isotopic agreement between ambient Hg^0 and PBM associated with nearly complete AMDEs, as would be expected. Moreover, for less quantitative oxidation, PBM is isotopically lighter than Hg^0, analogous to kinetic isotope fractionation during oxidation and subsequent uptake of $Hg^{II}(g)$ on particles (such as Arctic haze). As described above, halogen atom-driven gas-phase oxidation induces a negative $\Delta^{199}Hg^{II}$ (Sun et al., 2016; Auyang et al., 2022), which is consistent with the observed signature in PBM. The interpretation of Zheng et al. (2021) that gas-phase oxidation uniquely shapes isotopic fractionation has been challenged by Araujo et al. (2022), who instead consider (–)MgIE photoreduction in aerosols as the imprinting source. The Antarctic coast has shown uniquely high positive $\delta^{202}Hg^{II}(p)$ values (up to ~3‰ and anticorrelated with $\Delta^{199}Hg^{II}(p)$) in air masses transported by katabatic winds from the continental shelf, where oxidation of Hg^0 persists during summer (Li et al., 2020a). Under precipitation (**Section 8.2.3**), the high $\Delta^{200}Hg^{II}$ values measured in southern Canada are addressed, noting that this also applies to the particulate fraction in precipitation, which is included in the rural PBM category (**Fig. 13b**).

8.2.3 Hg in precipitation

Measurements of Hg isotopes in precipitation samples (including fog and cloud water) have been reported at sites in the Northern Hemisphere (map in **Fig. 13c**), mostly in North America. Compared with the Hg^0 and PBM samples, the precipitation samples presented the greatest scatter in both $\Delta^{199}Hg$ and $\Delta^{200}Hg$. Nevertheless, the isotopic distribution pattern in precipitation water is generally similar to that of PBM, which is scavenged in precipitation during rainout and washout processes. Precipitation in the vicinity of anthropogenic emission sources (such as CFPPs) tends to be isotopically distinct, with particularly negative $\delta^{202}Hg^{II}$ values (Sherman et al., 2012). Precipitation from more pristine areas has a $\delta^{202}Hg^{II}$ that is shifted in a positive direction (significant for marine, polar and rural categories, Wilcoxon t test, $p < 0.01$) compared with urban precipitation and precipitation near point sources. The general differences between Hg^0 and precipitation/PBM in terms of MIF signatures (negative $\Delta^{199}Hg^0$ & $\Delta^{201}Hg^0$ vs. positive $\Delta^{199}Hg^{II}$ & $\Delta^{201}Hg^{II}$ and negative $\Delta^{200}Hg^0$ & positive $\Delta^{204}Hg^0$ vs. positive $\Delta^{200}Hg^{II}$ & negative $\Delta^{204}Hg^{II}$, respectively) are explained by atmospheric redox processes (Auyang et al., 2022; Kwon et al., 2020). In the case of even-MIF, chlorine atom-initiated gas-phase oxidation is known to induce a limited positive $\Delta^{200}Hg^{II}$ in the product. However, its observed magnitude cannot explain the highest $\Delta^{200}Hg^{II}$ measured in precipitation (Kurz et al., 2021; Chen et al., 2012; Yuan et al., 2022) in North America. Cai and Chen (2015) reported a trend toward increasing $\Delta^{200}Hg^{II}$ in background precipitation as moving northward along the mid-latitudes of the Northern Hemisphere (~20–45°N), but only with data from a unique station anomalous with greater statistical significance. A one-year measurement north of Lake Ontario (Chen et al., 2012), separated by a full decade from measurements at the same site limited to the colder parts of the year (Yuan et al., 2022), has shown that precipitation in winter often contains high values of $\Delta^{200}Hg^{II}$ (and, at the same time, strongly negative $\Delta^{204}Hg^{II}$ values). During the full-year measurement in 2010, filtered precipitation samples presented a $\Delta^{200}Hg^{II}$ in the range of 0.21 to 1.24‰, whereas during the colder months around the turn of the year 2020-21, the same category of samples contained between 0.25 to 1.19‰ and between –1.97 to 0.37‰ for $\Delta^{200}Hg^{II}$ and $\Delta^{204}Hg^{II}$, respectively. During the last campaign, isotopic analysis was also performed on precipitation particles, which presented significantly lower positive $\Delta^{200}Hg^{II}$ values (up to 0.37‰) and less negative $\Delta^{204}Hg^{II}$ values (down to –0.84‰). Intermittently, the particle phase has the opposite sign to the solute phase in the same precipitation sample with respect to both odd- and even-MIF. This, together with a time series of unrelated odd-MIF and even-MIF trends during events with large fluctuations in these values, has been interpreted as the influence of the circumpolar vortex with varying contributions of tropospheric and stratospheric air, with the transport of the latter air masses

tog bort: particles transported domestically or transboundary
formaterade ... [714]
tog bort: ‰)
formaterade ... [715]
tog bort: reduced
formaterade ... [716]
tog bort: the aerosol that initially has a near-zero $\Delta^{199}Hg^{II}(p)$,
formaterade ... [717]
tog bort: for the
formaterade ... [718]
tog bort: with
formaterade ... [719]
tog bort: , respectively, as the major potential source area
formaterade ... [720]
tog bort: the
formaterade ... [721]
tog bort: Asian region plausibly due to
formaterade ... [722]
tog bort: higher
formaterade ... [723]
tog bort: aerosol
formaterade ... [724]
tog bort: can be seen
formaterade ... [725]
tog bort: 83°N
formaterade ... [726]
tog bort: At the same time
formaterade ... [727]
tog bort: found to be
formaterade ... [728]
tog bort:)…, who instead consider (–)MgIE photoreduct ... [729]
formaterade ... [730]
tog bort: measured in coastal Antarctica interpreted as or ... [731]
formaterade ... [732]
tog bort: inland plateau
formaterade ... [733]
formaterade ... [734]
Formaterat ... [735]
tog bort: most
formaterade ... [736]
tog bort: Precipitation
formaterade ... [737]
tog bort: show the largest
formaterade ... [738]
tog bort: compared to Hg^0 and PBM.
formaterade ... [739]
tog bort: generically
formaterade ... [740]
tog bort: CFPP
formaterade ... [741]
tog bort: -
formaterade ... [742]
tog bort: to
formaterade ... [743]
tog bort: General
formaterade ... [744]
tog bort: definitely
formaterade ... [745]
tog bort: towards
formaterade ... [746]
tog bort: one moves northwards
formaterade ... [747]
tog bort: 45°N
formaterade ... [748]
tog bort: higher
formaterade ... [749]
tog bort: have together
formaterade ... [750]

explaining more extreme even-MIF values (Yuan et al., 2022). Compared with snow samples from the Canadian station north of Lake Ontario, rain samples from the Canadian station north of Lake Ontario generally have more moderately positive $\Delta^{200}Hg^{II}$ values, which is consistent with precipitation observations in the mid-latitudinal USA (Kurz et al., 2021; Demers et al., 2013; Gratz et al., 2010; Sherman et al., 2015), Europe (Fu et al., 2021; Enrico et al., 2016), the Tibetan Plateau (Yuan et al., 2015) and the Pacific Ocean (Motta et al., 2019; Washburn et al., 2021). Although cloud water (Fu et al., 2021; Zhen et al., 2024) and fog water (Washburn et al., 2021) have been isotopically analyzed, there are no apparent differences between them or significant differences from rain samples. In cloud water, Hg speciation with increasing complexation with DOM has been shown to correlate with odd-MIF values (Zhen et al., 2024), which is consistent with the view that these mercuric complexes are photolabile. Polar precipitation samples (only those from AMDEs are reported in the literature, Araujo et al., 2022; Sherman et al., 2012; Zheng et al., 2021) consistently have slightly negative $\Delta^{200}Hg^{II}$ values, which differ from those of precipitation samples from all other provenances, which have positive median values. The reason for these observations is plausibly that oxidation is so advanced during these AMDEs that the Hg^{II} scavenged by precipitation approaches the same isotopic values as the Hg^0 in the polar air before the AMDE.

8.2.4 Even-MIF ($\Delta^{200}Hg/\Delta^{204}Hg$) ratios in atmospheric samples

Early studies by Gratz et al. (2010) and Chen et al. (2012) revealed that MIF anomalies of even mass number isotope ^{200}Hg are regularly present in atmospheric precipitation. Later, measurements (Demers et al., 2013) were also made at $\Delta^{204}Hg$, which is more challenging due to the limitations of ion beam collector designs (Blum and Johnson, 2017). The anomaly of $\Delta^{204}Hg$ was generally larger and opposite to that of $\Delta^{200}Hg$. The $\Delta^{200}Hg/\Delta^{204}Hg$ ratio has been calculated based on spatial averages and exclusively on precipitation samples, which are usually above measurement uncertainty. For example, a slope of –0.5 was previously reported (Blum and Johnson, 2017) and later adjusted to –0.4 (Kwon et al., 2020) using this method as more data became available. However, when all individual precipitation data up to 2020 were combined, Kwon et al. (2020) obtained a significantly lower regression slope of –0.24. **Fig. 14** shows the even-MIF data ($\Delta^{200}Hg$ vs. $\Delta^{204}Hg$) binned into geographical regions (categorized as Hg^0, rain/mist/cloud, PBM, RM, and snowfall samples). Linear regression of York-type $\Delta^{200}Hg$ against $\Delta^{204}Hg$ yields slopes between –0.07 and –0.53 for data grouped by site and category for data of statistical significance ($p \leq 0.05$, indicated by *). When the global data grouped by sample type are analyzed separately, significant ($p < 0.001$***) slopes of –0.51±0.02 (n = 45, Kurz et al., 2021; Yuan et al., 2022), –0.41±0.03 (n = 108, Fu et al., 2021; Demers et al., 2015; Enrico et al., 2016; Sherman et al., 2012; Yuan et al., 2022; Demers et al., 2013; Donovan et al., 2013; Motta et al., 2019; Washburn et al., 2021), –0.29±0.06 (n = 58, Fu et al., 2019b) and –0.11±0.02 (n = 295, Fu et al., 2021; Kurz et al., 2020; Demers et al., 2015; Tate et al., 2023; Araujo et al., 2022; Enrico et al., 2016; Kurz et al., 2021; Demers et al., 2013; Yamakawa et al., 2017; Jiskra et al., 2019; Fu et al., 2016a; Wu et al., 2023a) are obtained for snowfall, rain and fog, particulate matter and Hg^0 respectively. The reaction mechanism triggering even-MIF could be photodissociation in the gas phase (Sun et al., 2022) or on surfaces (Fu et al., 2021). This should lead to varying degrees of fractionation depending on the species undergoing decomposition. As a result, the fractionation of atmospheric Hg^I and Hg^{II} species differs from one another, possibly explaining the divergent $\Delta^{200}Hg/\Delta^{204}Hg$ values for $Hg^{II}(aq)$, $Hg^{II}(p)$, and $Hg^0(g)$.

tog bort: Rain samples compared to
formaterade: Kondenserad med 0,2 pt
tog bort: show
formaterade: Kondenserad med 0,2 pt
formaterade: Kondenserad med 0,2 pt
formaterade: Teckenfärg: Dekorfärg 2, Kondenserad med 0,2 pt
formaterade: Kondenserad med 0,2 pt
formaterade: Teckenfärg: Blå, Kondenserad med 0,2 pt
formaterade: Kondenserad med 0,2 pt
tog bort: over
formaterade: Kondenserad med 0,2 pt
tog bort: with
formaterade: Kondenserad med 0,2 pt
tog bort: to
formaterade: Kondenserad med 0,2 pt
formaterade: Teckenfärg: Blå, Kondenserad med 0,2 pt
formaterade: Kondenserad med 0,2 pt
formaterade: Kondenserad med 0,2 pt
formaterade: Kondenserad med 0,2 pt
tog bort: show
formaterade: Kondenserad med 0,2 pt
formaterade: Kondenserad med 0,2 pt
tog bort: differs
formaterade: Kondenserad med 0,2 pt
formaterade: Kondenserad med 0,2 pt
tog bort: of
formaterade: Kondenserad med 0,2 pt
tog bort: show
formaterade: Kondenserad med 0,2 pt
formaterade: Kondenserad med 0,2 pt
tog bort: had
formaterade: Kondenserad med 0,2 pt
formaterade: Kondenserad med 0,2 pt
tog bort: showed
tog bort: of the
tog bort: sign
formaterade: Teckenfärg: Dekorfärg 2
tog bort:
tog bort: gives
tog bort: due to photo-dissociation
tog bort: will differ in fractionation

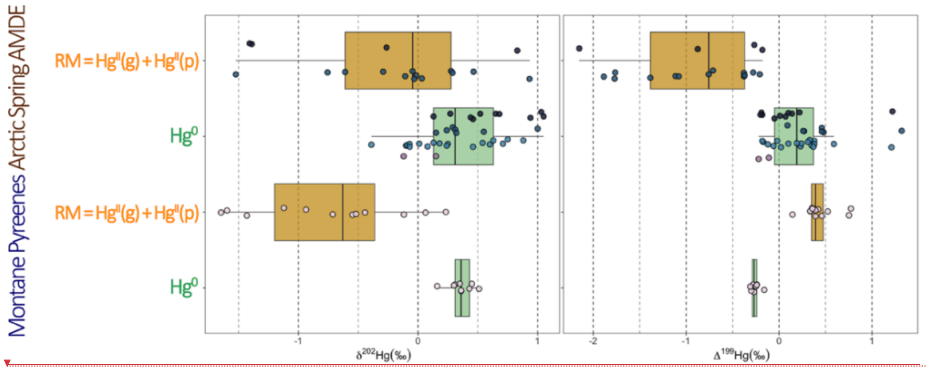

Figure 12. A comparison of the TMDF and odd-MIF signatures for atmospheric Hg^0 and RM, measured during Arctic AMDEs and in the Pyrenees during winter, reveals notable contrasts.

4605

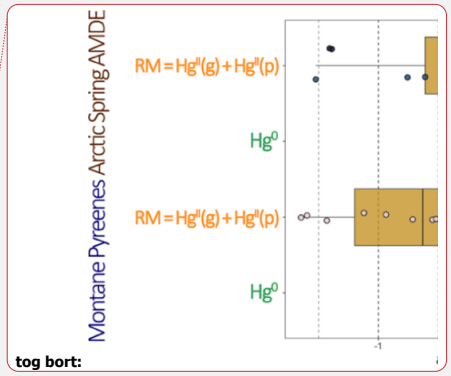

tog bort:

tog bort: MDF

Gaseous Hg (~Hg⁰)

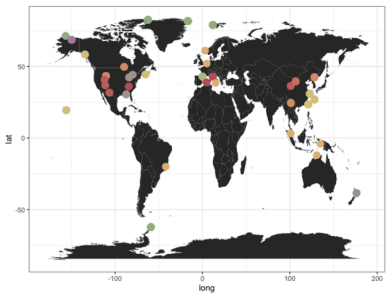

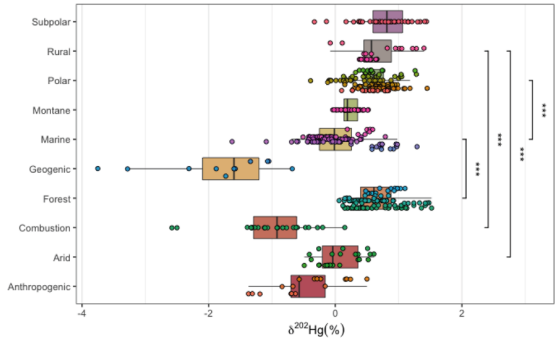

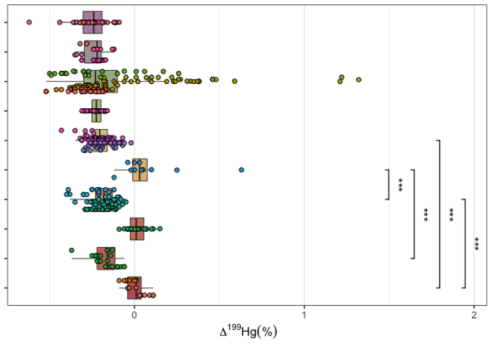

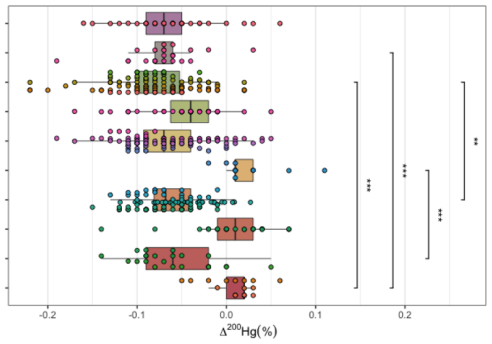

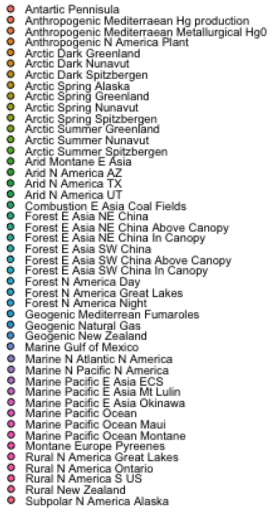

PBM

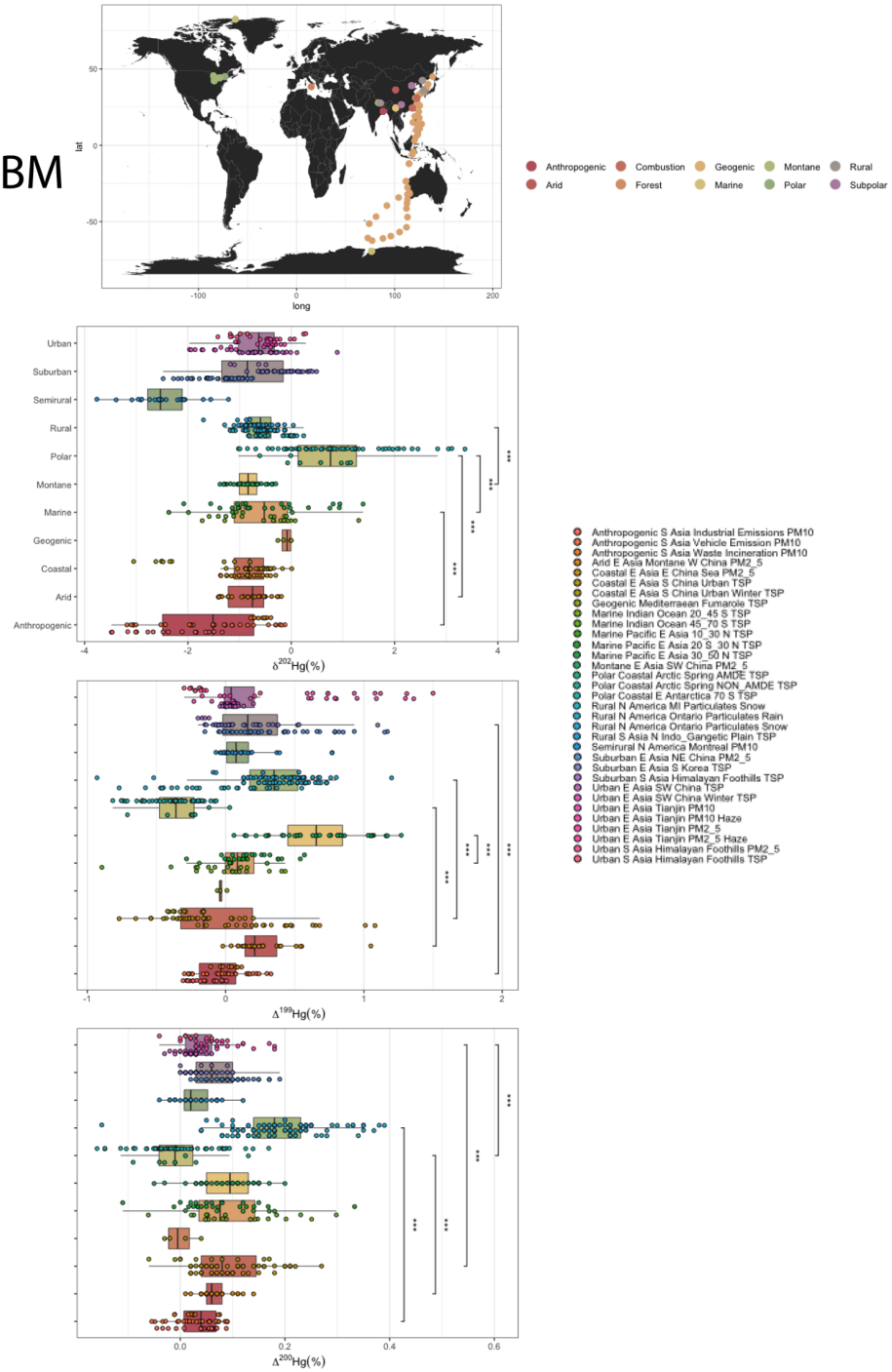
lat
long
50
0
-50
-100
0
100
200
Anthropogenic
Arid
Combustion
Forest
Geogenic
Marine
Montane
Polar
Rural
Subpolar
Urban
Suburban
Semirural
Rural
Polar
Montane
Marine
Geogenic
Coastal
Arid
Anthropogenic
δ202Hg(%)
Δ199Hg(%)
Δ200Hg(%)
Anthropogenic S Asia Industrial Emissions PM10
Anthropogenic S Asia Vehicle Emission PM10
Anthropogenic S Asia Waste Incineration PM10
Arid E Asia Montane W China PM2_5
Coastal E Asia E China Sea PM2_5
Coastal E Asia S China Urban TSP
Coastal E Asia S China Urban Winter TSP
Geogenic Mediterraean Fumarole TSP
Marine Indian Ocean 20_45 S TSP
Marine Indian Ocean 45_70 S TSP
Marine Pacific E Asia 10_30 N TSP
Marine Pacific E Asia 20 S_30 N TSP
Marine Pacific E Asia 30_50 N TSP
Montane E Asia SW China PM2_5
Polar Coastal Arctic Spring AMDE TSP
Polar Coastal Arctic Spring NON_AMDE TSP
Polar Coastal E Antarctica 70 S TSP
Rural N America MI Particulates Snow
Rural N America Ontario Particulates Rain
Rural N America Ontario Particulates Snow
Rural S Asia N Indo_Gangetic Plain TSP
Semirural N America Montreal PM10
Suburban E Asia NE China PM2_5
Suburban E Asia S Korea TSP
Suburban S Asia Himalayan Foothills TSP
Urban E Asia SW China TSP
Urban E Asia SW China Winter TSP
Urban E Asia Tianjin PM10
Urban E Asia Tianjin PM10 Haze
Urban E Asia Tianjin PM2_5
Urban E Asia Tianjin PM2_5 Haze
Urban S Asia Himalayan Foothills PM2_5
Urban S Asia Himalayan Foothills TSP

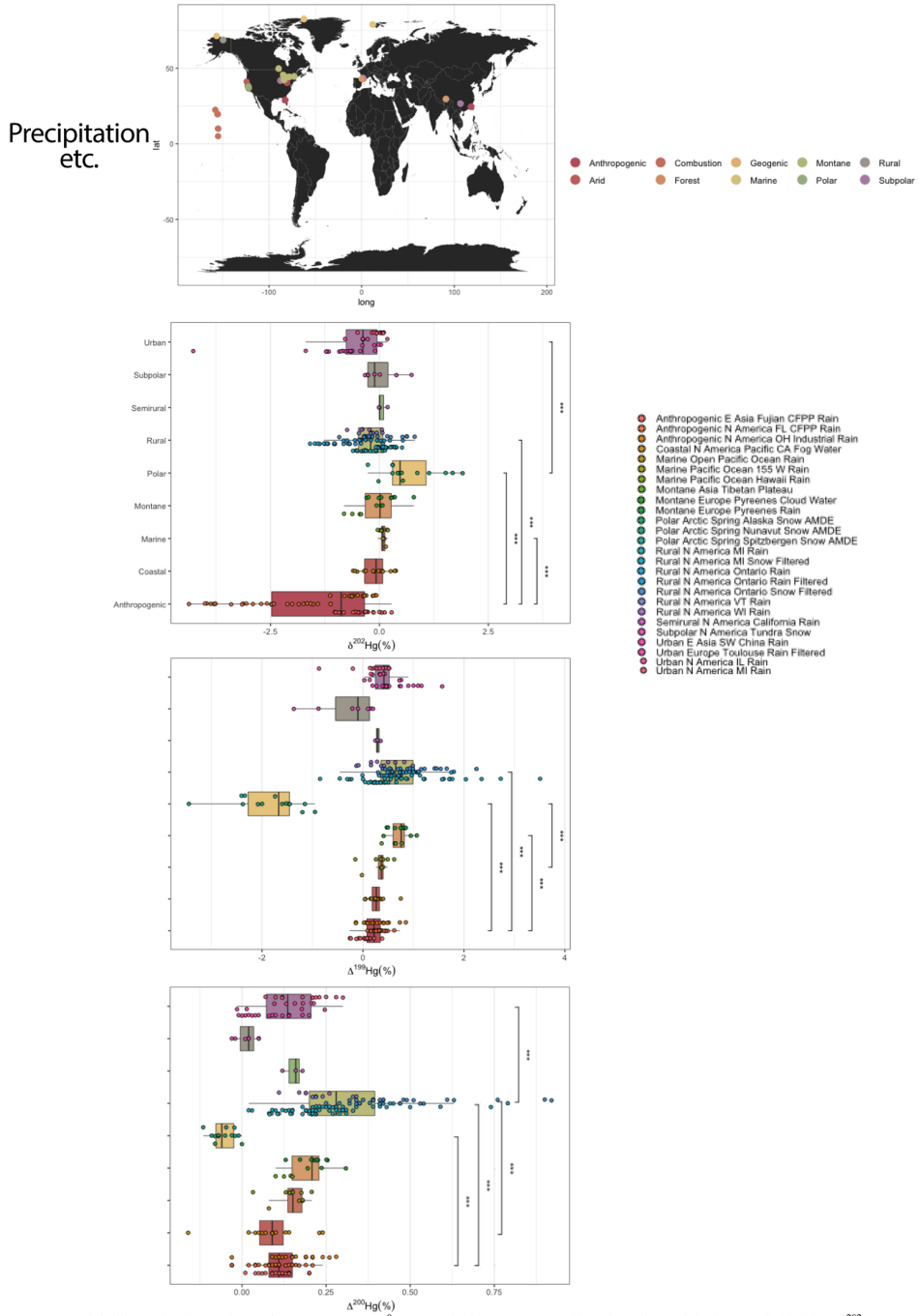

Figure 13. Global isotopic observations of gaseous Hg (~Hg^0) (a), particulate Hg (PBM) (b) and Hg in precipitation (c) divided into $\delta^{202}Hg$ (top), $\Delta^{199}Hg$ (middle) and $\Delta^{200}Hg$ (bottom).

formaterade: Kondenserad med 0,2 pt

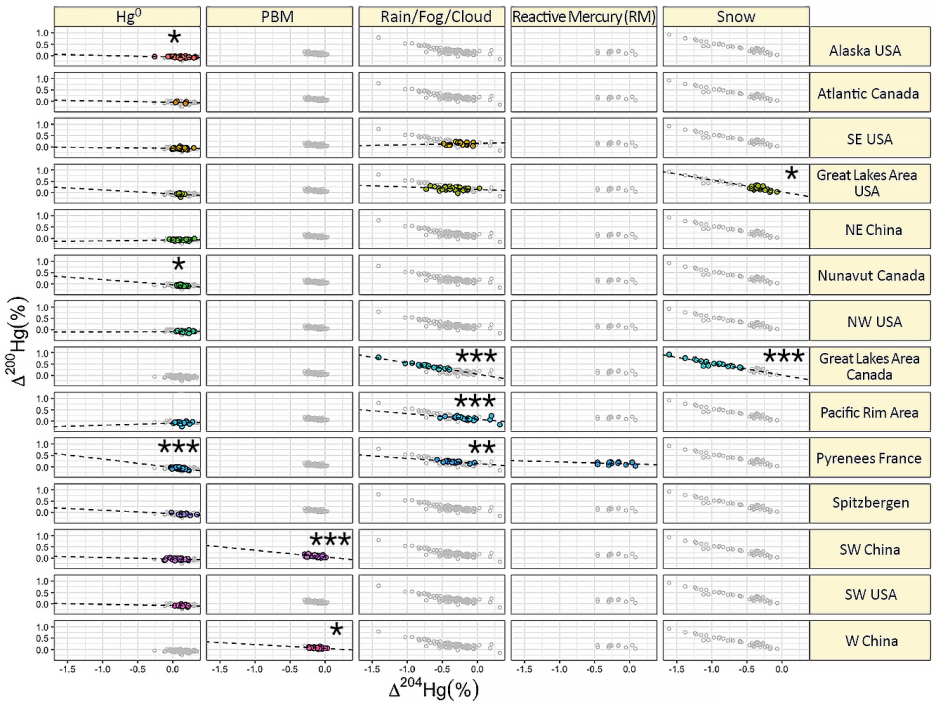

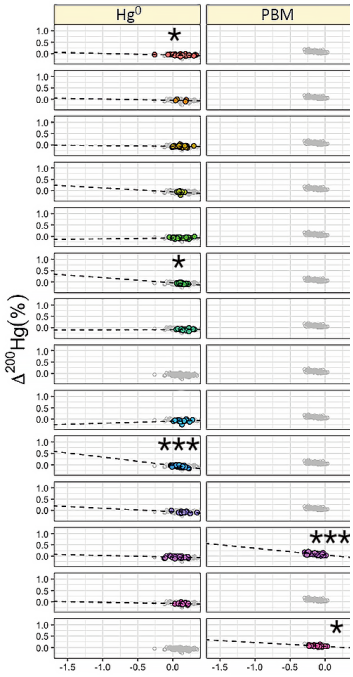

Figure 14. Global observations of even-MIF (Δ^{200}Hg vs. Δ^{204}Hg) by, from left, Hg^0, PBM, rain/fog/cloud, reactive mercury (RM), and snow.

8.3 Isotope fractionation during gas-phase oxidation

Data on the stable isotopic fractionation of Hg during gas-phase chemical reactions are limited. However, in addition to the published studies on fractionation during the oxidation of Hg^0 initiated by Cl and Br atoms (Sun et al., 2016) and during the oxidation of electronically excited Hg^0 in the presence of synthetic air (Sun et al., 2022), the corresponding thesis provides additional data (Sun, 2018), which are highlighted here.

8.3.1 Ground-state Hg^0 oxidation in air

Isotope fractionation during the oxidation of Hg^0 vapor in the ground state has been studied for reactions initiated by $Cl^{\bullet}/Br^{\bullet}/{}^{\bullet}OH/O_3/BrO^{\bullet}$ in air at 750 Torr and 298 K, as listed in **Table 7**. **Fig. 15** shows that the $Br^{\bullet}$ and ${}^{\bullet}OH$ reactions produce a lighter isotope enrichment in the reactant Hg^0, unlike the other reactions that follow KIE. This deviation from KIE occurs because the Hg^0 to Hg^I step (**Rxn G1–G3**, **Table 3**) in the overall Hg^0 to Hg^{II} oxidation is reversible. EIE is especially notable for the $Br^{\bullet}$ and ${}^{\bullet}OH$ channels being affected by thermal and photolytic dissociation (**Rxn G14 & G53**), creating a cyclic replenishment of Hg^0 at higher temperatures, as discussed in **Section 5.1.2**. EIE predicts the enrichment of heavier isotopes in species with a stronger bonding environment (e.g., $HgBr_2$, $Hg(OH)_2$, Schauble, 2007). However, at temperatures in the upper atmosphere and during AMDEs in polar regions, the rate of **Rxn G14a & G53a** becomes much lower, and the oxidation mechanism moves toward irreversibility, potentially leading to the dominance of KIE at lower temperatures. The chlorine atom-initiated reaction already displays a KIE at 298 K, which is related to the relative thermal stability of the HgCl intermediate. All the atmospherically relevant reactions investigated ($Cl^{\bullet}$, $Br^{\bullet}$ and ${}^{\bullet}OH$) give rise to (+) odd-MIF, which is most pronounced for the Cl-initiated reaction ($E^{199}Hg$ = –0.37‰) compared with the other reactions ($E^{199}Hg$ = –0.23‰ and –0.18‰ for the Br and OH reactions, respectively). Analogous to ${}^{\bullet}OH$ + ${}^{\bullet}OH$ recombination, which yields H_2O_2 in the gas phase (Velivetskaya et al., 2016; Velivetskaya et al., 2018), odd-MIF

tog bort:
tog bort: Reactive Mercury
tog bort: Hg
tog bort: of Hg
tog bort: the
tog bort: a
tog bort: work of
tog bort: the
tog bort: torr
tog bort: the kinetic isotope effect (
tog bort:).
tog bort: -
tog bort: The equilibrium isotope effect (
tog bort:)
tog bort: invoked
tog bort: ·OH
tog bort: Br·
tog bort: Br1, OH1
tog bort: Br1b/OH1b
tog bort: towards
tog bort: -
tog bort: to
tog bort: others
tog bort: yielding

plausibly occurs due to MgIE triggered by radical–radical ($^{\bullet}Hg^{I}X + Y^{\bullet}$) interactions that occur during reactions, leading to the formation of $XHg^{II}Y$ species. The diagnostic ratio of $\Delta^{199}Hg/\Delta^{201}Hg$ ~1.9, which is observed for the $Hg^0 + Cl^{\bullet}$ system, differs

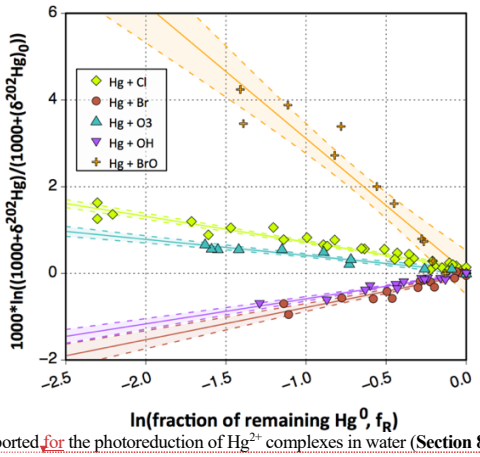

significantly from the ratios reported for the photoreduction of Hg^{2+} complexes in water (**Section 8.4.1**).

Figure 15. Linearized Rayleigh diagram for $\delta^{202}Hg$ in Hg^0 during Cl, Br, OH, O_3 and BrO oxidation experiments at ~298 K showing normal and inverse KIEs. Each point represents a single experiment.

Table 7. Experimental fractionation factors determined in gas-phase oxidation studies.

Oxidant	Precursor	Bath gas	$\varepsilon^{202}Hg$ (‰)	$E^{199}Hg$ (‰)	$E^{200}Hg$ (‰)
$Cl^{\bullet}$	$CCl_3C(O)Cl + h\nu$	air	–0.590	–0.370	0.06
$Br^{\bullet}$	$CHBr_3 + h\nu$	air	0.740	–0.230	
O_3	n/a	air	–0.370	–0.120	
$^{\bullet}OH$	$H_2O_2 + h\nu$	air	0.580	–0.180	
"$BrO^{\bullet}$"	$CHBr_3 + O_3 + h\nu$	air	–3.105	1.009	

8.3.2 Hg^0 oxidation initiated by photosensitized reactions

Ancient rock samples show a significant occurrence of even-MIF in the Archean atmosphere (~2.5 Ga, Zerkle et al., 2020), which lacked an O_3 layer to filter out deep UV light in the actinic zone. However, in the modern atmosphere, even MIF does not appear to occur significantly in Hg redox processes at the Earth's surface. The current atmospheric budget reveals notable imbalances between $\Delta^{200}Hg$ in Hg emissions from and deposition to the Earth's surface (0.025 ± 0.032‰ vs. 0.073 ± 0.019‰, Fu et al., 2021). To maintain a steady state, even-MIF sources in the atmosphere are necessary. Studies have shown that UVC-induced Hg^0 vapor in the electronically excited state, $Hg(^3P_1)$, undergoes chemical transformation under both artificial (Mead et al., 2013) and modern (Sun et al., 2022) atmospheres, resulting in a large MIF of both odd and even Hg isotopes. There are claims (Blum and Johnson, 2017; Mead et al., 2013) that the $\Delta^{200}Hg/\Delta^{204}Hg$ ratios found in nature are similar to those present in the glass housing of compact fluorescent lamps (CFLs). However, the $\Delta^{199}Hg^{II}$, $\Delta^{200}Hg^{II}$, and $\Delta^{204}Hg^{II}$ values in the CFL housing exhibit opposite signs to those observed in nature (cf. **Figs. 13 & 14**). Laboratory experiments have shown that the net oxidation of Hg^0 by the reaction between excited-state Hg^0 and atmospheric O_2, which is identical to the driving photosensitized reaction for the turnover of Hg^0 in the upper stratosphere (**Rxn G12b** counteracted by **Rxn G72**, **Table 3**), scrambles the systematics of all Hg isotopes in an entirely mass-independent manner. These laboratory experiments and atmospheric samples show similar observations for the $\Delta^{200}Hg/\Delta^{204}Hg$ ratio, suggesting that photodissociation is a potential chemical mechanism for triggering even-MIF in the atmosphere (Sun et al., 2022). This review outlines new findings on atmospheric Hg chemistry, supporting the fundamental importance of photodissociation processes (**Sections 5.1.2 and 5.1.4**). In addition to the gas phase, surface-mediated photolysis of mercurous halide species has also been proposed as a mechanism for generating even-MIF (Fu et al., 2021). However, theoretical challenges still need to be solved at the quantum

tog bort: -
tog bort: It should be noted that the
tog bort: *<object>*
tog bort: in
tog bort: KIE
tog bort: (ε, E)
tog bort: the
tog bort: Even-MIF
tog bort: detected
tog bort: light
tog bort: A
tog bort: the
tog bort: Fig
tog bort:
tog bort: G71
formaterade: Teckenfärg: Blå
tog bort: to give rise to

mechanics level to generically expand our understanding of anomalous isotope effects for traditional and non-traditional elements (Lin and Thiemens, 2024). Further field and laboratory research in this area should be encouraged.

8.4 Isotope fractionation during aqueous-phase red-ox transformation

Hg transformation in the aqueous phase has been reviewed extensively, including stable Hg isotope studies (Hintelmann and Zheng, 2011). The present study does not focus on biotic processes, such as microbial reduction, methylation and demethylation, or phototrophic microbial reduction. Kritee et al. (2013) and Tsui et al. (2020) provide overviews of this field. The focus is on abiotic processes, excluding those involving coordination with macromolecular heterogeneous ligands such as DOM or fractions, and instead on low-molecular-weight ligands, including those with N–, O–, S–, or (pseudo)halide donors. This includes inorganic and organic ligands and oxidizing and reducing processes (**Section 6**).

8.4.1 Reduction

To recapitulate **Section 8.1**, in addition to MDF, isotopic effects in NFS and MgIE occur for Hg during chemical transformation in the aqueous phase. MDF and NFS are present in all reactions to varying magnitudes and in all mechanisms and have a thermodynamic nature. In contrast, MgIE is a kinetic effect and is indicative of spin-selective reactions involving a paramagnetic intermediate. Therefore, MgIE is the only isotope effect that detects the reaction mechanism. MgIE can be both thermally and photolytically induced and can be two-dimensional (+ or – depending on the reaction conditions, Zheng and Hintelmann, 2010b) or one-dimensional (exclusively +), depending on the identity of the Hg^{II} complex (Motta et al., 2020a). In cases where the spin-selective reaction can be induced thermally, the radical pair is generated almost exclusively as a singlet (Buchachenko, 2018), which is spin-forbidden to react (dissociate) further into products. For a singlet spin forbidden reaction compared to a triplet spin allowed reaction, the magnitude of the MgIE-MIF is more limited. However, many Hg^{II} complexes have a narrow energy separation of a variety of excited states, indicating that the intermediate radical pair can evolve into a triplet or singlet state. Studies of Hg^{2+} photoreduction in the presence of organic ligands (which consistently follow a pseudo-first-order kinetic pathway) have shown that, depending on the degree of Hg^{2+}(aq) turnover, weak MIF is initially induced by NFS, and then, when most of the Hg^{2+}(aq) has been converted, there is a shift to strong MIF induced by MgIE, the onset of which coincides with strong suppression of MDF (Motta et al., 2020b; Zheng and Hintelmann, 2010b). One explanation for why MgIE first appears closer to complete Hg^{II} reduction is, at least in part, that the termination radical–radical step when Hg^0 is split off (in a bimolecular reaction, such as $Hg^{+\bullet} + C_2O_4^{\bullet-}/CO_2^{\bullet-}$ in the photoreduction of $Hg(\eta^2\text{-}C_2O_4)$) is favored by a decreasing concentration ratio of oxidized Hg to bulk ligand (Zhao et al., 2021). As shown in **Fig. 11**, (–)MgIE is induced when the radical pair is generated in a singlet state, and (+)MgIE is induced when the excitation occurs in a triplet state. Ligand field strength, in combination with atomic orbital hybridization theory, has been used to illustrate MgIE in the (photo)reduction of Hg^{II} complexes. This phenomenon has been suggested to vary as a function of, among other things, the arrangement of the ligands around Hg^{2+}, the coordination strength of the ligands, and the presence/absence of light along with its wavelength (Epov, 2011a; Epov, 2011b). As discussed in **Section 4.4**, reduced S- and reduced N-containing groups are soft (strong field) ligands, whereas O-donating groups are hard (weak field) ligands. Epov (2011a) rationalized mercuric complexes with strong field ligands such as cysteine ($Hg(cys)_2^{2-}$) and ethylenediamine ($Hg(en)^{2+}$) as bright singlets (i.e., in the presence of light) with sp-hybridization at the central Hg atom in two binding orbitals. To undergo singlet-triplet evolution by hyperfine coupling between magnetic nuclei (^{199}Hg and ^{201}Hg) and electrons to a paramagnetic state, the orbital hydridization of Hg must change from sp-linear to sp^2d-planar square so that the transfer of electrons from the soft ligand to Hg can be accomplished.

tog bort: Nevertheless, further
tog bort: , including both field studies and laboratory experiments
formaterade: Teckenfärg: Dekorfärg 2
tog bort: This article will
tog bort: and
tog bort: dissolved organic matter
tog bort:
tog bort:
tog bort: ,
tog bort:
tog bort: conventional
formaterade: Teckenfärg: Blå
formaterade: Teckenfärg: Blå
tog bort: magnitude
tog bort: the
formaterade: Teckenfärg: Dekorfärg 2
tog bort: of the reaction
tog bort: +)
tog bort: in
tog bort: From studies
tog bort:), it has been
formaterade: Teckenfärg: Blå
tog bort: -
tog bort: -
tog bort: 2
tog bort: .
tog bort: an
tog bort: Hg
tog bort: a
tog bort: nucleus
tog bort: Hg must change its
formaterade: Teckenfärg: Dekorfärg 2
tog bort:

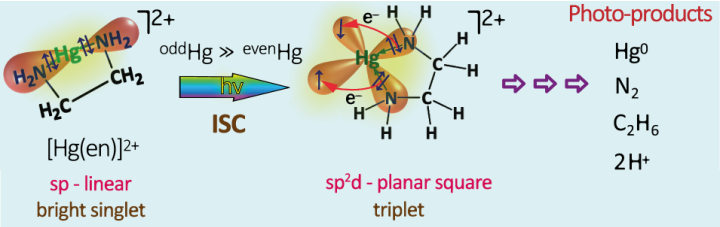

Figure 16. Mechanism proposed by Epov (2011b) for the photoreduction of $Hg(en)^{2+}$ via a bright singlet excited complex undergoing intersystem crossing preferentially for the odd isotope to the closest triplet state, which can dissociate following a complex reaction.

Fig. 16 shows the schematic for $Hg(en)^{2+}$ + light with (–)MgIE. It is postulated that mercuric complexes with O-binding ligands possess a bright triplet state that is more likely (spin allowed) to undergo Hg reduction via 1e-LMCT with an imprint of (+)MgIE.

For a change in the spin state to occur, spin–orbit coupling (SOC) must be induced, but if the SOC is elevated, spin relaxation or phosphorescence can be induced, which prevents the formation of a separating radical pair during dissociation, making MgIE less relevant (cf. **Fig. 11**). Coupling constants are known experimentally for only a few Hg-containing radicals ($CH_3Hg^{\bullet}$, Karakyriakos and Mckinley, 2004; $^{\bullet}HgF$, Knight Jr. et al., 1981; $^{\bullet}HgCN$, Knight Jr. and Lin, 1972; $^{\bullet}HgH/^{\bullet}HgD$, Stowe and Knight Jr., 2002). Recently, published theoretical electronic structure simulations have been performed on environmentally interesting Hg halides (Cl, Br, I) and pseudohalides (methanethiol). The study (Motta et al., 2020a) reported that the coupling for reactions involving $^{\bullet}Hg^{I}Br$ and $^{\bullet}HgI$ is so high that radical pair formation is inhibited, whereas for $^{\bullet}Hg^{I}Cl$ and $CH_3SHg^{I\bullet}$, coupling is sufficient in the caged pair as well as at a low level in the separated pair geometries, allowing MgIE to form. Depending on the identity of the Hg–ligand bond that undergoes homolysis to a radical pair, either quadruple (X = Cl, S) or double (Y = C) degeneracy can occur between the low-lying electronically excited levels and the ground state in the HgX_2 and HgXY compounds, respectively, allowing the photoreduction of HgX_2 to exhibit (+)MgIE or (–)MgIE while that of HgXY (i.e., MMHgX) exhibits only (+)MgIE. This is based on the premise that the photolysis of MMHgX is exclusively by cleavage of the weaker Hg–C bond rather than the stronger Hg–X bond. (+)MgIE is most evident for the photoreduction of $MMHg^+$ species, as its $^3\sigma\sigma^*$ 1e-LMCT state is energetically separated from other excited states in the paramagnetic intermediate, leading to the maximization of MgIE (Motta et al., 2020a). Stable Hg isotopes provide insight into the dynamics and metabolism of inorganic and methylated Hg in biota. Exposure to the former results in subtle odd-MIF with a $\Delta^{199}Hg/\Delta^{201}Hg$ ratio close to unity at sampling, while for the latter, this ratio is greater (~1.3) with a large odd-MIF (up to ~5‰ in fish, Li et al., 2022b).

From **Table 8**, which summarizes the isotopic effects quantitatively observed in aqueous-phase laboratory studies, MgIE can have different signs for the same reactant depending on the reaction conditions, as exemplified by the Hg-cysteine-light system. Depending on the degree of photoconversion, the reduction of Hg^{II} in the presence of water-soluble diesel soot (aromatic polyacids and humic-like structures) exhibits swings in the direction of MgIE (Huang et al., 2021). Another example of the impact of pH/complexation on the evolution of MgIE can be seen in the UVC photodegradation of $MMHg^+$ in acidic and alkaline (adjusted with NH_3) solutions. In the former, (+)MgIE is significant, but it is limited in the latter. For traditional elements with the same reaction mechanism, the strength development of MgIE depends on various factors, including viscosity, triplet sensitizer, and excited-state quenchers (Turro, 1983; Buchachenko, 2013). As seen in the laboratory experiments, both (+) and (–) net Hg MgIE were observed in samples related to the natural atmosphere, as previously reported in **Section 8.2**. The reaction conditions also affect the degree of turnover of the Hg reactant at which the onset of MgIE occurs, which incidentally does not correlate with a change in the overall reduction rate. To better interpret odd-MIF signatures and systematically elaborate the roles of reaction parameters (pH, presence of O_2, light wavelength, etc., Rose et al., 2015) in excited-state kinetic isotope effects, experimental research is needed. For example, dissolved O_2 is a well-known quencher of excited triplet states, but radical-O_2 reactions have also been described to induce significant MgIE (Pliss et al., 2019). For the photoreduction of Hg in the presence of multifunctional ligands (such as DOM), the stoichiometry (Hg:L

tog bort: The figure above
tog bort: Analogously, it
formaterade: Teckenfärg: Blå
tog bort: this schematically
tog bort: showing
tog bort: -
tog bort: ,
formaterade: Teckenfärg: Blå
tog bort: shows
tog bort: while
tog bort: • it
tog bort: .
formaterade: Teckensnitt:Symbol
tog bort: In particular, exposure
tog bort: higher
tog bort: A further
formaterade: Teckenfärg: Blå
tog bort: influence
formaterade: Teckenfärg: Blå
tog bort: solution, where
formaterade: Teckenfärg: Blå
tog bort: in the first case
formaterade: Teckenfärg: Blå
tog bort: very
formaterade: Teckenfärg: Blå
formaterade: Teckenfärg: Dekorfärg 2
tog bort: second
formaterade: Teckenfärg: Blå
tog bort:
tog bort: have been
tog bort: Experimental research is needed to
formaterade: Teckenfärg: Blå
formaterade: Teckenfärg: Blå
tog bort: , etc.)
formaterade: Teckenfärg: Blå
tog bort:
formaterade: Teckenfärg: Blå
tog bort: .
tog bort:
tog bort: NOM),
formaterade: Teckenfärg: Dekorfärg 2

ratio) has been shown to play an important role in the magnitude of MgIE induced. Zhang and Hintelmann (2009) observed an $E^{199}Hg$ optimum (≳5%) in anoxic photo-experiments with the DOM fraction from Dorset Lake, Ontario. This optimum is associated with a ligation mode in which all S-bonding functional groups are saturated by Hg^{2+} cations, increasing the proportion of Hg–O bonds and the ratio of bright triplets to bright singlets, thus making the MgIE increasingly positive. As the Hg:L ratio is further increased, the reduction rate (driven by Hg–O complexes) is significantly affected. The triplet-singlet spin evolution is limited to fewer HgL radical pairs, resulting in a lower $–E^{199}Hg$ (Epov, 2011a). In contrast to freshwater DOM, photo experiments with Hg^{II} in the presence of DOM extracted from marine phytoplankton yield (–)MgIE during reduction (Kritee et al., 2018).

tog bort: For the dissolved organic matter (DOM) fraction from Dorset Lake, Ontario,
formaterade: Teckenfärg: Blå
formaterade: Teckenfärg: Blå
tog bort: an $–E^{199}Hg$
formaterade: Teckenfärg: Blå
tog bort: (≳5‰)
formaterade: Teckenfärg: Blå
tog bort: where
tog bort: –
tog bort: increases, which increases
formaterade: Teckenfärg: Blå
tog bort: –
formaterade: Teckenfärg: Blå
tog bort: Hg^{2+}
formaterade: Teckenfärg: Blå
tog bort: and
formaterade: Teckenfärg: Blå
formaterade: Teckenfärg: Blå
formaterade: Teckenfärg: Blå
tog bort: and
formaterade: Teckenfärg: Blå
tog bort: becomes
formaterade: Teckenfärg: Blå
tog bort: Photo
formaterade: Teckenfärg: Blå
tog bort: give rise to
tog bort: , in contrast to freshwater DOM

Table 8. Experimental fractionation factors determined for a variety of Hg red-ox transformations.

Initial Hg conc. (electrolyte)	Reactant	Experimental conditions: L/Hg ratio	Anoxic/ Oxic	Major Hg species	ε^{202}Hg (‰, ±2σ)	E^{199}Hg (‰)	Δ^{199}Hg/ Δ^{201}Hg	Isotope effects	Reference
Photoreduction of Hg^{II}									
0.5 µM NIST-3133 (Cl^-)	Cysteine (Hcys)	Quartz glass, ~2000:1 (M/M), Xe lamp (UVC-filter), pH 3.6	A	$Hg(cys)_2$	−1.32 ± 0.07	1.02	1.46 ± 0.03	MDF, NFS, (−)MgIE	Zheng & Hintelmann, 2010b
0.17±0.04 µM		FEP Teflon, ≥2000:1 (M/M), natural sunlight, pH 3.2			−1.04 ± 0.09	–	1.34 ± 0.03		Motta et al., 2020b
		FEP Teflon, ≥2000:1 (M/M), natural sunlight, pH 7.2				−0.25	0.99 ± 0.06	MDF, (+)MgIE	
		FEP Teflon, ≥2000:1 (M/M), natural sunlight, pH 7.2	O			−1.15	1.11 ± 0.09		
0.5 µM NIST-3133 (Cl^-)	Serine (Hser)	Quartz glass, 2000:1 (M/M), Xe lamp (UVC-filter), pH 3.8	A	$Hg(ser)_2$	−1.71 ± 0.03	0.17	1.67 ± 0.28	MDF, NFS, (+)MgIE[36]	Zheng & Hintelmann, 2010b
0.17± 0.04 µM		FEP Teflon, ≥2000:1 (M/M), natural sunlight	A/O		−1.81 ± 0.04	0.06 ~−1.3	~1.6 1.08 ± 0.01	MDF, NFS (+)MgIE[37]	Motta et al., 2020b
0.17± 0.04 µM	Ethylenediamine (en)	FEP Teflon, ≥20000:1 (M/M), natural sunlight, pH 7.4	O	$Hg(en)_2^{2+}$ $HgOH(en)^+$	−0.9 ± 0.3	0.16	0.85 ± ±0.14	MDF, (−)MgIE	Motta et al., 2020b
1 µM (ClO_4^-)	Oxalate (ox^{2-})	Pyrex, 300:1 (M/M), UV-B light, pH 3.9 & 5.2	A/O	Hg-η-ox	−1.45 ± 0.06	0.15	1.39 ± 0.38	MDF, NFS[38]	Zhao et al., 2021
	AQDS	Pyrex, 300:1 (M/M), UV-B light, pH 3.4	A	?	−0.66 ± 0.10	−0.86	1.00 ± 0.02	MDF, (+)MgIE	
	Salicylic acid (Hsal)	Pyrex, 300:1 (M/M), UV-B light, pH 4.3	A	$Hg(sal)^+$?	−1.79 ± 0.30	~0.10	1.53 ± 0.02	MDF, NFS	This work
	4-hydroxy-benzoic acid (HOBz)	Pyrex, 300:1 (M/M), UV-B light, pH 4.9	A	$Hg(OBz)^+$?	−2.25 ± 0.10				
	4-aminobenzoic acid (HNBz)	Pyrex, 300:1 (M/M), UV-B light, pH 5.9	A	$Hg(NBz)^+$?	−2.75 ± 0.40				
0.3 – 0.5 µM	Suwannee River fulvic acid	Quartz glass, ~10 – 17 (m/m), sunlight	O		−0.60	−0.45	1.00 ± 0.02	MDF, (+)MgIE	Bergquist & Blum, 2007
~10 µM	NIST-3133 (Cl^-)	Quartz glass, ~29000 (m/m), Xe lamp (UVC-filter)	A	The proportion of Hg-O bonding increases as we move downward, and so does the reaction rate.	−0.77 ± 0.18	−2.94	1.19 ± 0.02	MDF, (+)MgIE	Zheng & Hintelmann, 2009
		Quartz glass, ~6000 (m/m), Xe lamp (UVC-filter)			−0.72 ± 0.10	−4.12	1.22 ± 0.02		
~50 µM		Quartz glass, ~1200 (m/m), Xe lamp (UVC-filter)			−1.26 ± 0.07	−6.29	1.24 ± 0.02		
		Quartz glass, ~1200 (m/m), sunlight			−0.99 ± 0.02	−5.57	1.26 ± 0.01		
~500 µM		Quartz glass, ~120 (m/m), Xe lamp (UVC-filter)			−1.06 ± 0.02	−1.94	1.30 ± 0.02		
~50 µM					−1.09 ± 0.04	−1.99	1.31 ± 0.01		
29 nM (NO_3^-)	Marine algal DOM (intracellular)	Teflon, 1.41 nmol $chla^{-1}$, UVB-light	O		−0.70	1.03	1.06	MDF, (−)MgIE	Kritee et al., 2018
82 nM (Cl^-)	Water-soluble diesel soot extracts	Quartz glass, ~67:1 (M/M), Xe lamp, Instanteous removal of product (Hg^0)	A		−1.30± ± 0.11	−2.49	1.15	MDF, (+)MgIE	Huang et al., 2021
10 nM (NO_3^-)	Dissolved black carbon (< 0.45 µm)	Glass, ~42000:1 (M/M), Xe lamp	A				1.20 ± 0.10	MDF, (−)MgIE	Li et al., 2020b
Photoreduction of $MMHg^+$									
50 µM	CH_3HgCl	Hg-lamp (λ = 254 nm), pH 4.0	O	CH_3HgCl	~−0.25	~−0.5	1.26 ±0.06	MDF, (+)MgIE	Malinovsky et al., 2010
	CH_3HgOH	Hg-lamp (λ = 254 nm), pH 8.6		CH_3HgOH	~−0.3	< −0.06		MDF, supressed (+)MgIE	
0.3 – 0.5 µM?	CH_3Hg^+	Suwannee River fulvic acid, sunlight	10 mg C/L		−1.70± 0.30	−7.9	1.36 ±0.02	MDF, (+)MgIE	Bergquist & Blum, 2007
			1 mg C/L		~−1.30 ± 0.20	−3.3			
102 nM	(Cl^-)	Suwannee River fulvic acid, Xe lamp (UVC-filter)	2.13[39]		−1.74 ±0.50	−0.9	1.30 ±0.07		Chandan et al., 2015
86 nM			0.72		−4.64 ±1.64	−5.0	1.28 ±0.09		
101 nM			0.42		−1.91 ±0.25	−7.2	1.32 ±0.03		
80 nM			0.17		−1.77 ±0.81	−7.2	1.30 ±0.03		

[36] Appears at 4 h photoreduction and beyond with a $\Delta^{199}Hg/\Delta^{201}Hg$ of 1.10–1.18

[37] Onset of (+)MgIE at f_R = 0.40–0.76 depending on reaction conditions.

[38] A single experiment (anoxic, pH 6) on oxalate indicates (+)MgIE at f_R = 0.11

[39] MMHg/organic bound reduced sulfur (M/M)

97 nM				0.10			−1.50 ±0.50	−13.4	1.40 ±0.03		
94 nM			Pony Lake fulvic acid, Xe lamp (UVC-filter)	0.07			−2.24 ±0.44	−16.2	1.37 ±0.03		
96 nM				0.01			−1.13 ±0.36	−15.3	1.36 ±0.01		
104 nM			Nordic Lake DOM, Xe lamp (UVC-filter)	0.41			−1.33 ± 0.17	−1.3	1.17 ± 0.04		
95 nM				0.05			−2.23 ± 0.68	−14.6	1.41 ± 0.02		
Dark reduction of Hg^{II}											
1 µM (ClO_4^-)		Benzoquinone $C_6H_4(OH)_2$, QH_2	Pyrex, 300:1, dark, pH 4.6	O	Hg–QH^+?		−1.25 ±0.19	0.12	1.39 ±0.38		Zhao et al., 2021
0.5 µM NIST-3133 (Cl^-)		$SnCl_2$	Quartz, dark, low pH	A	$HgCl_4^{2-}$		−1.56 ±0.11	0.17	1.59 ±0.22		Zheng & Hintelmann, 2010a
1 µM (ClO_4^-)		Ascorbic acid	Pyrex, 300:1, dark, pH 5.1	O/A	?		−1.79 ±0.13	0.08	1.48 ±0.35		This work
NIST-3133 (Cl^-)		Dorset Lake bulk DOM	Quartz, dark, pH 6.5	A			−1.52 ± 0.06	0.19	1.54 ±0.34	MDF, NFS	Zheng & Hintelmann, 2009
1 µM NIST-3133 (NO_3^-)		$FeCl_2$	Glass, 12.5:1, dark, pH 6.5, 0.5 mM Cl^-	A	$Hg(OH)_2$		−2.20 ± 0.16 −2.44 ± 0.17[40]	0.21 0.34	1.58 ± 0.08 1.60 ± 0.05		Schwab et al., 2023
			Glass, 12.5:1, dark, pH 6.5, 10 mM Cl^-		$HgCl_2$, $Hg(OH)Cl$		−2.14 ± 0.09	0.24 ± 0.01			
Methylation of Hg^{II}											
0.5 – 5 µM NIST-3133 (Cl^-)		Methylcobalamin	1000:1, pH 5, (UV–A lamp) (λ~325 nm)	O			~−1.5[41]	0.21[42]	1.20 ± 0.17	MDF, (−)MgIE	Malinovsky & Vanhaecke, 2011
		Acetate						0.22	1.20 ± 0.26		
Oxidation of Hg^0											
200 – 280 nM		Hydroxyl radicals	Pyrex, ≤ 600:1 ($NaNO_3$), pH 7, UV-lamp (λ > 300 nM)	A	$Hg(OH)_2$		1.20 ± 0.14				Stathopoulos, 2014
~60 nM		Sulphanyl-acetic acid	Glass, 80:1 (M/M), dark, pH 7	A			1.25 ±0.11	−0.14	1.28 ±0.38	EIE-MDF, NFS	Zheng et al., 2019
		2-sulphanyl-propanoic acid		A			1.10 ±0.08				
115 nM		Reduced natural Elliott soil humic acid	Glass, ~0.6–1.2 S:Hg (M/M)	A			1.54 ±0.10	−0.18			

As shown in **Table 8**, photoreduction of Hg^{2+} often, but by no means always, is associated with high odd-MIF. For macromolecular entities such as DOM and fulvic acids and a selection of smaller organic ligands that use O–, N– and S-donor atoms to complex with Hg^{2+}, MgIE is initially induced in the photoreduction process, whereas for the amino acid serine, MgIE is triggered only after a significant turnover of Hg^{2+}, the onset of which varies significantly depending on the reaction conditions (Zheng and Hintelmann, 2010b; Motta et al., 2020b). The experimental $\Delta^{199}Hg/\delta^{202}Hg$ data are described to follow the same trajectory, regardless of when MgIE kicks in during serine-assisted photo-reduction. When oxalic acid was screened with a single light experiment (anoxic, pH 6, $f_R = 0.11$), (+)MgIE was observed, anoxic time series experiments with UV-B irradiation at pH 3.9 and 5.2 revealed no evidence of MgIE in the range investigated down to $f_R = 0.01$. This is evidence that Hg oxalate complexes can be directly photodegraded by homolysis ($Hg(\eta^2\text{–}C_2O_4) \xrightarrow{h\nu} Hg^{\bullet+} + C_2O_4^{\bullet-}$) as well as heterolysis ($Hg(\eta^2\text{–}C_2O_4) \xrightarrow{h\nu} Hg + 2\,CO_2$). Heterolytic photoreduction does not induce MgIE but results in NFS with limited (−)odd-MIF, as is the case for ligation with the substituted aromatic carboxylic acids shown in the table. This also applies to thermal (dark) reduction by a uni− (e.g., $Hg\text{–}QH^+ \rightarrow Hg^0 + Q + H^+$) or bimolecular (e.g., $Hg^{2+} + Sn^{2+} \rightarrow Hg^0 + Sn^{IV}$) processes. Although NFS is a general isotopic effect, its magnitude depends on the shift in the 6s orbital electron density, which is greater for a red-ox reaction than for ligand exchange or evaporation. In turn, ionic Hg complexes have greater NFS than more covalent complexes upon reduction to Hg^0. NFS typically produces a characteristic $\Delta^{199}Hg/\Delta^{201}Hg$ slope of ~1.54 to 1.66, as determined from experimental studies and theoretical calculations. However, the application of linear regression to NFS odd-MIF data ($\Delta^{199}Hg$ vs. $\Delta^{201}Hg$) is limited in several cases because the observations are distributed over such a small range that they approach the scale of the corresponding analytical precision. **Table 8** gives two standard deviations of the slope of the linear fits using York's regression, and the uncertainty is so large that it does not allow a definitive $\Delta^{199}Hg/\Delta^{201}Hg$ ratio to be determined. In these cases, it has been suggested that a better indicator of NFS is

[40] Refers to a closed system

[41] Applies to dark conditions, under UVA irradiation demethylation gradually counteracts $MMHg^+$ formation.

[42] Potentially explained by photodegradation of $MMHg^+$

formaterade: Teckenfärg: Blå
formaterade: Inte Expanderad med / Kondenserad med
tog bort: NVE
formaterade: Kondenserad med 0,2 pt
formaterade: Kondenserad med 0,2 pt
flyttade (infogning) [9]
formaterade: Teckenfärg: Dekorfärg 2
flyttade upp [9]: 0.24 ± 0.01
formaterade: Kondenserad med 0,6 pt
formaterade: Teckenfärg: Dekorfärg 2
formaterade: Inte Expanderad med / Kondenserad med
formaterade: Inte Expanderad med / Kondenserad med
formaterade: Kondenserad med 0,2 pt
tog bort: NVE
formaterade: Kondenserad med 0,2 pt
tog bort: photo reduction
tog bort: is
formaterade: Teckenfärg: Blå
tog bort: ,
tog bort: induced
tog bort: the
tog bort: while
tog bort: showed
tog bort: ,
tog bort: shows
formaterade: Teckenfärg: Blå
tog bort: .
tog bort: .
tog bort: the
formaterade: Teckenfärg: Blå
tog bort: a
formaterade: Teckenfärg: Blå
tog bort: it approaches
tog bort: intermittently
tog bort: iApplies
tog bort: photo-degradation

instead to confirm that the patterns of Hg isotope fractionation observed mimic the odd–even staggering pattern of nuclear charge radii (Motta et al., 2020b). The description of NFS is limited to equilibrium fractionation (**Eq. 25**) and predicts, similar to EIE-MDF (**Eq. 23**), the enrichment of heavier isotopes in the oxidized fraction of the red–ox pair. Calculations performed for a series of Hg^{II} complexes, both binary and heterogeneous, containing simple hard and soft ligands relative to Hg^0, show that NFS makes the most significant contribution to $\varepsilon^{202}Hg$ (ranging in total from 46 to 85% at 25 °C; Jiskra et al., 2012). The expected mass-independent enrichment $E^{199}Hg_{NFS}$ can be calculated based on the calculation of $\varepsilon^{202}Hg_{NFS}$, using the scale factors $\beta_{KIE-MDF}$ and β_{NFS} (Jiskra et al., 2012):

$$E^{199}Hg_{NFS} = \varepsilon^{202}Hg_{NFS} \cdot (\beta_{NFS} - \beta_{KIE\text{-}MDF}) \approx -0.2 \cdot \varepsilon^{202}Hg_{NFS} \quad (26)$$

Reduction by Fe^{II} and p-substituted benzoic acids results in one of the highest magnitudes of experimentally observed kinetic MDF (**Table 8**). The former system has been studied anoxically both as an open and closed system (Schwab et al., 2023), where the fractionation is of the Rayleighian model (kinetic) and equilibrium type, respectively. The closed system permits overprinting with the signature of isotopic equilibrium fractionation between Hg^0 and hydrolyzed Hg^{2+}, which has been consistently determined in two independent studies to be –2.63 (Wang et al., 2021) and –2.44‰ (Schwab et al., 2023), respectively. As demonstrated below, the magnitude of the equilibrium isotope enrichment factor ($\varepsilon^{202}Hg$) between Hg^0 and thiol-bound Hg^{II} is significantly lower (1.1–1.6‰), which is related to the lower vibrational energy of Hg-S bonds than that of Hg-O/Cl bonds.

8.4.2 Oxidation

To the extent that isotopic effects in aqueous-phase Hg^0 oxidation have been studied in the laboratory, it has been observed that oxidized Hg becomes isotopically heavier than the reactant. The observed fractionation does not conform to the Rayleigh model, but it is consistent with EIE in a closed system. Consequently, the isotope ratio of the product(s) linearly approaches that of the reactant at the beginning of the reaction. An example of atmospherically relevant oxidation is the rapid reaction with $^{\bullet}OH$ (**Rxn W2**, generated by photolysis of NO_3^-) with $\varepsilon^{202}Hg = 1.20 \pm 0.14$ ‰ (Stathopoulos, 2014). Experiments with thiol-substituted carboxylic acids in the dark produced similar fractionation results (**Table 8**, **Rxn W7**). Additionally, NFS produces a small odd-MIF signal that consistently acts in the opposite direction of mass-dependent fractionation (Zheng et al., 2019). The reason for observing EIE despite the continuous oxidation of Hg^0 without any indication of reversibility in the form of back reactions has been attributed to the rapid exchange of Hg isotopes between the remaining Hg^0 and the formed Hg^{II} complexes (Wang et al., 2020). There is currently debate surrounding the mechanism by which this exchange occurs (Wang et al., 2020; Zheng et al., 2019; Wang et al., 2021). In the presence of humic acid, the oxidation of dissolved Hg^0 exhibits two kinetic regimes where the EIE is not fully established in the initial regime (Zheng et al., 2019). KIE-MDF during dark reduction in the presence of DOM and EIE-MDF during dark oxidation caused by humic acid results in fractionation in the same direction and magnitude, so unmasking the controlling redox process from isotopic measurements can be difficult.

8.5 Isotope fractionation during complexation, sorption and surface-catalyzed reduction

8.5.1 Processes interfacing the aqueous phase

Theoretical computations of EIE based on the MDF and NFS generally agree with experimentally determined fractionation factors for complexation. Competitive complexation of Hg^{II} between one of the typical hard ligands HO^- and Cl^- and a soft ligand in the form of a thiol resin results in a lighter isotopic signature of the sulfur-bound Hg^{II} pool ($\varepsilon^{202}Hg$ values of –0.62 and –0.53‰, respectively), which is related to increased covalent bonding and electron density in the 6s Hg orbital (Wiederhold et al., 2010). For the sorption of dissolved Hg^{II} on α-FeOOH, the observed isotopic fractionation ($\varepsilon^{202}Hg \sim -0.4$‰) is exclusively determined by the process in solution, where a vanishingly small pool (< 0.1%) of isotopically lighter cations is in equilibrium with a bulk of neutral Hg^{II} molecules, with only the former being sorption active (Jiskra et al., 2012). Equilibration and kinetic fractionation have been reported to describe the precipitation process of β-HgS and HgO, respectively, from an initially acidic solution, with $\varepsilon^{202}Hg$ values between the precipitate and the supernatant being –0.63‰ and –0.32‰, respectively (Smith et al., 2015). Like adsorption on goethite, the observed fractionation during the precipitation of metacinnabar is interpreted as an effect of solution chemistry, in this case, a transition from O– to S–bonding for Hg^{II}. In addition to the homogeneous phase reduction of Hg^{II} by Fe^{II} in aqueous solutions (**Table 8**), the heterogeneous phase reduction of Hg^{II} by surface-bound (adsorbed Fe^{II} on goethite/boehmite) or structural Fe^{II} (magnetite $Fe^{II}Fe_2^{III}O_4$, Schwab et al., 2023 and siderite/green rust $FeCO_3$, Wang et al., 2021) has been studied isotopically. As shown in **Table 9**, the isotopic fractionation in heterogeneous reduction

tog bort: -
tog bort: 21
tog bort: like
tog bort: 19
tog bort: -
formaterade: Teckenfärg: Blå
tog bort: in most cases
tog bort: ,
formaterade: Teckenfärg: Dekorfärg 2
Formaterat: Avstånd Efter: 6 pt
tog bort: 23
Formaterat: Avstånd Efter: 3 pt
tog bort: will be
tog bort: factors
tog bort: as
tog bort: a
tog bort: in
tog bort: in
Formaterat: Radavstånd: enkelt
formaterade: Kondenserad med 0,3 pt
formaterade: Kondenserad med 0,3 pt
tog bort: NVE
formaterade: Kondenserad med 0,3 pt
tog bort: one
formaterade: Kondenserad med 0,3 pt
formaterade: Kondenserad med 0,3 pt
formaterade: Kondenserad med 0,3 pt
formaterade: Kondenserad med 0,3 pt
formaterade: Kondenserad med 0,3 pt
formaterade: Kondenserad med 0,3 pt
tog bort: As with the
formaterade: Kondenserad med 0,3 pt
formaterade: Kondenserad med 0,3 pt
formaterade: Kondenserad med 0,3 pt

is closely related in magnitude to that of homogeneous fractionation by Fe^{II} (**Table 8**), except in the case of magnetite (whose iron structure is present in different oxidation states), which has a much more limited TMDF and MIF ($\varepsilon^{202}Hg$ = –1.38‰ and $E^{199}Hg$ = 0.13‰, respectively). All these processes, when determined with confidence, demonstrate $\Delta^{199}Hg/\Delta^{201}Hg$ ratios within the range of 1.56 to 1.62, which indicates that the observed MIF ($E^{199}Hg$ in the range of 0.13 to 0.34‰) is caused by NFS.

8.5.2 Processes interfacing the gas phase

Section 8.4.1 and **Table 8** refer to a study of Hg^{II} photoreduction of aqueous diesel soot, which includes experiments with a stationary soot phase mixed with $HgCl_2$ on a quartz plate over which a slow flow of Ar gas passes, as discussed below (Huang et al., 2021). In comparison, photoreduction in aqueous- and solid-phase diesel soot shows equivalent enrichment of heavier isotopes in the Hg reactant of 1.26–1.75‰. This value overlaps with the values typical of Hg redox chemistry (**Table 8**). In contrast to the aqueous phase, the photoreduction in the solid phase shows a continuous strong MIF (this time, positive MgIE induced in the Hg^0 product) throughout the reaction, whereas in the latter case, a large MIF of the opposite sign occurs after only ~60% of the reaction. Furthermore, the reduction rate increases with increasing carrier gas humidity. The photo-triggered MgIE is highest when the carrier gas is dehumidified, but decreases rapidly as the RH increases (**Table 9**).

Table 9. Experimental fractionation factors determined for Hg^{II} complexation, sorption, surface-catalyzed reduction and processes interfacing the gas phase.

Initial Hg^{II} conc. (electrolyte)	Reactant	Experimental conditions: L/Hg ratio		Anoxic (A)/Oxic (O)	$\varepsilon^{202}Hg$ (‰, ±2σ)	$E^{199}Hg$ (‰)	$\Delta^{199}Hg/\Delta^{201}Hg$	Isotope effects	Reference
Complexation, sorption, precipitation of aqueous Hg^{II}									
196 µM (Cl^-)	$HgCl_2$	Complexation between Hg^{II} and thiol resins		O	–0.53± 0.15			EIE-MDF, NFS	Wiederhold et al., 2010
207 µM (NO_3^-)	$Hg(OH)_2$				–0.62± 0.17				
5–25 µM	$HgOH^+$ $HgCl^+$	Hg^{II} sorption to α–FeOOH		O	–0.37± 0.03	–0.06			Jiskra et al., 2012
100 µM	$Hg(OAc)_2$	Sub-stoichiometric (10, 30, 50, 70%) amounts of S^{2-} added at a start pH of 2.3–3.0		A	–0.63± 0.04				Smith et al., 2015
	Hg^{2+}	Sub-stoichiometric (10, 30, 50, 70%) amounts of OH^- added at a start pH of 1.		A	–0.32			KIE-MDF, NFS	
Hg^{II} – Hg^0 equilibration									
300–328 nM Hg^{II} 150–173 nM Hg^0	$Hg(OH)_2/Hg^0$	Water		A	2.63± 0.37	0.28± 0.21	1.44	EIE-MDF, NFS	Wang et al., 2021
	$HgCl_2/Hg^0$	10 mM NaCl			2.77± 0.70				
Heterogeneous Hg^{II} reduction by surface-bound and structural Fe^{II}									
285 nM (NO_3^-)	$Hg(OH)_2$	Hg^{II} reduction to Hg^0 by suspended $FeCO_3$ (s)	Siderite (0.1 g L^{-1}, pH 7.1)	A	2.43 ± 0.38	0.09		EIE–MDF NFS	Wang et al., 2021
			Green rust (0.01 g L^{-1}, pH 7.2)		2.28 ± 0.40				
1 µM (NO_3^-)	$Hg(OH)_2$	Hg^{II} reduction by suspended magnetite ($Fe^{II}Fe^{III}_2O_4$, surface area ~2 m^2 L^{-1}		A	–1.37 ± 0.07	0.13 ± 0.01	1.59 ± 0.09		Schwab et al., 2023
Photoreduction of Hg^{II} doped on a diesel soot matrix									
12 µM (Cl^-)		Hg/C 7.8 × 10^{-5} (M/M)	Relative humidity 28%	A	–1.75 ±0.05	2.43 ±0.19	1.15 ± 0.01	MDF, (–)MgIE	Huang et al., 2021
			Relative humidity 68%		–1.48 ±0.02	0.20 ±0.05			

8.6 Isotopic fractionation during air-surface Hg^0 gas exchange

The interaction between atmospheric Hg and the Earth's reservoirs has been discussed only briefly in Section 3.2, as this area has recently been covered by a literature review (Sommar et al., 2020). Importantly, the gas exchange of volatile Hg is bidirectional. Consequently, the net flux of Hg over an ecosystem may represent a delicate balance between opposing processes, including deposition/uptake versus re-emission. The end members of Hg exchange between the surface (biosphere, pedosphere, lithosphere, hydrosphere, and cryosphere) and atmosphere are all isotopically distinguishable (Liu et al., 2024). A combination of bulk measurements and analysis of stable Hg isotopic compositions enables separation of the contributions from atmospheric Hg^{II} and Hg^0 deposition, as well as local partitioning between Hg^0 deposition and re-emission. The isotopic composition of atmospheric Hg is presented and discussed in **Section 8.2**. In addition to the data, an updated compilation of complementary isotopic Hg data for reservoirs that are in contact with

tog bort: well
tog bort: one
formaterade: Kondenserad med 0,3 pt
tog bort: the
formaterade: Kondenserad med 0,3 pt
formaterade: Kondenserad med 0,3 pt
tog bort: in
formaterade ... [756]
tog bort: iron
formaterade: Kondenserad med 0,3 pt
tog bort:) with
formaterade: Kondenserad med 0,3 pt
tog bort: MDF
formaterade: Kondenserad med 0,3 pt
tog bort: possible to be
formaterade: Kondenserad med 0,3 pt
tog bort: NVE
formaterade: Kondenserad med 0,3 pt
Formaterat: Radavstånd: Flera 1,43 li
tog bort: …phase diesel soot shows equivalent enrichment of heavier isotopes in the Hg reactant of 1.26-…1.75‰. This value overlaps with the value ... [757]
tog bort: sets in only…ccurs after only ~60% of the reaction. Furthermore, the reduction rate increases with the…ncreasing carrier gas's…as humidity. ... [758]
tog bort:)
tog bort:
tog bort: NVE
tog bort: NVE
tog bort: NVE
tog bort: 4
formaterade: Teckenfärg: Blå
tog bort: It is crucial to acknowledge that
formaterade: Kondenserad med 0,2 pt
tog bort: the
formaterade ... [759]
tog bort: isotope composition allows to separate
formaterade: Kondenserad med 0,2 pt
tog bort: contribution of,
formaterade: Kondenserad med 0,2 pt
tog bort: the
formaterade: Kondenserad med 0,2 pt
tog bort: has been
formaterade: Kondenserad med 0,2 pt
tog bort: these
formaterade: Kondenserad med 0,2 pt
tog bort: the
formaterade: Kondenserad med 0,2 pt

the atmosphere and thus can undergo gas exchange has been produced during the preparation of this review (Liu et al., 2024). In the following, we express absolute deposition with negative values and vice versa for emission throughout.

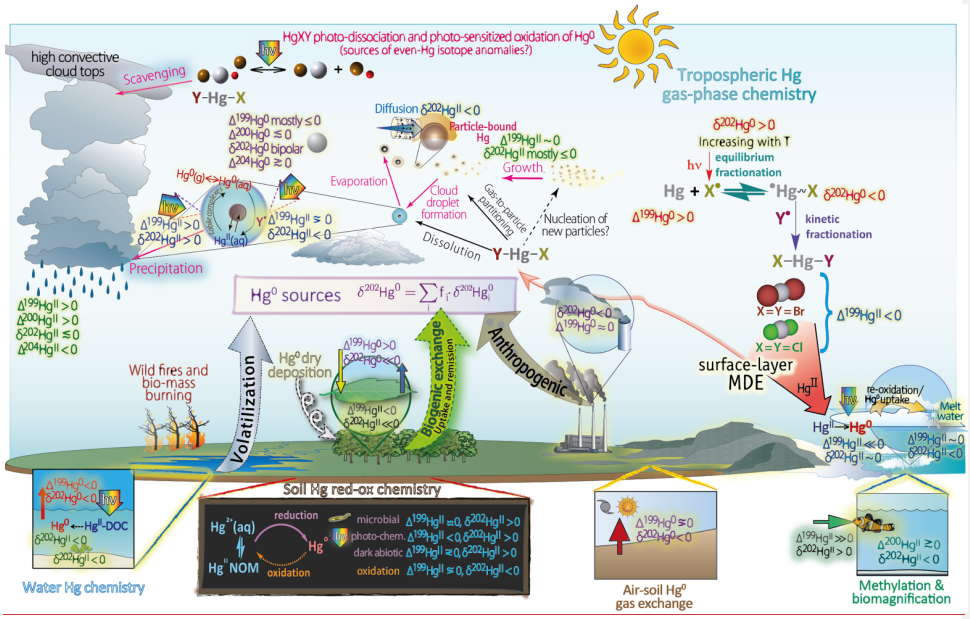

Figure 17. Schematic illustration showing key biogeochemical Hg processes in Earth's surface reservoirs and their associated Hg isotope fractionation along with corresponding isotopic composition observations focused on the atmosphere. **Section 8.2** addresses the isotopic characteristics of atmospheric mercury. The existing isotopic information on the gas-phase and water-phase redox transformations of mercury is presented in **Sections 8.3** and **8.4**, respectively. **Sections 8.5** and **8.6** describe isotopic fractionation in heterogeneous chemical processes and processes involving Hg^0 gas exchange between the atmosphere and the Earth's surface reservoirs, respectively.

8.6.1 Mixing and fractionation modeling of Hg^0 deposition and post-depositional processes

Deposition

Isotope-based modeling by binary (e.g., **Eq. 27**) and ternary mixing with MDF, odd-MIF, and even-MIF signatures of atmospheric Hg^0 and other Hg pools as end members has been applied to distinguish the fraction of Hg^0 deposition via vegetated surfaces (Wang et al., 2020b; Enrico et al., 2016; Obrist et al., 2017; Wang et al., 2019b; Li et al., 2022a; Li et al., 2023a; Li et al., 2023b), soil (Zheng et al., 2016; Obrist et al., 2017; Wang et al., 2019b; Wang et al., 2020a), water (Jiskra et al., 2021; Zhang et al., 2023a), throughfall (Wang et al., 2020b) and snow run-off (Douglas and Blum, 2019), estimated to be 60–90%, 32–105%, 50–85%, 34–82% and > 75% of total deposition, respectively. As a proxy for atmospheric Hg^0, foliage/litter Hg has been used as an end-member in mixing modeling of Hg^0 inputs to soil (Demers et al., 2013; Jiskra et al., 2015; Zhang et al., 2013), runoff (Jiskra et al., 2017), and stream water (Woerndle et al., 2018), which may introduce bias because a significant fraction of the gross air Hg^0 incorporated as Hg^{II} in foliage is re-emitted after photoreduction (Yuan et al., 2019b). The contribution of Hg^0 deposition to vegetation Hg uptake is greatest in foliage, followed by branches, bark, stems and roots (Wang et al., 2020b; Liu et al., 2021a; Sun et al., 2017). The new Hg isotope evidence has demonstrated that Hg throughfall via the canopy and along stems, which was previously assumed to be derived mainly from wet and dry deposition of atmospheric RM (Wright et al., 2016), contains a larger proportion of Hg excreted from biomass, where it originated mainly from Hg^0 uptake followed by translocation. The isotope mixing formula is used to determine the proportions of different isotope sources in a mixture, the simplest form of which is as follows:

$$(\delta^{xxx}Hg)_{mix} = f_1 \cdot (\delta^{xxx}Hg)_1 + f_2 \cdot (\delta^{xxx}Hg)_2 \quad (27)$$

$$f_1 + f_2 = 1$$

tog bort: exert
formaterade: Kondenserad med 0,2 pt
formaterade: Kondenserad med 0,2 pt
Formaterat: Avstånd Före: 6 pt, Radavstånd: Flera 1,15 li
formaterade: Teckenfärg: Dekorfärg 2
Formaterat: Avstånd Före: 9 pt, Radavstånd: 1,5 rader
formaterade: Kondenserad med 0,2 pt
Formaterat: Avstånd Efter: 6 pt, Radavstånd: 1,5 rader
formaterade: Kondenserad med 0,2 pt
formaterade: Kondenserad med 0,2 pt
tog bort: stem
formaterade: Kondenserad med 0,2 pt
formaterade: Kondenserad med 0,2 pt
tog bort: were
formaterade: Kondenserad med 0,2 pt
formaterade: Kondenserad med 0,2 pt

Post-deposition

Isotopic and concentration measurements of Hg^0 jointly in near-surface air and surface pore air/water, in addition to other isotopic data, allow the inference of processes by mass balance or Rayleigh-type models at the air–soil interface and in the surface soil (Jiskra et al., 2019; Li et al., 2023a; Yuan et al., 2021; Chen et al., 2023). For poorly drained boreal organic soil horizons (histosols), in contrast to podzols, mixing modeling indicates significant reductive loss (24–33%) to the atmosphere by abiotic reduction (Jiskra et al., 2015). A further multi-process model is presented here, which is designed to elucidate the dynamic evolution of post-depositional Hg (>90% from litterfall) on the subtropical forest floor over a 500-year period (Yuan et al., 2020). The results indicate that photolytic and microbial reduction processes exert an influence during the initial few years, but are subsequently superseded by dark redox processes (exhibiting NFS) in the compost, where Hg^{II} finally becomes inert at depths of >10 cm in the horizon after approximately 420 years. Studies of forest soils in different climatic zones have shown that microbial reduction ($\varepsilon^{202}Hg = -0.4‰$, $E^{199}Hg \approx 0$, Kritee et al., 2007) plays a dominant role (Yuan et al., 2021; Chen et al., 2023), which, for rainforests, can explain up to 90% of the Hg^{II} reduction in the upper soil horizon (Yuan et al., 2023b). In an open boreal peatland, photoreduction dominated the post-depositional process, accounting for the transformation of 30% of the annually deposited Hg (Li et al., 2023a).

8.6.2 Enclosure and related flux measurements

Experimental investigations employing dynamic flux chambers (DFCs) have been conducted in both ambient and controlled environments with the objective of elucidating the isotopic dynamics of Hg^0 exchange between the atmosphere and vegetation at the branch level (Yuan et al., 2019b; Chen et al., 2023), as well as between air and soil (Yuan et al., 2021; Chen et al., 2023; Zhu et al., 2022; Zhang et al., 2020), water (Zhang et al., 2023a), and snow (Sherman et al., 2010). For this application, in addition to traditional chambers (Demers et al., 2013; Chen et al., 2023; Zhu et al., 2024), a type was used that produces a uniform surface friction velocity over flat ground to couple with ambient shear conditions to scale to the ambient flux (Yuan et al., 2021; Yuan et al., 2023b; Lin et al., 2012). The surface-atmosphere Hg^0 flux is the result of complicated bidirectional processes, including Hg^0 efflux from the surface and direct atmospheric Hg^0 deposition.

Deposition and sink processes

When direct Hg^0 deposition is measured absolutely and isotopically with a DFC, enrichment factors for TMDF ($\varepsilon^{202}Hg_{air/surface}$) and odd-MIF ($E^{199}Hg_{air/surface}$) may be calculated via a linearized Rayleigh fractionation model (Zhu et al., 2022; Mariotti et al., 1981):

$$\delta^{202}Hg^0_{DFC} - \delta^{202}Hg^0_{air} = \varepsilon^{202}Hg_{surface-air} \cdot \ln\left(c^{Hg^0}_{DFC} / c^{Hg^0}_{air}\right)$$
$$\Delta^{199}Hg^0_{DFC} - \Delta^{199}Hg^0_{air} = E^{199}Hg_{surface-air} \cdot \ln\left(c^{Hg^0}_{DFC} / c^{Hg^0}_{air}\right) \quad (28)$$

where c represents the concentration and the indices air and DFC refer to the air entering and exiting the DFC, respectively. Alternatively, **Eq. 28** is applied to extract $\varepsilon^{202}Hg_{surface-air}$ using measurements of c^{Hg^0} and $\delta^{202}Hg^0$ at two pristine sites with and without vegetation (Enrico et al., 2016) or using day- vs. night-time segregated ambient air data at the same site (Jiskra et al., 2019). When direct deposition is measured isotopically with a DFC, the residual Hg^0 in the chamber outlet shifts to be preferentially isotopically heavier, with a large but variable discrimination observed over soils ($\varepsilon^{202}Hg_{soil-air} = \sim 0$ to $-5.8‰$, Chen et al., 2023; Yuan et al., 2023b; Zhu et al., 2022) and over vegetation ($\varepsilon^{202}Hg_{foliage/air} = \sim -1$ to $-4.2‰$, Yuan et al., 2019b; Enrico et al., 2016; Demers et al., 2013; Jiskra et al., 2019; Chen et al., 2023). Deposition in contact with any surface does not result in a significant change in $\Delta^{199}Hg^0$, unlike the situation with $\delta^{202}Hg^0$.

Information on the sink processes of Hg^0 in the soil can be obtained by pursuing measurements of isotopic Hg^0 in the soil pore air under sub-ambient concentration regimes. In tundra (Jiskra et al., 2019) and peatlands (Li et al., 2023a), the isotopic differences between ambient Hg^0 and pore gas Hg^0, whose concentrations is sub-ambient (~0.4 – ~0.6 and ~0.2 – ~0.7 ng m^{-3}) and therefore mediate Hg^0 net diffusion into the substrate via **Eq. 28**, have been linked to DOM-driven anaerobic oxidation in soil water exhibiting EIE (Zheng et al., 2019). Investigations of the Hg^0 level in the pore air of forest soils provide a mixed picture, ranging from sites with highly depleted air (Obrist et al., 2014) to sites with up to ten times enriched pore air (Yuan et al., 2019a) compared with the ambient concentrations above. In subtropical (Yuan et al., 2019a) and subalpine (Chen et al., 2023) forest soils, the concentration of Hg^0 in pore air is typically higher than that in near-surface ambient air and shows seasonal isotopic variations (TMDF and odd-MIF), suggesting complexity in Hg^0 gas exchange between air and soil. In tropical forest soils, pore air shifts from being nearly ambient

Formaterat: Radavstånd: Flera 1,15 li, Ingen kontroll av enstaka rader, Håll inte ihop med nästa
Formaterat: Avstånd Efter: 4 pt, Radavstånd: 1,5 rader
tog bort: to infer
tog bort: -
tog bort: boreal
tog bort: a
tog bort: –
tog bort: herewith
tog bort: of 500 yr.
tog bort: ,
tog bort: NVE
tog bort: became
Formaterat: Radavstånd: Flera 1,15 li
Formaterat: Radavstånd: Flera 1,15 li
tog bort: MDF
tog bort: using
Formaterat: Avstånd Efter: 0 pt, Radavstånd: enkelt
Formaterat: Avstånd Efter: 0 pt
Formaterat: Avstånd Efter: 0 pt
tog bort: 24
Formaterat: Radavstånd: exakt 17 pt
tog bort: refers
tog bort: 24
tog bort: for extracting
formaterade: Teckenfärg: Dekorfärg 2
tog bort: difference
tog bort: the
tog bort: concentration
tog bort: mediates
tog bort: , have
tog bort: 24
formaterade: Teckenfärg: Anpassad färg(RGB(31;56;100))
formaterade: Teckenfärg: Blå
tog bort: give
tog bort: to
tog bort: above
tog bort: in MDF
tog bort: near-

during the rainy season to being markedly sub-ambient during the dry season (Yuan et al., 2023b). To resolve Hg^0 flux partitioning here, a combination of DFC measurements of net fluxes and forced unidirectional efflux, soil pore air, and Hg isotopic composition in forest soil depth profiles are employed as inputs into isotope mass balance models based on odd-MIF (Yuan et al., 2021). Net fluxes measured by DFC are interpreted as a ternary mixing of deposition, Hg^0 losses from the surface soil via Hg^{II} photoreduction, and a term generated by Hg redox processes (dark/microbial reduction vs. oxidation) in the organic soil horizon. Although associated with considerable uncertainties, the estimated gross deposition to the forest floor is between -7.8 and -1.8 ng m^{-2} h^{-1} for the subtropical site (Yuan et al., 2021) and between -6.7 and -4.4 ng m^{-2} h^{-1} for the tropical site (Yuan et al., 2023b), depending on the season, and between -4.9 and -2.0 ng m^{-2} h^{-1} for the subalpine site, depending on the type of forest floor (Chen et al., 2023).

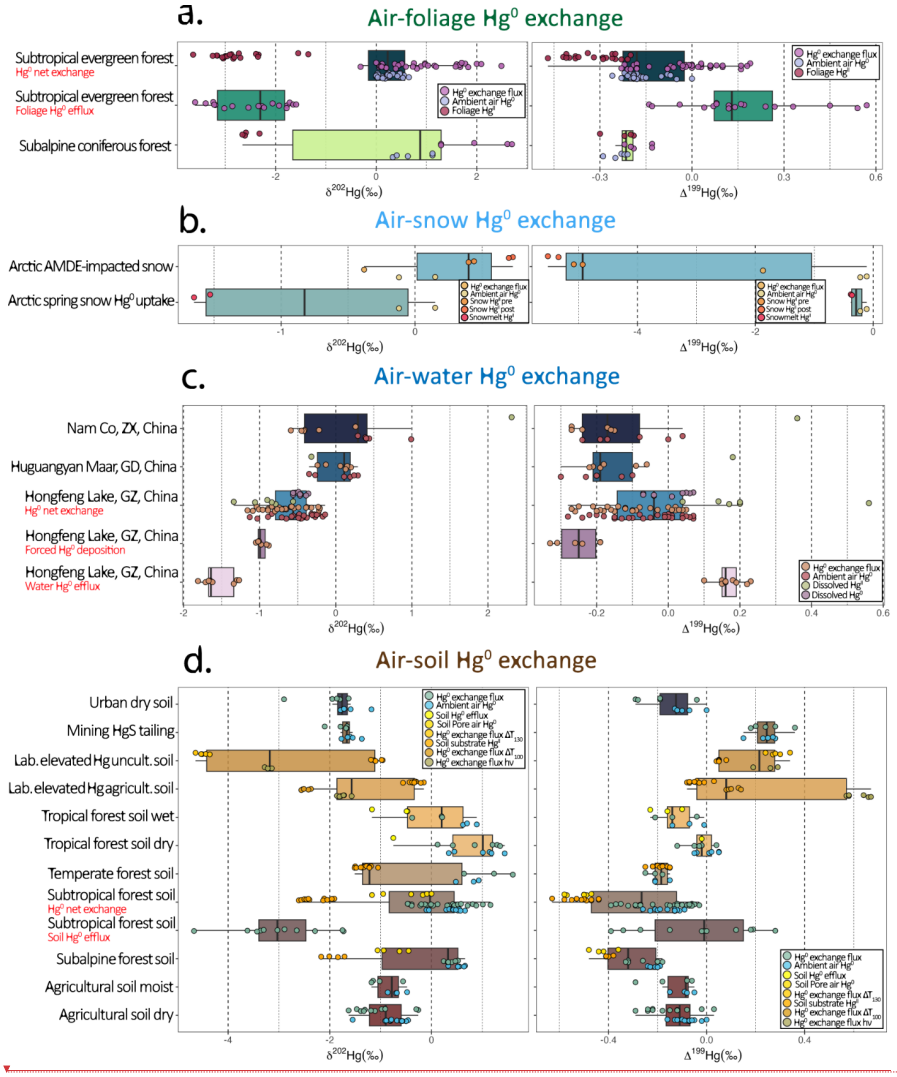

Figure 18. Statistical summary of observations from isotopic studies of Hg^0 exchange between the atmosphere and various groups of surface reservoirs on Earth. In the air-foliage group, data were taken from Yuan et al. (2019b) and Chen et al. (2023). For the air–snow group, data were taken from Sherman

tog bort: isotope

tog bort: input

tog bort:

formaterade: Kondenserad med 0,3 pt

tog bort: 17

formaterade: Kondenserad med 0,3 pt

tog bort: Earth's

formaterade: Kondenserad med 0,3 pt

formaterade: Kondenserad med 0,3 pt

tog bort: In

formaterade: Kondenserad med 0,3 pt

tog bort: -

formaterade: Kondenserad med 0,3 pt

et al. (2010) and Douglas and Blum (2019). For the air–water group, data were taken from Zhang et al. (2023a; 2021a). For the air–soil group, data were taken from Zhang et al. (2020), Zhu et al. (2022), Yuan et al. (2021; 2023b) and Chen et al. (2023).

Foliar oxidation of Hg^0 drives its reactive uptake and is the most important step in the accumulation of initially Hg^0 uptake by plants (Liu et al., 2021b). Direct bio-oxidation from Hg^0 to Hg^{II} has been traced to heme enzymes that catalyze the degradation of H_2O_2, specifically to a ferryl ($O=Fe^{IV}$) catalase radical cation complex (Ogata and Aikoh, 1984) that swiftly oxidizes Hg^0 (1.4×10^4 M^{-1} s^{-1}, Wigfield and Tse, 1986):

$$H_2O_2 + \langle Fe^{II}–E^{\bullet+} \leftrightarrow Fe^{III}–E\rangle \longrightarrow H_2O + \langle O=Fe^{IV}–E^{+\bullet} \leftrightarrow O=Fe^{III}–E\rangle$$
$$Hg^0 + \langle O=Fe^{IV}–E^{+\bullet} \leftrightarrow O=Fe^{III}–E\rangle + 2\,H^+ \longrightarrow Hg^{2+} + \langle Fe^{II}–E^{\bullet+} \leftrightarrow Fe^{III}–E\rangle + H_2O \quad \text{(Rxn 14)}$$

here, E represents the heme group attached to the enzyme, which can provide an electron, reducing the formal oxidation number of iron from five to four. Divalent Hg readily binds to soft functional groups on the enzyme as soon as it is formed. MDF fractionation during oxidation of the absorbed isotopically light Hg^0 causes the product pool to be heavier than the reactant, which is consistent with observations that Hg^{II} incorporated into leaf shoots is only slightly lighter than Hg^0 in ambient air. Notably, in contrast to the Hg pool in the leaf shoots, the Hg in the growing foliage of the current year shifted rapidly in the first months toward clearly negative $\delta^{202}Hg^{II}$ signatures, the causes of which have been discussed elsewhere (Yuan et al., 2019b).

In contrast to the observations regarding the air modified by interactions with soil and foliage, the residual Hg^0 in the outgoing air is significantly lighter than that in the incoming air ($\delta^{202}Hg^0_{air} - \delta^{202}Hg^0_{DFC} = 0.38‰$), as observed by DFC, for deposition regimes over freshwater surfaces (Zhang et al., 2023a). This may be interpreted as the dissolved $Hg^0(aq)$ being consumed by oxidation, whereby the rapid exchange of Hg isotopes between the remaining Hg^0 and the formed Hg^{II} (**Section 8.4.2**) causes the former, which is partially returned to the gas phase, to exhibit a more negative $\delta^{202}Hg^0$. In surface waters, photolytic re-reduction is also possible, which can be used for determining the isotopic composition of dissolved Hg^0 (Zhang et al., 2021a).

During colder seasons with limited solar radiation, there is a small but persistent net Hg^0 dry deposition over the snow-covered Arctic interior tundra (Obrist et al., 2017), whose interstitial snow air has sub-ambient concentrations (0.69 vs. 1.07 ng m^{-3}) with comparatively more positive $\delta^{202}Hg^0$ values (1.08 vs. 0.77‰, Jiskra et al., 2019). Using the exclusion method, this trajectory may reflect Hg^0 uptake by ground lichens (Olson et al., 2019). Compared with the hinterland snowpack (~50 ng m^{-2}), the Arctic coastal snowpack has regionally much higher Hg^{II} pools (>2000 ng m^{-2}), which are characteristically released as an ionic pulse in the runoff during snowmelt. High Hg^{II} concentrations in the coastal marine cryosphere are partially explained by AMDEs (described in **Section 3.2**, Douglas et al., 2017). However, coastal AMDE deposition is mostly re-emitted as Hg^0 to the atmosphere before snow melts (see below). In contrast, the pulse in runoff appears to be related mainly to the reactive uptake of Hg^0 on marine snow, which is rich in halogen compounds and other reactive species (see **Section 7.3**) (Douglas et al., 2017). In support of the significant reactive uptake of Hg^0 on salt-laden snow, analogous odd-MIF signatures between ambient air Hg^0 and snowmelt Hg^{II} have been reported ($\Delta^{199}Hg$ values documented in **Fig. 18b**, Douglas and Blum, 2019).

Net exchange, source processes and flux partitioning

Owing to the length of time (typically a few days) required to accumulate sufficient Hg to perform isotopic analysis, samples from a DFC measurement are a composite of periods of net emission and net deposition, unless the Hg^0 concentration in the inlet is manipulated so that emission or deposition becomes persistent within the chamber. The TMDF and odd-MIF signatures from DFC measurements in ambient air ("net Hg^0 exchange") are calculated as follows (Zhu et al., 2022):

$$\delta^{202}Hg^0_{exchange} = \left(\delta^{202}Hg^0_{DFC} \cdot c^{Hg^0}_{DFC} - \delta^{202}Hg^0_{air} \cdot c^{Hg^0}_{air}\right) / \left(c^{Hg^0}_{DFC} - c^{Hg^0}_{air}\right)$$
$$\Delta^{199}Hg^0_{exchange} = \left(\Delta^{199}Hg^0_{DFC} \cdot c^{Hg^0}_{DFC} - \Delta^{199}Hg^0_{air} \cdot c^{Hg^0}_{air}\right) / \left(c^{Hg^0}_{DFC} - c^{Hg^0}_{air}\right) \quad (29)$$

In the special case of using Hg-free air (zero air) to feed the DFC, $\delta^{202}Hg^0_{emission}$ and $\Delta^{199}Hg^0_{emission}$ can be determined. The enrichment factors during net Hg^0 exchange and emission are calculated using the following set of equations:

$$\varepsilon^{202}Hg_{exchange} = \delta^{202}Hg^0_{exchange} - \delta^{202}Hg_{surface} \quad , \quad E^{199}Hg_{exchange} = \Delta^{199}Hg^0_{exchange} - \Delta^{199}Hg_{surface} \quad (30)$$
$$\varepsilon^{202}Hg_{emission} = \delta^{202}Hg^0_{emission} - \delta^{202}Hg_{surface} \quad E^{199}Hg_{emission} = \Delta^{199}Hg^0_{emission} - \Delta^{199}Hg_{surface}$$

tog bort: In
tog bort: -
formaterade: Kondenserad med 0,3 pt
tog bort: In
formaterade: Kondenserad med 0,3 pt
formaterade: Kondenserad med 0,3 pt
tog bort: -
formaterade: Kondenserad med 0,3 pt
tog bort: dry deposited
formaterade: Teckenfärg: Dekorfärg 2
formaterade: Kondenserad med 0,2 pt
formaterade: Teckenfärg: Dekorfärg 2
tog bort: 15
formaterade: Teckenfärg: Dekorfärg 2
tog bort: The divalent
tog bort: will
tog bort: bind
tog bort: Then it should be mentioned that
tog bort: shifts
tog bort: towards
tog bort:
tog bort: interaction
formaterade: Teckensnitt:9,5 pt
formaterade: Teckensnitt:9,5 pt
formaterade: Teckensnitt:9,5 pt
tog bort: is another source involved in
formaterade: Teckenfärg: Dekorfärg 2
tog bort: -
tog bort: to
tog bort: 5.1.1
tog bort: most of the
tog bort: the
tog bort: the
tog bort: the
tog bort: a
tog bort: the
tog bort: referenced
tog bort: 17b
tog bort: Due
tog bort: MDF
tog bort: 25
tog bort: 26
tog bort: E^{199}

In a series of light, temperature and substrate moisture controlled laboratory experiments with untilled (forest) and tilled (agricultural) soils, both with elevated Hg levels, enclosed in a DFC fed with Hg-free air, large Hg^0 fluxes (≥500 ng m^{-2} h^{-1}) were unanimously associated with the most negative $\delta^{202}Hg^0_{emisson}$ values (−2.9 to −2.2‰ and −4.4 to −4.2‰ for agricultural and forest soils, respectively) when substrates were exposed to elevated temperatures in the dark (100–130 °C vs. 40 °C), while treatments with light, moisture, or a combination of both at room temperature produced more moderately negative $\delta^{202}Hg^0_{emisson}$ values (−2.1 to −1.6‰ and −3.3 to −2.6‰ for agricultural and forest soils, respectively, Zhang et al., 2020). $E^{199}Hg_{emission}$ of agricultural and forest soils displays a value of approximately 0.2 ‰, and $\Delta^{199}Hg/\Delta^{201}Hg$ was ~ 1.55 for the temperature controls, suggesting that the treatment caused Hg^0 loss propelled by the thermally driven reduction in Hg^{II} in the dark (**Section 8.4.1**). In the light and light–moisture exposure controls, the substrates differed in terms of the observed $E^{199}Hg_{emission}$, which for agricultural soils was 0.67 to 0.76‰ (mean) and for forest soils of a small magnitude, both positive and negative (−0.03 to 0.18‰, mean). The $E^{199}Hg_{emission}$ dichotomy may be interpreted as derived from a composite with $\Delta^{199}Hg$ contributions from both (−)MgIE and (+)MgIE-induced Hg^{II} photoreduction pathways, almost completely dominated by (−)MgIE processes (Hg^{II} bound to, e.g., N, S-containing ligands) for agricultural soils and for forest soils with a larger contribution from (+)MgIE processes (Hg^{II} bound to, e.g., O-containing ligands), balancing odd-MIF fractionation from (−)MgIE processes. However, the agricultural soil placed under water (rice paddy) photoemits Hg^0 characterized by a negative $\Delta^{199}Hg^0$ ($\Delta^{199}Hg^0_{emission}$ = −0.38 ± 0.18‰, Zhang et al., 2024), which is indicative of all observed Hg^{II} photoreduction in natural freshwaters studied in the laboratory as well as in situ.

A field study with DFC of cultivated or managed soils measured exchange fluxes (an MDF Rayleigh model yielded a 10-27 % contribution from deposition), which revealed net Hg^0 emissions (fraction) associated with average $\varepsilon^{202}Hg_{exchange}$ of −1.1 to −0.1‰ and −1.6 to −0.2‰ and average $E^{199}Hg_{ex}$ values of −0.27 to −0.13‰ and 0.00 to 0.14‰ for rural and urban soils, respectively. The above enrichment factors and $E^{199}Hg_{exchange} \approx E^{201}Hg_{exchange}$ indicate that the emitted Hg^0 comes mainly from the pool produced by photoreduction. The air concentration positively influences the magnitude of deposition in soils so that at a critical concentration level (compensation point), the net flux tends to change direction. This is reflected in the apparent $\varepsilon^{202}Hg_{exchange}$, which varies with the ambient Hg^0 concentration (Zhu et al., 2022). Analogous to laboratory experiments, in situ experiments on the subtropical forest floor have revealed that soil emissions of Hg^0 are strongly negative $\delta^{202}Hg^0_{emission}$ (mean −3.0‰, Yuan et al., 2021), while the magnitude of $\delta^{202}Hg^0_{emission}$ for the tropical rainforest floor is much smaller but still negative (mean −0.7‰, Yuan et al., 2023b). $E^{199}Hg_{emission}$ for subtropical forest soils exhibit positive values for all seasons over a considerable range (mean 0.1–0.7‰), whereas for rainforests, $E^{199}Hg_{emission}$ is consistently positive, albeit to a lesser extent (mean 0.2–0.3‰). Limited negative $\delta^{202}Hg^0_{exchange}$ values (mean values of –0.26, –0.54, –0.07 and –0.09 ‰) and consistently positive $E^{199}Hg_{exchange}$ values (mean values of 0.42, 0.23, 0.39 and 0.30 ‰) are observed in net Hg^0 gas exchange experiments over subtropical (Yuan et al., 2021), tropical (Yuan et al., 2023b), subalpine (Chen et al., 2023) and temperate (Demers et al., 2013) forest soils, respectively. In conclusion, bare or cultivated soils result in a greater degree of MDF isotope fractionation associated with Hg^0 gas exchange with the atmosphere than do forest soils, where the effects of photic and thermal processes are limited by canopy shading. Temporally extensive chamber measurements conducted globally over the forest floor indicate net emissions (Yuan et al., 2019a). For the first three forest soil studies mentioned above, the DFC dataset also contains sufficient isotope data to enable the modeling of net flux partitioning into gross emission and gross deposition.

Re-emissions of Hg^0 from perennial foliage of three beech species show an average positive $\varepsilon^{202}Hg_{emission}$ and $E^{199}Hg_{emission}$ of 0.6 and 0.3‰, respectively. The studied net exchange of Hg^0 between foliage and air for montane evergreen deciduous (Yuan et al., 2019b) and spruce (Chen et al., 2023) forests is mostly on the uptake side, which indicates that $\delta^{202}Hg^0_{DFC}$ is generally more positive than that of ambient air (**Fig. 18a**, mean shift of 0.72‰ for the latter site). The presence of bidirectional fluxes is, however, reflected in the observation that the $E^{199}Hg_{exchange}$ for both sites is consistently positive (mean 0.08 and 0.13‰, respectively), albeit modestly, due to a contribution from Hg^0 emissions resulting from (−)MgIE-induced photoreduction.

Isotopic studies of air–snow Hg^0 interactions and post-depositional processes have typically been conducted in the Arctic (Araujo et al., 2022; Sherman et al., 2010; Zheng et al., 2021; Jiskra et al., 2019; Obrist et al., 2017; Douglas and Blum, 2019), with occasional

tog bort: were observed
tog bort: -
tog bort: $Hg^0_{emisson}$
tog bort: ‰
tog bort: in
tog bort: dark
tog bort: Hg^{II}
tog bort: -
formaterade: Teckenfärg: Dekorfärg 2
tog bort: deriving
tog bort: inducing
tog bort: ,
tog bort: .
tog bort:)
tog bort: the
tog bort: aforementioned
formaterade: Teckenfärg: Dekorfärg 2
tog bort:) that showed
tog bort: of
tog bort: $E^{199}Hg_{exchange}$
tog bort: the
tog bort: to
tog bort:)
tog bort: the
tog bort: show
tog bort: that have
tog bort: ,
tog bort: exhibits
tog bort: –
tog bort: –
tog bort: sub-alpine
tog bort: , compared to
tog bort: effect
tog bort: is
tog bort: data set
tog bort: the
tog bort: gives
tog bort: 17a
tog bort: -
tog bort: interaction

studies at mid-latitudes (Kurz et al., 2021; Yuan et al., 2022). Hg in aging snowpacks exhibits by far the most extensive distribution of $\Delta^{199}Hg^{II}$ among Earth's surface reservoirs, with observations of $\Delta^{199}Hg$ progression reported in both positive (Kurz et al., 2021) and negative (Sherman et al., 2010; Zheng et al., 2021; Douglas and Blum, 2019) directions relative to fresh snow. As discussed in **Section 8.2.1**, the larger $\Delta^{199}Hg$ spread observed in polar airborne Hg (Hg^0 and RM) than in, for instance, high-altitude air from mid-latitudes can be attributed to the influence of AMDEs (during spring after sunrise and during summer) on a significant proportion of the collected polar data. Snow(fall) during the polar night is characterized by positive or near-zero $\Delta^{199}Hg$ signatures, as is the case for most global precipitation data (**Fig. 13c**), while the $\Delta^{199}Hg$ values of polar Hg^0 for the same period are all slightly negative, which is consistent with the global Hg^0 background pool (**Fig. 13a**). Only sporadic isotopic DFC measurements have been conducted over snow, yet ample measurements of polar air and snow as endmembers still offer an understanding of air-surface Hg^0 exchange following Hg^{II} deposition associated with AMDE. A seminal set of isotope data (Sherman et al., 2010) demonstrating a substantial odd-MIF triggered because of Hg^{II} photoreduction in snow was obtained from samples collected during a 9-day AMDE at the Alaskan Arctic coastline in conjunction with periods of minimal snowfall carrying high concentrations of scavenged Hg^{II} (0.5 ± 0.4 μg L^{-1}, Johnson et al., 2008). Fresh snow, surface snow, and drifting snow presented, in order, rapidly increasing negative $\Delta^{199}Hg^{II}$ values of –0.95 to –1.20‰, –2.41 to –2.63‰, and –3.84 to –5.08‰, which, according to Rayleigh fractionation, can correspond to 5–30%, 35–50%, and 65–75% photoreduced Hg^{II}, respectively. A chamber measurement was conducted on AMDE-impacted drifting snow that had undergone substantial photoreduction ($\Delta^{199}Hg$ ~–5.0‰) for 10.5 h of sunlight. The total DFC throughput, including the Hg^0 emissions corresponding to 6% of the total Hg^{II} in the snow plot (whose $\Delta^{199}Hg^{II}$ dropped to ~–5.4‰), exhibited a $\Delta^{199}Hg^0$ of –1.87‰. Mid-latitude snow (MI, USA), derived from polar vortex-transported air masses originating in AMDE-affected subarctic regions, shows, when $\Delta^{199}Hg$ is plotted against $\delta^{202}Hg$, a regression of -3.32 ± 1.19 (Kurz et al., 2021), which, given the uncertainty in the line fit, appears to agree well with the corresponding regression of data from the Alaska DFC snow experiment of -3.44 ± 0.70 (Sherman et al., 2010).

Perennial data from the Canadian High Arctic show that Hg^{II} deposited on snow during the most frequent phase of AMDEs just after polar sunrise until early May, which is partly characterized by low temperatures and Arctic haze, has a significantly greater susceptibility to photoreduction and loss as Hg^0 (up to 60%) than that deposited later (<20%, Zheng et al., 2021). As previously stated in **Section 5.1.4**, airborne Hg^{II} originating from high Arctic AMDEs undergoes rapid conversion to the particle phase between March and April, whereas unconverted GOM remains the dominant form between May and June. The cause of the reactivity of deposited Hg^{II} is unclear (Sherman et al., 2010; Kurz et al., 2021). It has been speculated that components of Arctic haze, such as black carbon, that cause photoreactivity of particulate Hg^{II} are the cause of the observed (–)MgIE signature (Zheng et al., 2021), which is supported by water-phase experiments with Hg^{II} and dissolved black carbon (**Table 8**, Li et al., 2020b). Concurrently, the restricted Hg^{II} reduction observed in Arctic snow toward the conclusion of spring is consistent with concurrent observations of substantial reactive uptake of Hg^0 (see above; Douglas and Blum, 2019), indicating that the snowpack then contains species with a predominant oxidative capacity. However, during snowmelt on the inland tundra, net Hg^0 deposition is disrupted by shifts in the isotopic signatures of snow interstitial air to those indicative of photoreduction, with $\Delta^{199}Hg$ values decreasing to –1.37‰ in snow and –0.62‰ in snow interstitial air, which are consistently lower than those in ambient air (-0.23 ± 0.06‰). In contrast to Arctic snow, snow sampling in the U.S. Great Lakes area (with the exceptions noted above) generally results in increasing positive $\Delta^{199}Hg^{II}$ values (up to 3.51‰) in aging snow (Kurz et al., 2021). Indicative of (–) and (+) MgIE triggering photoreduction, respectively, the snow data from coastal Alaska (Sherman et al., 2010; Douglas and Blum, 2019) and the Great Lakes region (Kurz et al., 2021) show steeper $\Delta^{199}Hg/\delta^{202}Hg$ trajectories than is the case for any of the well-studied Hg^{II} complex photoreductions in the laboratory (**Tables 8 & 9**), leaving the question of which snow Hg^{II} complexes are involved.

The mean MIF values ($\Delta^{199}Hg^{II}$ and $\Delta^{200}Hg^{II}$) in the pools of fresh and seawater are between the mean values of global atmospheric Hg^0 and wet precipitation. However, the variation is particularly pronounced for $\Delta^{199}Hg^{II}$ in coastal seawater, lakes, and river water (Liu et al., 2024). After three different categories of lakes with DFC were studied, a $\Delta^{200}Hg$ isotope mass balance model was used to partition the overall net emission fluxes into gross emission and deposition fluxes, which ranged from 2.1 to 4.2 ng m^{-2} h^{-1} and from –2.3 to –1.2 ng m^{-2} h^{-1}, depending on the lake (Zhang et al., 2023a). Hg^0 gross deposition exceeds the measured wet deposition across

tog bort: snowpack
tog bort: previously
tog bort: when compared to
tog bort: ,
tog bort: is
tog bort: the
formaterade ... [760]
tog bort: as a consequence
formaterade ... [761]
tog bort: ,
tog bort: showed
tog bort: of photo-reduced
tog bort: inclusive of
tog bort: A
formaterade ... [762]
tog bort: (-
formaterade ... [763]
tog bort: ,
formaterade ... [764]
tog bort: .,
formaterade ... [765]
tog bort:)
formaterade ... [766]
tog bort: to
formaterade ... [767]
formaterade ... [768]
tog bort: $\Delta^{199}Hg$ plotted against $\delta^{202}Hg$ data (-
formaterade ... [769]
tog bort: ,
formaterade ... [770]
tog bort: .,
formaterade ... [771]
tog bort:) has also been observed, given the uncertainty ... [772]
tog bort: higher
tog bort: 2021). Regression of the Alaskan DFC experim ... [773]
tog bort: while
tog bort: co-
tog bort: would be
tog bort: towards
tog bort: down
tog bort: ,
formaterade ... [774]
tog bort: shows
tog bort: the
tog bort: Table
tog bort:
tog bort: pool
tog bort: seawaters
tog bort: situated
tog bort: studying
tog bort: over

these lakes and accounts for 56–85% of the total deposition (Feng et al., 2022). The anomalous observation of preferential deposition of heavier Hg isotopes over water has already been discussed. The results of the volatilization experiments of dissolved Hg^0 in water indicate an MDF enrichment factor ($\varepsilon^{202}Hg^0_{air\text{-}water}$) of −0.45‰ and a negligible $E^{199}Hg^0_{air\text{-}water}$ (Zheng et al., 2007). Emission-controlled experiments for one of the lakes yielded $E^{199}Hg_{emission}$ of –0.38‰ and $\varepsilon^{202}Hg_{emission}$ of –0.31‰, which are subject to large uncertainties, with a resulting $E^{199}Hg_{emission}/\varepsilon^{202}Hg_{emission}$ trajectory of 1.26 ± 0.72, which is within the margin of error for Hg^{II} photoreduction mediated by fulvic acids (1.15 ± 0.07, Bergquist and Blum, 2007). The isotopic tracing of the formation of dissolved Hg^0 in peat-covered groundwater from Hg^{II} in rainwater (1.24 ± 0.68) has also suggested that this process is the same type of photoreduction (Li et al., 2023a). The $E^{199}Hg_{exchange}$ was between –0.76 and –0.32‰, with the highest absolute value for a clear mountain lake fed mainly glacial water, indicating that (+)MgIE photoreduction plays an important role, as has been shown early in laboratory experiments on natural freshwater (Bergquist and Blum, 2007; Zheng and Hintelmann, 2009). The observed substantial positive $\Delta^{199}Hg^{II}$ shift of the sampled lake surface waters relative to Hg^{II} in precipitation can be interpreted as an effect of partial photoreduction of Hg^{II}. However, other sources, including MMHg photodegradation, have been suggested (Chen et al., 2016). As discussed in **Section 4.2**, Hg^0 emissions from the ocean represent a primary source of Hg in the atmosphere. However, the isotopic signatures of this emission source remain largely unknown. In the absence of in-situ sampling, photoexperiments with Hg^{II} in the presence of DOM extracted from marine phytoplankton produce (–)MgIE during reduction, in contrast to freshwater DOM (Kritee et al., 2018).

9. Future perspectives

9.1 Theoretical chemistry contributions & challenges

This examination of the advancements made in our comprehension of the mercury cycle in the troposphere and stratosphere reveals iterative interactions among three distinct branches of atmospheric chemistry (modeling, field measurements, and laboratory measurements). Advances in computational chemistry have made seminal contributions to our understanding of gas-phase $Hg^{(I,II)}$ molecules in terms of their geometries, energies, UV–VIS spectra, and reaction kinetics. The treatment of strong relativistic effects, which largely determine the chemistry of Hg-containing species, is crucial for accurate results. Ab initio thermochemical calculations for atmospheric Hg species are performed at a higher level of theory, which incorporates core–valence electron correlation and coupled-cluster methods. This approach yields a significantly improved accuracy of ≤ 4 kJ mol^{-1}, in accordance with high-quality experimental data. However, significant uncertainties in the estimates of the binding strength and thermal and photolytic stability of $^{\bullet}Hg^{I}I$ (**Section 5.1.2**) remain, limiting the ability to assess the occurrence and significance of iodine-induced Hg^0 oxidation in the troposphere and lower stratosphere, as has been suggested from atmospheric observations (Murphy et al., 2006; Lee et al., 2024).

Compared with ab initio thermodynamics, the calculation of ab initio kinetics is a much more challenging task, for which transition state theory (TST) and RRKM theory are often used for barrier and non-barrier bimolecular reactions, respectively. More flexible methods (e.g., variational TST) are now applied to optimize the position of the transition state (TS) by varying it along the reaction coordinate to minimize the free activation energy, which more accurately estimates the rate than traditional TST, which assumes a single, fixed TS that irreversibly leads to products. The calculation of TS energies is more challenging than the calculation of energies of relative minima (metastable species) because of the involvement of extended bonds where the electronic wave function is less dominated by a single electronic configuration. Obtaining a correct barrier energy is crucial for calculating reliable rate constants, as a bias of ~4 kJ/mol in the barrier height can lead to an error of nearly an order of magnitude in the resulting rate constant (Ariya and Peterson, 2005; Ariya et al., 2009).

For gas-phase reactions (**Section 5**), calculated rate constants have been presented and compared with those experimentally determined in the laboratory. The level of agreement varies from relatively good (≤ 30% as **Rxn G1 - G3**) to inconsistent (**Rxn G20a,b & G22**). Owing to the complex shape of their potential energy surfaces, the rates of assumed key reactions such as **Rxn G27**, **G45**, and **G63** are inherently difficult to constrain theoretically (**Section 5.1.4**) and thus require empirical verification, preferably using PLP-LIF or similar techniques. A direct reaction between water vapor and $YHg^{II}O^{\bullet}$ has recently been proposed for

tog bort: is
tog bort: -
tog bort: (DGM)
tog bort: give
tog bort: that agrees
tog bort: with that
tog bort: of
tog bort: by
tog bort: on
formaterade: Teckenfärg: Blå
tog bort:
formaterade: Teckenfärg: Blå
tog bort: Knowledge
formaterade: Teckenfärg: Blå
tog bort: cycle of mercury has increased significantly in recent decades, as described in this paper. This is particularly evident in the
formaterade: Teckenfärg: Blå
tog bort: of
formaterade: Teckenfärg: Blå
formaterade: Teckenfärg: Blå
tog bort: , which has
formaterade: Teckenfärg: Blå
tog bort: -
formaterade: Teckenfärg: Blå
tog bort: -
formaterade: Teckenfärg: Blå
tog bort: extended basis sets (
formaterade: Teckenfärg: Blå
tog bort:).
formaterade: Teckenfärg: Blå
tog bort: more accurate results, with an
tog bort: ≤1 kcal
formaterade: Teckenfärg: Blå
formaterade: Teckenfärg: Blå
tog bort: The undertaking
formaterade: Teckenfärg: Blå
tog bort: ab initio kinetics calculations is a considerably more arduous task than that
formaterade: Teckenfärg: Blå
tog bort: ab initio thermodynamics calculations. It is mor... [775]
formaterade: Teckenfärg: Blå
tog bort: calculate
formaterade: Teckenfärg: Blå
tog bort: energies
formaterade: Teckenfärg: Blå
tog bort: transition states (TS) with high accuracy than th... [776]
formaterade: Teckenfärg: Blå
flyttade (infogning) [10]
tog bort: 2009
formaterade: Teckenfärg: Blå
tog bort: Absolute

Y = OH (**Rxn G60**, Saiz-Lopez et al., 2022). If this reaction is realized with the given rate expression in models, it will result in the conversion of essentially all $HOHg^{II}O^{\bullet}$ to the completely stable $Hg(OH)_2$ in the tropics. This type of reaction also requires empirical verification and should be given priority in laboratory experiments.

9.2 Laboratory measurement techniques & limitations

The absolute determination of rate constants experimentally with pulsed laser-assisted methods (reaction times typically < 0.1 ms), such as PLP-LIF, is more easily facilitated when secondary reactions are negligible and therefore does not contribute to the measured values. In general, absolute determination is conducted by obtaining pseudo-first-order conditions, whereby the more stable reactant is present in a density more than tenfold that of the other reactant. However, for Hg, this method is viable only for studies that are conducted at elevated temperatures (typically ≥ 100 °C). At atmospheric temperatures, the relatively low vapor pressure of Hg^0 (in comparison to, for instance, DMHg) precludes the possibility of such experiments. Despite the challenges for Hg^0, a flow PLP-LIF system has many advantages, including the ability to measure the rate coefficient over a wide range of temperatures and pressures and to test the effect of a change in the bath gas (third body). Nevertheless, to exploit these advantages, alternative methods have been used in which the Hg species is not in excess, but in which the excess is X = Cl and Br when the reaction $Hg + X^{\bullet} + M$ is studied, while it is instead Y = O_3, NO_2, NO, and O_2 when the interaction between $^{\bullet}Hg^{I}Br$ and Y is studied. In the study of the former reaction type, $X^{\bullet}$ is present in excess, but its concentration decreases over time owing to the rapid three-body recombination of the species into X_2 and M. This results in additional Hg^0 exponential decay. To achieve a fit to the observed Hg^0 time profiles, rate coefficients must be obtained through numerical integration. This requires monitoring both the $X^{\bullet}$ and Hg^0 time profiles using LIF, with the absolute concentration of X atoms known with precision. The experimental measurements of the rate coefficients for the $Hg + X^{\bullet} + M$ reaction by Donohoue et al. (2005; 2006) are in accordance with the findings of theoretical computational studies.

The conversion of $^{\bullet}Hg^{I}Br$ by bimolecular elimination reduction (**Rxn G18 & G20b**; Wu et al., 2020; Wu et al., 2022), addition (oxidation assisted by M, [**Rxn G20a**]; Wu et al., 2020), or abstraction (**Rxn G22**, Gómez Martín et al., 2022) is constrained by the capacity to generate sufficiently high densities of $^{\bullet}Hg^{I}Br$ through the gas-phase photolysis of $HgBr_2$ in deep UV. Because the vapor pressure of $HgBr_2$ is low (less than one-tenth that of Hg^0), it is necessary to keep the $HgBr_2$ source at least 30 °C and the flow tube reactor at least 10 °C higher to prevent vapor condensation. A higher temperature increases the thermal dissociation of $^{\bullet}Hg^{I}Br$; therefore, a large excess of Y is required for the $^{\bullet}Hg^{I}Br + Y$ reaction to dominate the conversion of $^{\bullet}Hg^{I}Br$. In the context of laboratory experiments necessitating deep UV irradiation, it is essential to consider that oxygen atoms are formed through the partial photolysis of O_3 and NO_2, thereby enabling $O(^3P)$ to react with $^{\bullet}Hg^{I}Br$ ($O + HgBr^{\bullet} \rightarrow Hg + BrO^{\bullet}$; **Rxn G23**). Experiments to study the reactions of $^{\bullet}Hg^{I}Br$ with NO_2 and O_3 will inevitably result in the observation of a partially reversible oxidation process. This is due to the occurrence of secondary chemistry, including reactions **G14**, **G23**, **G24**, and **G29**, which take place concurrently with the title reactions **G20** and **G22**. Furthermore, to elucidate the influence of secondary chemistry on the observed $^{\bullet}Hg^{I}Br$ disappearance, a comprehensive series of experiments must be conducted, with pressure, temperature, [$^{\bullet}Hg^{I}Br$], [Y], and [O] as variables. This necessitates numerical modeling to isolate the individual rate constants. While the laboratory study of $^{\bullet}Hg^{I}Br + O_3$ gives an experimental rate constant for the reaction **G22** that is in good agreement with computational predictions (Castro Pelaez et al., 2022), experimental kinetic data for $^{\bullet}Hg^{I}Br + NO_2$ (**Rxn G20**), which must be decoupled into termolecular oxidation (**Rxn G20a**) and reduction (**Rxn G20b**) reactions, respectively, indicate that computational methods overestimate the rate constants for both channels (Wu et al., 2020). Later, experimental investigations revealed that **Rxn G20** cannot fully account for observations but that significant losses of $^{\bullet}Hg^{I}Br$ must occur via side reactions, probably involving **Rxn G23**, which was unexplored at the time. These intractable shortcomings present a challenge to validating a majority of the proposed reaction steps by computational quantum chemistry in the atmospheric Hg redox cycle, including $YHg^{II}O^{\bullet}$ chemistry, through experimental means. As requested by theoretical chemists (Edirappulige et al., 2023) and modelers (Shah et al., 2021), better rate constants are needed for $YHgO^{\bullet} + CH_4$ and $YHgO^{\bullet} + CO$ reactions, especially for Y = Br and OH, to better assess the atmospheric fate of $YHgO^{\bullet}$, i.e., whether $YHgO^{\bullet}$ will be mainly reduced or form closed-shell Hg^{II} compounds under different atmospheric conditions. As a workaround in the absence of experimentally

tog bort: time
formaterade ... [777]
tog bort:)
formaterade ... [778]
formaterade ... [779]
tog bort: do
formaterade ... [780]
tog bort: the
formaterade ... [781]
tog bort:
formaterade ... [782]
tog bort: exceeding
formaterade ... [783]
tog bort: .
tog bort: standard
tog bort: conditions
formaterade ... [784]
formaterade ... [785]
formaterade ... [786]
tog bort: These
formaterade ... [787]
tog bort: have been exploited by
formaterade ... [788]
tog bort: where
formaterade ... [789]
tog bort: where
formaterade ... [790]
tog bort: in the study of
formaterade ... [791]
tog bort: •
formaterade ... [792]
tog bort: this
formaterade ... [793]
tog bort: in the study of
formaterade ... [794]
tog bort: •
formaterade ... [795]
tog bort: . Despite being
formaterade ... [796]
tog bort: the X•
formaterade ... [797]
tog bort: due
formaterade ... [798]
tog bort: to
formaterade ... [799]
tog bort: a non-trivial
formaterade ... [800]
tog bort: •
formaterade ... [801]
tog bort: •
formaterade ... [802]
tog bort: experimentally
formaterade ... [803]
tog bort: the
formaterade ... [804]
tog bort:
formaterade ... [805]
tog bort: study of the
formaterade ... [806]
tog bort: •
formaterade ... [807]
tog bort: (
formaterade ... [808]
tog bort: ,
formaterade ... [809]
tog bort: •
formaterade ... [810]
tog bort: the

determined rate constants, Khiri et al. (2020) proposed efforts to perform molecular dynamics simulations via computationally more sophisticated variational TST with multidimensional tunneling.

Many of the proposed key gas-phase Hg species lack experimental characterization (such as spectral proofs). The main method for studying such gas-phase molecules has been spectroscopy after preparation by matrix isolation, which has thus far been used to study the products of photochemical reactions of excited Hg atoms, e.g., O_3 (Butler et al., 1979), O_2 (Andrews et al., 2023), H_2 (Wang and Andrews, 2005b), H_2O (Wang and Andrews, 2005a), F_2 (Wang et al., 2007), and OF_2 (Andrews et al., 2012), in a matrix host of solid Ar and Ne at a cold (typically 4–7 K) surface. **Section 5.1.4** has already described some of the isolated molecules of interest, namely, $Hg(OH)_2$ (Wang and Andrews, 2005a) and the fluorine analog of $YHg^{II}O^{\bullet}$ (Andrews et al., 2012). Other studies involve mercury halide molecules (Loewenschuss et al., 1969) and their adducts (Tevault et al., 1977). The reaction mechanism for the formation of $Hg(OH)_2$ tentatively involves insertion as a first step: $Hg(^3P) + O_2 + H_2 \rightarrow (OHgO)^* + H_2 \rightarrow HOHgOH$, where $OHgO$ ($^3\Sigma_g^-$) is implicitly indicated as a reactive intermediate (c.f., **Rxn G12**, although, unlike the analogous complexes for the other Group 12 metals, OZnO and OCdO, it has yet to be identified by IR spectra, Chertihin and Andrews, 1997). Apart from MS experiments of the laser desorption ionization and time-of-flight type with solid HgO as the source and detection of $(HgO)_x$ clusters in the gas phase (Jayasekharan and Sahoo, 2014), there is one early (Butler et al., 1979) and one recent (Andrews et al., 2023) matrix study of the products of the $Hg(^3P) + O_2$ system, where both $^{16}O_2$ and $^{18}O_2$ were used as reagents. The former experiments required co-deposition of Hg with 0.5 to 5% O_3 in excess of Ar under deep UV photolysis for oxidation to occur, while the latter experiments used laser-ablated Hg atoms energetic enough to form oxygen atoms when deposited in a cryogenic matrix doped with 0.3% $^{16}O_2$ or $^{18}O_2$, which reacts upon annealing to form O_3 and a series of HgO_x species (x = 1 to 3). The observed fundamental harmonic vibrational frequencies in different cryogenic matrices for the simple oxide Hg–O are in the range of 500-600 cm^{-1}, as predicted by high-level calculations (Shepler and Peterson, 2003; Peterson et al., 2007), indicating the presence of a weakly ionic molecule. This is also true for HgO_2 and HgO_3, which have superoxide ($Hg^{\bullet+}O_2^{\bullet-}$) and ozonide ($Hg^{\bullet+}O_3^{\bullet-}$) characteristics, respectively (Andrews et al., 2023). Notably, the study did not isolate linear mercury dioxide, OHgO, and evidence for this species remains weak. Nevertheless, this species is included as a metastable adduct in the **Rxn G12** scheme, the key reaction for Hg^0 turnover in the stratosphere, whose complex potential energy surface forms the basis of ab initio kinetic calculations. In these calculations (Saiz-Lopez et al., 2022), the energy of the Hg–O bond is assumed to be 27.3 kJ mol^{-1}, which is significantly higher than the most recently published high-level calculation values (Peterson et al., 2007; Cremer et al., 2008). Increased activity and innovation in advanced experimental studies characterizing key species and reactions are needed to verify models of atmospheric Hg chemistry that currently appear overly reliant on computational chemistry. The innovation could be, for example, finding a laboratory method to capture the temporal behavior of HgO (perhaps generated by the spin-allowed $Hg(^1S) + O(^1D)$ reaction or by reacting DMHg with $O(^3P)$) in the presence of gas-phase coreactants (with reference to **Rxn G73 & G74**), performing a detailed study of **Rxn G8 & 12**, or finding a synthetic route to matrix-isolate species such as $BrHgO^{\bullet}$ from laser-ablated Hg atoms.

9.3 Laboratory measurement techniques & limitations

Current limitations and challenges in accurately measuring speciated atmospheric mercury (Gustin et al., 2024; **Section 3.1**) mean that the basis for verifying models in detail is insufficient, despite reliable measurements of Hg^0 in air and Hg^{II} in wet deposition. Nevertheless, some models have been developed by including KCl-denuder-based Hg^{II} measurements in the reference material (Shah et al., 2021; Fu et al., 2024), which are known to suffer from low bias, and others (Saiz-Lopez et al., 2020; Saiz-Lopez et al., 2025), which seem to stick strictly to RM data for validation or include KCl-denuder-based Hg^{II} measurements corrected according to Marusczak et al. (2017); consequently, the evaluation is qualitative (Shah et al., 2021) and consistently fails to simulate the magnitude of recurring episodes of highly oxidized mercury originating in the free troposphere (underestimation by up to several hundred percent, Elgiar et al., 2025; Gustin et al., 2023). In **Section 3.2**, we highlighted the discrepancies that exist in terms of the atmospheric budget and the fluxes into and out of it. Particularly, new model results concerning the importance of the stratosphere are inconsistent with existing empirical data and require further elaboration, as does the stratospheric chemistry discussed above. Recent observations

formaterade: Teckenfärg: Blå

tog bort: From a computational chemistry standpoint, the reaction between $YHg^{II}O^{\bullet}$ and CO has been identified as crucial in assessing the atmospheric burden of Hg^{II}. However, the calculated rate constant is subject to significant uncertainty, within a factor of 10 being a reasonable estimate. A direct reaction between water vapor and $YHg^{II}O^{\bullet}$ has recently been proposed for Y = OH (Saiz-Lopez et al., 2022). If this reaction is realized with the given rate expression in models, it will result in the conversion of essentially all $HOHg^{II}O^{\bullet}$ to the completely stable $Hg(OH)_2$ in the tropics. The question of whether iodine-induced Hg^0 oxidation is a significant process in the troposphere and lower stratosphere has been raised based on atmospheric observations (Murphy et al.,

have shown that there are abundant anthropogenic emissions of reactive halogens (e.g., Br_2 and BrCl) over continental, densely populated areas of South and East Asia that also have high Hg emissions. This is now beginning to be modeled as a key component of the regional atmospheric Hg redox cycle (Fu et al., 2024), but more field measurements are needed for confirmation.

The difficulties of accurately determining the speciation of Hg^{II} in atmospheric water through equilibrium modeling and thus identifying the pool of reducible complexes have been described (**Section 4.3**). Additionally, the potential for simulating the gas-particle distribution of atmospherically oxidized Hg has been explored (**Section 7.1.1**). Stable isotope data have been analyzed to constrain Hg redox chemistry in the atmosphere (Song et al., 2024; Zhen et al., 2024), but there are profound knowledge gaps that require state-of-the-art theoretical and experimental investigations. **Section 8.2** describes the isotopic composition of atmospheric samples, a pool generally consisting of filtered air divided into PBM and gaseous mercury (~Hg^0), and precipitation samples, including those of cloud and fog water. The isotope measurements on RM, which are now also performed, are briefly presented here (Fu et al., 2021). With a measuring line consisting of a CEM (Hg^{II}(g)), a filter (Hg^{II}(p)) and a trap consisting of halogen-impregnated activated carbon (Hg^0) in series, the analysis shows that the three groups are clearly isotopically separated from each other and that the resulting samples can thus provide further insights into atmospheric processes (X. Fu, pers. comm). The discovery, made over a decade ago, that atmospheric samples contain a significant level of the even-mass-number isotope MIF with seasonal and geospatial variations has been a source of both benefit and puzzlement for scientists (**Sections 8.2.3 & -4**). As even Hg MIF variation is limited to samples from a few localities thus far (compare **Figs. 13 & 14**), Δ^{200}Hg and Δ^{204}Hg in the environment are considered conservative tracers because of their generally narrow range, and values of Δ^{200}Hg and Δ^{204}Hg on the land surface and in water confine the relative contribution of Hg^0 to the Hg^{II} exchange process with the atmosphere. Nevertheless, the underlying chemical processes that give rise to anomalous MIF and the atmospheric conditions that facilitate its occurrence remain to be elucidated in greater detail. In addition to laboratory-based investigations, future field experiments that report vertical profiles of isotopic Hg^0 and Hg^{II} in the atmosphere may prove invaluable in further constraining the sources of even-MIF.

Author contributions

J. O. S. prepared the manuscript with contributions from all co-authors.

Competing interests

The authors declare that they have no conflicts of interest.

Financial support

This work was supported by the National Natural Science Foundation of China (grant nos. 42150710535 and 42373068).

References

Ababneh, F. A., Scott, S. L., Al-Reasi, H. A., and Lean, D. R. S.: Photochemical reduction and reoxidation of aqueous mercuric chloride in the presence of ferrioxalate and air, Science of the Total Environment, 367, 831-839, 10.1016/j.scitotenv.2006.02.018, 2006.

Agnan, Y., Le Dantec, T., Moore, C. W., Edwards, G. C., and Obrist, D.: New constraints on terrestrial surface-atmosphere fluxes of gaseous elemental mercury using a global database, Environmental Science & Technology, 50, 507 - 520, 10.1021/acs.est.5b04013, 2016.

Ahmed, S., Thomas, J. L., Angot, H., Dommergue, A., Archer, S. D., Bariteau, L., Beck, I., Benavent, N., Blechschmidt, A. M., Blomquist, B., Boyer, M., Christensen, J. H., Dahlke, S., Dastoor, A., Helmig, D., Howard, D., Jacobi, H. W., Jokinen, T., Lapere, R., Laurila, T., Quelever, L. L. J., Richter, A., Ryjkov, A., Mahajan, A. S., Marelle, L., Pfaffhuber, K. A., Posman, K., Rinke, A., Saiz-Lopez, A., Schmale, J., Skov, H., Steffen, A., Stupple, G., Stutz, J., Travnikov, O., and Zilker, B.: Modeling the coupled mercury-halogen-ozone cycle in the central Arctic during spring, Elementa-Science of the Anthropocene, 11, ARTN 00129, 10.1525/elementa.2022.00129, 2023.

Ai, Y., Wang, C., Videen, G., and Pan, Y.-L.: Optically levitated, single-particle reactor for the study of surface and heterogeneous chemistry-reactions of particulate-bound mercury with ozone in air, Chemical Physics Letters, 817, 140428,

flyttade upp [10]: 2006; Lee et al.,
formaterade ... [839]
tog bort: 2024) and the emerging role that O_3 is thought t ... [840]
formaterade ... [841]
tog bort: modelling,
formaterade ... [842]
tog bort: ,
formaterade ... [843]
tog bort: elucidated
formaterade ... [844]
tog bort: -
formaterade ... [845]
tog bort: The use of
formaterade ... [846]
tog bort: the
formaterade ... [847]
tog bort: has begun
formaterade ... [848]
tog bort: art theoretical and experimental investigations.
formaterade ... [849]
tog bort: , which has been observed to exhibit
formaterade ... [850]
tog bort: ,
formaterade ... [851]
tog bort: ever since (Section
formaterade ... [852]
tog bort: the
formaterade ... [853]
tog bort: so
formaterade ... [854]
tog bort: &
formaterade ... [855]
tog bort: is
formaterade ... [856]
tog bort: a
formaterade ... [857]
tog bort: tracer due to its
formaterade ... [858]
tog bort: &
formaterade ... [859]
tog bort: the
formaterade ... [860]
tog bort: on the
formaterade ... [861]
tog bort: ----------Sidbrytning----------
formaterade ... [862]
tog bort: ....Avsnittsbrytning (nästa sida)..........
tog bort: contribution
tog bort: conflict
tog bort: no
formaterade ... [863]
tog bort: ,
formaterade ... [864]
Formaterat ... [865]
formaterade ... [866]
flyttade (infogning) [11]
formaterade ... [867]
formaterade ... [868]
Formaterat ... [869]
tog bort: Modelling
formaterade ... [870]

10.1016/j.cplett.2023.140428, 2023.

Akagi, H., Fujita, Y., and Tkabatake, E.: Photochemical methylation of inorganic mercuric compounds in aqueous acetic acid solutions, Nippon Kagaku Kaishi, 1974, 1180, 1974.

Alberts, J. J., Schindler, J. E., Miller, R. W., and Nutter, D. E.: Elemental mercury evolution mediated by humic acid, Science, 184, 895-896, 1974.

Ambrose, J. L.: Improved methods for signal processing in measurements of mercury by Tekran® 2537A and 2537B instruments, Atmospheric Measurement Techniques, 10, 5063-5073, 10.5194/amt-10-5063-2017, 2017.

Amirbahman, A., Kent, D. B., Curtis, G. P., and Marvin-DiPasquale, M. C.: Kinetics of homogeneous and surface-catalyzed mercury(II) reduction by iron(II), Environmental Science & Technology, 47, 7204-7213, 10.1021/es401459p, 2013.

Amos, H. M., Jacob, D. J., Holmes, C. D., Fisher, J. A., Wang, Q., Yantosca, R. M., Corbitt, E. S., Galarneau, E., Rutter, A. P., Gustin, M. S., Steffen, A., Schauer, J. J., Graydon, J. A., St Louis, V. L., Talbot, R. W., Edgerton, E. S., Zhang, Y., and Sunderland, E. M.: Gas-particle partitioning of atmospheric Hg(II) and its effect on global mercury deposition, Atmospheric Chemistry and Physics, 12, 591-603, 2012.

Amos, H. M., Sonke, J. E., Obrist, D., Robins, N., Hagan, N., Horowitz, H. M., Mason, R. P., Witt, M., Hedgecock, I. M., Corbitt, E. S., and Sunderland, E. M.: Observational and modeling constraints on global anthropogenic enrichment of mercury, Environmental Science & Technology, 49, 4036-4047, 10.1021/es5058665, 2015.

Amyot, M., Morel, F. M. M., and Ariya, P. A.: Dark oxidation of dissolved and liquid elemental mercury in aquatic environments, Environmental Science & Technology, 39, 110-114, 10.1021/es035444k, 2005.

Andersson, M. E., Gårdfeldt, K., Wängberg, I., and Strömberg, D.: Determination of Henry's law constant for elemental mercury, Chemosphere, 73, 587-592, 10.1016/j.chemosphere.2008.05.067, 2008.

Andrews, L., Wang, X., Gong, Y., Schloeder, T., Riedel, S., and Franger, M. J.: Spectroscopic observation of a group 12 oxyfluoride: A matrix-isolation and quantum-chemical investigation of mercury oxyfluorides, Angewandte Chemie-International Edition, 51, 8235-8238, 10.1002/anie.201204331, 2012.

Andrews, L. S., Tsegaw, Y. A., Cho, H.-G., and Riedel, S.: Observation and characterization of the Hg-O diatomic molecule: A matrix-isolation and quantum-chemical investigation, Chemistry – A European Journal, 29, e202202740, 10.1002/chem.202202740, 2023.

Angot, H., Dastoor, A., De Simone, F., Gårdfeldt, K., Gencarelli, C. N., Hedgecock, I. M., Langer, S., Magand, O., Mastromonaco, M. N., Nordstrøm, C., Pfaffhuber, K. A., Pirrone, N., Ryjkov, A., Selin, N. E., Skov, H., Song, S., Sprovieri, F., Steffen, A., Toyota, K., Travnikov, O., Yang, X., and Dommergue, A.: Chemical cycling and deposition of atmospheric mercury in polar regions: review of recent measurements and comparison with models, Atmospheric Chemistry and Physics, 16, 10735-10763, 10.5194/acp-16-10735-2016, 2016.

Araujo, B. F., Osterwalder, S., Szponar, N., Lee, D., Petrova, M. V., Pernov, J. B., Ahmed, S., Heimburger-Boavida, L. E., Laffont, L., Teisserenc, R., Tananaev, N., Nordstrom, C., Magand, O., Stupple, G., Skov, H., Steffen, A., Bergquist, B., Pfaffhuber, K. A., Thomas, J. L., Scheper, S., Petaja, T., Dommergue, A., and Sonke, J. E.: Mercury isotope evidence for Arctic summertime re-emission of mercury from the cryosphere, Nature Communications, 13, ARTN 4956, 10.1038/s41467-022-32440-8, 2022.

Ariya, P. and Peterson, K. A.: Chemical transformation of gaseous elemental mercury in the atmosphere, in: Dynamics of Mercury Pollution on Regional and Global Scales: Atmospheric Processes and Human Exposures Around the World, edited by: Pirrone, N., and Mahaffey, K. R., Springer, 261-294, 2005.

Ariya, P. A., Khalizov, A., and Gidas, A.: Reactions of gaseous mercury with atomic and molecular halogens: Kinetics, product studies, and atmospheric implications, Journal of Physical Chemistry A, 106, 7310-7320, 2002.

Ariya, P. A., Peterson, K., Snider, G., and Amyot, M.: Mercury chemical transformations in the gas, aqueous and heterogeneous phases: state-of-the-art science and uncertainties, in: Mercury fate and transport in the global atmosphere. Emissions, measurements and models., edited by: Mason, R., and Pirrone, N., Springer, 459-501, 2009.

Ariya, P. A., Skov, H., Grage, M. M. L., and Goodsite, M. E.: Gaseous elemental mercury in the ambient atmosphere: Review of the application of theoretical calculations and experimental studies for determination of reaction coefficients and mechanisms with halogens and other reactants, in: Advances in Quantum Chemistry: Applications of Theoretical Methods to Atmospheric Science, edited by: Sabin, J. R., and Brandas, E. J., Academic Press, 43-55, 10.1016/s0065-3276(07)00204-3, 2008.

Ariya, P. A., Amyot, M., Dastoor, A., Deeds, D., Feinberg, A., Kos, G., Poulain, A., Ryjkov, A., Semeniuk, K., Subir, M., and Toyota, K.: Mercury physicochemical and biogeochemical transformation in the atmosphere and at atmospheric interfaces: A

tog bort: Methylation of Inorganic Mercuric Compounds in Aqueous Acetic Acid Solutions
formaterade: Teckenfärg: Blå
tog bort: Mercury Evolution Mediated by Humic Acid
formaterade: Teckenfärg: Blå
tog bort: Homogeneous
formaterade: Teckenfärg: Blå
tog bort: Surface-Catalyzed Mercury
formaterade: Teckenfärg: Blå
tog bort: Reduction
formaterade: Teckenfärg: Blå
tog bort: Iron
formaterade: Teckenfärg: Blå
formaterade: Teckenfärg: Blå
Formaterat: Avstånd Efter: 0,6 Rad, Radavstånd: Flera 1,1 li
tog bort: Oxidation
formaterade: Teckenfärg: Blå
tog bort: Dissolved
formaterade: Teckenfärg: Blå
tog bort: Liquid Elemental Mercury
formaterade: Teckenfärg: Blå
tog bort: Aquatic Environments
formaterade: Teckenfärg: Blå
tog bort: Observation
formaterade: Teckenfärg: Blå
tog bort: Group
formaterade: Teckenfärg: Blå
tog bort: Oxyfluoride
formaterade: Teckenfärg: Blå
tog bort: Matrix-Isolation
formaterade: Teckenfärg: Blå
tog bort: Quantum-Chemical Investigation
formaterade: Teckenfärg: Blå
tog bort: Mercury Oxyfluorides
formaterade: Teckenfärg: Blå
formaterade: Teckenfärg: Blå
Formaterat: Avstånd Efter: 0,6 Rad, Radavstånd: Flera 1,1 li
tog bort: Physicochemical
formaterade: Teckenfärg: Blå
tog bort: Biogeochemical Transformation
formaterade: Teckenfärg: Blå
tog bort: Atmosphere
formaterade: Teckenfärg: Blå
tog bort: Atmospheric Interfaces
formaterade: Teckenfärg: Blå

review and future directions, Chemical Reviews, 10.1021/cr500667e, 2015.

AuYang, D., Chen, J., Zheng, W., Zhang, Y., Shi, G., Sonke, J., Cartigny, P., Hongming, C., Yuan, W., Liu, L., Gai, P., and Liu, C.: South-hemispheric marine aerosol Hg and S isotope compositions reveal different oxidation pathways, National Science Open, 1, 20220014, 10.1360/nso/20220014, 2022.

Auzmendi-Murua, I., Castillo, Á., and Bozzelli, J. W.: Mercury oxidation via chlorine, bromine, and iodine under atmospheric conditions: Thermochemistry and kinetics, Journal of Physical Chemistry A, 118, 2959-2975, 10.1021/jp412654s, 2014.

Åkerblom, S., Meili, M., and Bishop, K.: Organic matter in rain: An overlooked influence on mercury deposition, Environmental Science & Technology Letters, 2, 128-132, 10.1021/acs.estlett.5b00009, 2015.

Babaev, N. S., Cheltsov, A. N., Sazykin, A. A., Sosnin, L. Y., and Kuchelev, A. P.: Centrifugal enrichment of mercury isotopes, Nuclear Instruments and Methods in Physics Research Section A: Accelerators, Spectrometers, Detectors and Associated Equipment, 613, 473-476, 10.1016/j.nima.2009.10.006, 2010.

Balabanov, N. B. and Peterson, K. A.: Mercury and reactive halogens: The thermochemistry of Hg + [Cl_2, Br_2, BrCl, ClO, and BrO], Journal of Physical Chemistry A, 107, 7465-7470, 2003.

Balabanov, N. B. and Peterson, K. A.: Accurate theoretical near-equilibrium potential energy and dipole moment surfaces of HgClO and HgBrO, Journal of Chemical Physics, 120, 6585-6592, 2004.

Balabanov, N. B., Shepler, B. C., and Peterson, K. A.: Accurate global potential energy surface and reaction dynamics for the ground state of $HgBr_2$, Journal of Physical Chemistry A, 109, 8765-8773, 2005.

Banic, C. M., Beauchamp, S. T., Tordon, R. J., Schroeder, W. H., Steffen, A., Anlauf, K. A., and Wong, H. K. T.: Vertical distribution of gaseous elemental mercury in Canada, Journal of Geophysical Research-Atmospheres, 108, art. no.-4264, 2003.

Bartels-Rausch, T., Huthwelker, T., Jori, M., Gaggeler, H. W., and Ammann, M.: Interaction of gaseous elemental mercury with snow surfaces: laboratory investigation, Environmental Research Letters, 3, 10.1088/1748-9326/3/4/045009, 2008.

Bartels-Rausch, T., Krysztofiak, G., Bernhard, A., Schläppi, M., Schwikowski, M., and Ammann, M.: Photoinduced reduction of divalent mercury in ice by organic matter, Chemosphere, 82, 199-203, 2011.

Bash, J. O., Bresnahan, P., and Miller, D. R.: Dynamic surface interface exchanges of mercury: A review and compartmentalized modeling framework, Journal of Applied Meteorology and Climatology, 46, 1606-1618, 10.1175/jam2553.1, 2007.

Bash, J. O., Carlton, A. G., Hutzell, W. T., and Bullock, O. R.: Regional air quality model application of the aqueous-phase photo reduction of atmospheric oxidized mercury by dicarboxylic acids, Atmosphere, 5, 1-15, 10.3390/atmos5010001, 2014.

Bauer, D., Campuzano-Jost, P., and Hynes, A. J.: Rapid, ultra-sensitive detection of gas phase elemental mercury under atmospheric conditions using sequential two-photon laser induced fluorescence, Journal of Environmental Monitoring, 4, 339-343, 2002.

Bauer, D., D'Ottone, L., Campuzano-Jost, P., and Hynes, A. J.: Gas phase elemental mercury: A comparison of LIF detection techniques and study of the kinetics of reaction with the hydroxyl radical, Journal of Photochemistry and Photobiology, A: Chemistry, 157, 247-256, 2003.

Bauer, D., Everhart, S., Remeika, J., Tatum Ernest, C., and Hynes, A. J.: Deployment of a sequential two-photon laser-induced fluorescence sensor for the detection of gaseous elemental mercury at ambient levels: fast, specific, ultrasensitive detection with parts-per-quadrillion sensitivity, Atmospheric Measurement Techniques, 7, 4251-4265, 10.5194/amt-7-4251-2014, 2014.

Baxendale, J. H. and Bridge, N. K.: Photoreduction of ferric compounds in aqueous solution, Journal of Physical Chemistry, 59, 783-788, 10.1021/j150530a022, 1955.

Baya, P. A., Gosselin, M., Lehnherr, I., St Louis, V. L., and Hintelmann, H.: Determination of monomethylmercury and dimethylmercury in the Arctic marine boundary layer, Environmental Science & Technology, 49, 223-232, 2015.

Bencardino, M., D'Amore, F., Angot, H., Angiuli, L., Bertrand, Y., Cairns, W., Diéguez, M. C., Dommergue, A., Ebinghaus, R., Esposito, G., Komínková, K., Labuschagne, C., Mannarino, V., Martin, L., Martino, M., Neves, L. M., Mashyanov, N., Magand, O., Nelson, P., Norstrom, C., Read, K., Sholupov, S., Skov, H., Tassone, A., Vítková, G., Cinnirella, S., Sprovieri, F., and Pirrone, N.: Patterns and trends of atmospheric mercury in the GMOS network: Insights based on a decade of measurements, Environmental Pollution, 363, 125104, 10.1016/j.envpol.2024.125104, 2024.

Bergquist, B. A. and Blum, J. D.: Mass-dependent and -independent fractionation of Hg isotopes by photoreduction in aquatic systems, Science, 318, 417-420, 2007.

tog bort: Review
formaterade ... [871]
tog bort: Future Directions
formaterade ... [872]
tog bort: Oxidation
formaterade ... [873]
tog bort: Chlorine, Bromine
formaterade ... [874]
tog bort: Iodine
formaterade ... [875]
tog bort: Atmospheric Conditions
formaterade ... [876]
tog bort: Kinetics
formaterade ... [877]
tog bort: Matter
formaterade ... [878]
tog bort: Rain
formaterade ... [879]
tog bort: Overlooked Influence
formaterade ... [880]
tog bort: Mercury Deposition
formaterade ... [881]
tog bort: Reactive Halogens
formaterade ... [882]
tog bort: Thermochemistry
formaterade ... [883]
tog bort: Global Potential Energy Surface
formaterade ... [884]
tog bort: Reaction Dynamics
formaterade ... [885]
tog bort: Ground State
formaterade ... [886]
flyttade (infogning) [12]
formaterade ... [887]
formaterade ... [888]
Formaterat ... [889]
formaterade ... [890]
tog bort: Air Quality Model Application
formaterade ... [891]
tog bort: Aqueous-Phase Photo Reduction
formaterade ... [892]
tog bort: Atmospheric Oxidized Mercury
formaterade ... [893]
tog bort: Dicarboxylic Acids
formaterade ... [894]
tog bort: a
formaterade ... [895]
tog bort: Ferric Compounds
formaterade ... [896]
tog bort: Aqueous Solution, The
formaterade ... [897]
tog bort: Monomethylmercury
formaterade ... [898]
tog bort: Dimethylmercury
formaterade ... [899]
tog bort: Marine Boundary Layer
formaterade ... [900]

Berkovic, A. M., Bertolotti, S. G., Villata, L. S., Gonzalez, M. C., Pis Diez, R., and Mártire, D. O.: Photoinduced reduction of divalent mercury by quinones in the presence of formic acid under anaerobic conditions, Chemosphere, 89, 1189-1194, 2012.

Berkovic, A. M., Gonzalez, M. C., Russo, N., Del Carmen Michelini, M., Diez, R. P., and Mártire, D. O.: Reduction of mercury(II) by the carbon dioxide radical anion: A theoretical and experimental investigation, Journal of Physical Chemistry A, 114, 12845-12850, 2010.

Bianco, A., Deguillaume, L., Vaïtilingom, M., Nicol, E., Baray, J.-L., Chaumerliac, N., and Bridoux, M.: Molecular characterization of cloud water samples collected at the Puy de Dôme (France) by Fourier transform ion cyclotron resonance mass spectrometry, Environmental Science & Technology, 52, 10275-10285, 10.1021/acs.est.8b01964, 2018.

Bieser, J., Slemr, F., Ambrose, J., Brenninkmeijer, C., Brooks, S., Dastoor, A., DeSimone, F., Ebinghaus, R., Gencarelli, C. N., Geyer, B., Gratz, L. E., Hedgecock, I. M., Jaffe, D., Kelley, P., Lin, C. J., Jaegle, L., Matthias, V., Ryjkov, A., Selin, N. E., Song, S. J., Travnikov, O., Weigelt, A., Luke, W., Ren, X. R., Zahn, A., Yang, X., Zhu, Y., and Pirrone, N.: Multi-model study of mercury dispersion in the atmosphere: vertical and interhemispheric distribution of mercury species, Atmospheric Chemistry and Physics, 17, 6925-6955, 10.5194/acp-17-6925-2017, 2017

Bigeleisen, J. and Wolfsberg, M.: Theoretical and experimental aspects of isotope effects in chemical kinetics, in: Advances in Chemical Physics, 15-76, https://doi.org/10.1002/9780470143476.ch2, 1957.

Bittrich, D. R., Chadwick, S. P., Babiarz, C. L., Manolopoulos, H., Rutter, A. P., Schauer, J. J., Armstrong, D. E., Collett, J., and Herckes, P.: Speciation of mercury (II) and methylmercury in cloud and fog water, Aerosol and Air Quality Research, 11, 161-U181, Doi 10.4209/Aaqr.2010.08.0067, 2011.

Bloom, N. S., Grout, A. K., and Prestbo, E. M.: Development and complete validation of a method for the determination of dimethyl mercury in air and other media, Analytica Chimica Acta, 546, 92-101, 2005.

Blum, J. D. and Bergquist, B. A.: Reporting of variations in the natural isotopic composition of mercury, Analytical and Bioanalytical Chemistry, 388, 353-359, 2007.

Blum, J. D. and Johnson, M. W.: Recent developments in mercury stable isotope analysis, Reviews in Mineralogy and Geochemistry, 82, 733-757, 2017.

Breitinger, D. and Brodersen, K.: Development of and problems in the chemistry of mercury-nitrogen compounds, Angewandte Chemie International Edition in English, 9, 357-367, 10.1002/anie.197003571, 1970.

Brønsted, J. N. and de Hevesy, G.: The separation of the isotopes of mercury, Nature, 106, 144-144, 1921.

Buchachenko, A. L.: Mass-independent isotope effects, Journal of Physical Chemistry B, 117, 2231-2238, 10.1021/jp308727w, 2013.

Buchachenko, A. L.: Mercury isotopes in Earth and environmental chemistry, Russian Journal of Physical Chemistry B, 12, 635-644, 10.1134/s1990793118040048, 2018.

Burkholder, J. B., Sander, S. P., Abbatt, J., Barker, J. R., Cappa, C., Crounse, J. D., Dibble, T. S., Huie, R. E., Kolb, C. E., Kurylo, M. J., Orkin, V. L., Percival, C. J., Wilmouth, D. M., and Wine, P. H.: Chemical kinetics and photochemical data for use in atmospheric studies, Evaluation No. 19, Jet Propulsion Laboratory, Pasadena, 2019.

Burnard, P.: The noble gases as geochemical tracers, Springer, 2013.

Butler, R., Katz, S., Snelson, A., and Stephens, J. B.: Identification of HgO_2 species by matrix-isolation spectroscopy, Journal of Physical Chemistry, 83, 2578-2580, 1979.

Buxton, G. V., Mulazzani, Q. G., and Ross, A. B.: Critical review of rate constants for reactions of transients from metal ions and metal complexes in aqueous solution, Journal of Physical and Chemical Reference Data, 24, 1055-1349, 10.1063/1.555966, 1995.

Cai, H. and Chen, J.: Mass-independent fractionation of even mercury isotopes, Science Bulletin, 1-9, 10.1007/s11434-015-0968-8, 2015.

Callear, A. B.: Excited mercury complexes, Chemical Reviews, 87, 335-355, 1987.

Callear, A. B. and Shiundu, P. M.: Temperature-dependence of the Hg 6s6p($^3P_0 \rightarrow {}^3P_1$) transition induced by nitrogen, Chemical Physics Letters, 136, 342-345, 10.1016/0009-2614(87)80263-4, 1987.

Callear, A. B., Patrick, C. R., and Robb, J. C.: Reaction of excited mercury (Hg 6^3P_1) with oxygen, Transactions of the Faraday Society, 55, 280 - 287, 1959.

Calvert, J. G. and Lindberg, S. E.: Mechanisms of mercury removal by O_3 and OH in the atmosphere, Atmospheric Environment,

tog bort: Characterization
tog bort: Cloud Water Samples Collected
formaterade ... [902]
tog bort: Transform Ion Cyclotron Resonance Mass Spectrometry
formaterade ... [901]
formaterade ... [903]
flyttade (infogning) [13]
formaterade ... [904]
formaterade ... [905]
Formaterat ... [906]
tog bort: Experimental Aspects of Isotope Effects in Che ... [907]
formaterade ... [908]
tog bort: Mercury
formaterade ... [909]
tog bort: Methylmercury
formaterade ... [910]
tog bort: Cloud
formaterade ... [911]
tog bort: Fog Water
formaterade ... [912]
tog bort: Problems
formaterade ... [913]
tog bort: Chemistry
formaterade ... [914]
tog bort: Mercury-Nitrogen Compounds
formaterade ... [915]
tog bort: https://doi.org/
formaterade ... [916]
tog bort: Independent Isotope Effects
formaterade ... [917]
tog bort: Isotopes
formaterade ... [918]
tog bort: Environmental Chemistry
formaterade ... [919]
tog bort: Kinetics
formaterade ... [920]
tog bort: Photochemical Data
formaterade ... [921]
tog bort: Use
formaterade ... [922]
tog bort: Atmospheric Studies
formaterade ... [923]
formaterade ... [924]
Formaterat ... [925]
tog bort: Review
formaterade ... [926]
tog bort: Rate Constants
formaterade ... [927]
tog bort: Reactions
formaterade ... [928]
tog bort: Transients
formaterade ... [929]
tog bort: Metal Ions
formaterade ... [930]
tog bort: Metal Complexes
formaterade ... [931]
tog bort: Aqueous Solution
formaterade ... [932]
tog bort: Byun, Y., Cho,
flyttade upp [12]: M.,
formaterade ... [933]
tog bort: Namkung,
flyttade upp [11]: W.,
formaterade ... [934]
tog bort: Lee, K., Koh, D. J., and Shin, D. N.: Insight int ... [935]
formaterade ... [936]
tog bort: Mercury Complexes
formaterade ... [937]

39, 3355-3367, 2005.

Calvert, J. G., Orlando, J. J., Stockwell, W. R., and Wallington, T. J.: The mechanisms of reactions influencing atmospheric ozone, Oxford University Press, 2015.

Cardiano, P., Cucinotta, D., Foti, C., Giuffrè, O., and Sammartano, S.: Potentiometric, calorimetric, and ^{1}H NMR investigation on Hg^{2+}-mercaptocarboxylate interaction in aqueous solution, Journal of Chemical & Engineering Data, 56, 1995-2004, 10.1021/je101007n, 2011.

Cario, G. and Franck, J.: Über Zerlegung von Wasserstoffmolekülen durch angeregte Quecksilberatome, Zeitschrift für Physik, 11, 161-166, 10.1007/BF01328410, 1922.

Carmona-Garcia, J., Saiz-Lopez, A., Mahajan, A. S., Wang, F., Borrego-Sanchez, A., Acuna, A. U., Cuevas, C. A., Davalos, J. Z., Feinberg, A., Spolaor, A., Ruiz-Lopez, M. F., Francisco, J. S., and Roca-Sanjuan, D.: Photoreduction of mercuric bromides in polar ice, Proceedings of the National Academy of Sciences of the United States of America, 122, e2422885122, 10.1073/pnas.2422885122, 2025.

Carpi, A.: Mercury from combustion sources: A review of the chemical species emitted and their transport in the atmosphere, Water Air and Soil Pollution, 98, 241-254, 1997.

Castro Pelaez, P., Kellö, V., Cernusak, I., and Dibble, T.: Together, not separately, OH and O_3 oxidize $Hg^{(0)}$ to $Hg^{(II)}$ in the atmosphere, Journal of Physical Chemistry A, 126, 10.1021/acs.jpca.2c04364, 2022.

Chandan, P., Ghosh, S., and Bergquist, B. A.: Mercury isotope fractionation during aqueous photo-reduction of monomethylmercury in the presence of dissolved organic matter, Environmental Science & Technology, 49, 259-267, 10.1021/es5034553, 2015.

Chen, C., Huang, J.-H., Li, K., Osterwalder, S., Yang, C., Waldner, P., Zhang, H., Fu, X., and Feng, X.: Isotopic characterization of mercury atmosphere–foliage and atmosphere–soil exchange in a Swiss subalpine coniferous forest, Environmental Science & Technology, 57, 15892-15903, 10.1021/acs.est.3c03576, 2023.

Cheng, I., Xu, X., and Zhang, L.: Overview of receptor-based source apportionment studies for speciated atmospheric mercury, Atmospheric Chemistry and Physics, 15, 7877-7895, 10.5194/acp-15-7877-2015, 2015.

Chen, J., Pehkonen, S. O., and Lin, C. J.: Degradation of monomethylmercury chloride by hydroxyl radicals in simulated natural waters, Water Research, 37, 2496-2504, 2003.

Chen, J., Hintelmann, H., Feng, X., and Dimock, B.: Unusual fractionation of both odd and even mercury isotopes in precipitation from Peterborough, ON, Canada, Geochimica et Cosmochimica Acta, 90, 3346, 2012.

Chen, J., Hintelmann, H., Zheng, W., Feng, X., Cai, H., Wang, Z., Yuan, S., and Wang, Z.: Isotopic evidence for distinct sources of mercury in lake waters and sediments, Chemical Geology, 426, 33-44, 10.1016/j.chemgeo.2016.01.030, 2016.

Chen, L., Wang, H. H., Liu, J. F., Tong, Y. D., Ou, L. B., Zhang, W., Hu, D., Chen, C., and Wang, X. J.: Intercontinental transport and deposition patterns of atmospheric mercury from anthropogenic emissions, Atmospheric Chemistry & Physics, 14, 10163-10176, 10.5194/acp-14-10163-2014, 2014.

Chen, Y., Zhang, Q., Zhang, L., Liu, X., Li, Y., Liu, R., Wang, Y., Song, Y., Li, Y., Yin, Y., and Cai, Y.: Light-induced degradation of dimethylmercury in different natural waters, Journal of Hazardous Materials, 470, 10.1016/j.jhazmat.2024.134113, 2024.

Cheng, Y. C., Watari, T., Seccatore, J., Nakajima, K., Nansai, K., and Takaoka, M.: A review of gold production, mercury consumption, and emission in artisanal and small-scale gold mining (ASGM), Resources Policy, 81, 3370-3370, 10.1016/j.resourpol.2023.103370, 2023.

Chertihin, G. V. and Andrews, L.: Reactions of laser-ablated Zn and Cd atoms with O_2: Infrared spectra of ZnO, OZnO, CdO, and OCdO in solid argon, Journal of Chemical Physics, 106, 3457-3465, 10.1063/1.473441, 1997.

Chi, Y., Yan, N. Q., Qu, Z., Qiao, S. H., and Jia, J. P.: The performance of iodine on the removal of elemental mercury from the simulated coal-fired flue gas, Journal of Hazardous Materials, 166, 776-781, 10.1016/j.jhazmat.2008.11.130, 2009.

Cohen-Atiya, M. and Mandler, D.: Studying thiol adsorption on Au, Ag and Hg surfaces by potentiometric measurements, Journal of Electroanalytical Chemistry, 550, 267-276, 10.1016/S0022-0728(02)01145-2, 2003.

Cole, A. S., Steffen, A., Pfaffhuber, K. A., Berg, T., Pilote, M., Poissant, L., Tordon, R., and Hung, H.: Ten-year trends of atmospheric mercury in the high Arctic compared to Canadian sub-Arctic and mid-latitude sites, Atmospheric Chemistry and Physics, 13, 1535-1545, 2013.

Cole, A. S., Steffen, A., Eckley, C. S., Narayan, J., Pilote, M., Tordon, R., Graydon, J. A., St Louis, V. L., Xu, X. H., and

tog bort: Mechanisms
formaterade: Teckenfärg: Blå, Kondenserad med 0,2 pt
tog bort: Reactions Influencing Atmospheric Ozone
formaterade: Teckenfärg: Blå, Kondenserad med 0,2 pt
tog bort: Investigation
formaterade ... [942]
tog bort: Calorimetric
formaterade: Teckenfärg: Blå, Kondenserad med 0,3 pt
formaterade ... [943]
tog bort: Mercaptocarboxylate Interaction
formaterade: Teckenfärg: Blå, Kondenserad med 0,3 pt
tog bort: Aqueous Solution
formaterade ... [944]
formaterade: Teckenfärg: Blå
tog bort: Carmona García, J.: Atmospheric chemistry of mercury and sulfur induced by sunlight: Quantum-chemical modelling and environmental implications, Ph D. thesis, Institut de Ciènci ... [945]
formaterade: Teckenfärg: Blå
Formaterat ... [946]
tog bort: Not Separately
formaterade: Teckenfärg: Blå
tog bort: Oxidize
formaterade: Teckenfärg: Blå
tog bort: Atmosphere, The
formaterade: Teckenfärg: Blå
formaterade: Teckenfärg: Blå, Kondenserad med 0,3 pt
tog bort: Isotope Fractionation
formaterade: Teckenfärg: Blå, Kondenserad med 0,3 pt
tog bort: Aqueous Photo-Reduction
formaterade: Teckenfärg: Blå, Kondenserad med 0,3 pt
tog bort: Monomethylmercury
formaterade: Teckenfärg: Blå
tog bort: Presence
formaterade: Teckenfärg: Blå
tog bort: Dissolved Organic Matter
formaterade: Teckenfärg: Blå
tog bort: Characterization
formaterade: Teckenfärg: Blå
tog bort: Mercury Atmosphere–Foliage
formaterade: Teckenfärg: Blå
tog bort: Atmosphere–Soil Exchange
formaterade: Teckenfärg: Blå
tog bort: Subalpine Coniferous Forest
formaterade: Teckenfärg: Blå
formaterade: Teckenfärg: Blå
Formaterat ... [947]
Formaterat ... [948]
formaterade ... [949]
formaterade: Teckenfärg: Blå
Formaterat ... [950]
formaterade: Teckenfärg: Blå, Kondenserad med 0,2 pt

Branfireun, B. A.: A survey of mercury in air and precipitation across Canada: patterns and trends, Atmosphere, 5, 635-668, 2014.

Conaway, C. H., Black, F. J., Weiss-Penzias, P., Gault-Ringold, M., and Flegal, A. R.: Mercury speciation in Pacific coastal rainwater, Monterey Bay, California, Atmospheric Environment, 44, 1788-1797, 2010.

Conaway, C. H., Black, F. J., Gault-Ringold, M., Pennington, J. T., Chavez, F. P., and Flegal, A. R.: Dimethylmercury in coastal upwelling waters, Monterey Bay, California, Environmental Science & Technology, 43, 1305-1309, 10.1021/es802705t, 2009.

Cooke, C. A., Martínez-Cortizas, A., Bindler, R., and Gustin, M. S.: Environmental archives of atmospheric Hg deposition - A review, Science of the Total Environment, 709, 10.1016/j.scitotenv.2019.134800, 2020.

Cremer, D., Kraka, E., and Filatov, M.: Bonding in mercury molecules described by the normalized elimination of the small component and coupled cluster theory, Physical Chemistry Chemical Physics, 9, 2510-2521, 2008.

Criss, R. E.: Principles of stable isotope distribution, Oxford University Press, 1999.

Custódio, D., Ebinghaus, R., Spain, T., and Bieser, J.: Source apportionment of atmospheric mercury in the remote marine atmosphere: Mace Head GAW station, Irish western coast, Atmospheric Chemistry and Physics, 20, 7929-7939, 10.5194/acp-20-7929-2020, 2020.

Custódio, D., Pfaffhuber, K. A., Spain, T. G., Pankratov, F. F., Strigunova, I., Molepo, K., Skov, H., Bieser, J., and Ebinghaus, R.: Odds and ends of atmospheric mercury in Europe and over the North Atlantic Ocean: temporal trends of 25 years of measurements, Atmospheric Chemistry and Physics, 22, 3827-3840, 10.5194/acp-22-3827-2022, 2022.

Davis, M. and Lu, J. L.: Calibration sources for gaseous oxidized mercury: A review of source design, performance, and operational parameters, Critical Reviews in Analytical Chemistry, 54, 1748-1757, 10.1080/10408347.2022.2131373, 2024.

Deacon, G. B., Faulks, S. J., and Pain, G. N.: The synthesis of organometallics by decarboxylation reactions, in: Advances in Organometallic Chemistry, edited by: Stone, F. G. A., and West, R., Academic Press, 237-276, 10.1016/S0065-3055(08)60576-6, 1986.

Deeds, D. A., Ghoshdastidar, A., Raofie, F., Guérette, É.-A., Tessier, A., and Ariya, P. A.: Development of a particle-trap preconcentration-soft ionization mass spectrometric technique for the quantification of mercury halides in air, Analytical Chemistry, 87, 5109-5116, 10.1021/ac504545w, 2015.

Demers, J. D., Blum, J. D., and Zak, D. R.: Mercury isotopes in a forested ecosystem: Implications for air-surface exchange dynamics and the global mercury cycle, Global Biogeochemical Cycles, 27, 222-238, 2013.

Demers, J. D., Sherman, L. S., Blum, J. D., Marsik, F. J., and Dvonch, J. T.: Coupling atmospheric mercury isotope ratios and meteorology to identify sources of mercury impacting a coastal urban-industrial region near Pensacola, Florida, USA, Global Biogeochemical Cycles, 29, 1689-1705, 10.1002/2015GB005146, 2015.

Dibble, T. S. and Schwid, A. C.: Thermodynamics limits the reactivity of BrHg radical with volatile organic compounds, Chemical Physics Letters, 659, 289-294, 10.1016/j.cplett.2016.07.065, 2016.

Dibble, T. S., Zelie, M. J., and Jiao, Y.: Quantum chemistry guide to PTRMS studies of as-yet undetected products of the bromine-atom initiated oxidation of gaseous elemental mercury, Journal of Physical Chemistry A, 118, 7847-7854, 10.1021/jp5041426, 2014.

Dibble, T. S., Zelie, M. J., and Mao, H.: Thermodynamics of reactions of ClHg and BrHg radicals with atmospherically abundant free radicals, Atmospheric Chemistry and Physics, 12, 10271-10279, 2012.

Dibble, T. S., Tetu, H. L., Jiao, Y. G., Thackray, C. P., and Jacob, D. J.: Modeling the OH-initiated oxidation of mercury in the global atmosphere without violating physical laws, Journal of Physical Chemistry A, 124, 444-453, 10.1021/acs.jpca.9b10121, 2020.

Dickinson, R. G. and Sherrill, M. S.: Formation of ozone by optically excited mercury vapor, Proceedings of the National Academy of Sciences of the United States of America, 12, 175-178, 1926.

Dommergue, A., Bahlmann, E., Ebinghaus, R., Ferrari, C., and Boutron, C.: Laboratory simulation of Hg^0 emissions from a snowpack, Analytical and Bioanalytical Chemistry, 388, 319-327, 2007.

Dommergue, A., Sprovieri, F., Pirrone, N., Ebinghaus, R., Brooks, S., Courteaud, J., and Ferrari, C. P.: Overview of mercury measurements in the Antarctic troposphere, Atmospheric Chemistry and Physics, 10, 3309-3319, 2010.

Dong, W., Bian, Y., Liang, L., and Gu, B.: Binding constants of mercury and dissolved organic matter determined by a modified ion exchange technique, Environmental Science & Technology, 45, 3576-3583, 2011.

Donohoue, D. L.: Kinetic studies of the oxidation pathways of gaseous elemental mercury, Ph. D. Thesis, Department of Marine and Atmospheric Chemistry, University of Miami, Coral Gables, Florida, 261 pp., 2008.

tog bort: Survey
formaterade ... [951]
tog bort: Mercury
formaterade ... [952]
tog bort: Air
formaterade ... [953]
tog bort: Precipitation
formaterade ... [954]
tog bort: Patterns
formaterade ... [955]
tog bort: Trends
formaterade ... [956]
formaterade ... [957]
formaterade ... [958]
tog bort: Coastal Upwelling Waters
formaterade ... [959]
tog bort: Mercury Molecules Described
formaterade ... [960]
Formaterat ... [961]
formaterade ... [962]
tog bort: Normalized Elimination
formaterade ... [963]
tog bort: Small Component
formaterade ... [964]
tog bort: Coupled Cluster Theory
formaterade ... [965]
formaterade ... [966]
Formaterat ... [967]
tog bort: Synthesis
formaterade ... [968]
tog bort: Organometallics
formaterade ... [969]
tog bort: Decarboxylation Reactions
formaterade ... [970]
formaterade ... [971]
tog bort: Particle-Trap Preconcentration-Soft Ionization ... [972]
formaterade ... [973]
tog bort: Quantification
formaterade ... [974]
tog bort: Mercury Halides
formaterade ... [975]
tog bort: Air
formaterade ... [976]
tog bort: Chemistry Guide
formaterade ... [977]
tog bort: Studies
formaterade ... [978]
tog bort: As-Yet Undetected Products
formaterade ... [979]
tog bort: Bromine-Atom Initiated Oxidation
formaterade ... [980]
tog bort: Gaseous Elemental Mercury
formaterade ... [981]
tog bort: Initiated Oxidation
formaterade ... [982]
tog bort: Mercury
formaterade ... [983]
tog bort: Global Atmosphere
formaterade ... [984]
tog bort: Violating Physical Laws
formaterade ... [985]
formaterade ... [986]
tog bort: Ozone
formaterade ... [987]
tog bort: Optically Excited Mercury Vapor
formaterade ... [988]
formaterade ... [989]
Formaterat ... [990]

Donohoue, D. L., Bauer, D., and Hynes, A. J.: Temperature and pressure dependent rate coefficients for the reaction of Hg with Cl and the reaction of Cl with Cl: A pulsed laser photolysis-pulsed laser induced fluorescence study, Journal of Physical Chemistry A, 109, 7732-7741, 2005.

Donohoue, D. L., Bauer, D., Cossairt, B., and Hynes, A. J.: Temperature and pressure dependent rate coefficients for the reaction of Hg with Br and the reaction of Br with Br: A pulsed laser photolysis-pulsed laser induced fluorescence study, Journal of Physical Chemistry A, 110, 6623-6632, 2006.

Donovan, P. M., Blum, J. D., Yee, D., Gehrke, G. E., and Singer, M. B.: An isotopic record of mercury in San Francisco Bay sediment, Chemical Geology, 349, 87 - 98, 2013.

Douglas, T. A. and Blum, J. D.: Mercury isotopes reveal atmospheric gaseous mercury deposition directly to the Arctic coastal snowpack, Environmental Science & Technology Letters, 6, 235-242, 10.1021/acs.estlett.9b00131, 2019.

Douglas, T. A., Sturm, M., Blum, J. D., Polashenski, C., Stuefer, S., Hiemstra, C., Steffen, A., Filhol, S., and Prevost, R.: A Pulse of mercury and major ions in snowmelt runoff from a small Arctic Alaska watershed, Environmental Science & Technology, 51, 11145-11155, 10.1021/acs.est.7b03683, 2017.

Dumarey, R., Dams, R., and Hoste, J.: Comparison of the collection and desorption efficiency of activated-charcoal, silver, and gold for the determination of vapor-phase atmospheric mercury, Analytical Chemistry, 57, 2638-2643, 1985.

Dunham-Cheatham, S. M., Lyman, S., and Gustin, M. S.: Comparison and calibration of methods for ambient reactive mercury quantification, Science of the Total Environment, 856, ARTN 159219, 10.1016/j.scitotenv.2022.159219, 2023.

Eder, J. M.: Ein neues chemisches Photometer mittelst Quecksilberoxalat zur Bestimmung der Intensität der ultravioletten Strahlen des Tageslichtes und Beiträge zur Photochemie des Quecksilberchlorides, Berichte der deutschen chemischen Gesellschaft, 13, 166-168, 10.1002/cber.18800130150, 1880.

Edirappulige, D. T. H., Cheng, L., Castro Pelaez, P., and Dibble, T.: Nitrate radical cannot initiate oxidation of Hg(0) to Hg(II) in the laboratory or at ground level in the atmosphere, Submitted to Environmental Science & Technology (preprint), 10.26434/chemrxiv-2024-qwh3w, 2024.

Edirappulige, D. T. H., Kirby, I. J., Beckett, C. K., and Dibble, T. S.: Atmospheric chemistry of $HOHg^{II}O\bullet$ mimics that of a hydroxyl radical, Journal of Physical Chemistry A, 10.1021/acs.jpca.3c04159, 2023.

Edwards, B. A., Kushner, D. S., Outridge, P. M., and Wang, F.: Fifty years of volcanic mercury emission research: Knowledge gaps and future directions, Science of the Total Environment, 757, 143800-143800, 10.1016/j.scitotenv.2020.143800, 2021.

Elgiar, T. R., Gratz, L., Hallar, A. G., Volkamer, R., and Lyman, S. N.: Underestimation of atmospheric oxidized mercury at a mountaintop site by the GEOS-Chem chemical transport model, EGUsphere, 2025, 1-23, 10.5194/egusphere-2025-977, 2025.

Enrico, M., Le Roux, G., Marusczak, N., Heimbürger, L. E., Claustres, A., Fu, X. W., Sun, R. Y., and Sonke, J. E.: Atmospheric mercury transfer to peat bogs dominated by gaseous elemental mercury dry deposition, Environmental Science & Technology, 50, 2405-2412, 2016.

Epov, V.: Mechanisms of oxidation–reduction reactions can be predicted by the magnetic isotope effect, Advances in Physical Chemistry, 2011, 10.1155/2011/450325, 2011a.

Epov, V. N.: Magnetic isotope effect and theory of atomic orbital hybridization to predict a mechanism of chemical exchange reactions, Physical Chemistry Chemical Physics, 13, 13222-13231, 10.1039/c1cp21012b, 2011b.

Faïn, X., Helmig, D., Hueber, J., Obrist, D., and Williams, M. W.: Mercury dynamics in the Rocky Mountain, Colorado, snowpack, Biogeosciences, 10, 3793-3807, 10.5194/bg-10-3793-2013, 2013.

Fang, Y., Liu, G., Wang, Y., Liu, Y., Yin, Y., Cai, Y., Mebel, A. M., and Jiang, G.: Transformation of mercurous [Hg^{I}] species during laboratory standard preparation and analysis: Implication for environmental analysis, Environmental Science & Technology, 58, 6825-6834, 10.1021/acs.est.4c00718, 2024.

Feinberg, A., Dlamini, T., Jiskra, M., Shah, V., and Selin, N. E.: Evaluating atmospheric mercury (Hg) uptake by vegetation in a chemistry-transport model, Environmental Science: Processes & Impacts, 24, 1303-1318, 10.1039/D2EM00032F, 2022.

Feinberg, A. I., Kurien, U., and Ariya, P. A.: The kinetics of aqueous mercury(II) reduction by sulfite over an array of environmental conditions, Water Air and Soil Pollution, 226, 10.1007/s11270-015-2371-0, 2015.

Feinberg, A., Selin, N. E., Braban, C. F., Chang, K.-L., Custodio, D., Jaffe, D. A., Kyllonen, K., Landis, M. S., Leeson, S. R., Luke, W., Molepo, K. M., Murovec, M., Mastromonaco, M. G. N., Pfaffhuber, K. A., Ruediger, J., Sheu, G.-R., and St. Louis, V. L.: Unexpected anthropogenic emission decreases explain recent atmospheric mercury concentration declines, Proceedings

tog bort: Pressure Dependent Rate Coefficients
formaterade ... [996]
tog bort: Reaction
formaterade ... [997]
tog bort: Reaction
formaterade ... [998]
tog bort: Pulsed Laser Photolysis-Pulsed Laser Induced ... [999]
formaterade ... [1000]
tog bort: Pressure Dependent Rate Coefficients
formaterade ... [1001]
tog bort: Reaction
formaterade ... [1002]
tog bort: Reaction
formaterade ... [1003]
tog bort: Pulsed Laser Photolysis-Pulsed Laser Induced ... [1004]
formaterade ... [1005]
tog bort: Isotopes Reveal Atmospheric Gaseous Mercur ... [1006]
formaterade ... [1007]
tog bort: Coastal Snowpack
formaterade ... [1008]
tog bort: Mercury
formaterade ... [1009]
tog bort: Major Ions
formaterade ... [1010]
tog bort: Snowmelt Runoff
formaterade ... [1011]
tog bort: Small
formaterade ... [1012]
tog bort: Watershed
formaterade ... [1013]
tog bort: . S.: Computational chemistry re-interprets lab ... [1015]
formaterade ... [1016]
tog bort: initiation of
formaterade ... [1017]
tog bort:), ACS Spring Meeting 2023, Indianapolis
formaterade ... [1014]
formaterade ... [1018]
formaterade ... [1019]
tog bort: Chemistry
formaterade ... [1020]
tog bort: Mimics That
formaterade ... [1021]
tog bort: Hydroxyl Radical
formaterade ... [1022]
tog bort: 2023b
Formaterat ... [1023]
formaterade ... [1024]
tog bort: Mercury Transfer
formaterade ... [1025]
tog bort: Peat Bogs Dominated
formaterade ... [1026]
tog bort: Gaseous Elemental Mercury Dry Deposition
formaterade ... [1027]
tog bort: Oxidation-Reduction Reactions Can Be Predicted
formaterade ... [1028]
tog bort: Magnetic Isotope Effect
formaterade ... [1029]
tog bort: Mercurous
formaterade ... [1030]
tog bort: Species
formaterade ... [1031]
tog bort: Laboratory Standard Preparation
tog bort: Analysis
formaterade ... [1033]
tog bort: Environmental Analysis
formaterade ... [1032]
formaterade ... [1034]
tog bort: Kinetics

of the National Academy of Sciences of the United States of America, 121, 10.1073/pnas.2401950121, 2024.

Feldmann, J., Grumping, R., and Hirner, A. V.: Determination of volatile metal and metalloid compounds in gases from domestic waste deposits with GC ICP-MS, Fresenius Journal of Analytical Chemistry, 350, 228-234, 1994.

Feng, X., Li, P., Fu, X., Wang, X., Zhang, H., and Lin, C.-J.: Mercury pollution in China: implications on the implementation of the Minamata Convention, Environmental Science: Processes & Impacts, 24, 634-648, 10.1039/D2EM00039C, 2022.

Filatov, M. and Cremer, D.: Revision of the dissociation energies of mercury chalcogendies - Unusual types of mercury bonding, Chemical Physics Physical Chemistry, 5, 1547-1557, 10.1002/cphc.200301207, 2004.

Finlayson-Pitts, B. J. and Pitts, J. N.: Chemistry of the upper and lower atmosphere: Theory, experiments and applications, 1st Ed., Academic Press, San Diego, 2000.

Foti, C., Giuffre, O., Lando, G., and Sammartano, S.: Interaction of inorganic mercury(II) with polyamines, polycarboxylates, and amino acids, Journal of Chemical and Engineering Data, 54, 893-903, 10.1021/je800685c, 2009.

Francés-Monerris, A., Carmona-García, J., Acuña, A. U., Dávalos, J. Z., Cuevas, C. A., Kinnison, D. E., Francisco, J. S., Saiz-Lopez, A., and Roca-Sanjuán, D.: Photodissociation mechanisms of major mercury(II) species in the atmospheric chemical cycle of mercury, Angewandte Chemie International Edition, 59, 7605-7610, 2020.

Fu, X., Marusczak, N., Wang, X., Gheusi, F., and Sonke, J. E.: Isotopic composition of gaseous elemental mercury in the free troposphere of the Pic du Midi observatory, France, Environmental Science & Technology, 10.1021/acs.est.6b00033, 2016a.

Fu, X., Zhang, H., Liu, C., Zhang, H., Lin, C.-J., and Feng, X.: Significant seasonal variations in isotopic composition of atmospheric total gaseous mercury at forest sites in China caused by vegetation and mercury sources, Environmental Science & Technology, 53, 13748-13756, 10.1021/acs.est.9b05016, 2019a.

Fu, X., Zhang, H., Feng, X., Tan, Q., Ming, L., Liu, C., and Zhang, L.: Domestic and transboundary sources of atmospheric particulate bound mercury in remote areas of China: Evidence from mercury isotopes, Environmental Science & Technology, 53, 1947-1957, 2019b.

Fu, X., Jiskra, M., Yang, X., Marusczak, N., Enrico, M., Chmeleff, J., Heimbürger-Boavida, L.-E., Gheusi, F., and Sonke, J. E.: Mass-independent fractionation of even and odd mercury isotopes during atmospheric mercury redox reactions, Environmental Science & Technology, 55, 10164-10174, 2021.

Fu, X., Zhu, W., Zhang, H., Sommar, J., Yu, B., Yang, X., Wang, X., Lin, C. J., and Feng, X.: Depletion of atmospheric gaseous elemental mercury by plant uptake at Mt. Changbai, Northeast China, Atmospheric Chemistry and Physics, 16, 12861-12873, 10.5194/acp-16-12861-2016, 2016b.

Fu, X. W., Zhang, H., Yu, B., Wang, X., Lin, C. J., and Feng, X. B.: Observations of atmospheric mercury in China: a critical review, Atmospheric Chemistry and Physics, 15, 9455-9476, 10.5194/acp-15-9455-2015, 2015.

Fu, X., Sun, X., Travnikov, O., Li, Q., Qin, C., Cuevas, C. A., Fernandez, R. P., Mahajan, A. S., Wang, S., Wang, T., and Saiz-Lopez, A.: Anthropogenic short-lived halogens increase human exposure to mercury contamination due to enhanced mercury oxidation over continents, Proceedings of the National Academy of Sciences, 121, e2315058121, 10.1073/pnas.2315058121, 2024.

Fujita, S., Horii, H., and Taniguchi, S.: Pulse radiolysis of mercuric ion in aqueous solutions, Journal of Physical Chemistry, 77, 2868-2871, 10.1021/j100642a009, 1973.

Fujita, S., Horii, H., Mori, T., and Taniguchi, S.: Pulse radiolysis of mercuric oxide in neutral aqueous solutions, Journal of Physical Chemistry, 79, 960-964, 10.1021/j100577a003, 1975.

Gačnik, J., Zivkovic, I., Guevara, S. R., Kotnik, J., Berisha, S., Nair, S. V., Jurov, A., Cvelbar, U., and Horvat, M.: Calibration approach for gaseous oxidized mercury based on nonthermal plasma oxidation of elemental mercury, Analytical Chemistry, 94, 8234-8240, 10.1021/acs.analchem.2c00260, 2022.

Gačnik, J., Lyman, S., Dunham-Cheatham, S. M., and Gustin, M. S.: Limitations and insights regarding atmospheric mercury sampling using gold, Analytica Chimica Acta, 1319, 342956, 10.1016/j.aca.2024.342956, 2024.

Gaffney, J. and Marley, N.: In-depth review of atmospheric mercury: sources, transformations, and potential sinks, Energy and Emission Control Technologies, 2, 10.2147/eect.s37038, 2014.

Gao, Z. Y., Bailey, N., and Wang, F. Y.: Experimental determination of mercury photoreduction rates in cloudwater, Journal of Geophysical Research-Atmospheres, 128, 10.1029/2022jd038183, 2023.

Gao, Z. Y., Geilfus, N. X., Saiz-Lopez, A., and Wang, F. Y.: Reproducing Arctic springtime tropospheric ozone and mercury

formaterade ... [1041]
Formaterat ... [1042]
tog bort: Volatile Metal
tog bort: Metalloid Compounds
formaterade ... [1043]
formaterade ... [1044]
tog bort: Gases
formaterade ... [1045]
tog bort: Domestic Waste Deposits
formaterade ... [1046]
tog bort: theory
formaterade ... [1047]
tog bort: Inorganic Mercury
formaterade ... [1048]
tog bort: Polyamines, Polycarboxylates
formaterade ... [1049]
tog bort: Amino Acids
formaterade ... [1050]
tog bort: Mechanisms
formaterade ... [1051]
tog bort: Major Mercury
formaterade ... [1052]
tog bort: Species
formaterade ... [1053]
tog bort: Atmospheric Chemical Cycle
formaterade ... [1054]
tog bort: Mercury
formaterade ... [1055]
tog bort: Composition
formaterade ... [1056]
tog bort: Gaseous Elemental Mercury
formaterade ... [1057]
tog bort: Free Troposphere
formaterade ... [1058]
tog bort: Observatory
formaterade ... [1059]
tog bort: Seasonal Variations
formaterade ... [1060]
tog bort: Isotopic Composition
formaterade ... [1061]
tog bort: Atmospheric Total Gaseous Mercury
formaterade ... [1062]
tog bort: Forest Sites
formaterade ... [1063]
tog bort: Caused
formaterade ... [1064]
tog bort: Vegetation
formaterade ... [1065]
tog bort: Mercury Sources
formaterade ... [1066]
tog bort: Transboundary Sources
formaterade ... [1067]
tog bort: Atmospheric Particulate Bound Mercury
formaterade ... [1068]
tog bort: Remote Areas
formaterade ... [1069]
tog bort: Mercury Isotopes
formaterade ... [1070]
tog bort: Independent Fractionation
formaterade ... [1071]
tog bort: Even
formaterade ... [1072]
tog bort: Odd Mercury Isotopes
formaterade ... [1073]
tog bort: Atmospheric Mercury Redox Reactions
formaterade ... [1074]
formaterade ... [1075]
Formaterat ... [1076]

depletion events in an outdoor mesocosm sea ice facility, Atmospheric Chemistry and Physics, 22, 1811-1824, 10.5194/acp-22-1811-2022, 2022.

Gay, D. A., Schmeltz, D., Prestbo, E., Olson, M., Sharac, T., and Tordon, R.: The Atmospheric Mercury Network: Measurement and initial examination of an ongoing atmospheric mercury record across North America, Atmospheric Chemistry and Physics, 13, 11339-11349, 2013.

Gerson, J. R., Driscoll, C. T., Demers, J. D., Sauer, A. K., Blackwell, B. D., Montesdeoca, M. R., Shanley, J. B., and Ross, D. S.: Deposition of mercury in forests across a montane elevation gradient: Elevational and seasonal patterns in methylmercury inputs and production, Journal of Geophysical Research - Biogeosciences, 122, 1922-1939, 10.1002/2016JG003721, 2017.

Geyman, B. M., Streets, D. G., Thackray, C. P., Olson, C. L., Schaefer, K., and Sunderland, E. M.: Projecting global mercury emissions and deposition under the shared socioeconomic pathways, Earth's Future, 12, e2023EF004231, 10.1029/2023EF004231, 2024.

Ghoshdastidar, A. J. and Ariya, P. A.: The existence of airborne mercury nanoparticles, Scientific Reports, 910733, 10.1038/s41598-019-47086-8, 9, 2019.

Ghoshdastidar, J., Ramamurthy, J., Morissette, M., and Ariya, P.: Development of methodology to generate, measure, and characterize the chemical composition of oxidized mercury nanoparticles, Analytical and Bioanalytical Chemistry, 10.1007/s00216-019-02279-y, 2019.

Giannakopoulos, E., Deligiannakis, Y., and Salahas, G.: Electrochemical interfacial adsorption mechanism of polyphenolic molecules onto Hanging Mercury Drop Electrode surface (HMDE), Journal of Electroanalytical Chemistry, 664, 117-125, 10.1016/j.jelechem.2011.11.008, 2012.

Gómez Martín, J. C., Lewis, T. R., Douglas, K. M., Blitz, M. A., Saiz-Lopez, A., and Plane, J. M. C.: The reaction between HgBr and O_3: kinetic study and atmospheric implications, Physical Chemistry Chemical Physics, 24, 12419-12432, 10.1039/D2CP00754A, 2022.

Goodsite, M., Plane, J. M. C., and Skov, H.: A theoretical study of the oxidation of Hg^0 to $HgBr_2$ in the troposphere, Environmental Science & Technology, 38, 2004.

Goodsite, M. E., Plane, J. M. C., and Skov, H.: A theoretical study of the oxidation of Hg^0 to $HgBr_2$ in the troposphere (vol 38, pg 1772, 2004), Environmental Science & Technology, 46, 5262-5262, 10.1021/es301201c, 2012.

Gratz, L. E., Keeler, G. J., Blum, J. D., and Sherman, L. S.: Isotopic composition and fractionation of mercury in Great Lakes precipitation and ambient air, Environmental Science & Technology, 44, 7764-7770, 2010.

Gratz, L. E., Ambrose, J. L., Jaffe, D. A., Shah, V., Jaeglé, L., Stutz, J., Festa, J., Spolaor, M., Tsai, C., Selin, N. E., Song, S., Zhou, X., Weinheimer, A. J., Knapp, D. J., Montzka, D. D., Flocke, F. M., Campos, T. L., Apel, E., Hornbrook, R., Blake, N. J., Hall, S., Tyndall, G. S., Reeves, M., Stechman, D., and Stell, M.: Oxidation of mercury by bromine in the subtropical Pacific free troposphere, Geophysical Research Letters, 2015GL066645, 10.1002/2015GL066645, 2015.

Greig, G., Gunning, H. E., and Strausz, O. P.: Reactions of metal atoms. II. The combination of mercury and bromine atoms and the dimerization of HgBr, Journal of Chemical Physics, 52, 3684, 10.1063/1.1673544, 1970.

Greig, G., Young, P. J., and Strausz, O. P.: Reactions of metal atoms. IV. The UV Spectra of CdBr, CdI, ZnBr, and ZnI, Journal of Chemical Physics, 54, 983 - 991, 1971.

Gruß, A. F., Rodriguez, R., and Mazyck, D. W.: Mercury oxidation by UV irradiation: Effect of contact time, UV wavelength, and moisture content, Industrial & Engineering Chemistry Research, 56, 6131-6135, 10.1021/acs.iecr.7b00032, 2017.

Gu, B. H., Bian, Y. R., Miller, C. L., Dong, W. M., Jiang, X., and Liang, L. Y.: Mercury reduction and complexation by natural organic matter in anoxic environments, Proceedings of the National Academy of Sciences of the United States of America, 108, 1479-1483, 2011.

Guérette, E.-A.: Kinetic and mass-spectrometric studies of atmospherically relevant mercury-bromine chemistry, M.Sc. thesis, Department of Chemistry, McGill University, Montreal, Canada, 114 pp., 2011.

Gunning, H. E. and Strausz, O. P.: Isotopic effects and the mechanism of energy transfer in mercury photosensitization, in: Advances in Photochemistry Vol. 1, edited by: Noyes Jr, W. A., Hammond, G. S., and Pitts Jr, J. N., John Wiley & Sons, 209-274, 10.1002/9780470133316.ch7, 1963.

Gustin, M. S., Amos, H. M., Huang, J., Miller, M. B., and Heidecorn, K.: Measuring and modeling mercury in the atmosphere: A critical review, Atmospheric Chemistry and Physics, 15, 5697 - 5713, 2015.

Gustin, M. S., Dunham-Cheatham, S. M., Huang, J. Y., Lindberg, S., and Lyman, S. N.: Development of an understanding of

tog bort: :
formaterade ... [1083]
Formaterat ... [1085]
tog bort: Existence
formaterade ... [1084]
formaterade ... [1086]
tog bort: Airborne Mercury Nanoparticles
formaterade ... [1087]
formaterade ... [1088]
tog bort: Theoretical Study
formaterade ... [1089]
tog bort: Oxidation
formaterade ... [1090]
tog bort: Troposphere
formaterade ... [1091]
tog bort: Theoretical Study
formaterade ... [1092]
tog bort: Oxidation
formaterade ... [1093]
tog bort: Troposphere
formaterade ... [1094]
tog bort: Composition
formaterade ... [1095]
tog bort: Fractionation
formaterade ... [1096]
tog bort: Mercury
formaterade ... [1097]
tog bort: Precipitation
formaterade ... [1098]
tog bort: Ambient Air
formaterade ... [1099]
tog bort: Metal Atoms
formaterade ... [1100]
tog bort: Combination
formaterade ... [1101]
tog bort: Mercury
formaterade ... [1102]
tog bort: Bromine Atoms
formaterade ... [1103]
tog bort: Dimerization
formaterade ... [1104]
tog bort: The
formaterade ... [1105]
tog bort: Metal Atoms
formaterade ... [1106]
tog bort: uv
formaterade ... [1107]
tog bort: The
formaterade ... [1108]
tog bort: Gruss
formaterade ... [1109]
tog bort: Oxidation
formaterade ... [1110]
tog bort: Irradiation
formaterade ... [1111]
tog bort: Contact Time
formaterade ... [1112]
tog bort: Wavelength
formaterade ... [1113]
tog bort: Moisture Content
formaterade ... [1114]
formaterade ... [1115]
formaterade ... [1116]
tog bort: Effects
formaterade ... [1117]
tog bort: Mechanism
formaterade ... [1118]
tog bort: Energy Transfer

reactive mercury in ambient air: A review, Atmosphere, 12, ARTN 73, 10.3390/atmos12010073, 2021.

Gustin, M. S., Dunham-Cheatham, S. M., Allen, N., Choma, N., Johnson, W., Lopez, S., Russell, A., Mei, E. R., Magand, O., Dommergue, A., and Elgiar, T.: Observations of the chemistry and concentrations of reactive Hg at locations with different ambient air chemistry, Science of the Total Environment, 904, 166-184, 10.1016/j.scitotenv.2023, 2023.

Gustin, M. S., Dunham-Cheatham, S. M., Lyman, S., Horvat, M., Gay, D. A., Gačnik, J., Gratz, L., Kempkes, G., Khalizov, A., Lin, C.-J., Lindberg, S. E., Lown, L., Martin, L., Mason, R. P., Macsween, K., Nair, S. V., Nguyen, L. S. P., O'Neil, T., Sommar, J., Zhang, L., Weiss-Penzias, P., and Zivkovic, I.: Measurement of atmospheric mercury: Current limitations and suggestions for paths forward, Environmental Science & Technology, 58, 12853-12864, 10.1021/acs.est.4c06011, 2024.

Guzman, F. J. and Bozzelli, J.: Thermodynamics of OHgX, XHgOH, XHgOCl, XHgOBr, and HOHgY gaseous oxidized mercury molecules from isodesmic, isogyric, and atomization work reactions (X = halogen, Y = OH, OCl, OBr), Journal of Physical Chemistry A, 123, 4452-4464, 10.1021/acs.jpca.9b01358, 2019.

Gårdfeldt, K. and Jonsson, M.: Is bimolecular reduction of Hg(II) complexes possible in aqueous systems of environmental importance?, Journal of Physical Chemistry A, 107, 4478- 4482, 2003.

Gårdfeldt, K., Munthe, J., Strömberg, D., and Lindqvist, O.: A kinetic study on the abiotic methylation of divalent mercury in the aqueous phase, Science of the Total Environment, 304, 127-136, https://doi.org/10.1016/S0048-9697(02)00562-4, 2003.

Gårdfeldt, K., Sommar, J., Strömberg, D., and Feng, X. B.: Oxidation of atomic mercury by hydroxyl radicals and photoinduced decomposition of methylmercury in the aqueous phase, Atmospheric Environment, 35, 3039-3047, 2001.

Görner, H.: Quinone Photochemistry, in: CRC Handbook of Organic Photochemistry and Photobiology, 3rd Ed. Volume 1, edited by: Griesbeck, A., Oelgemöller, M., and Ghetti, F., CRC Press, 683 - 714, 2019.

Haitzer, M., Aiken, G. R., and Ryan, J. N.: Binding of mercury(II) to dissolved organic matter: The role of the mercury-to-DOM concentration ratio, Environmental Science & Technology, 36, 3564-3570, 10.1021/es025699i, 2002.

Hall, B.: An experimental study of mercury reactions in combustion flue gases, Ph. D. Thesis, Department of Inorganic Chemistry, Chalmers University of Technology and Göteborg University, Sweden, 76 pp., 1992.

Hall, B.: The gas-phase oxidation of elemental mercury by ozone, Water Air and Soil Pollution, 80, 301-315, 1995.

Hall, B., Schager, P., and Weesmaa, J.: The homogeneous gas-phase reaction of mercury with oxygen, and the corresponding heterogeneous reactions in the presence of activated carbon and fly ash, Chemosphere, 30, 611-627, 1995.

Hammerschmidt, C. R., Lamborg, C. H., and Fitzgerald, W. F.: Aqueous phase methylation as a potential source of methylmercury in wet deposition, Atmospheric Environment, 41, 1663-1668, 10.1016/j.atmosenv.2006.10.032, 2007.

Han, X. X., Li, Y. B., Li, D., and Liu, C.: Role of free radicals/reactive oxygen species in MeHg photodegradation: Importance of utilizing sppropriate scavengers, Environmental Science & Technology, 51, 3784-3793, 10.1021/acs.est.7b00205, 2017.

Harkins, W. D. and Mulliken, R. S.: The separation of mercury into isotopes, Nature, 108, 146, 10.1038/108146a0, 1921.

Hayashi, K., Kawai, S., Ohno, T., and Maki, Y.: Photomethylation of inorganic mercury by aliphatic α-amino-acids, Journal of the Chemical Society-Chemical Communications, 158-159, 10.1039/c39770000158, 1977.

He, F., Zhao, W., Liang, L., and Gu, B.: Photochemical oxidation of dissolved elemental mercury by carbonate radicals in water, Environmental Science & Technology Letters, 1, 499 - 503, 2014.

He, F., Zheng, W., Liang, L. Y., and Gu, B. H.: Mercury photolytic transformation affected by low-molecular-weight natural organics in water, Science of the Total Environment, 416, 429-435, 10.1016/j.scitotenv.2011.11.081, 2012.

He, X.-C., Tham, Y. J., Dada, L., Wang, M., Finkenzeller, H., Stolzenburg, D., Iyer, S., Simon, M., Kürten, A., Shen, J., Rörup, B., Rissanen, M., Schobesberger, S., Baalbaki, R., Wang, D. S., Koenig, T. K., Jokinen, T., Sarnela, N., Beck, L. J., Almeida, J., Amanatidis, S., Amorim, A., Ataei, F., Baccarini, A., Bertozzi, B., Bianchi, F., Brilke, S., Caudillo, L., Chen, D., Chiu, R., Chu, B., Dias, A., Ding, A., Dommen, J., Duplissy, J., El Haddad, I., Gonzalez Carracedo, L., Granzin, M., Hansel, A., Heinritzi, M., Hofbauer, V., Junninen, H., Kangasluoma, J., Kemppainen, D., Kim, C., Kong, W., Krechmer, J. E., Kvashin, A., Laitinen, T., Lamkaddam, H., Lee, C. P., Lehtipalo, K., Leiminger, M., Li, Z., Makhmutov, V., Manninen, H. E., Marie, G., Marten, R., Mathot, S., Mauldin, R. L., Mentler, B., Möhler, O., Müller, T., Nie, W., Onnela, A., Petäjä, T., Pfeifer, J., Philippov, M., Ranjithkumar, A., Saiz-Lopez, A., Salma, I., Scholz, W., Schuchmann, S., Schulze, B., Steiner, G., Stozhkov, Y., Tauber, C., Tomé, A., Thakur, R. C., Väisänen, O., Vazquez-Pufleau, M., Wagner, A. C., Wang, Y., Weber, S. K., Winkler, P. M., Wu, Y., Xiao, M., Yan, C., Ye, Q., Ylisirniö, A., Zauner-Wieczorek, M., Zha, Q., Zhou, P., Flagan, R. C., Curtius, J., Baltensperger, U., Kulmala, M., Kerminen, V.-M., Kurtén, T., Donahue, N. M., Volkamer, R., Kirkby, J., Worsnop, D. R., and Sipilä, M.: Role of

tog bort: Reactive Mercury
formaterade ... [1122]
tog bort: Ambient Air
formaterade ... [1123]
tog bort: Review
formaterade ... [1124]
tog bort: Gacnik
formaterade ... [1125]
tog bort: Atmospheric Mercury
formaterade ... [1126]
tog bort: Limitations
formaterade ... [1127]
tog bort: Suggestions
formaterade ... [1128]
tog bort: Paths Forward
formaterade ... [1129]
tog bort: Gaseous Oxidized Mercury Molecules
formaterade ... [1130]
tog bort: Isodesmic, Isogyric
formaterade ... [1131]
tog bort: Atomization Work Reactions
formaterade ... [1132]
tog bort: Halogen
formaterade ... [1133]
tog bort: The
formaterade ... [1134]
tog bort: Mercury
formaterade ... [1135]
tog bort: Dissolved Organic Matter
formaterade ... [1136]
tog bort: Role
formaterade ... [1137]
tog bort: Mercury
formaterade ... [1138]
tog bort: Concentration Ratio
formaterade ... [1139]
tog bort: Homogeneous Gas-Phase Reaction
formaterade ... [1140]
tog bort: Mercury
formaterade ... [1141]
tog bort: Oxygen
formaterade ... [1142]
tog bort: Corresponding Heterogeneous Reactions
formaterade ... [1143]
tog bort: Presence
formaterade ... [1144]
tog bort: Activated Carbon
formaterade ... [1145]
tog bort: Fly-Ash
formaterade ... [1146]
tog bort: Free Radicals/Reactive Oxygen Species
formaterade ... [1147]
tog bort: Photodegradation
formaterade ... [1148]
tog bort: Utilizing Appropriate Scavengers
formaterade ... [1149]
tog bort: Inorganic Mercury by Aliphatic Alpha-Amino-Acids
formaterade ... [1150]

iodine oxoacids in atmospheric aerosol nucleation, Science, 371, 589-595, 10.1126/science.abe0298, 2021.

He, Y. P. and Mason, R. P.: Comparison of reactive gaseous mercury measured by KCl-coated denuders and cation exchange membranes during the Pacific GEOTRACES GP15 expedition, Atmospheric Environment, 244, 10.1016/j.atmosenv.2020.117973, 2021.

He, Y. P., Shi, X. M., Huffman, W. W., Lamborg, C. H., and Mason, R. P.: Description of a dimethylmercury automatic analyzer for the high-resolution measurement of dissolved gaseous mercury species in surface ocean waters, Environmental Science & Technology, 10.1021/acs.est.2c02908, 2022.

Hepler, L. G. and Olofsson, G.: Mercury – Thermodynamic properties, chemical equilibria, and standard potentials, Chemical Reviews, 75, 585-602, 10.1021/cr60297a003, 1975.

Hietanen, S. and Sillén, L. G.: On the standard potentials of mercury, and the equilibrium $Hg^{2+} + Hg^{0}(l) = Hg_2^{2+}$ in nitrate and perchlorate solutions, Arkiv för Kemi, 10, 103-125, 1956.

Hintelmann, H. and Zheng, W.: Tracking geochemical transformations and transport of mercury through isotope fractionation, in: Environmental Chemistry and Toxicology of Mercury, edited by: Liu, G., Cai, Y., and O'Driscoll, N., John Wiley & Sons, 293 - 328, 2011.

Hippler, H., Wendt, H. R., and Hunziker, H. E.: Excited intermediates in Hg-photosensitized reaction of O_2 detected by energy-transfer, Journal of Chemical Physics, 68, 5103-5111, 1978.

Holmes, C. D., Jacob, D. J., Mason, R. P., and Jaffe, D. A.: Sources and deposition of reactive gaseous mercury in the marine atmosphere, Atmospheric Environment, 43, 2278-2285, 10.1016/j.atmosenv.2009.01.051, 2009.

Holmes, C. D., Jacob, D. J., Corbitt, E. S., Mao, J., Yang, X., Talbot, R., and Slemr, F.: Global atmospheric model for mercury including oxidation by bromine atoms, Atmospheric Chemistry and Physics, 10, 12037-12057, 2010.

Hong, Q., Xie, Z., Liu, C., Wang, F., Xie, P., Kang, H., Xu, J., Wang, J., Wu, F., He, P., Mou, F., Fan, S., Dong, Y., Zhan, H., Yu, X., Chi, X., and Liu, J.: Speciated atmospheric mercury on haze and non-haze days in an inland city in China, Atmospheric Chemistry and Physics, 16, 13807-13821, 10.5194/acp-16-13807-2016, 2016.

Horne, D. G., Gosavi, R., and Strausz, O. P.: Reactions of metal atoms. I. The combination of mercury and chlorine atoms and the dimerization of HgCl, Journal of Chemical Physics, 48, 4758 - 4764, 1968.

Horowitz, H. M., Jacob, D. J., Zhang, Y. X., Dibble, T. S., Slemr, F., Amos, H. M., Schmidt, J. A., Corbitt, E. S., Marais, E. A., and Sunderland, E. M.: A new mechanism for atmospheric mercury redox chemistry: implications for the global mercury budget, Atmospheric Chemistry and Physics, 17, 6353-6371, 10.5194/acp-17-6353-2017, 2017.

Howard, D., Nelson, P. F., Edwards, G. C., Morrison, A. L., Fisher, J. A., Ward, J., Harnwell, J., van der Schoot, M., Atkinson, B., Chambers, S. D., Griffiths, A. D., Werczynski, S., and Williams, A. G.: Atmospheric mercury in the Southern Hemisphere tropics: seasonal and diurnal variations and influence of inter-hemispheric transport, Atmospheric Chemistry and Physics, 17, 11623-11636, 10.5194/acp-17-11623-2017, 2017.

Huang, J., Lyman, S. N., Hartman, J. S., and Gustin, M. S.: A review of passive sampling systems for ambient air mercury measurements, Environmental Sciences: Processes and Impacts, 16, 374-392, 2014.

Huang, J., Miller, M. B., Edgerton, E., and Sexauer Gustin, M.: Deciphering potential chemical compounds of gaseous oxidized mercury in Florida, USA, Atmospheric Chemistry and Physics, 17, 1689-1698, 10.5194/acp-17-1689-2017, 2017.

Huang, J., Kang, S., Tian, L., Guo, J., Zhang, Q., Cong, Z., Sillanpää, M., Sun, S., and Tripathee, L.: Influence of long-range transboundary transport on atmospheric water vapor mercury collected at the largest city of Tibet, Science of the Total Environment, 566-567, 1215-1222, 10.1016/j.scitotenv.2016.05.177, 2016a.

Huang, Q., He, X., Huang, W., and Reinfelder, J. R.: Mass-Independent fractionation of mercury isotopes during photoreduction of soot particle bound Hg(II), Environmental Science & Technology, 55, 13783-13791, 10.1021/acs.est.1c02679, 2021.

Huang, Q., Liu, Y., Chen, J., Feng, X., Huang, W., Yuan, S., Cai, H., and Fu, X.: An improved dual-stage protocol to pre-concentrate mercury from airborne particles for precise isotopic measurement, Journal of Analytical Atomic Spectrometry, 30, 957-966, 10.1039/C4JA00438H, 2015.

Huang, Q., Chen, J., Huang, W., Reinfelder, J. R., Fu, P., Yuan, S., Wang, Z., Yuan, W., Cai, H., Ren, H., Sun, Y., and He, L.: Diel variation in mercury stable isotope ratios records photoreduction of $PM_{2.5}$-bound mercury, Atmospheric Chemistry and Physics, 19, 315-325, 10.5194/acp-19-315-2019, 2019.

Huang, Q., Chen, J., Huang, W., Fu, P., Guinot, B., Feng, X., Shang, L., Wang, Z., Wang, Z., Yuan, S., Cai, H., Wei, L., and Yu, B.: Isotopic composition for source identification of mercury in atmospheric fine particles, Atmospheric Chemistry and

formaterade: Teckenfärg: Blå
Formaterat: Avstånd Efter: 0,6 Rad, Radavstånd: Flera 1,1 li
formaterade: Teckenfärg: Blå, Kondenserad med 0,3 pt
formaterade: Teckenfärg: Blå, Kondenserad med 0,5 pt
formaterade: Teckenfärg: Blå, Kondenserad med 0,3 pt
formaterade: Teckenfärg: Blå, Kondenserad med 0,5 pt
tog bort: Dimethylmercury Automatic Analyzer
formaterade: Teckenfärg: Blå
formaterade: Teckenfärg: Blå
tog bort: High-Resolution Measurement
formaterade: Teckenfärg: Blå
tog bort: Dissolved Gaseous Mercury Species
formaterade: Teckenfärg: Blå
tog bort: Surface Ocean Waters
formaterade: Teckenfärg: Blå
tog bort: thermodynamic
formaterade: Teckenfärg: Blå
tog bort: Geochemical Transformations
formaterade: Teckenfärg: Blå
tog bort: Transport
formaterade: Teckenfärg: Blå
tog bort: Mercury
formaterade: Teckenfärg: Blå
tog bort: Isotope Fractionation
formaterade: Teckenfärg: Blå
tog bort: The
formaterade: Teckenfärg: Blå

Formaterat: Avstånd Efter: 0,6 Rad, Radavstånd: Flera 1,1 li
formaterade: Teckenfärg: Blå
tog bort: The
formaterade: Teckenfärg: Blå
formaterade: Teckenfärg: Blå, Kondenserad med 0,2 pt
tog bort: Fractionation
formaterade: Teckenfärg: Blå, Kondenserad med 0,2 pt
tog bort: Mercury Isotopes
formaterade: Teckenfärg: Blå, Kondenserad med 0,2 pt
tog bort: Photoreduction
formaterade: Teckenfärg: Blå, Kondenserad med 0,2 pt
tog bort: Soot Particle Bound
formaterade: Teckenfärg: Blå, Kondenserad med 0,2 pt
formaterade: Teckenfärg: Blå
formaterade: Teckenfärg: Blå, Nedsänkt
formaterade: Teckenfärg: Blå

Physics, 16, 11773-11786, 10.5194/acp-16-11773-2016, 2016b.

Huber, M. L., Laesecke, A., and Friend, D. G.: Correlation for the vapor pressure of mercury, Industrial & Engineering Chemistry Research, 45, 7351-7361, 10.1021/ie060560s, 2006.

Humphries, R. S., Schofield, R., Keywood, M. D., Ward, J., Pierce, J. R., Gionfriddo, C. M., Tate, M. T., Krabbenhoft, D. P., Galbally, I. E., Molloy, S. B., Klekociuk, A. R., Johnston, P. V., Kreher, K., Thomas, A. J., Robinson, A. D., Harris, N. R. P., Johnson, R., and Wilson, S. R.: Boundary layer new particle formation over East Antarctic sea ice – possible Hg-driven nucleation?, Atmospheric Chemistry and Physics, 15, 13339-13364, 2015.

Hynes, A. J., Donohoue, D. L., Goodsite, M. E., and Hedgecock, I. M.: Our current understanding of major chemical and physical processes affecting mercury dynamics in the atmosphere and at the air–water/terrestrial interfaces, in: Mercury Fate and Transport in the Global Atmosphere - Emissions, Measurements and Models, edited by: Mason, R. P., and Pirrone, N., Springer, 427 - 457, 2009.

Hynes, A. J., Everhart, S., Bauer, D., Remeika, J., and Tatum Ernest, C.: In situ and denuder-based measurements of elemental and reactive gaseous mercury with analysis by laser-induced fluorescence – results from the Reno Atmospheric Mercury Intercomparison Experiment, Atmospheric Chemistry and Physics, 17, 465-483, 10.5194/acp-17-465-2017, 2017.

Iverfeldt, Å. and Lindqvist, O.: Atmospheric oxidation of elemental mercury by ozone in the aqueous phase, Atmospheric Environment, 20, 1567-1573, 10.1016/0004-6981(86)90245-3, 1986.

Jackson, T. A.: Long-range atmospheric transport of mercury to ecosystems, and the importance of anthropogenic emissions - a critical review and evaluation of the published evidence, Environmental Reviews, 5, 99-120, 1997.

Jackson, T. A.: Reply: Variations in the isotope composition of mercury in a freshwater sediment sequence and food web, Canadian Journal of Fisheries and Aquatic Sciences, 00058, 2312-2317, 2001.

Jaffe, D. A., Lyman, S., Amos, H. M., Gustin, M. S., Huang, J., Selin, N. E., Levin, L., ter Schure, A., Mason, R. P., Talbot, R., Rutter, A., Finley, B., Jaegle, L., Shah, V., McClure, C., Arnbrose, J., Gratz, L., Lindberg, S., Weiss-Penzias, P., Sheu, G.-R., Feddersen, D., Horvat, M., Dastoor, A., Hynes, A. J., Mao, H., Sonke, J. E., Slemr, F., Fisher, J. A., Ebinghaus, R., Zhang, Y., and Edwards, G.: Progress on understanding atmospheric mercury hampered by uncertain measurements, Environmental Science & Technology, 48, 7204-7206, 10.1021/es5026432, 2014.

Jayasekharan, T. and Sahoo, N. K.: Mercury mono oxide cluster ions $(HgO)_n^+$ by laser desorption ionization time of flight mass spectrometry, Journal of Mass Spectrometry, 49, 248-250, 2014.

Jerzykiewicz, M.: The effect of Hg(II) ions on the free radicals of humic substances and their model compounds, Chemosphere, 92, 445-450, 10.1016/j.chemosphere.2013.01.048, 2013.

Jerzykiewicz, M., Witwicki, M., and Jezierska, J.: pH-dependent formation of Hg(II)-semiquinone complexes from natural phenols, Chemosphere, 138, 233-238, 10.1016/j.chemosphere.2015.06.006, 2015.

Jiang, H., Li, J., Tang, J., Cui, M., Zhao, S., Mo, Y., Tian, C., Zhang, X., Jiang, B., Liao, Y., Chen, Y., and Zhang, G.: Molecular characteristics, sources, and formation pathways of organosulfur compounds in ambient aerosol in Guangzhou, South China, Atmospheric Chemistry and Physics, 22, 6919-6935, 10.5194/acp-22-6919-2022, 2022.

Jiao, Y. and Dibble, T. S.: Structures, vibrational frequencies, and bond energies of the BrHgOX and BrHgXO species formed in atmospheric mercury depletion events, Journal of Physical Chemistry A, 121, 7976-7985, 10.1021/acs.jpca.7b06829, 2017a.

Jiao, Y. G. and Dibble, T. S.: First kinetic study of the atmospherically important reactions $BrHg^{\bullet} + NO_2$ and $BrHg^{\bullet} + HOO$, Physical Chemistry Chemical Physics, 19, 1826-1838, 10.1039/c6cp06276h, 2017b.

Jimenez, J. L., Canagaratna, M. R., Donahue, N. M., Prevot, A. S. H., Zhang, Q., Kroll, J. H., DeCarlo, P. F., Allan, J. D., Coe, H., Ng, N. L., Aiken, A. C., Docherty, K. S., Ulbrich, I. M., Grieshop, A. P., Robinson, A. L., Duplissy, J., Smith, J. D., Wilson, K. R., Lanz, V. A., Hueglin, C., Sun, Y. L., Tian, J., Laaksonen, A., Raatikainen, T., Rautiainen, J., Vaattovaara, P., Ehn, M., Kulmala, M., Tomlinson, J. M., Collins, D. R., Cubison, M. J., E., Dunlea, J., Huffman, J. A., Onasch, T. B., Alfarra, M. R., Williams, P. I., Bower, K., Kondo, Y., Schneider, J., Drewnick, F., Borrmann, S., Weimer, S., Demerjian, K., Salcedo, D., Cottrell, L., Griffin, R., Takami, A., Miyoshi, T., Hatakeyama, S., Shimono, A., Sun, J. Y., Zhang, Y. M., Dzepina, K., Kimmel, J. R., Sueper, D., Jayne, J. T., Herndon, S. C., Trimborn, A. M., Williams, L. R., Wood, E. C., Middlebrook, A. M., Kolb, C. E., Baltensperger, U., and Worsnop, D. R.: Evolution of organic aerosols in the atmosphere, Science, 326, 1525-1529, 10.1126/science.1180353, 2009.

Jiskra, M., Wiederhold, J. G., Bourdon, B., and Kretzschmar, R.: Solution speciation controls mercury isotope fractionation of Hg(II) sorption to Goethite, Environmental Science & Technology, 46, 6654-6662, 10.1021/es3008112, 2012.

tog bort: Vapor Pressure
formaterade: Teckenfärg: Blå
tog bort: Mercury
formaterade: Teckenfärg: Blå
tog bort: -
formaterade: Teckenfärg: Blå
tog bort: A
formaterade: Teckenfärg: Blå
tog bort: Understanding Atmospheric Mercury Hampered
formaterade: Teckenfärg: Blå
tog bort: Uncertain Measurements
formaterade: Teckenfärg: Blå
tog bort: Vibrational Frequencies
formaterade: Teckenfärg: Blå
tog bort: Bond Energies
formaterade: Teckenfärg: Blå
tog bort: Species Formed
formaterade: Teckenfärg: Blå
tog bort: Atmospheric Mercury Depletion Events, The
formaterade: Teckenfärg: Blå
tog bort: Organic Aerosols
formaterade: Teckenfärg: Blå
tog bort: Atmosphere
formaterade: Teckenfärg: Blå
tog bort: Speciation Controls Mercury Isotope Fractionation
formaterade: Teckenfärg: Blå
tog bort: Sorption
formaterade: Teckenfärg: Blå

Jiskra, M., Sonke, J. E., Agnan, Y., Helmig, D., and Obrist, D.: Insights from mercury stable isotopes on terrestrial–atmosphere exchange of Hg^0 in the Arctic tundra, Biogeosciences, 16, 4051-4064, 2019.

Jiskra, M., Wiederhold, J. G., Skyllberg, U., Kronberg, R.-M., and Kretzschmar, R.: Source tracing of natural organic matter bound mercury in boreal forest runoff with mercury stable isotopes, Environmental Science-Processes & Impacts, 19, 1235-1248, 10.1039/c7em00245a, 2017.

Jiskra, M., Wiederhold, J. G., Skyllberg, U., Kronberg, R. M., Hajdas, I., and Kretzschmar, R.: Mercury deposition and re-emission pathways in boreal forest soils investigated with Hg isotope signatures, Environmental Science & Technology, 49, 7188-7196, 2015.

Jiskra, M., Heimbürger-Boavida, L.-E., Desgranges, M.-M., Petrova, M. V., Dufour, A., Ferreira-Araujo, B., Masbou, J., Chmeleff, J., Thyssen, M., Point, D., and Sonke, J. E.: Mercury stable isotopes constrain atmospheric sources to the ocean, Nature, 597, 678-682, 10.1038/s41586-021-03859-8, 2021.

Jiskra, M., Sonke, J. E., Obrist, D., Bieser, J., Ebinghaus, R., Myhre, C. L., Pfaffhuber, K. A., Wängberg, I., Kyllönen, K., Worthy, D., Martin, L. G., Labuschagne, C., Mkololo, T., Ramonet, M., Magand, O., and Dommergue, A.: A vegetation control on seasonal variations in global atmospheric mercury concentrations, Nature Geoscience, 11, 244-251, 10.1038/s41561-018-0078-8, 2018.

Johnson, K. P., Blum, J. D., Keeler, G. J., and Douglas, T. A.: Investigation of the deposition and emission of mercury in arctic snow during an atmospheric mercury depletion event, Journal of Geophysical Research-Atmospheres, 113, 10.1029/2008jd009893, 2008.

Jones, C. P., Lyman, S. N., Jaffe, D. A., Allen, T., and O'Neil, T. L.: Detection and quantification of gas-phase oxidized mercury compounds by GC/MS, Atmospheric Measurement Techniques, 9, 2195-2205, 10.5194/amt-9-2195-2016, 2016.

Jordan, K. J., Bascal, H. A., Lipson, R. H., and Melchior, M.: The $B^2\Sigma^+ \leftarrow X^2\Sigma^+$ transition of HgI, Journal of Molecular Spectroscopy, 159, 144-155, 10.1006/jmsp.1993.1113, 1993.

Jungbluth, H., Beyrich, J., and Asmus, K. D.: Reduction of mercuric halides and pseudohalides in aqueous solution. Formation and some physicochemical properties of HgCl, HgBr, HgI, HgSCN, and HgCN radical molecules, Journal of Physical Chemistry, 80, 1049-1053, 10.1021/j100551a004, 1976.

Kallend, A. S. and Purnell, J. H.: Gas-Phase thermal decomposition of dimethyl mercury. 2. Homogeneous reaction, Transactions of the Faraday Society, 60, 103-&, 10.1039/tf9646000103, 1964.

Kaluza, U. and Boehm, H. P.: Titanium dioxide catalyzed photooxidation of mercury, Journal of Catalysis, 22, 347-358, 10.1016/0021-9517(71)90206-5, 1971.

Karakyriakos, E. and McKinley, A. J.: Matrix isolated $HgCH_3$ radical: An ESR investigation, Journal of Physical Chemistry A, 108, 4619-4626, 10.1021/jp0400925, 2004.

Khalizov, A. and Mao, N.: Heterogeneous reaction of gaseous mercuric chloride with atmospherically relevant organic films, ACS Earth and Space Chemistry, 7, 10.1021/acsearthspacechem.3c00268, 2023.

Khalizov, A., Guzman, F., Cooper, M., Mao, N., Antley, J., and Bozzelli, J.: Direct detection of gas-phase mercuric chloride by ion drift - Chemical ionization mass spectrometry, Atmospheric Environment, 238, 117687, 10.1016/j.atmosenv.2020.117687, 2020.

Khalizov, A. F., Viswanathan, B., Larregaray, P., and Ariya, P. A.: A theoretical study on the reactions of Hg with halogens: Atmospheric implications, Journal of Physical Chemistry A, 107, 6360-6365, 2003.

Khiri, D., Louis, F., Cernusak, I., and Dibble, T. S.: $BrHgO^{\bullet}$ + CO: Analogue of OH plus CO and reduction path for Hg(II) in the atmosphere, ACS Earth and Space Chemistry, 4, 1777-1784, 2020.

Kim, P. R., Han, Y. J., Holsen, T. M., and Yi, S. M.: Atmospheric particulate mercury: Concentrations and size distributions, Atmospheric Environment, 61, 94-102, 2012.

Kleszczewska, E.: The spectrophotometry determination of chelate complex: L-ascorbic acid with cuprum (II) and mercury (II) in alkaline solution, Polish Journal of Environmental Studies, 8, 313-318, 1999.

Kobayashi, T.: Oxidantion of metallic mercury in aqueous solution by hydrogen peroxide and chlorine, Journal of Japan Society of Air Pollution, 22, 230-236, 10.11298/taiki1978.22.230, 1987.

Knight Jr., L. B. and Lin, K. C.: ESR spectroscopy and chemical bonding in CdCN and HgCN molecules, Journal of Chemical Physics, 56, 6044-6049, 10.1063/1.1677153, 1972.

Knight Jr., L. B., Fisher, T. A., and Wise, M. B.: Photolytic codeposition generation of the HgF radical in an argon matrix at 12 K: An ESR investigation, The Journal of Chemical Physics, 74, 6009-6013, 10.1063/1.441040, 1981.

tog bort: Deposition
formaterade ... [1151]
tog bort: Re
formaterade ... [1152]
tog bort: Pathways
formaterade ... [1153]
tog bort: Boreal Forest Soils Investigated
formaterade ... [1154]
tog bort: Isotope Signatures
formaterade ... [1155]
formaterade ... [1156]
formaterade ... [1157]
formaterade ... [1158]
tog bort: Transition
formaterade ... [1159]
flyttade ned [14]: Knight Jr., L. B. and Lin, K. C.: ES ... [1160]
tog bort: Spectroscopy and Chemical Bonding in CdCN ... [1161]
flyttade ned [16]: Knight Jr., L. B., Fisher, T. A., and Wise, M.
formaterade ... [1162]
formaterade ... [1163]
tog bort: Thermal Decomposition
formaterade ... [1164]
tog bort: Dimethyl Mercury
formaterade ... [1165]
tog bort: Reaction
formaterade ... [1166]
formaterade ... [1167]
tog bort: Isolated
formaterade ... [1168]
tog bort: Radical
tog bort: Investigation, The
formaterade ... [1169]
formaterade ... [1170]
formaterade ... [1171]
tog bort: Reaction
formaterade ... [1172]
tog bort: Gaseous Mercuric Chloride
formaterade ... [1173]
tog bort: Atmospherically Relevant Organic Films
formaterade ... [1174]
formaterade ... [1175]
formaterade ... [1176]
tog bort: Reduction Path
formaterade ... [1177]
tog bort: Atmosphere
formaterade ... [1178]
flyttade (infogning) [17]
flyttade upp [17]: Kim, P. R., Han, Y. J., Holsen, T. M., and Yi,
tog bort: Spectrophotometry Determination
formaterade ... [1179]
tog bort: Chelate Complex
formaterade ... [1180]
tog bort: Ascorbic Acid
formaterade ... [1181]
tog bort: Cuprum
formaterade ... [1182]
tog bort: Mercury
formaterade ... [1183]
tog bort: Alkaline Solution
formaterade ... [1184]
tog bort: Metallic Mercury
formaterade ... [1185]
tog bort: Aqueous Solution
formaterade ... [1186]
tog bort: Hydrogen Peroxide
formaterade ... [1187]
tog bort: Chlorine
formaterade ... [1188]

Koenig, A., Sonke, J., Magand, O., Andrade, M., Moreno R, C. I., Velarde, F., Forno, R., Gutierrez, R., Blacutt, L., Laj, P., Ginot, P., Bieser, J., Zahn, A., Slemr, F., and Dommergue, A.: Evidence for interhemispheric mercury exchange in the Pacific Ocean upper troposphere, Journal of Geophysical Research: Atmospheres, 127, 10.1029/2021JD036283, 2022.

Koenig, T. K., Baidar, S., Campuzano-Jost, P., Cuevas, C. A., Dix, B., Fernandez, R. P., Guo, H., Hall, S. R., Kinnison, D., Nault, B. A., Ullmann, K., Jimenez, J. L., Saiz-Lopez, A., and Volkamer, R.: Quantitative detection of iodine in the stratosphere, Proceedings of the National Academy of Sciences, 117, 1860-1866, doi:10.1073/pnas.1916828117, 2020.

Kominar, R. J. and Price, S. J.: Determination of bond dissociation energy D(CH_3Hg-CH_3) by toluene carrier method, Canadian Journal of Chemistry, 47, 991-&, 10.1139/v69-156, 1969.

Kornev, V. I. and Kardapol'tsev, A. A.: Heteroligand mercury(II) complexes with aspartic, tartaric, and citric acids, Russian Journal of Coordination Chemistry, 34, 896-900, 10.1134/s107032840812004x, 2008.

Kozin, L. F. and Hansen, S. C.: Mercury Handbook: Chemistry, Applications and Environmental Impact, Royal Society of Chemistry, London, UK, 2013.

Kramida, A., Ralchenko, Y., Reader, J., and Team, N. A.: NIST Atomic Spectra Database (version 5.11), 10.18434/T4W30F, 2023.

Kritee, K., Blum, J. D., Reinfelder, J. R., and Barkay, T.: Microbial stable isotope fractionation of mercury: A synthesis of present understanding and future directions, Chemical Geology, 336, 13-25, 10.1016/j.chemgeo.2012.08.017, 2013.

Kritee, K., Blum, J. D., Johnson, M. W., Bergquist, B. A., and Barkay, T.: Mercury stable isotope fractionation during reduction of Hg(II) to Hg(0) by mercury resistant microorganisms, Environmental Science & Technology, 41, 1889-1895, 2007.

Kritee, K., Motta, L. C., Blum, J. D., Tsui, M. T. K., and Reinfelder, J. R.: Photomicrobial visible light-induced magnetic mass independent fractionation of mercury in a marine microalga, ACS Earth and Space Chemistry, 2, 432-440, 10.1021/acsearthspacechem.7b00056, 2018.

Kurien, U., Hu, Z., Lee, H., Dastoor, A. P., and Ariya, P. A.: Radiation enhanced uptake of Hg^0(g) on iron (oxyhydr)oxide nanoparticles, RSC Advances, 7, 45010-45021, 10.1039/C7RA07401H, 2017.

Kurz, A., Blum, J., Johnson, M., Nadelhoffer, K., and Zak, D.: Isotopic composition of mercury deposited via snow into mid-latitude ecosystems, Science of the Total Environment, 784, 147252, 10.1016/j.scitotenv.2021.147252, 2021.

Kurz, A. Y., Blum, J. D., Gratz, L. E., and Jaffe, D. A.: Contrasting controls on the diel isotopic variation of Hg^0 at two high elevation sites in the Western United States, Environmental Science & Technology, 54, 10502-10513, 2020.

Kwon, S. Y., Blum, J. D., Yin, R., Tsui, M. T.-K., Yang, Y. H., and Choi, J. W.: Mercury stable isotopes for monitoring the effectiveness of the Minamata Convention on Mercury, Earth-Science Reviews, 203, 103-111, 2020.

Lalonde, J. D., Poulain, A. J., and Amyot, M.: The role of mercury redox reactions in snow on snow-to-air mercury transfer, Environmental Science & Technology, 2002, 36, 174-178, 2002.

Lalonde, J. D., Amyot, M., Doyon, M. R., and Auclair, J. C.: Photo-induced Hg(II) reduction in snow from the remote and temperate Experimental Lakes Area (Ontario, Canada), Journal of Geophysical Research-Atmospheres, 108, art. no.-4200, 2003.

Lalonde, J. D., Amyot, M., Kraepiel, A. M. L., and Morel, F. M. M.: Photooxidation of Hg(0) in artificial and natural waters, Environmental Science & Technology, 35, 1367-1372, 2001.

Lam, K. T.: Chemistry and implications of a previously unknown intermediate in the atmospheric mercury oxidation, Ph. D. thesis, College of Environmental Science and Forestry, State University of New York, Syracuse, NY, 2019.

Lam, K. T., Wilhelmsen, C. J., and Dibble, T. S.: $BrHgO^{\bullet}$ + C_2H_4 and $BrHgO^{\bullet}$ + HCHO in atmospheric oxidation of mercury: determining rate constants of reactions with prereactive complexes and bifurcation, Journal of Physical Chemistry A, 123, 6045-6055, 10.1021/acs.jpca.9b05120, 2019a.

Lam, K. T., Wilhelmsen, C. J., Schwid, A. C., Jiao, Y., and Dibble, T. S.: Computational study on the photolysis of BrHgONO and the reactions of $BrHgO^{\bullet}$ with CH_4, C_2H_6, NO, and NO_2: Implications for formation of Hg(II) compounds in the atmosphere, Journal of Physical Chemistry A, 123, 1637-1647, 2019b.

Lamborg, C. H., Fitzgerald, W. F., O'Donnell, J., and Torgersen, T.: A non-steady-state compartmental model of global-scale mercury biogeochemistry with interhemispheric atmospheric gradients, Geochimica et Cosmochimica Acta, 66, 1105-1118, 2002.

Lan, X., Talbot, R., Castro, M., Perry, K., and Luke, W.: Seasonal and diurnal variations of atmospheric mercury across the US determined from AMNet monitoring data, Atmospheric Chemistry and Physics, 12, 10569-10582, 10.5194/acp-12-10569-2012, 2012.

tog bort: Interhemispheric Mercury Exchange
formaterade ... [1192]
tog bort: Upper Troposphere
formaterade ... [1193]
tog bort: Toluene Carrier Method
formaterade ... [1194]
formaterade ... [1196]
Formaterat ... [1195]
tog bort: Bond Dissociation Energy
formaterade ... [1197]
tog bort: Of
formaterade ... [1198]
tog bort: Stable Isotope Fractionation
formaterade ... [1199]
tog bort: Reduction
formaterade ... [1200]
tog bort: Mercury Resistant Microorganisms
formaterade ... [1201]
formaterade ... [1202]
tog bort: Visible Light-Induced Magnetic Mass Indepen ... [1203]
formaterade ... [1204]
formaterade ... [1205]
tog bort: The
formaterade ... [1206]
tog bort: Controls
formaterade ... [1207]
tog bort: Diel Isotopic Variation
formaterade ... [1208]
tog bort: Two High Elevation Sites
formaterade ... [1209]
formaterade ... [1210]
formaterade ... [1211]
tog bort: Implications
formaterade ... [1212]
tog bort: Previously-Unknown Intermediate
formaterade ... [1213]
tog bort: Atmospheric Mercury Oxidation
formaterade ... [1214]
tog bort: Atmospheric Oxidation
formaterade ... [1215]
tog bort: Mercury: Determining Rate Constants
formaterade ... [1216]
tog bort: Reactions
formaterade ... [1217]
tog bort: Prereactive Complexes
formaterade ... [1218]
tog bort: Bifurcation
formaterade ... [1219]
tog bort: Study
formaterade ... [1220]
tog bort: Photolysis
formaterade ... [1221]
tog bort: Reactions
formaterade ... [1222]
tog bort: Formation
formaterade ... [1223]
tog bort: Compounds
formaterade ... [1224]
tog bort: Atmosphere, The
formaterade ... [1225]
formaterade ... [1226]
Formaterat ... [1227]
formaterade ... [1228]

Landis, M. S., Stevens, R. K., Schaedlich, F., and Prestbo, E. M.: Development and characterization of an annular denuder methodology for the measurement of divalent inorganic reactive gaseous mercury in ambient air, Environmental Science & Technology, 36, 3000-3009, 10.1021/es015887t, 2002.

Lauretta, D. S., Klaue, B., Blum, J. D., and Buseck, P. R.: Mercury abundances and isotopic compositions in the Murchison (CM) and Allende (CV) carbonaceous chondrites, Geochimica et Cosmochimica Acta, 65, 2807-2818, 10.1016/S0016-7037(01)00630-5, 2001.

Lee, C. F., Elgiar, T., David, L. M., Wilmot, T. Y., Reza, M., Hirshorn, N., McCubbin, I. B., Shah, V., Lin, J. C., Lyman, S. N., Hallar, A. G., Gratz, L. E., and Volkamer, R.: Elevated tropospheric iodine over the central continental United States: Is iodine a major oxidant of atmospheric mercury?, Geophysical Research Letters, 51, e2024GL109247, 10.1029/2024GL109247, 2024.

Lee, H., Kurien, U., and Ariya, P. A.: Uptake of Hg^0 (g) on TiO_2, Al_2O_3, and Fe_2O_3 nanoparticles: Importance in atmospheric chemical and physical processes, Journal of Physical Chemistry A, 10.1021/acs.jpca.2c03428, 2022.

Lee, S., Kim, D.-H., and Kim, K.-W.: The enhancement and inhibition of mercury reduction by natural organic matter in the presence of Shewanella oneidensis MR-1, Chemosphere, 194, 515-522, 10.1016/j.chemosphere.2017.12.007, 2018.

Lee, Y. H., Wängberg, I., and Munthe, J.: Sampling and analysis of gas-phase methylmercury in ambient air, Science of the Total Environment, 304, 107-113, 2003.

Lehtipalo, K., Nieminen, T., Schobesberger, S., Ehn, M., Kulmala, M., and Kerminen, V.-M.: How the understanding of atmospheric new particle formation has evolved along with the development of measurement and analysis methods, Journal of Aerosol Science, 184, 106494, 10.1016/j.jaerosci.2024.106494, 2025.

Leonori, D. and Sturgeon, R. E.: A unified approach to mechanistic aspects of photochemical vapor generation, Journal of Analytical Atomic Spectrometry, 34, 636-654, 10.1039/c8ja00354h, 2019.

Li, C., Enrico, M., Magand, O., Araujo, B., Le Roux, G., Osterwalder, S., Dommergue, A., Bertrand, Y., Brioude, J., Vleeschouwer, F., and Sonke, J.: A peat core Hg stable isotope reconstruction of Holocene atmospheric Hg deposition at Amsterdam Island (37.8°S), Geochimica et Cosmochimica Acta, 341, 10.1016/j.gca.2022.11.024, 2022a.

Li, C., Jiskra, M., Nilsson, M., Osterwalder, S., Zhu, W., Mauquoy, D., Skyllberg, U., Enrico, M., Haijun, P., Song, Y., Björn, E., and Bishop, K.: Mercury deposition and redox transformation processes in peatland constrained by mercury stable isotopes, Nature Communications, 14, 10.1038/s41467-023-43164-8, 2023a.

Li, C., Chen, J., Angot, H., Zheng, W., Shi, G., Ding, M., Du, Z., Zhang, Q., Ma, X., Kang, S., Xiao, C., Ren, J., and Qin, D.: Seasonal variation of mercury and its isotopes in atmospheric particles at the coastal Zhongshan station, eastern Antarctica, Environmental Science & Technology, 54, 11344-11355, 10.1021/acs.est.0c04462, 2020a.

Li, L., Wang, X., Fu, H., Qu, X., Chen, J., Tao, S., and Zhu, D.: Dissolved black carbon facilitates photoreduction of Hg(II) to Hg(0) and reduces mercury uptake by lettuce (*Lactuca sativa L.*), Environmental Science & Technology, 54, 11137-11145, 10.1021/acs.est.0c01132, 2020b.

Li, M.-L., Kwon, S. Y., Poulin, B. A., Tsui, M. T.-K., Motta, L. C., and Cho, M.: Internal dynamics and metabolism of mercury in biota: A review of insights from mercury stable isotopes, Environmental Science & Technology, 56, 9182-9195, 10.1021/acs.est.1c08631, 2022b.

Li, T., Wang, Y., Mao, H., Wang, S., Talbot, R. W., Zhou, Y., Wang, Z., Nie, X., and Qie, G.: Insights on chemistry of mercury species in clouds over northern China: Complexation and adsorption, Environmental Science & Technology, 52, 5125-5134, 10.1021/acs.est.7b06669, 2018.

Li, X., Wang, X., Zhang, H., and Lu, Z.: Mosses and lichens enhance atmospheric elemental mercury deposition in a subtropical montane forest, Environmental Chemistry, 20, 105-113, 10.1071/EN22124, 2023b.

Li, X. S., Yan, M., Dibble, T. S., and Zhang, L. Q.: Reaction mechanism and kinetics of the important but neglected reaction of Hg with NO_2 at low temperature, Chemical Engineering Journal, 432, 10.1016/j.cej.2021.134373, 2022c.

Lian, P., Guo, L., Devarajan, D., Parks, J. M., Painter, S. L., Brooks, S. C., and Smith, J. C.: The AQUA-MER databases and aqueous speciation server: A web resource for multiscale modeling of mercury speciation, Journal of Computational Chemistry, 41, 147-155, 10.1002/jcc.26081, 2020.

Lide, D. R. (Ed.) CRC handbook of chemistry and physics, 89th Ed., CRC Press/Taylor and Francis, Boca Raton, FL, 2008.

Lin, C.-J., Singhasuk, P., and Pehkonen, S. O.: Atmospheric chemistry of mercury, in: Environmental chemistry and toxicology of mercury, edited by: Liu, G., Cai, Y., and O'Driscoll, N., John Wiley & Sons, 113 - 154, 2011.

Lin, C.-J., Zhu, W., Li, X., Feng, X., Sommar, J., and Shang, L.: Novel dynamic flux chamber for measuring air-surface exchange of Hg^0 from soils, Environmental Science & Technology, 46, 8910-8920, 10.1021/es3012386, 2012.

formaterade ... [1229]
formaterade ... [1230]
formaterade ... [1231]
tog bort: Tropospheric Iodine Over
tog bort: Central Continental
tog bort: Iodine
formaterade ... [1232]
formaterade ... [1233]
formaterade ... [1234]
tog bort: Major Oxidant
formaterade ... [1235]
tog bort: Atmospheric Mercury
formaterade ... [1236]
tog bort: Nanoparticles
tog bort: Atmospheric Chemical
formaterade ... [1237]
formaterade ... [1238]
tog bort: Physical Processes
formaterade ... [1239]
formaterade ... [1240]
tog bort: Wangberg
formaterade ... [1241]
formaterade ... [1242]
Formaterat ... [1243]
formaterade ... [1244]
formaterade ... [1245]
formaterade ... [1246]
formaterade ... [1247]
tog bort: Variation
formaterade ... [1248]
tog bort: Mercury
formaterade ... [1249]
tog bort: Its Isotopes
formaterade ... [1250]
tog bort: Atmospheric Particles
formaterade ... [1251]
tog bort: Coastal
formaterade ... [1252]
tog bort: Station, Eastern
formaterade ... [1253]
tog bort: Black Carbon Facilitates Photoreduction
formaterade ... [1254]
tog bort: Reduces Mercury Uptake
formaterade ... [1255]
tog bort: Lettuce
formaterade ... [1256]
formaterade ... [1257]
tog bort: Dynamics
formaterade ... [1258]
tog bort: Metabolism
formaterade ... [1259]
tog bort: Mercury
formaterade ... [1260]
tog bort: Biota
formaterade ... [1261]
tog bort: Review
formaterade ... [1262]
tog bort: Insights
formaterade ... [1263]
tog bort: Mercury Stable Isotopes
formaterade ... [1264]
formaterade ... [1265]
tog bort: Chemistry
formaterade ... [1266]
tog bort: Mercury Species
formaterade ... [1267]
tog bort: Clouds
formaterade ... [1268]

Lin, C. J. and Pehkonen, S. O.: Aqueous free radical chemistry of mercury in the presence of iron oxides and ambient aerosol, Atmospheric Environment, 31, 4125-4137, 1997.

Lin, C. J. and Pehkonen, S. O.: Two-phase model of mercury chemistry in the atmosphere, Atmospheric Environment, 32, 2543-2558, 1998a.

Lin, C. J. and Pehkonen, S. O.: Oxidation of elemental mercury by aqueous chlorine ($HOCl/OCl^-$): Implications for tropospheric mercury chemistry, Journal of Geophysical Research-Atmospheres, 103, 28093-28102, 1998b.

Lin, C. J. and Pehkonen, S. O.: The chemistry of atmospheric mercury: A review, Atmospheric Environment, 33, 2067-2079, 1999.

Lin, C. J., Pongprueksa, P., Lindberg, S. E., Pehkonen, S. O., Byun, D., and Jang, C.: Scientific uncertainties in atmospheric mercury models I: Model science evaluation, Atmospheric Environment, 40, 2911-2928, 2006.

Lin, C. J., Pongprueksa, P., Russell Bullock Jr, O., Lindberg, S. E., Pehkonen, S. O., Jang, C., Braverman, T., and Ho, T. C.: Scientific uncertainties in atmospheric mercury models II: Sensitivity analysis in the CONUS domain, Atmospheric Environment, 41, 6544-6560, 2007.

Lin, M. and Thiemens, M. H.: 40 years of theoretical advances in mass-independent oxygen isotope effects and applications in atmospheric chemistry: A critical review and perspectives, Applied Geochemistry, 161, 10.1016/j.apgeochem.2023.105860, 2024.

Lindberg, S. E. and Stratton, W. J.: Atmospheric mercury speciation: Concentrations and behavior of reactive gaseous mercury in ambient air, Environmental Science & Technology, 32, 49-57, 1998.

Lindberg, S. E., Southworth, G., Prestbo, E. M., Wallschlager, D., Bogle, M. A., and Price, J.: Gaseous methyl- and inorganic mercury in landfill gas from landfills in Florida, Minnesota, Delaware, and California, Atmospheric Environment, 39, 249-258, 2005.

Lindqvist, O. and Rodhe, H.: Atmospheric Mercury - A Review, Tellus Series B, 37, 136-159, 1985.

Lindqvist, O., Johansson, K., Aastrup, M., Andersson, A., Bringmark, L., Hovsenius, G., Håkanson, L., Iverfeldt, Å., Meili, M., and Timm, B.: Mercury in the Swedish environment - Recent research on causes, Consequences and corrective methods, Water Air and Soil Pollution, 55, 1-261, 1991.

Liu, E., Makarov, I. E., and Pikaev, A. K.: Pulse-radiolysis of alkaline aqueous-solutions of divalent mercury compounds, High Energy Chemistry, 17, 41-46, 1983.

Liu, K., Wu, Q., Wang, S., Chang, X., Tang, Y., Wang, L., Liu, T., Zhang, L., Zhao, Y., Wang, Q., and Chen, J.: Improved atmospheric mercury simulation using updated gas-particle partition and organic aerosol concentrations, Journal of Environmental Sciences, 119, 106-118, 10.1016/j.jes.2022.04.007, 2022.

Liu, Q. and Margerum, D. W.: Equilibrium and kinetics of bromine chloride hydrolysis, Environmental Science & Technology, 35, 1127-1133, 2001.

Liu, T.: Oxidation of aqueous elemental mercury through the Fenton reaction, M Sc. Thesis, Tennessee Technological University, USA, 106 pp., 2011.

Liu, Y., Lin, C.-J., Yuan, W., Lu, Z., and Feng, X.: Translocation and distribution of mercury in biomasses from subtropical forest ecosystems: evidence from stable mercury isotopes, Acta Geochimica, 40, 42-50, 10.1007/s11631-020-00441-3, 2021a.

Liu, Y., Liu, H., Guo, Y., lu, D., Hou, X., Shi, J., Yin, Y., Cai, Y., and Jiang, G.: Atmospheric Hg(0) dry deposition over environmental surfaces: Insights from mercury isotope fractionation, Eco-Environment & Health, 10.1016/j.eehl.2024.04.009, 2024.

Liu, Y., Tao, H., Wang, Y., Fang, Y., Xiang, Y., Liu, G., Guo, Y., Liu, J., Yin, Y., Cai, Y., and Jiang, G.: Gaseous elemental mercury [$Hg^{(0)}$] oxidation in poplar leaves through a two-step single-electron transfer process, Environmental Science & Technology Letters, 8, 1098-1103, 10.1021/acs.estlett.1c00735, 2021b.

Loewenschuss, A., Ron, A., and Schnepp, O.: Vibrational spectra of group IIB halides. II. The halides of cadmium and mercury, Journal of Chemical Physics, 50, 2502-2512, 10.1063/1.1671408, 1969.

Love, L. O.: Electromagnetic separation of isotopes at Oak Ridge, Science, 182, 343-352, 10.1126/science.182.4110.343, 1973.

Lu, X., Zhao, J., Liang, X., Zhang, L., Liu, Y., Yin, X., Li, X., and Gu, B.: The application and potential artifacts of Zeeman cold vapor atomic absorption spectrometry in mercury stable isotope analysis, Environmental Science & Technology Letters, 6, 165-170, 10.1021/acs.estlett.9b00067, 2019.

Lyman, S. and Jaffe, D.: Formation and fate of oxidized mercury in the upper troposphere and lower stratosphere, Nature Geoscience, 5, 114 - 117, 2012.

tog bort: Environment
tog bort: Research
formaterade: Teckenfärg: Blå, Kondenserad med 0,2 pt
tog bort: Causes
formaterade: Teckenfärg: Blå, Kondenserad med 0,2 pt
formaterade: Teckenfärg: Blå, Kondenserad med 0,2 pt
tog bort: Corrective Methods
formaterade: Teckenfärg: Blå, Kondenserad med 0,2 pt
formaterade: Teckenfärg: Blå, Kondenserad med 0,4 pt
tog bort: . g
formaterade: Teckenfärg: Blå, Kondenserad med 0,4 pt
formaterade: Teckenfärg: Blå, Kondenserad med 0,3 pt
formaterade: Teckenfärg: Blå, Kondenserad med 0,2 pt
formaterade: Teckenfärg: Blå, Kondenserad med 0,3 pt
tog bort: Elemental Mercury
formaterade: Teckenfärg: Blå, Kondenserad med 0,2 pt
formaterade: Teckenfärg: Blå, Kondenserad med 0,2 pt
tog bort: Oxidation
formaterade: Teckenfärg: Blå, Kondenserad med 0,2 pt
tog bort: Poplar Leaves
formaterade: Teckenfärg: Blå, Kondenserad med 0,2 pt
tog bort: Two-Step Single-Electron Transfer Process
formaterade: Teckenfärg: Blå, Kondenserad med 0,2 pt
formaterade: Teckenfärg: Blå, Kondenserad med 0,2 pt
Formaterat: Avstånd Efter: 0,6 Rad, Radavstånd: Flera 1,1 li
tog bort: Separation
formaterade: Teckenfärg: Blå, Kondenserad med 0,2 pt
tog bort: Isotopes
formaterade: Teckenfärg: Blå, Kondenserad med 0,2 pt
tog bort: Application
tog bort: Potential Artifacts
formaterade: Teckenfärg: Blå, Kondenserad med 0,2 pt
tog bort: Cold Vapor Atomic Absorption Spectrometry
formaterade: Teckenfärg: Blå, Kondenserad med 0,2 pt
formaterade: Teckenfärg: Blå, Kondenserad med 0,2 pt
tog bort: Mercury Stable Isotope Analysis
formaterade: Teckenfärg: Blå, Kondenserad med 0,2 pt

Lyman, S. N., Jaffe, D. A., and Gustin, M. S.: Release of mercury halides from KCl denuders in the presence of ozone, Atmospheric Chemistry and Physics, 10, 8197-8204, 10.5194/acp-10-8197-2010, 2010.

Lyman, S. N., Cheng, I., Gratz, L. E., Weiss-Penzias, P., and Zhang, L.: An updated review of atmospheric mercury, Science of The Total Environment, 707, 135575, 2020a.

Lyman, S. N., Gratz, L. E., Dunham-Cheatham, S. M., Gustin, M. S., and Luippold, A.: Improvements to the accuracy of atmospheric oxidized mercury measurements, Environmental Science & Technology, 54, 13379-13388, 10.1021/acs.est.0c02747, 2020b.

Lyman, S. N., Elgiar, T., Gustin, M. S., Dunham-Cheatham, S. M., David, L. M., and Zhang, L.: Evidence against rapid mercury oxidation in photochemical smog, Environmental Science & Technology, 10.1021/acs.est.2c02224, 2022.

Maguire, R. J. and Anand, S.: Kinetics of acidolysis of dimethyl mercury, Journal of Inorganic & Nuclear Chemistry, 38, 1167-1169, 1976.

Malcolm, E. G., Keeler, G. J., Lawson, S. T., and Sherbatskoy, T. D.: Mercury and trace elements in cloud water and precipitation collected on Mt. Mansfield, Vermont, Journal of Environmental Monitoring, 5, 584-590, 2003.

Malcolm, E. G., Ford, A. C., Redding, T. A., Richardson, M. C., Strain, B. M., and Tetzner, S. W.: Experimental investigation of the scavenging of gaseous mercury by sea salt aerosol, Journal of Atmospheric Chemistry, 63, 221-234, 2009.

Malinovsky, D. and Vanhaecke, F.: Mercury isotope fractionation during abiotic transmethylation reactions, International Journal of Mass Spectrometry, 307, 214-224, 2011.

Malinovsky, D., Latruwe, K., Moens, L., and Vanhaecke, F.: Experimental study of mass-independence of Hg isotope fractionation during photodecomposition of dissolved methylmercury, Journal of Analytical Atomic Spectrometry, 25, 950-956, 2010.

Mangiante, D. M., Schaller, R. D., Zarzycki, P., Banfield, J. F., and Gilbert, B.: Mechanism of ferric oxalate photolysis, ACS Earth and Space Chemistry, 1, 270-276, 10.1021/acsearthspacechem.7b00026, 2017.

Mao, H., Cheng, I., and Zhang, L.: Current understanding of the driving mechanisms for spatiotemporal variations of atmospheric speciated mercury: A review, Atmospheric Chemistry and Physics, 16, 12897-12924, 10.5194/acp-16-12897-2016, 2016.

Mao, H., Talbot, R. W., Sigler, J. M., Sive, B. C., and Hegarty, J. D.: Seasonal and diurnal variations of Hg^0 over New England, Atmospheric Chemistry and Physics, 8, 1401-1421, 2008.

Mao, N. and Khalizov, A.: Exchange reactions alter molecular speciation of gaseous oxidized mercury, ACS Earth and Space Chemistry, 5, 10.1021/acsearthspacechem.1c00178, 2021.

Mao, N., Antley, J., Cooper, M., Shah, N., Kadam, A., and Khalizov, A.: Heterogeneous chemistry of mercuric chloride on inorganic salt surfaces, Journal of Physical Chemistry A, 125, 10.1021/acs.jpca.1c02220, 2021.

Mariotti, A., Germon, J. C., Hubert, P., Kaiser, P., Letolle, R., Tardieux, A., and Tardieux, P.: Experimental determination of nitrogen kinetic isotope fractionation - Some principles - Illustration for the denitrification and nitrification processes, Plant and Soil, 62, 413-430, 10.1007/Bf02374138, 1981.

Martell, A. and Smith, R. M.: Critical stability constants: Vol. 3 Other Organic Ligands, Springer Science, 495 pp., 1977.

Martell, A. E. and Smith, R. M.: Critical stability constants: Vol. 4 Inorganic complexes, Springer Science, 257 pp., 1976.

Martell, A. E. and Smith, R. M.: Critical stability constants: Vol. 5 First Supplement, Springer Science, 604 pp., 1982.

Martens, J., Uchtmann, H., and Hensel, F.: Homogeneous nucleation of mercury vapor, Journal of Physical Chemistry, 91, 2489-2492, 10.1021/j100294a010, 1987.

Marusczak, N., Sonke, J. E., Fu, X., and Jiskra, M.: Tropospheric GOM at the Pic du Midi observatory—Correcting bias in denuder based observations, Environmental Science & Technology, 51, 863-869, 10.1021/acs.est.6b04999, 2017.

Maya, J.: Ultraviolet-absorption cross-sections of HgI_2, $HgBr_2$, and tin(II) halide vapors, Journal of Chemical Physics, 67, 4976-4980, 1977.

McClure, C. D., Jaffe, D. A., and Edgerton, E. S.: Evaluation of the KCl denuder method for gaseous oxidized mercury using $HgBr_2$ at an in-service AMNet site, Environmental Science & Technology, 48, 11437-11444, 2014.

McElroy, W. J. and Munthe, J.: The oxidation of mercury(I) by ozone in acidic aqueous solutions, Acta Chemica Scandinavica, 45, 254-257, 10.3891/acta.chem.scand.45-0254, 1991.

McKeown, F. P., Iyer, R. S., and Rowland, F. S.: Methyl fluoride formation from thermal ^{18}F reaction with dimethylmercury, Journal of Physical Chemistry, 87, 3972-3975, 10.1021/j100243a035, 1983.

tog bort: Accuracy
formaterade ... [1286]
tog bort: Atmospheric Oxidized Mercury Measurements
formaterade ... [1287]
formaterade ... [1288]
formaterade ... [1289]
tog bort: Rapid Mercury Oxidation in Photochemical Smog
formaterade ... [1290]
tog bort: Acidolysis
formaterade ... [1291]
tog bort: Dimethyl Mercury
formaterade ... [1292]
tog bort: Ferric Oxalate Photolysis
formaterade ... [1293]
formaterade ... [1294]
tog bort: a
formaterade ... [1295]
tog bort: Reactions Alter Molecular Speciation of Gase ... [1296]
formaterade ... [1297]
formaterade ... [1298]
tog bort: Chemistry of Mercuric Chloride on Inorganic ... [1299]
formaterade ... [1300]
tog bort: -Determination
formaterade ... [1301]
tog bort: Nitrogen Kinetic Isotope Fractionation
formaterade ... [1302]
tog bort: Principles
formaterade ... [1303]
tog bort: Denitrification
formaterade ... [1304]
tog bort: Nitrification Processes
formaterade ... [1305]
Formaterat ... [1306]
formaterade ... [1307]
tog bort: Critical stability constants,
formaterade ... [1308]
tog bort: .
formaterade ... [1309]
formaterade ... [1310]
Formaterat ... [1311]
tog bort: Plenum Pr., New York u.a.
formaterade ... [1312]
Formaterat ... [1313]
formaterade ... [1314]
formaterade ... [1315]
Formaterat ... [1316]
tog bort: Absorption Cross-Sections
formaterade ... [1317]
tog bort: Tin
formaterade ... [1318]
tog bort: Halide Vapors
formaterade ... [1319]
formaterade ... [1320]

Mead, C., Lyons, J. R., Johnson, T. M., and Anbar, A. D.: Unique Hg stable isotope signatures of compact fluorescent lamp-sourced Hg, Environmental Science & Technology, 47, 2542-2547, 2013.

Medhekar, A. K., Rokni, M., Trainor, D. W., and Jacob, J. H.: Surface catalyzed reaction of Hg + Cl_2, Chemical Physics Letters, 65, 600-604, 1979.

Miller, M. B., Dunham-Cheatham, S. M., Gustin, M. S., and Edwards, G. C.: Evaluation of cation exchange membrane performance under exposure to high Hg^0 and $HgBr_2$ concentrations, Atmospheric Measurement Techniques, 12, 1207-1217, 10.5194/amt-12-1207-2019, 2019.

Morand, J.-P. and Nief, G.: Oxydation isotopique du mercure par l'oxygène moléculaire sous l'influence de la radiation 2357 Å, Journal de Chimie Physique, 65, 2058-2068, 10.1051/jcp/1968652058, 1968.

Morton, D. C.: Atomic-data for resonance absorption lines. II. Wavelengths longward of the Lyman limit for heavy elements, Astrophysical Journal Supplement Series, 130, 403-436, 2000.

Moser, H. C. and Voigt, A. F.: Dismutation of the mercurous dimer in dilute solutions, Journal of the American Chemical Society, 79, 1837-1839, 10.1021/ja01565a019, 1957.

Motta, L. C., Chien, A. D., Rask, A. E., and Zimmerman, P. M.: Mercury magnetic isotope effect: A plausible photochemical mechanism, Journal of Physical Chemistry A, 124, 3711-3719, 2020a.

Motta, L. C., Kritee, K., Blum, J. D., Tsz-Ki Tsui, M., and Reinfelder, J. R.: Mercury isotope fractionation during the photochemical reduction of Hg(II) coordinated with organic ligands, Journal of Physical Chemistry A, 124, 2842-2853, 2020b.

Motta, L. C., Blum, J. D., Johnson, M. W., Umhau, B. P., Popp, B. N., Washburn, S. J., Drazen, J. C., Benitez-Nelson, C. R., Hannides, C. C. S., Close, H. G., and Lamborg, C. H.: Mercury cycling in the north Pacific subtropical gyre as revealed by mercury stable isotope ratios, Global Biogeochemical Cycles, 33, 777-794, 2019.

Mulliken, R. S.: The separation of isotopes application of systematic fractionation to mercury in a high-speed evaporation-diffusion apparatus, Journal of the American Chemical Society, 45, 1592-1604, 10.1021/ja01660a003, 1923.

Munthe, J.: The aqueous oxidation of elemental mercury by ozone, Atmospheric Environment. Part A, 26, 1461-1468, 10.1016/0960-1686(92)90131-4, 1992.

Munthe, J. and McElroy, W. J.: Some aqueous reactions of potential importance in the atmospheric chemistry of mercury, Atmospheric Environment Part A, 26, 553-557, 10.1016/0960-1686(92)90168-k, 1992.

Munthe, J., Xiao, Z. F., and Lindqvist, O.: The aqueous reduction of divalent mercury by sulfite, Water Air and Soil Pollution, 56, 621-630, 1991.

Murphy, D. M., Thomson, D. S., and Mahoney, M. J.: In situ measurements of organics, meteoritic material, mercury, and other elements in aerosols at 5 to 19 kilometers, Science, 282, 1664-1669, 1998.

Murphy, D. M., Hudson, P. K., Thomson, D. S., Sheridan, P. J., and Wilson, J. C.: Observations of mercury-containing aerosols, Environmental Science & Technology, 40, 3163-3167, 2006.

Murphy, D. M., Froyd, K. D., Schwarz, J. P., and Wilson, J. C.: Observations of the chemical composition of stratospheric aerosol particles, Quarterly Journal of the Royal Meteorological Society, 140, 1269-1278, 2014.

Nazhat, N. B. and Asmus, K. D.: Reduction of mercuric chloride by hydrated electrons and reducing radicals in aqueous-solutions - Formation and reactions of HgCl, Journal of Physical Chemistry, 77, 614-620, 1973.

Nerentorp Mastromonaco, M., Gårdfeldt, K., Jourdain, B., Abrahamsson, K., Granfors, A., Ahnoff, M., Dommergue, A., Méjean, G., and Jacobi, H. W.: Antarctic winter mercury and ozone depletion events over sea ice, Atmospheric Environment, 129, 125-132, 10.1016/j.atmosenv.2016.01.023, 2016.

Niki, H., Maker, P. D., Savage, C. M., and Breitenbach, L. P.: A long-path Fourier transform infrared study of the kinetics and mechanism for the HO-radical initiated oxidation of dimethylmercury, Journal of Physical Chemistry, 87, 4978-4981, 1983a.

Niki, H., Maker, P. S., Savage, C. M., and Breitenbach, L. P.: A Fourier transform infrared study of the kinetics and mechanism for the reaction Cl + CH_3HgCH_3, Journal of Physical Chemistry, 87, 3722-3724, 1983b.

Niksa, S., Helble, J. J., and Fujiwara, N.: Kinetic modeling of homogeneous mercury oxidation: The importance of NO and H_2O in predicting oxidation in coal- derived systems, Environmental Science & Technology, 35, 3701-3706, 2001.

Nriagu, J. (Ed.) The biogeochemistry of mercury in the environment, Elsevier/North- Holland Biomedical Press, 671 pp., 1979.

tog bort: Stable Isotope Signatures
formaterade ... [1321]
tog bort: Compact Fluorescent Lamp-Sourced
formaterade ... [1322]
formaterade ... [1323]
formaterade ... [1324]
tog bort: Catalyzed Reaction
formaterade ... [1325]
formaterade ... [1326]
formaterade ... [1327]
tog bort: J. Chim. Phys.,
formaterade ... [1328]
tog bort: lyman
formaterade ... [1329]
tog bort: Mercurous Dimer in Dilute Solutions
formaterade ... [1330]
formaterade ... [1331]
tog bort: Magnetic Isotope Effect
formaterade ... [1332]
formaterade ... [1333]
tog bort: Plausible Photochemical Mechanism
formaterade ... [1334]
tog bort: Isotope Fractionation
formaterade ... [1335]
tog bort: Photochemical Reduction
formaterade ... [1336]
tog bort: Coordinated
formaterade ... [1337]
tog bort: Organic Ligands
formaterade ... [1338]
tog bort: Cycling
formaterade ... [1339]
tog bort: North
formaterade ... [1340]
tog bort: Subtropical Gyre
formaterade ... [1341]
tog bort: Revealed
formaterade ... [1342]
tog bort: Mercury Stable Isotope Ratios
formaterade ... [1343]
formaterade ... [1344]
formaterade ... [1345]
tog bort: Aqueous Reduction
formaterade ... [1346]
tog bort: Divalent Mercury
formaterade ... [1347]
tog bort: Sulfite
formaterade ... [1348]
formaterade ... [1349]
Formaterat ... [1350]
formaterade ... [1351]
Formaterat ... [1352]
tog bort: Mercuric Chloride
formaterade ... [1353]
tog bort: Hydrated Electrons and Reducing Radicals
formaterade ... [1354]
tog bort: Aqueous-Solutions
formaterade ... [1355]
tog bort: Reactions
formaterade ... [1356]
tog bort: Long-Path
formaterade ... [1357]
tog bort: -Transform Infrared Study
formaterade ... [1358]
tog bort: Kinetics
formaterade ... [1359]
tog bort: Mechanism
formaterade ... [1360]

O'Concubhair, R., O'Sullivan, D., and Sodeau, J. R.: Dark oxidation of dissolved gaseous mercury in polar ice mimics, Environmental Science & Technology, 46, 4829-4836, 10.1021/es300309n, 2012.

Obrist, D., Pokharel, A. K., and Moore, C.: Vertical profile measurements of soil air suggest immobilization of gaseous elemental mercury in mineral soil, Environmental Science & Technology, 48, 2242-2252, 2014.

Obrist, D., Tas, E., Peleg, M., Matveev, V., Fain, X., Asaf, D., and Luria, M.: Bromine-induced oxidation of mercury in the mid-latitude atmosphere, Nature Geoscience, 4, 22-26, 2011.

Obrist, D., Agnan, Y., Jiskra, M., Olson, C. L., Colegrove, D. P., Hüber, J., Moore, C. W., Sonke, J. E., and Helmig, D.: Tundra uptake of atmospheric elemental mercury drives Arctic mercury pollution, Nature, 547, 201-204, 10.1038/nature22997, 2017.

Obrist, D., Roy, E. M., Harrison, J. L., Kwong, C. F., Munger, J. W., Moosmüller, H., Romero, C. D., Sun, S., Zhou, J., and Commane, R.: Previously unaccounted atmospheric mercury deposition in a midlatitude deciduous forest, Proceedings of the National Academy of Sciences, 118, e2105477118, 10.1073/pnas.2105477118, 2021.

Ogata, M. and Aikoh, H.: Mechanism of metallic mercury oxidation in vitro by catalase and peroxidase, Biochemical Pharmacology, 33, 490-493, 10.1016/0006-2952(84)90246-6, 1984.

Ogg, R. A., Martin, H. C., and Leighton, P. A.: Kinetics of the vapor phase reaction of mercury and halogens, Journal of the American Chemical Society, 58, 1922-1924, 10.1021/ja01301a026, 1936.

Olson, C. L., Jiskra, M., Sonke, J. E., and Obrist, D.: Mercury in tundra vegetation of Alaska: Spatial and temporal dynamics and stable isotope patterns, Science of the Total Environment, 660, 1502-1512, 10.1016/j.scitotenv.2019.01.058, 2019.

Osterwalder, S., Eugster, W., Feigenwinter, I., and Jiskra, M.: Eddy covariance flux measurements of gaseous elemental mercury over a grassland, Atmospheric Measurement Techniques, 13, 2057-2074, 10.5194/amt-13-2057-2020, 2020.

Osterwalder, S., Nerentorp, M., Zhu, W., Jiskra, M., Nilsson, E., Nilsson, M. B., Rutgersson, A., Soerensen, A. L., Sommar, J., Wallin, M. B., Wängberg, I., and Bishop, K.: Critical observations of gaseous elemental mercury air-sea exchange, Global Biogeochemical Cycles, 35, e2020GB006742, 10.1029/2020GB006742, 2021.

Pal, B. and Ariya, P. A.: Gas-phase HO-initiated reactions of elemental mercury: Kinetics, product studies, and atmospheric implications, Environmental Science & Technology, 38, 5555-5566, 2004a.

Pal, B. and Ariya, P. A.: Studies of ozone initiated reactions of gaseous mercury: kinetics, product studies, and atmospheric implications, Physical Chemistry Chemical Physics, 6, 572-579, 2004b.

Pandey, S. K., Kim, K. H., and Brown, R. J. C.: Measurement techniques for mercury species in ambient air, TrAC - Trends in Analytical Chemistry, 30, 899-917, 2011.

Pankow, J. F.: An absorption model of the gas/aerosol partitioning involved in the formation of secondary organic aerosol, Atmospheric Environment, 41, 75-79, https://doi.org/10.1016/j.atmosenv.2007.10.060, 2007.

Parks, J. M., Johs, A., Podar, M., Bridou, R., Hurt, R. A., Smith, S. D., Tomanicek, S. J., Qian, Y., Brown, S. D., Brandt, C. C., Palumbo, A. V., Smith, J. C., Wall, J. D., Elias, D. A., and Liang, L.: The genetic basis for bacterial mercury methylation, Science, 339, 1332-1335, doi:10.1126/science.1230667, 2013.

Pasakarnis, T., Boyanov, M., Kemner, K., Mishra, B., O'Loughlin, E., Parkin, G., and Scherer, M.: Influence of chloride and Fe(II) content on the reduction of Hg(II) by magnetite, Environmental Science & Technology, 47, 10.1021/es304761u, 2013.

Pehkonen, S. O. and Lin, C. J.: Aqueous photochemistry of mercury with organic acids, Journal of the Air & Waste Management Association, 48, 144-150, 1998.

Peleg, M., Tas, E., Obrist, D., Matveev, V., Moore, C., Gabay, M., and Luria, M.: Observational evidence for involvement of nitrate radicals in nighttime oxidation of mercury, Environmental Science & Technology, 49, 14008-14018, 10.1021/acs.est.5b03894, 2015.

Pertel, R. and Gunning, H. E.: Photochemical separation of mercury isotopes 2. The reaction of $^{202}Hg(6^3P_1)$ atoms, photoexcited in natural mercury vapor, with water vapor and other HgO-forming substrates, Canadian Journal of Chemistry, 37, 35-42, 1959.

Peterson, K. A., Shepler, B. C., and Singleton, J. M.: The group 12 metal chalcogenides: an accurate multireference configuration interaction and coupled cluster study, Molecular Physics, 105, 1139-1155, 2007.

Pikaev, A. K., Sibirskaya, G. K., and Spitsyn, V. I.: Pulse radiolysis of aqueous solutions of bivalent mercury compounds, Doklady Akademii Nauk SSSR, 224, 638-641, 1975.

Pleijel, K. and Munthe, J.: Modeling the atmospheric chemistry of mercury, Water, Air, & Soil Pollution, 80, 317324, 10.1007/BF01189681, 1995.

tog bort: Oxidation
formaterade: Teckenfärg: Blå, Kondenserad med 0,2 pt
tog bort: Dissolved Gaseous Mercury
formaterade: Teckenfärg: Blå, Kondenserad med 0,2 pt
tog bort: Polar Ice Mimics
formaterade: Teckenfärg: Blå, Kondenserad med 0,2 pt
tog bort: Observations
formaterade: Teckenfärg: Blå, Kondenserad med 0,2 pt
tog bort: Gaseous Elemental Mercury Air-Sea Exchange
formaterade: Teckenfärg: Blå, Kondenserad med 0,2 pt
tog bort: Phase
formaterade: Teckenfärg: Blå, Kondenserad med 0,2 pt
tog bort: Initiated Reactions
formaterade: Teckenfärg: Blå, Kondenserad med 0,2 pt
tog bort: Elemental Mercury
formaterade: Teckenfärg: Blå, Kondenserad med 0,2 pt
tog bort: Product Studies
formaterade: Teckenfärg: Blå, Kondenserad med 0,2 pt
tog bort: Atmospheric Implications
formaterade: Teckenfärg: Blå, Kondenserad med 0,2 pt
formaterade: Teckenfärg: Blå, Kondenserad med 0,2 pt
Formaterat: Avstånd Efter: 0,6 Rad, Radavstånd: Flera 1,1 li
tog bort: Genetic Basis
formaterade: Teckenfärg: Blå, Kondenserad med 0,2 pt
tog bort: Bacterial Mercury Methylation
formaterade: Teckenfärg: Blå, Kondenserad med 0,2 pt
tog bort: Chloride
formaterade: Teckenfärg: Blå, Kondenserad med 0,2 pt
tog bort: Content
formaterade: Teckenfärg: Blå, Kondenserad med 0,2 pt
tog bort: Reduction
formaterade: Teckenfärg: Blå, Kondenserad med 0,2 pt
tog bort: Magnetite
formaterade: Teckenfärg: Blå, Kondenserad med 0,2 pt
formaterade: Teckenfärg: Blå, Kondenserad med 0,3 pt
tog bort: Evidence
formaterade: Teckenfärg: Blå, Kondenserad med 0,3 pt
tog bort: Involvement
formaterade: Teckenfärg: Blå, Kondenserad med 0,3 pt
tog bort: Nitrate Radicals
formaterade: Teckenfärg: Blå, Kondenserad med 0,3 pt
tog bort: Nighttime Oxidation
formaterade: Teckenfärg: Blå, Kondenserad med 0,3 pt
tog bort: Mercury, Environ. Sci. Technol.,
formaterade: Teckenfärg: Blå, Kondenserad med 0,3 pt
formaterade: Teckenfärg: Blå, Kondenserad med 0,2 pt
tog bort: -Revue Canadienne De Chimie
formaterade: Teckenfärg: Blå, Kondenserad med 0,2 pt
formaterade: Teckenfärg: Blå

Pliss, E. M., Grobov, A. M., Kuzaev, A. K., and Buchachenko, A. L.: Magnetic field effect on the oxidation of organic substances by molecular oxygen, Journal of Physical Organic Chemistry, 32, 10.1002/poc.3915, 2019.

Poissant, L., Pilote, M., Yumvihoze, E., and Lean, D.: Mercury concentrations and foliage/atmosphere fluxes in a maple forest ecosystem in Quebec, Canada, Journal of Geophysical Research-Atmospheres, 10.1029/2007jd009510, 2008.

Pongratz, R. and Heumann, K. G.: Production of methylated mercury, lead, and cadmium by marine bacteria as a significant natural source for atmospheric heavy metals in polar regions, Chemosphere, 39, 89-102, 1999.

Poulain, A. J., Lalonde, J. D., Amyot, M., Shead, J. A., Raofie, F., and Ariya, P. A.: Redox transformations of mercury in an Arctic snowpack at springtime, Atmospheric Environment, 38, 6763-6774, 10.1016/j.atmosenv.2004.09.013, 2004.

Powell, K. J., Brown, P. L., Byrne, R. H., Gajda, T., Hefter, G. T., Sjöberg, S., and Wanner, H.: Chemical speciation of environmentally significant heavy metals with inorganic ligands. Part 1: The Hg^{2+}– Cl^-, OH^-, CO_3^{2-}, SO_4^{2-}, and PO_4^{3-} aqueous systems, Pure and Applied Chemistry, 77, 739-800, 2005.

Puigdomenech, I.: SPANA and DATABASE (modified JAVA versions of earlier software MEDUSA, HYDRA and INPUT-SED-PREDOM) Dept. of Inorganic Chemistry, Royal Institute of Technology (KTH), 2013.

Pyykkö, P.: Relativistic Effects in Structural Chemistry, Chemical Reviews, 88, 10.1021/cr00085a006, 1988.

Qiu, Y., Gai, P., Yue, F., Zhang, Y., He, P., Kang, H., Yu, X., Chen, J., and Xie, Z.: Potential factors impacting $PM_{2.5}$-Hg during haze evolution revealed by mercury isotope: Emission sources and photochemical processes, Atmospheric Research, 277, 10.1016/j.atmosres.2022.106318, 2022.

Qu, Z., Yan, N. Q., Liu, P., Chi, Y. P., and Jia, J.: Bromine chloride as an oxidant to improve elemental mercury removal from coal-fired flue gas, Environmental Science & Technology, 43, 8610-8615, 10.1021/es901803s, 2009.

Radke, L. F., Friedli, H. R., and Heikes, B. G.: Atmospheric mercury over the NE Pacific during spring 2002: Gradients, residence time, upper troposphere lower stratosphere loss, and long-range transport, Journal of Geophysical Research-Atmospheres, 112, 10.1029/2005jd005828, 2007.

Raofie, F. and Ariya, P. A.: Product study of the gas-phase BrO-initiated oxidation of Hg^0: evidence for stable Hg^{1+} compounds, Environmental Science & Technology, 38, 4319-4326, 2004.

Raofie, F., Snider, G., and Ariya, P. A.: Reaction of gaseous mercury with molecular iodine, atomic iodine, and iodine oxide radicals - Kinetics, product studies, and atmospheric implications, Canadian Journal of Chemistry, 86, 811-820, 10.1139/v08-088, 2008.

Riccardi, D., Guo, H.-B., Parks, J. M., Gu, B., Summers, A. O., Miller, S. M., Liang, L., and Smith, J. C.: Why mercury prefers soft ligands, Journal of Physical Chemistry Letters, 4, 2317-2322, 10.1021/jz401075b, 2013.

Richard, J. H., Bischoff, C., Ahrens, C. G. M., and Biester, H.: Mercury (II) reduction and co-precipitation of metallic mercury on hydrous ferric oxide in contaminated groundwater, Science of the Total Environment, 539, 36-44, 10.1016/j.scitotenv.2015.08.116, 2016.

Rolison, J. M., Landing, W. M., Luke, W., Cohen, M., and Salters, V. J. M.: Isotopic composition of species-specific atmospheric Hg in a coastal environment, Chemical Geology, 336, 37-49, 2013.

Rose, C. H., Ghosh, S., Blum, J. D., and Bergquist, B. A.: Effects of ultraviolet radiation on mercury isotope fractionation during photo-reduction for inorganic and organic mercury species, Chemical Geology, 405, 102-111, 10.1016/j.chemgeo.2015.02.025, 2015.

Rosenthal, J. E. and Breit, G.: The isotope shift in hyperfine structure, Physical Review, 41, 459-470, 10.1103/PhysRev.41.459, 1932.

Rutter, A. P. and Schauer, J. J.: The impact of aerosol composition on the particle to gas partitioning of reactive mercury, Environmental Science & Technology, 41, 3934-3939, 2007a.

Rutter, A. P. and Schauer, J. J.: The effect of temperature on the gas-particle partitioning of reactive mercury in atmospheric aerosols, Atmospheric Environment, 41, 8647-8657, 10.1016/J.Atmosenv.2007.07.024, 2007b.

Rutter, A. P., Shakya, K. M., Lehr, R., Schauer, J. J., and Griffin, R. J.: Oxidation of gaseous elemental mercury in the presence of secondary organic aerosols, Atmospheric Environment, 59, 86-92, 10.1016/j.atmosenv.2012.05.009, 2012.

Saiz-Lopez, A., Sitkiewicz, S. P., Roca-Sanjuán, D., Oliva-Enrich, J. M., Dávalos, J. Z., Notario, R., Jiskra, M., Xu, Y., Wang, F., Thackray, C. P., Sunderland, E. M., Jacob, D. J., Travnikov, O., Cuevas, C. A., Acuña, A. U., Rivero, D., Plane, J. M. C., Kinnison, D. E., and Sonke, J. E.: Photoreduction of gaseous oxidized mercury changes global atmospheric mercury speciation, transport and deposition, Nature Communications, 9, 4796, 2018.

Saiz-Lopez, A., Ulises Acuna, A., Trabelsi, T., Carmona-Garcia, J., Davalos, J. Z., Rivero, D., Cuevas, C. A., Kinnison, D. E.,

formaterade: Teckenfärg: Blå, Kondenserad med 0,2 pt

tog bort: Amyot,

flyttade upp [13]: M.,

formaterade: Teckenfärg: Blå, Svenska

tog bort: Kwan, M., and Bégin, M.: Atmospheric mercury transport, oxidation and fallout in northern Québec (Nunavik): an important potential route of contamination., Environment Canada, Montréal, Northern Contaminants Program, Synopsis of Research 2000-2001, Indian and Northern Affairs Canada, 125-129, 2001.¶ Poissant, L.,

formaterade: Teckenfärg: Blå, Kondenserad med 0,2 pt

formaterade: Teckenfärg: Blå, Kondenserad med 0,2 pt

formaterade: Teckenfärg: Blå, Kondenserad med 0,4 pt

formaterade: Teckenfärg: Blå, Kondenserad med 0,3 pt

formaterade: Teckenfärg: Blå, Kondenserad med 0,2 pt

tog bort:

formaterade: Teckenfärg: Blå, Kondenserad med 0,2 pt

tog bort: Chloride

formaterade: Teckenfärg: Blå, Kondenserad med 0,2 pt

tog bort: Oxidant

formaterade: Teckenfärg: Blå, Kondenserad med 0,2 pt

tog bort: Improve Elemental Mercury Removal

formaterade: Teckenfärg: Blå, Kondenserad med 0,2 pt

tog bort: Coal-Fired Flue Gas

formaterade: Teckenfärg: Blå, Kondenserad med 0,2 pt

formaterade: Teckenfärg: Blå, Kondenserad med 0,2 pt

Formaterat: Avstånd Efter: 0,6 Rad, Radavstånd: Flera 1,1 li

formaterade: Teckenfärg: Blå, Kondenserad med 0,3 pt

tog bort: -Revue Canadienne De Chimie

formaterade: Teckenfärg: Blå, Kondenserad med 0,3 pt

formaterade: Teckenfärg: Blå, Kondenserad med 0,2 pt

tog bort: Mercury Prefers Soft Ligands

formaterade: Teckenfärg: Blå, Kondenserad med 0,2 pt

formaterade: Teckenfärg: Blå, Kondenserad med 0,4 pt

formaterade: Teckenfärg: Blå, Kondenserad med 0,2 pt

Sitkiewicz, S. P., Roca-Sanjuan, D., and Francisco, J. S.: Gas-phase photolysis of Hg(I) radical species: A new atmospheric mercury reduction process, Journal of the American Chemical Society, 141, 8698-8702, 10.1021/jacs.9b02890, 2019.

Saiz-Lopez, A., Travnikov, O., Sonke, J. E., Thackray, C. P., Jacob, D. J., Carmona-Garcia, J., Frances-Monerris, A., Roca-Sanjuan, D., Acuna, A. U., Davalos, J. Z., Cuevas, C. A., Jiskra, M., Wang, F., Bieser, J., Plane, J. M. C., and Francisco, J. S.: Photochemistry of oxidized Hg(I) and Hg(II) species suggests missing mercury oxidation in the troposphere, Proceedings of the National Academy of Sciences of the United States of America, 117, 30949-30956, 2020.

Saiz-Lopez, A., Acuña, A., Mahajan, A., Dávalos, J., Wuhu, F., Roca-Sanjuán, D., Carmona-García, J., Cuevas, C. A., Kinnison, D., Gomez Martin, J. C., Francisco, J., and Plane, J.: The chemistry of mercury in the stratosphere, Geophysical Research Letters, 49, e2022GL097953, 10.1029/2022GL097953, 2022.

Saiz-Lopez, A., Cuevas, C. A., Acuña, A. U., Añel, J. A., Mahajan, A. S., de la Torre, L., Feng, W., Dávalos, J. Z., Roca-Sanjuán, D., Kinnison, D. E., Carmona-García, J., Fernandez, R. P., Li, Q., Sonke, J. E., Feinberg, A., Martín, J. C. G., Villamayor, J., Zhang, P., Zhang, Y., Blaszczak-Boxe, C. S., Travnikov, O., Wang, F., Bieser, J., Francisco, J. S., and Plane, J. M. C.: Role of the stratosphere in the global mercury cycle, Science Advances, 11, eads1459, 10.1126/sciadv.ads1459, 2025.

Salter, C., Tellinghuisen, P. C., Ashmore, J. G., and Tellinghuisen, J.: The emission spectrum of $^{200}Hg^{127}I$, Journal of Molecular Spectroscopy, 120, 334-358, 10.1016/0022-2852(86)90009-3, 1986.

Sander, R.: Modeling Atmospheric Chemistry: Interactions between gas-phase species and liquid cloud/aerosol particles, Surveys in Geophysics, 20, 1-31, 10.1023/A:1006501706704, 1999.

Sanemasa, I.: Solubility of elemental mercury-vapor in water, Bulletin of the Chemical Society of Japan, 48, 1795-1798, 10.1246/bcsj.48.1795, 1975.

Schartup, A. T., Soerensen, A. L., and Heimburger-Boavida, L. E.: Influence of the Arctic Sea-ice regime shift on sea-ice methylated mercury trends, Environmental Science & Technology Letters, 7, 708-713, 10.1021/acs.estlett.0c00465, 2020.

Schauble, E. A.: Role of nuclear volume in driving equilibrium stable isotope fractionation of mercury, thallium, and other very heavy elements, Geochimica et Cosmochimica Acta, 71, 2170-2189, 2007.

Schmolke, S. R., Schroeder, W. H., Kock, H. H., Schneeberger, D., Munthe, J., and Ebinghaus, R.: Simultaneous measurements of total gaseous mercury at four sites on a 800 km transect: spatial distribution and short-time variability of total gaseous mercury over central Europe, Atmospheric Environment, 33, 1725-1733, 1999.

Schroeder, W. H. and Munthe, J.: Atmospheric mercury - An overview, Atmospheric Environment, 32, 809-822, 1998.

Schroeder, W. H., Yarwood, G., and Niki, H.: Transformation processes involving mercury species in the atmosphere - Results from a literature survey, Water Air and Soil Pollution, 56, 653-666, 1991.

Schroeder, W. H., Anlauf, K. G., Barrie, L. A., Lu, J. Y., Steffen, A., Schneeberger, D. R., and Berg, T.: Arctic springtime depletion of mercury, Nature, 394, 331-332, 1998.

Schwab, L., Gallati, N., Reiter, S. M., Kimber, R. L., Kumar, N., McLagan, D. S., Biester, H., Kraemer, S. M., and Wiederhold, J. G.: Mercury isotope fractionation during dark abiotic reduction of Hg(II) by dissolved, surface-bound, and structural Fe(II), Environmental Science & Technology, 57, 15243-15254, 10.1021/acs.est.3c03703, 2023.

Schwartz, S. E.: Mass-transport considerations pertinent to aqueous phase reactions of gases in liquid-water clouds, in: Chemistry of multiphase atmospheric systems, edited by: Jäschke, W., NATO ASI Series, G6, Springer-Verlag Berlin Heidelberg, 415-471, 1986.

Scott, S. L., Yusuf, H., Lahoutifard, N., and Maunder, K.: Homogeneous and heterogeneous reactions of atmospheric mercury(II) with sulfur(IV), Journal de Physique IV, 107, 1201-1204, 2003.

Seigneur, C., Wrobel, J., and Constantinou, E.: A chemical kinetic mechanism for atmospheric inorganic mercury, Environmental Science & Technology, 28, 1589-1597, 1994.

Seinfeld, J. H. and Pandis, S. N.: Atmospheric chemistry and physics: from air pollution to climate change, Wiley, Hoboken, 2006.

Selin, N. E.: Global biogeochemical cycling of mercury: A review, Environment and Resources, 10.1146/annurev.environ.051308.084314, 2009.

Sexauer Gustin, M., Pierce, A. M., Huang, J., Miller, M. B., Holmes, H. A., and Loria-Salazar, S. M.: Evidence for different reactive Hg sources and chemical compounds at adjacent valley and high elevation locations, Environmental Science & Technology, 50, 12225-12231, 10.1021/acs.est.6b03339, 2016.

Shah, V., Jacob, D., Thackray, C., Wang, X., Sunderland, E., Dibble, T., Saiz-Lopez, A., Cernusak, I., Kellö, V., Castro, P., Wu,

tog bort: Phase Photolysis
formaterade ... [1367]
tog bort: Radical Species
formaterade ... [1368]
tog bort: New Atmospheric Mercury Reduction Process
formaterade ... [1369]
tog bort: Chemistry
formaterade ... [1370]
tog bort: Mercury
formaterade ... [1371]
tog bort: Stratosphere
formaterade ... [1372]
tog bort: Gas-Phase Species and Liquid Cloud/Aerosol Particles
formaterade ... [1373]
tog bort: Elemental Mercury-Vapor
formaterade ... [1374]
tog bort: Water
formaterade ... [1375]
tog bort: DOI
formaterade ... [1376]
tog bort: Ice Regime Shift on Sea-Ice Methylated Mercury Trends
formaterade ... [1377]
tog bort: Et
formaterade ... [1378]
tog bort: Processes Involving Mercury Species
formaterade ... [1379]
tog bort: Atmosphere
formaterade ... [1380]
tog bort: Literature Survey
formaterade ... [1381]
tog bort: Isotope Fractionation
formaterade ... [1382]
tog bort: Dark Abiotic Reduction
formaterade ... [1383]
tog bort: Dissolved, Surface-Bound
formaterade ... [1384]
tog bort: Structural
formaterade ... [1385]
formaterade ... [1386]
tog bort: Multiphase Atmospheric Systems
formaterade ... [1387]
formaterade ... [1388]
tog bort: De
formaterade ... [1389]
formaterade ... [1390]
Formaterat ... [1391]
tog bort: Different Reactive
formaterade ... [1392]
tog bort: Sources
formaterade ... [1393]
tog bort: Chemical Compounds
formaterade ... [1394]
tog bort: Adjacent Valley
formaterade ... [1395]
tog bort: High Elevation Locations
formaterade ... [1396]

R., and Wang, C.: Improved mechanistic model of the atmospheric redox chemistry of mercury, Environmental Science & Technology, 55, 14445 - 14456, 2021.

Shah, V., Jaeglé, L., Gratz, L. E., Ambrose, J. L., Jaffe, D. A., Selin, N. E., Song, S., Campos, T. L., Flocke, F. M., Reeves, M., Stechman, D., Stell, M., Festa, J., Stutz, J., Weinheimer, A. J., Knapp, D. J., Montzka, D. D., Tyndall, G. S., Apel, E. C., Hornbrook, R. S., Hills, A. J., Riemer, D. D., Blake, N. J., Cantrell, C. A., and Mauldin, R. L.: Origin of oxidized mercury in the summertime free troposphere over the southeastern US, Atmospheric Chemistry and Physics, 16, 1511-1530, 10.5194/acp-16-1511-2016, 2016.

Shepler, B. C.: Ab Initio Investigation of the thermochemistry, spectroscopy and dynamics of reactions between mercury and reactive halogen species, Ph. D. thesis, Department of Chemistry, Washington State University, Pullman, WA, 289 pp., 2006.

Shepler, B. C. and Peterson, K. A.: Mercury Monoxide: A systematic investigation of its ground electronic state, Journal of Physical Chemistry A, 107, 1783-1787, 2003.

Shepler, B. C., Balabanov, N. B., and Peterson, K. A.: Ab initio thermochemistry involving heavy atoms: An investigation of the reactions Hg + IX (X = I, Br, Cl, O), Journal of Physical Chemistry A, 109, 10363 - 10372, 2005.

Shepler, B. C., Balabanov, N. B., and Peterson, K. A.: Hg + Br → HgBr recombination and collision-induced dissociation dynamics, Journal of Chemical Physics, 127, 164304; 10.1063/1.27771422007, 2007.

Sherman, L. S., Blum, J. D., Dvonch, J. T., Gratz, L. E., and Landis, M. S.: The use of Pb, Sr, and Hg isotopes in Great Lakes precipitation as a tool for pollution source attribution, Science of the Total Environment, 502, 362-374, 2015.

Sherman, L. S., Blum, J. D., Keeler, G. J., Demers, J. D., and Dvonch, J. T.: Investigation of local mercury deposition from a coal-fired power plant using mercury isotopes, Environmental Science & Technology, 46, 382-390, 2012.

Sherman, L. S., Blum, J. D., Johnson, K. P., Keeler, G. J., Barres, J. A., and Douglas, T. A.: Mass-independent fractionation of mercury isotopes in Arctic snow driven by sunlight., Nature Geoscience, 3, 173–177, 2010.

Sholupov, S., Pogarev, S., Ryzhov, V., Mashyanov, N., and Stroganov, A.: Zeeman atomic absorption spectrometer RA-915+for direct determination of mercury in air and complex matrix samples, Fuel Processing Technology, 85, 473-485, 2004.

Si, L. and Ariya, P.: Recent advances in atmospheric chemistry of mercury, Atmosphere, 9, 76, 2018.

Si, L. and Ariya, P. A.: Reduction of oxidized mercury species by dicarboxylic acids (C_2–C_4): Kinetic and product studies, Environmental Science & Technology, 42, 5150-5155, 10.1021/es800552z, 2008.

Si, L. and Ariya, P. A.: Aqueous photoreduction of oxidized mercury species in presence of selected alkanethiols, Chemosphere, 84, 1079-1084, 2011.

Si, L. and Ariya, P. A.: Photochemical reactions of divalent mercury with thioglycolic acid: Formation of mercuric sulfide particles, Chemosphere, 119, 467-472, 10.1016/j.chemosphere.2014.07.022, 2015.

Si, L., Branfireun, B. A., and Fierro, J.: Chemical oxidation and reduction pathways of mercury relevant to natural waters: A review, Water, 14, 10.3390/w14121891, 2022

Siegler, R. W., Nierenberg, D. W., and Hickey, W. F.: Fatal poisoning from liquid dimethylmercury: A neuropathologic study, Human Pathology, 30, 720-723, 10.1016/s0046-8177(99)90101-6, 1999.

Sipilä, M., Sarnela, N., Jokinen, T., Henschel, H., Junninen, H., Kontkanen, J., Richters, S., Kangasluoma, J., Franchin, A., Peräkylä, O., Rissanen, M. P., Ehn, M., Vehkamäki, H., Kurten, T., Berndt, T., Petäjä, T., Worsnop, D., Ceburnis, D., Kerminen, V.-M., Kulmala, M., and O'Dowd, C.: Molecular-scale evidence of aerosol particle formation via sequential addition of HIO_3, Nature, 537, 532-534, 10.1038/nature19314, 2016.

Sitkiewicz, S. P., Rivero, D., Oliva-Enrich, J. M., Saiz-Lopez, A., and Roca-Sanjuán, D.: Ab initio quantum-chemical computations of the absorption cross sections of HgX_2 and HgXY (X, Y = Cl, Br, and I): Molecules of interest in the Earth's atmosphere, Physical Chemistry Chemical Physics, 21, 455-467, 10.1039/C8CP06160B, 2019.

Skyllberg, U.: Chemical speciation of mercury in soil and sediment, in: Advances in environmental chemistry and toxicology of mercury edited by: Liu, G., Cai, Y., and O'Driscoll, N., John Wiley & Sons, 218-258, 2011.

Slemr, F., Schuster, G., and Seiler, W.: Distribution, speciation, and budget of atmospheric mercury, Journal of Atmospheric Chemistry, 3, 407-434, 1985.

Slemr, F., Martin, L., Labuschagne, C., Mkololo, T., Angot, H., Magand, O., Dommergue, A., Garat, P., Ramonet, M., and Bieser, J.: Atmospheric mercury in the Southern Hemisphere – Part 1: Trend and inter-annual variations in atmospheric mercury at Cape Point, South Africa, in 2007–2017, and on Amsterdam Island in 2012–2017, Atmospheric Chemistry and Physics, 20, 7683-7692,

tog bort: Mechanistic Model
tog bort: Mercury
formaterade: Teckenfärg: Blå, Kondenserad med 0,2 pt
tog bort: Atmospheric Redox Chemistry
formaterade: Teckenfärg: Blå, Kondenserad med 0,2 pt
formaterade: Teckenfärg: Blå, Kondenserad med 0,2 pt
formaterade: Teckenfärg: Blå, Kondenserad med 0,3 pt
formaterade: Teckenfärg: Blå, Kondenserad med 0,2 pt
tog bort: Systematic Investigation
formaterade: Teckenfärg: Blå, Kondenserad med 0,2 pt
tog bort: Its Ground Electronic State
formaterade: Teckenfärg: Blå, Kondenserad med 0,2 pt
tog bort: Initio Thermochemistry Involving Heavy Atoms
formaterade: Teckenfärg: Blå, Kondenserad med 0,2 pt
tog bort: Investigation
formaterade: Teckenfärg: Blå, Kondenserad med 0,2 pt
tog bort: Reactions
formaterade: Teckenfärg: Blå, Kondenserad med 0,2 pt
tog bort: Local Mercury Deposition
formaterade: Teckenfärg: Blå, Kondenserad med 0,2 pt
tog bort: Coal-Fired Power Plant Using Mercury Isotopes
formaterade: Teckenfärg: Blå, Kondenserad med 0,2 pt
tog bort: Advances
formaterade: Teckenfärg: Blå, Kondenserad med 0,2 pt
tog bort: Atmospheric Chemistry
formaterade: Teckenfärg: Blå, Kondenserad med 0,2 pt
tog bort: Mercury
formaterade: Teckenfärg: Blå, Kondenserad med 0,2 pt
tog bort: Oxidized Mercury Species
formaterade: Teckenfärg: Blå, Kondenserad med 0,2 pt
tog bort: Dicarboxylic Acids
formaterade: Teckenfärg: Blå, Kondenserad med 0,2 pt
tog bort: Product Studies
formaterade: Teckenfärg: Blå, Kondenserad med 0,2 pt
formaterade: Teckenfärg: Blå, Kondenserad med 0,2 pt
Formaterat: Avstånd Efter: 0,6 Rad, Radavstånd: Flera 1,1 li
formaterade: Teckenfärg: Blå, Kondenserad med 0,3 pt
Formaterat: Avstånd Efter: 0,6 Rad, Radavstånd: Flera 1,1 li
tog bort: molecules
formaterade: Teckenfärg: Blå, Kondenserad med 0,3 pt
formaterade: Teckenfärg: Blå, Kondenserad med 0,2 pt

10.5194/acp-20-7683-2020, 2020.

Slemr, F., Weigelt, A., Ebinghaus, R., Kock, H. H., Bödewadt, J., Brenninkmeijer, C. A. M., Rauthe-Schöch, A., Weber, S., Hermann, M., Becker, J., Zahn, A., and Martinsson, B.: Atmospheric mercury measurements onboard the CARIBIC passenger aircraft, Atmospheric Measurement Techniques, 9, 2291-2302, 10.5194/amt-9-2291-2016, 2016.

Slemr, F., Weigelt, A., Ebinghaus, R., Bieser, J., Brenninkmeijer, C. A. M., Rauthe-Schoch, A., Hermann, M., Martinsson, B. G., van Velthoven, P., Bonisch, H., Neumaier, M., Zahn, A., and Ziereis, H.: Mercury distribution in the upper troposphere and lowermost stratosphere according to measurements by the IAGOS-CARIBIC observatory: 2014-2016, Atmospheric Chemistry and Physics, 18, 12329-12343, 2018.

Smith, R. M., Martell, A. E., and Motekaitis, R. J.: NIST critically selected stability constants of metal complexes database, 2004.

Smith, R. S., Wiederhold, J. G., and Kretzschmar, R.: Mercury isotope fractionation during precipitation of metacinnabar (β-HgS) and montroydite (HgO), Environmental Science & Technology, 49, 4325-4334, 2015.

Snelson, A.: Infrared matrix isolation spectrum of methyl radical produced by pyrolysis of methyl iodide and dimethyl mercury, Journal of Physical Chemistry, 74, 537-&, 10.1021/j100698a011, 1970.

Snider, G., Raofie, F., and Ariya, P. A.: Effects of relative humidity and CO(g) on the O_3-initiated oxidation reaction of Hg^0(g): Kinetic & product studies, Physical Chemistry Chemical Physics, 10, 5616-5623, 10.1039/b801226a, 2008.

Soerensen, A. L., Sunderland, E. M., Holmes, C. D., Jacob, D. J., Yantosca, R. M., Skov, H., Christensen, J. H., Strode, S. A., and Mason, R. P.: An improved global model for air-sea exchange of mercury: High concentrations over the North Atlantic, Environmental Science & Technology, 44, 8574-8580, 10.1021/es102032g, 2010.

Sommar, J., Feng, X. B., and Lindqvist, O.: Speciation of volatile mercury species present in digester and deposit gases, Applied Organometallic Chemistry, 13, 441-445, 1999.

Sommar, J., Hallquist, M., and Ljungstrom, E.: Rate of reaction between the nitrate radical and dimethyl mercury in the gas phase, Chemical Physics Letters, 257, 434-438, 1996.

Sommar, J., Lindqvist, O., and Strömberg, D.: Distribution equilibrium of mercury (II) chloride between water and air applied to flue gas scrubbing, Journal of the Air & Waste Management Association, 50, 1663-1666, 2000.

Sommar, J., Osterwalder, S., and Zhu, W.: Recent advances in understanding and measurement of Hg in the environment: Surface-atmosphere exchange of gaseous elemental mercury (Hg^0), Science of the Total Environment, 721, 137648, 10.1016/j.scitotenv.2020.137648, 2020.

Sommar, J., Gårdfeldt, K., Strömberg, D., and Feng, X. B.: A kinetic study of the gas-phase reaction between the hydroxyl radical and atomic mercury, Atmospheric Environment, 35, 3049-3054, 2001.

Sommar, J., Hallquist, M., Ljungstrom, E., and Lindqvist, O.: On the gas phase reactions between volatile biogenic mercury species and the nitrate radical, Journal of Atmospheric Chemistry, 27, 233-247, 1997.

Sommar, J., Wängberg, I., Berg, T., Gårdfeldt, K., Munthe, J., Richter, A., Urba, A., Wittrock, F., and Schroeder, W. H.: Circumpolar transport and air-surface exchange of atmospheric mercury at Ny-Ålesund (79°N), Svalbard, spring 2002., Atmospheric Chemistry and Physics, 7, 151-166, 2007.

Sommar, J., Zhu, W., Lin, C. J., and Feng, X.: Field approaches to measure Hg exchange between natural surfaces and the atmosphere - A review, Critical Reviews in Environmental Science and Technology, 43, 1657-1739, 2013

Song, Z. C., Huang, S. J., Zhang, P., Yuan, T. F., and Zhang, Y. X.: Isotope data constrains redox chemistry of atmospheric mercury, Environmental Science & Technology, 10.1021/acs.est.4c02600, 2024.

Sonke, J. E., Angot, H., Zhang, Y., Poulain, A., Björn, E., and Schartup, A.: Global change effects on biogeochemical mercury cycling, Ambio, 52, 853-876, 10.1007/s13280-023-01855-y, 2023.

Spicer, C. W., Satola, J., Abbgy, A. A., Plastridge, R. A., and Cowen, K. A.: Kinetics of gas-phase elemental mercury reactions with halogen species, ozone, and nitrate radical under atmospheric conditions, Florida Department of Environmental Protection, 2002.

Sprovieri, F., Pirrone, N., Ebinghaus, R., Kock, H., and Dommergue, A.: A review of worldwide atmospheric mercury measurements, Atmospheric Chemistry and Physics, 10, 8245-8265, 2010.

Sprovieri, F., Pirrone, N., Bencardino, M., D'Amore, F., Angot, H., Barbante, C., Brunke, E. G., Arcega-Cabrera, F., Cairns, W., Comero, S., Diéguez, M. D. C., Dommergue, A., Ebinghaus, R., Feng, X. B., Fu, X., Garcia, P. E., Gawlik, B. M., Hageström, U.,

formaterade ... [1397]
tog bort: Critically Selected Stability Constants
tog bort: Metal Complexes Database
formaterade ... [1398]
formaterade ... [1399]
formaterade ... [1400]
tog bort: Isotope Fractionation
formaterade ... [1401]
tog bort: Precipitation
formaterade ... [1402]
tog bort: Metacinnabar
formaterade ... [1403]
tog bort: Montroydite
formaterade ... [1404]
tog bort: Matrix Isolation Spectrum
formaterade ... [1405]
tog bort: Methyl Radical Produced
formaterade ... [1406]
tog bort: Pyrolysis
formaterade ... [1407]
tog bort: Methyl Iodide
formaterade ... [1408]
tog bort: Dimethyl Mercury
formaterade ... [1409]
tog bort: kinetic
formaterade ... [1410]
tog bort: Improved Global Model
formaterade ... [1411]
tog bort: Air-Sea Exchange
formaterade ... [1412]
tog bort: Mercury
formaterade ... [1413]
tog bort: Concentrations
formaterade ... [1414]
formaterade ... [1415]
tog bort: The
formaterade ... [1416]
formaterade ... [1417]
formaterade ... [1418]
formaterade ... [1419]
Formaterat ... [1420]
tog bort: Data Constrains Redox Chemistry
formaterade ... [1421]
tog bort: Atmospheric Mercury
formaterade ... [1422]
tog bort: Gas-Phase Elemental Mercury Reactions
formaterade ... [1423]
tog bort: Halogen Species, Ozone
formaterade ... [1424]
tog bort: Nitrate Radical
formaterade ... [1425]
tog bort: Atmospheric Conditions
formaterade ... [1426]
formaterade ... [1427]

Hansson, K., Horvat, M., Kotnik, J., Labuschagne, C., Magand, O., Martin, L., Mashyanov, N., Mkololo, T., Munthe, J., Obolkin, V., Ramirez Islas, M., Sena, F., Somerset, V., Spandow, P., Vardè, M., Walters, C., Wängberg, I., Weigelt, A., Yang, X., and Zhang, H.: Five-year records of mercury wet deposition flux at GMOS sites in the Northern and Southern hemispheres, Atmospheric Chemistry and Physics, 17, 2689-2708, 10.5194/acp-17-2689-2017, 2017.

Sprovieri, F., Pirrone, N., Bencardino, M., D'Amore, F., Carbone, F., Cinnirella, S., Mannarino, V., Landis, M., Ebinghaus, R., Weigelt, A., Brunke, E.-G., Labuschagne, C., Martin, L., Munthe, J., Wängberg, I., Artaxo, P., Morais, F., Barbosa, J. H. d. M., Brito, J., Cairns, W., Barbante, C., del Carmen Dieguez, M., Garcia, P. E., Dommergue, A., Angot, H., Magand, O., Skov, H., Horvat, M., Kotnik, J., Read, K. A., Neves, L. M., Gawlik, B. M., Sena, F., Mashyanov, N., Obolkin, V., Wip, D., Feng, X., Zhang, H., Fu, X., Ramachandran, R., Cossa, D., Knoery, J., Marusczak, N., Nerentorp, M., and Norstrom, C.: Atmospheric mercury concentrations observed at ground-based monitoring sites globally distributed in the framework of the GMOS network, Atmospheric Chemistry and Physics, 16, 11915-11935, 10.5194/acp-16-11915-2016, 2016.

St Louis, V. L., Hintelmann, H., Graydon, J. A., Kirk, J. L., Barker, J., Dimock, B., Sharp, M. J., and Lehnherr, I.: Methylated mercury species in Canadian high arctic marine surface waters and snowpacks, Environmental Science & Technology, 41, 6433-6441, 10.1021/es070692s, 2007.

Stathopoulos, D.: Fractionation of mercury isotopes in an aqueous environment: Chemical oxidation, M. Sc. Thesis, Faculty of Arts and Science, Trent University, Peterborough, Canada, 77 pp., 2014.

Steffen, A., Schroeder, W., Bottenheim, J., Narayan, J., and Fuentes, J. D.: Atmospheric mercury concentrations: Measurements and profiles near snow and ice surfaces in the Canadian Arctic during Alert 2000, Atmospheric Environment, 36, 2653-2661, 2002.

Steffen, A., Bottenheim, J., Cole, A., Ebinghaus, R., Lawson, G., and Leaitch, W. R.: Atmospheric mercury speciation and mercury in snow over time at Alert, Canada, Atmospheric Chemistry and Physics, 14, 2219-2231, 2014.

Steffen, A., Douglas, T. A., Amyot, M., Ariya, P. A., Aspmo, K., Berg, T., Bottenheim, J., Brooks, S., Cobbett, F., Dastoor, A., Dommergue, A., Ebinghaus, R., Ferrari, C. P., Gårdfeldt, K., Goodsite, M. E., Lean, D. R., Poulain, A. J., Scherz, C., Skov, H., Sommar, J., and Temme, C.: A synthesis of atmospheric mercury depletion event chemistry linking atmosphere, snow and water, Atmospheric Chemistry and Physics, 8, 1445-1482, 2008.

Steffen, A., Lehnherr, I., Cole, A., Ariya, P., Dastoor, A., Durnford, D., Kirk, J., and Pilote, M.: Atmospheric mercury in the Canadian Arctic. Part I: A review of recent field measurements, Science of the Total Environment, 509, 3-15, 2015.

Stephan, T. and Trappitsch, R.: Reliable uncertainties: Error correlation, rotated error bars, and linear regressions in three-isotope plots and beyond, International Journal of Mass Spectrometry, 491, 117053, 10.1016/j.ijms.2023.117053, 2023.

Stowe, A. C. and Knight, L. B.: Electron spin resonance studies of ^{199}HgH, ^{201}HgH, ^{199}HgD and ^{201}HgD isolated in neon and argon matrices at 4K: an electronic structure investigation, Molecular Physics, 100, 353-360, 10.1080/00268970110096443, 2002.

Strand, R., Lund, W., and Aaseth, J.: Complex formation of zinc, cadmium, and mercury with penicillamine, Journal of Inorganic Biochemistry, 19, 301-309, 10.1016/0162-0134(83)80003-8, 1983.

Strode, S. A., Jaegle, L., Selin, N. E., Jacob, D. J., Park, R. J., Yantosca, R. M., Mason, R. P., and Slemr, F.: Air-sea exchange in the global mercury cycle, Global Biogeochemical Cycles, 21, 10.1029/2006gb002766, 2007.

Strömberg, D., Gropen, O., and Wahlgren, U.: Non-relativistic and relativistic calculations on some Zn, Cd and Hg complexes, Chemical Physics, 133, 207-219, 10.1016/0301-0104(89)80202-2, 1989.

Strömberg, D. and Wahlgren, U. First-order relativistic calculations on Au_2 and Hg_2^{2+}, Chemical Physics Letters, 169, 109-115, 10.1016/0009-2614(90)85174-B, 1990

Strömberg, D., Strömberg, A., and Wahlgren, U.: Relativistic quantum calculations on some mercury sulfide molecules, Water Air & Soil Pollution, 56, 681-695, 10.1007/BF00342309, 1991.

Subir, M., Ariya, P. A., and Dastoor, A. P.: A review of uncertainties in atmospheric modeling of mercury chemistry I. Uncertainties in existing kinetic parameters - Fundamental limitations and the importance of heterogeneous chemistry, Atmospheric Environment, 45, 5664-5676, 2011.

Subir, M., Ariya, P. A., and Dastoor, A. P.: A review of the sources of uncertainties in atmospheric mercury modeling II. Mercury surface and heterogeneous chemistry - A missing link, Atmospheric Environment, 46, 1-10, 2012.

Suda, I., Suda, M., and Hirayama, K.: Degradation of methyl and ethyl mercury by singlet oxygen generated from sea-water exposed to sunlight or ultraviolet-light, Archives of Toxicology, 67, 365-368, 10.1007/Bf01973709, 1993.

Sumner, A. L., Spicer, C. W., Satola, J., Mangaraj, R., Cowen, K. A., Landis, M. S., Stevens, R. K., and Atkeson, T.: Environmental

formaterade: Teckenfärg: Blå, Kondenserad med 0,2 pt

formaterade: Teckenfärg: Blå, Kondenserad med 0,3 pt

formaterade: Teckenfärg: Blå, Kondenserad med 0,2 pt

tog bort: measurements

formaterade: Teckenfärg: Blå, Kondenserad med 0,2 pt

formaterade: Teckenfärg: Blå, Kondenserad med 0,3 pt

formaterade: Teckenfärg: Blå, Kondenserad med 0,2 pt

formaterade: Teckenfärg: Blå, Kondenserad med 0,2 pt

Formaterat: Avstånd Efter: 0,6 Rad, Radavstånd: Flera 1,1 li

formaterade: Teckenfärg: Blå, Kondenserad med 0,2 pt

Formaterat: Avstånd Efter: 0,6 Rad, Radavstånd: Flera 1,1 li

formaterade: Teckenfärg: Blå, Kondenserad med 0,2 pt

formaterade: Teckenfärg: Blå, Kondenserad med 0,2 pt

formaterade: Teckenfärg: Blå, Kondenserad med 0,3 pt

tog bort: Methyl

formaterade: Teckenfärg: Blå, Kondenserad med 0,2 pt

tog bort: Ethyl Mercury

formaterade: Teckenfärg: Blå, Kondenserad med 0,2 pt

tog bort: Singlet Oxygen Generated

formaterade: Teckenfärg: Blå, Kondenserad med 0,2 pt

tog bort: Sea-Water Exposed

formaterade: Teckenfärg: Blå, Kondenserad med 0,2 pt

formaterade: Teckenfärg: Blå, Kondenserad med 0,2 pt

tog bort: Sunlight

formaterade: Teckenfärg: Blå, Kondenserad med 0,2 pt

tog bort: Ultraviolet-Light

formaterade: Teckenfärg: Blå, Kondenserad med 0,2 pt

formaterade: Teckenfärg: Blå, Kondenserad med 0,3 pt

chamber studies of mercury reactions in the atmosphere, in: Dynamics of Mercury Pollution on Regional and Global Scales: Atmospheric Processes and Human Exposures Around the World, edited by: Pirrone, N., and Mahaffey, K. R., Springer US, 193-212, 10.1007/b105709, 2005.

Sun, G.: Isotope fractionation during major chemical transformations of atmospheric mercury, Ph D. thesis, Institute of Geochemistry, Chinese Academy of Sciences, Guiyang, 2018.

Sun, G., Feng, X., Yin, R., Wang, F., Lin, C.-J., Li, K., and Sommar, J. O.: Dissociation of mercuric oxides drives anomalous isotope fractionation during net photo-oxidation of mercury vapor in air, Environmental Science & Technology, 55, 13428–13438, 10.1021/acs.est.2c02722, 2022.

Sun, G., Sommar, J., Feng, X., Lin, C.-J., Ge, M., Wang, W., Yin, R., Fu, X., and Shang, L.: Mass -dependent and -independent fractionation of mercury isotope during gas-phase oxidation of elemental mercury vapor by atomic Cl and Br, Environmental Science & Technology, 50, 9232 - 9241, 2016.

Sun, L., Lu, B., Yuan, D., Hao, W., and Zheng, Y.: Variations in the isotopic composition of stable mercury isotopes in typical mangrove plants of the Jiulong estuary, SE China, Environmental Science and Pollution Research, 24, 1459-1468, 10.1007/s11356-016-7933-1, 2017.

Sun, R., Sonke, J. E., Heimbürger, L.-E., Belkin, H. E., Liu, G., Shome, D., Cukrowska, E., Liousse, C., Pokrovsky, O. S., and Streets, D. G.: Mercury stable isotope signatures of world coal deposits and historical coal combustion emissions, Environmental Science & Technology, 48, 7660, 2014.

Sun, R. Y., Jiskra, M., Amos, H. M., Zhang, Y. X., Sunderland, E. M., and Sonke, J. E.: Modelling the mercury stable isotope distribution of Earth surface reservoirs: Implications for global Hg cycling, Geochimica et Cosmochimica Acta, 246, 156-173, 2019.

Sun, R. Y., Cao, F., Dai, S. F., Shan, B., Qi, C. C., Xu, Z. J., Li, P. F., Liu, Y., Zheng, W., and Chen, J. B.: Atmospheric mercury isotope shifts in response to mercury emissions from underground coal fires, Environmental Science & Technology, 57, 8638-8649, 10.1021/acs.est.2c08637, 2023.

Svanberg, S.: Geophysical gas monitoring using optical techniques: Volcanoes, geothermal fields and mines, Optics and Lasers in Engineering, 37, 245-266, 2002.

Swartzendruber, P. C., Chand, D., Jaffe, D. A., Smith, J., Reidmiller, D., Gratz, L., Keeler, J., Strode, S., Jaegle, L., and Talbot, R.: Vertical distribution of mercury, CO, ozone, and aerosol scattering coefficient in the Pacific Northwest during the spring 2006 INTEX-B campaign, Journal of Geophysical Research-Atmospheres, 113, Artn D10305, 10.1029/2007jd009579, 2008.

Swartzendruber, P. C., Jaffe, D. A., and Finley, B.: Development and first results of an aircraft-based, high time resolution technique for gaseous elemental and reactive (oxidized) gaseous mercury, Environmental Science & Technology, 43, 7484-7489, 10.1021/es901390t, 2009.

Symons, M. C. R. and Yandell, J. K.: Unstable intermediates. Part LXXXVII. The dipositive radical cations of gallium, thallium, and mercury derived from aqueous solutions of gallium(III), thallium(III), and mercury(II) salts at 77 K by γ-irradiation, Journal of the Chemical Society A: Inorganic, Physical, Theoretical, 760-762, 10.1039/J19710000760, 1971.

Szponar, N., McLagan, D. S., Kaplan, R. J., Mitchell, C. P. J., Wania, F., Steffen, A., Stupple, G. W., Monaci, F., and Bergquist, B. A.: Isotopic characterization of atmospheric gaseous elemental mercury by passive air sampling, Environmental Science & Technology, 54, 10533-10543, 10.1021/acs.est.0c02251, 2020.

Tacey, S. A., Xu, L., Mavrikakis, M., and Schauer, J. J.: Heterogeneous reduction pathways for Hg(II) species on dry aerosols: A first-principles computational study, Journal of Physical Chemistry A, 120, 2106-2113, 10.1021/acs.jpca.5b12769, 2016.

Tacey, S. A., Szilvási, T., Xu, L., Schauer, J. J., and Mavrikakis, M.: The role of iron-oxide aerosols and sunlight in the atmospheric reduction of Hg(II) species: A DFT+U study, Applied Catalysis B, 234, 347-356, 10.1016/j.apcatb.2018.04.049, 2018a.

Tacey, S. A., Xu, L., Szilvási, T., Schauer, J. J., and Mavrikakis, M.: Quantum chemical calculations to determine partitioning coefficients for $HgCl_2$ on iron-oxide aerosols, Science of the Total Environment, 636, 580-587, 10.1016/j.scitotenv.2018.04.289, 2018b.

Talbot, R., Mao, H., Scheuer, E., Dibb, J., and Avery, M.: Total depletion of Hg degrees in the upper troposphere-lower stratosphere, Geophysical Research Letters, 34, 5, L23804,10.1029/2007gl031366, 2007.

Tang, K., Song, Z., Fu, X., Zhang, Y., Zhang, H., Sun, Y., Zhang, H., Wu, X., Deng, Q., Zhang, L., Suratman, S., Seng, T. H., and Feng, X.: An interhemispheric difference in atmospheric gaseous elemental mercury isotopes reveals a new insight in oceanic mercury emissions, Journal of Geophysical Research-Atmospheres, 130, 10.1029/2024jd042178, 2025.

Tas, E., Obrist, D., Peleg, M., Matveev, V., Faïn, X., Asaf, D., and Luria, M.: Measurement-based modelling of bromine-induced

formaterade ... [1428]
tog bort: Mercuric Oxides Drives Anomalous Isotope ... [1429]
formaterade ... [1430]
tog bort: Net Photo
tog bort: Air
formaterade ... [1431]
tog bort: Mercury Vapor
formaterade ... [1432]
formaterade ... [1433]
formaterade ... [1434]
tog bort: Et
formaterade ... [1435]
formaterade ... [1436]
tog bort: Mercury Isotope Shifts
tog bort: Response
formaterade ... [1438]
tog bort: Mercury Emissions
formaterade ... [1439]
tog bort: Underground Coal Fires
formaterade ... [1437]
formaterade ... [1440]
tog bort: Jaffe, D.
flyttade ned [18]: A., and Finley, B.: Development and
formaterade ... [1441]
tog bort: First Results of an Aircraft-Based, High Time ... [1442]
formaterade ... [1443]
flyttade (infogning) [18]
formaterade ... [1444]
formaterade ... [1445]
Formaterat ... [1446]
formaterade ... [1447]
tog bort: Characterization
formaterade ... [1448]
tog bort: Atmospheric Gaseous Elemental Mercury
formaterade ... [1449]
tog bort: Passive Air Sampling
formaterade ... [1450]
tog bort: Reduction Pathways
formaterade ... [1451]
tog bort: Species
formaterade ... [1452]
tog bort: Dry Aerosols
formaterade ... [1453]
tog bort: First-Principles Computational Study
formaterade ... [1454]
formaterade ... [1455]
formaterade ... [1456]
tog bort: The
formaterade ... [1457]
formaterade ... [1458]
formaterade ... [1459]
Formaterat ... [1460]

oxidation of mercury above the Dead Sea, Atmospheric Chemistry and Physics, 12, 2429-2440, 2012.

Tate, M. T., Janssen, S. E., Lepak, R. F., Flucke, L., and Krabbenhoft, D. P.: National-scale assessment of total gaseous mercury isotopes across the United States, Journal of Geophysical Research-Atmospheres, 128, e2022JD038276, 10.1029/2022JD038276, 2023.

Taylor, P. H., Mallipeddi, R., and Yamada, T.: LP/LIF study of the formation and consumption of mercury (I) chloride: Kinetics of mercury chlorination, Chemosphere, 61, 685-692, 2005.

Tellinghuisen, J. and Ashmore, J. G.: Mixed representations for diatomic spectroscopic data: application to mercury(I) bromide, Chemical Physics Letters, 102, 10-16, 1983.

Tellinghuisen, J., Tellinghuisen, P. C., Davies, S. A., Berwanger, P., and Viswanathan, K. S.: B → X transitions in HgCl and HgI, Applied Physics Letters, 41, 789-791, 10.1063/1.93704, 1982.

Terenin, A.: Photo-dissociation of the vapors of organo-metallic compounds, Journal of Chemical Physics, 2, 441-442, 10.1063/1.1749505, 1934.

Terenin, A. and Prileshajewa, N.: Photodissociation of the vapors of some organo-metallic compounds, Acta Physicochimica URSS, 1, 759-776, 1935.

Tevault, D., Strommen, D. P., and Nakamoto, K.: Reactions of mercury halides with carbon monoxide, nitric oxide, molecular nitrogen, and unsaturated hydrocarbons in argon matrices, Journal of the American Chemical Society, 99, 2997-3003, 10.1021/ja00451a024, 1977.

Thomsen, E. L. and Egsgaard, H.: Rate of reaction of dimethylmercury with oxygen atoms in the gas phase, Chemical Physics Letters, 125, 378-382, 1986.

Tong, Y., Eichhorst, T., Olson, M. R., Rutter, A. P., Shafer, M. M., Wang, X., and Schauer, J. J.: Comparison of heterogeneous photolytic reduction of Hg(II) in the coal fly ashes and synthetic aerosols, Atmospheric Research, 138, 324-329, 10.1016/j.atmosres.2013.11.015, 2014.

Tong, Y., Eichhorst, T., Olson, M. R., McGinnis, J. E., Turner, I., Rutter, A. P., Shafer, M. M., Wang, X., and Schauer, J. J.: Atmospheric photolytic reduction of Hg(II) in dry aerosols, Environmental Science-Processes & Impacts, 15, 1883-1888, 10.1039/c3em00249g, 2013.

Tong, Y. D., Zhang, H. F., Lin, H. M., de Foy, B., Chen, L., Zhang, W., Wang, X. J., and Guan, C. F.: A potential route for photolytic reduction of $HgCl_2$ and $HgBr_2$ in dry air and analysis about the impacts from ozone, Atmospheric Research, 249, 10.1016/j.atmosres.2020.105310, 2021.

Tossell, J. A.: Theoretical study of the photodecomposition of methyl Hg complexes, Journal of Physical Chemistry A, 102, 3587-3591, 10.1021/jp980244u, 1998.

Tossell, J. A.: Calculation of the energetics for oxidation of gas-phase elemental Hg by Br and BrO, Journal of Physical Chemistry A, 107, 7804-7808, 2003.

Tossell, J. A.: Calculation of the energetics for the oligomerization of gas phase HgO and HgS and for the solvolysis of crystalline HgO and HgS, Journal of Physical Chemistry A, 110, 2571-2578, 2006.

Tossell, J. A. and Vaughan, D. J.: Relationships between valence orbital binding-energies and crystal-structures in compounds of copper, silver, gold, zinc, cadmium, and mercury, Inorganic Chemistry, 20, 3333-3340, 10.1021/ic50224a038, 1981.

Toyota, K., Dastoor, A. P., and Ryzhkov, A.: Air-snowpack exchange of bromine, ozone and mercury in the springtime Arctic simulated by the 1-D model PHANTAS - Part 2: Mercury and its speciation, Atmospheric Chemistry and Physics, 14, 4135-4167, 2014.

Travnikov, O., Angot, H., Artaxo, P., Bencardino, M., Bieser, J., D'Amore, F., Dastoor, A., De Simone, F., Diéguez, M. D., Dommergue, A., Ebinghaus, R., Feng, X. B., Gencarelli, C. N., Hedgecock, I. M., Magand, O., Martin, L., Matthias, V., Mashyanov, N., Pirrone, N., Ramachandran, R., Read, K. A., Ryjkov, A., Selin, N. E., Sena, F., Song, S., Sprovieri, F., Wip, D., Wängberg, I., and Yang, X.: Multi-model study of mercury dispersion in the atmosphere: atmospheric processes and model evaluation, Atmospheric Chemistry and Physics, 17, 5271-5295, 10.5194/acp-17-5271-2017, 2017.

Tsui, M. T.-K., Blum, J. D., and Kwon, S. Y.: Review of stable mercury isotopes in ecology and biogeochemistry, Science of the Total Environment, 716, 135386, 2020.

Turro, N. J.: Influence of nuclear spin on chemical reactions: Magnetic isotope and magnetic field effects (A review), Proceedings of the National Academy of Sciences, 80, 609-621, 1983.

Ullrich, S. M., Tanton, T. W., and Abdrashitova, S. A.: Mercury in the aquatic environment: A review of factors affecting

tog bort: Scale Assessment
formaterade: Teckenfärg: Blå, Kondenserad med 0,4 pt
tog bort: Total Gaseous Mercury Isotopes Across
formaterade: Teckenfärg: Blå, Kondenserad med 0,4 pt
formaterade: Teckenfärg: Blå, Kondenserad med 0,3 pt
formaterade: Teckenfärg: Blå, Kondenserad med 0,2 pt

tog bort: Dissociation
formaterade: Teckenfärg: Blå, Kondenserad med 0,2 pt
tog bort: Vapors
formaterade: Teckenfärg: Blå, Kondenserad med 0,2 pt
tog bort: Organo-Metallic Compounds, The
formaterade: Teckenfärg: Blå, Kondenserad med 0,2 pt
tog bort:
formaterade: Teckenfärg: Blå, Kondenserad med 0,2 pt
formaterade: Teckenfärg: Blå, Kondenserad med 0,2 pt
Formaterat: Avstånd Efter: 0,6 Rad, Radavstånd: Flera 1,1 li
formaterade: Teckenfärg: Blå, Kondenserad med 0,3 pt
formaterade: Teckenfärg: Blå
formaterade: Teckenfärg: Blå, Kondenserad med 0,3 pt
formaterade: Teckenfärg: Blå, Kondenserad med 0,2 pt

tog bort: Valence Orbital Binding-Energies
formaterade: Teckenfärg: Blå, Kondenserad med 0,2 pt
tog bort: Crystal-Structures
formaterade: Teckenfärg: Blå, Kondenserad med 0,2 pt
tog bort: Compounds
formaterade: Teckenfärg: Blå, Kondenserad med 0,2 pt
tog bort: Copper, Silver, Gold, Zinc, Cadmium
formaterade: Teckenfärg: Blå, Kondenserad med 0,2 pt
tog bort: Mercury
formaterade: Teckenfärg: Blå, Kondenserad med 0,2 pt
formaterade: Teckenfärg: Blå, Kondenserad med 0,3 pt
formaterade: Teckenfärg: Blå, Kondenserad med 0,4 pt
formaterade: Teckenfärg: Blå, Kondenserad med 0,2 pt
Formaterat: Avstånd Efter: 0,6 Rad, Radavstånd: Flera 1,1 li
tog bort: The
formaterade: Teckenfärg: Blå, Kondenserad med 0,2 pt
tog bort: Review
formaterade: Teckenfärg: Blå, Kondenserad med 0,2 pt

methylation, Critical Reviews in Environmental Science and Technology, 31, 241-293, 2001.

UNEP: Global Mercury Assessment 2018: Sources, Emissions, Releases and Environmental Transport, UNEP Chemicals Branch, Geneva, Switzerland, 2018.

van der Linden, W. E. and Beers, C.: Determination of composition and stability-constants of complexes of mercury(II) with amino-acids, Analytica Chimica Acta, 68, 143-154, 10.1016/s0003-2670(01)85155-2, 1974.

van der Linden, W. E. and Beers, C.: Formation constants of mercury(II) with some buffer/masking agents and the formation of mixed-ligand complexes, Talanta, 22, 89-92, 10.1016/0039-9140(75)80148-2, 1975.

van Loon, L. L., Mader, E. A., and Scott, S. L.: Reduction of the aqueous mercuric ion by sulfite: UV spectrum of $HgSO_3$ and its intramolecular redox reaction, Journal of Physical Chemistry A, 104, 1621-1626, 2000.

van Loon, L. L., Mader, E. A., and Scott, S. L.: Sulfite stabilization and reduction of the aqueous mercuric ion: Kinetic determination of sequential formation constants, Journal of Physical Chemistry A, 105, 3190-3195, 2001.

Velivetskaya, T. A., Ignatiev, A. V., Yakovenko, V. V., and Vysotskiy, S. V.: Experimental studies of the oxygen isotope anomalies ($\Delta^{17}O$) of H_2O_2 and their relation to radical recombination reactions, Chemical Physics Letters, 693, 107-113, 10.1016/j.cplett.2018.01.012, 2018.

Velivetskaya, T. A., Ignatiev, A. V., Budnitskiy, S. Y., Yakovenko, V. V., and Vysotskiy, S. V.: Mass-independent fractionation of oxygen isotopes during H_2O_2 formation by gas-phase discharge from water vapour, Geochimica et Cosmochimica Acta, 193, 54-65, 10.1016/j.gca.2016.08.008, 2016.

Volman, D. H.: Reaction of optically excited mercury vapor with oxygen, Journal of Chemical Physics, 21, 2086-2087, 10.1063/1.1698769, 1953.

Vyazovetskii, Y. V.: Photochemical production of the ^{204}Hg isotope, Technical Physics, 57, 603-607, 2012.

Wallschläger, D., Hintelmann, H., Evans, R. D., and Wilken, R. D.: Volatilization of demethylmercury and elemental mercury from river Elbe floodplain soils, Water, Air, and Soil Pollution, 80, 1325-1329, 10.1007/BF01189798, 1995.

Wang, B., Yuan, W., Wang, X., Li, K., Lin, C.-J., Li, P., Lu, Z., Feng, X., and Sommar, J.: Canopy-level flux and vertical gradients of Hg^0 stable isotopes in remote evergreen broadleaf forest show year-around net Hg^0 deposition, Environmental Science & Technology, 56, 5950-5959, 10.1021/acs.est.2c00778, 2022.

Wang, C., Yang, S. C., Li, R. L., Yan, J. Y., Hu, Y. X., Lai, C. Y., Li, Z. G., Li, P., Zhang, L. M., and Feng, X. B.: Atmospheric mercury concentrations and isotopic compositions impacted by typical anthropogenic mercury emissions sources, Environmental Science & Technology, 58, 16855-16866, 10.1021/acs.est.4c07649, 2024.

Wang, Q., Zhang, L., Liang, X., Yin, X., Zhang, Y., Zheng, W., Pierce, E. M., and Gu, B.: Rates and dynamics of mercury isotope exchange between dissolved elemental Hg(0) and Hg(II) bound to organic and inorganic ligands, Environmental Science & Technology, 54, 15534-15545, 10.1021/acs.est.0c06229, 2020.

Wang, S., McNamara, S. M., Moore, C. W., Obrist, D., Steffen, A., Shepson, P. B., Staebler, R. M., Raso, A. R. W., and Pratt, K. A.: Direct detection of atmospheric atomic bromine leading to mercury and ozone depletion, Proceedings of the National Academy of Sciences, 116, 14479-14484, 10.1073/pnas.1900613116, 2019a.

Wang, X., Yuan, W., Lin, C.-J., Zhang, L., Zhang, H., and Feng, X.: Climate and vegetation as primary drivers for global mercury storage in surface soil, Environmental Science & Technology, 53, 10665-10675, 10.1021/acs.est.9b02386, 2019b.

Wang, X., Luo, J., Yuan, W., Lin, C.-J., Wang, F., Liu, C., Wang, G., and Feng, X.: Global warming accelerates uptake of atmospheric mercury in regions experiencing glacier retreat, Proceedings of the National Academy of Sciences of the United States of America, 117, 2049-2055, 10.1073/pnas.1906930117, 2020a.

Wang, X., Yuan, W., Lin, C.-J., Luo, J., Wang, F., Feng, X., Fu, X., and Liu, C.: Underestimated sink of atmospheric mercury in a deglaciated forest chronosequence, Environmental Science & Technology, 54, 8083-8093, 10.1021/acs.est.0c01667, 2020b.

Wang, X. F. and Andrews, L.: Infrared spectrum of $Hg(OH)_2$ in solid neon and argon, Inorganic Chemistry, 44, 108-113, 2005a.

Wang, X. F. and Andrews, L.: Mercury dihydride forms a covalent molecular solid, Physical Chemistry Chemical Physics, 7, 750-759, 2005b.

Wang, X. F., Andrews, L., Riedel, S., and Kaupp, M.: Mercury is a transition metal: The first experimental evidence for HgF_4, Angewandte Chemie-International Edition, 46, 8371-8375, 10.1002/anie.200703710, 2007.

Wang, Y., Liu, G., Fang, Y., Liu, P., Liu, Y., Guo, Y., Shi, J., Hu, L., Cai, Y., Yin, Y., and Jiang, G.: Dark oxidation of mercury

tog bort: Der
formaterade: Teckenfärg: Blå, Kondenserad med 0,2 pt
tog bort: Optically Excited Mercury Vapor
tog bort: Oxygen
formaterade: Teckenfärg: Blå, Kondenserad med 0,5 pt
formaterade: Teckenfärg: Blå, Kondenserad med 0,5 pt
formaterade: Teckenfärg: Blå, Kondenserad med 0,5 pt
formaterade: Teckenfärg: Blå, Kondenserad med 0,2 pt
tog bort: Level Flux
formaterade: Teckenfärg: Blå, Kondenserad med 0,2 pt
tog bort: Vertical Gradients
formaterade: Teckenfärg: Blå, Kondenserad med 0,2 pt
tog bort: Stable Isotopes
formaterade: Teckenfärg: Blå, Kondenserad med 0,2 pt
tog bort: Remote Evergreen Broadleaf Forest Show Year-Around Net…
formaterade: Teckenfärg: Blå, Kondenserad med 0,2 pt
tog bort: Deposition
formaterade: Teckenfärg: Blå, Kondenserad med 0,2 pt
formaterade: Teckenfärg: Blå, Kondenserad med 0,2 pt
Formaterat: Avstånd Efter: 0,6 Rad, Radavstånd: Flera 1,1 li
tog bort: Vegetation As Primary Drivers for Global Mercury Storage in Surface Soil
formaterade: Teckenfärg: Blå, Kondenserad med 0,2 pt
tog bort: Sink
formaterade: Teckenfärg: Blå, Kondenserad med 0,2 pt
tog bort: Atmospheric Mercury
formaterade: Teckenfärg: Blå, Kondenserad med 0,2 pt
tog bort: Deglaciated Forest Chronosequence
formaterade: Teckenfärg: Blå, Kondenserad med 0,2 pt
tog bort: 2005
formaterade: Teckenfärg: Blå, Kondenserad med 0,2 pt
formaterade: Teckenfärg: Blå, Kondenserad med 0,2 pt
Formaterat: Avstånd Efter: 0,6 Rad, Radavstånd: Flera 1,1 li

droplet: Mercurous Hg(I) species controls transformation kinetics, Water Research, 244, 10.1016/j.watres.2023.120472, 2023.

Wang, Y. W., Bartov, G., Wang, T., Reinfelder, J. R., Johnson, T. M., and Yee, N.: Rapid attainment of isotopic equilibrium after mercury reduction by ferrous iron minerals and isotopic exchange between Hg(II) and Hg(0), ACS Earth and Space Chemistry, 5, 1384-1394, 10.1021/acsearthspacechem.1c00026, 2021.

Wang, Z. and Pehkonen, S. O.: Oxidation of elemental mercury by aqueous bromine: atmospheric implications, Atmospheric Environment, 38, 3675-3688, 2004.

Wang, Z., Sun, T., Driscoll, C. T., Zhang, H., and Zhang, X.: Dimethylmercury in floodwaters of mercury contaminated rice paddies, Environmental Science & Technology, 53, 9453-9461, 10.1021/acs.est.8b07180, 2019c.

Warneck, P. (ed.) Sulfur compounds in the atmosphere, in: Chemistry of the Natural Atmosphere, International Geophysics vol. 71, Academic Press, 484-542, 10.1016/S0074-6142(08)60637-3, 1988.

Warneck, P.: In-cloud chemistry opens pathway to the formation of oxalic acid in the marine atmosphere, Atmospheric Environment, 37, 2423-2427, 10.1016/s1352-2310(03)00136-5, 2003.

Warneck, P. and Williams, J.: The atmospheric chemist's companion: numerical data for use in the atmospheric sciences, Springer Netherlands, New York, 10.1007/978-94-007-2275-0, 2012.

Washburn, S. J., Blum, J. D., Johnson, M. W., Tomes, J. M., and Carnell, P. J.: Isotopic characterization of mercury in natural gas via analysis of mercury removal unit catalysts, ACS Earth and Space Chemistry, 2, 462-470, 10.1021/acsearthspacechem.7b00118, 2018.

Washburn, S. J., Blum, J. D., Motta, L. C., Bergquist, B. A., and Weiss-Penzias, P.: Isotopic composition of Hg in fogwaters of coastal California, Environmental Science & Technology Letters, 8, 3-8, 2021.

Weigelt, A., Slemr, F., Ebinghaus, R., Pirrone, N., Bieser, J., Bodewadt, J., Esposito, G., and van Velthoven, P. F. J.: Mercury emissions of a coal-fired power plant in Germany, Atmospheric Chemistry and Physics, 16, 13653-13668, 10.5194/acp-16-13653-2016, 2016a.

Weigelt, A., Ebinghaus, R., Pirrone, N., Bieser, J., Bodewadt, J., Esposito, G., Slemr, F., van Velthoven, P. F. J., Zahn, A., and Ziereis, H.: Tropospheric mercury vertical profiles between 500 and 10,000 m in central Europe, Atmospheric Chemistry and Physics, 16, 4135-4146, 10.5194/acp-16-4135-2016, 2016b.

Weiss-Penzias, P., Sorooshian, A., Coale, K., Heim, W., Crosbie, E., Dadashazar, H., MacDonald, A. B., Wang, Z., and Jonsson, H.: Aircraft measurements of total mercury and monomethyl mercury in summertime marine stratus cloudwater from coastal California, USA, Environmental Science & Technology, 52, 2527-2537, 10.1021/acs.est.7b05395, 2018.

Weiss-Penzias, P. S., Ortiz, C., Acosta, R. P., Heim, W., Ryan, J. P., Fernandez, D., Collett, J. L., and Flegal, A. R.: Total and monomethyl mercury in fog water from the central California coast, Geophysical Research Letters, 39, L03804, 10.1029/2011gl050324, 2012.

West, J., Gindorf, S., and Jonsson, S.: Photochemical degradation of dimethylmercury in natural waters, Environmental Science & Technology, 56, 5920-5928, 10.1021/acs.est.1c08443, 2022.

Wiederhold, J. G.: Metal stable isotope signatures as tracers in environmental geochemistry, Environmental Science & Technology, 49, 2606-2624, 2015.

Wiederhold, J. G., Cramer, C. J., Daniel, K., Infante, I., Bourdon, B., and Kretzschmar, R.: Equilibrium mercury isotope fractionation between dissolved Hg(II) species and thiol-bound Hg, Environmental Science & Technology, 44, 4191-4197, 10.1021/es100205t, 2010.

Wigfield, D. C. and Perkins, S. L.: Oxidation of elemental mercury by hydroperoxides in aqueous solution, Canadian Journal of Chemistry, 63, 275-277, 10.1139/v85-045, 1985a.

Wigfield, D. C. and Perkins, S. L.: Oxidation state analysis of mercury: evidence of the formation of mercurous ion in the oxidation of mercury by peracetic acid, Journal of Applied Toxicology, 5, 339-341, 10.1002/jat.2550050514, 1985b.

Wigfield, D. C. and Tse, S.: The mechanism of biooxidation of mercury, Journal of Applied Toxicology, 6, 73-74, 10.1002/jat.2550060115, 1986.

Wilcox, J.: A Kinetic investigation of high-temperature mercury oxidation by chlorine, Journal of Physical Chemistry A, 113, 6633-6639, 10.1021/jp901050d, 2009.

Williston, S. H.: Mercury in atmosphere, Journal of Geophysical Research, 73, 7051-&, 1968.

Woerndle, G. E., Tsui, M. T. K., Sebestyen, S. D., Blum, J. D., Nie, X. P., and Kolka, R. K.: New insights on ecosystem mercury cycling revealed by stable isotopes of mercury in water flowing from a headwater peatland catchment, Environmental Science & Technology, 52, 1854-1861, 10.1021/acs.est.7b04449, 2018.

tog bort: Attainment
tog bort: Isotopic Equilibrium
formaterade ... [1461]
formaterade ... [1462]
tog bort: Mercury Reduction
formaterade ... [1463]
tog bort: Ferrous Iron Minerals
formaterade ... [1464]
tog bort: Isotopic Exchange
formaterade ... [1465]
tog bort: Floodwaters
formaterade ... [1466]
tog bort: Mercury Contaminated Rice Paddies
formaterade ... [1467]
tog bort: Compounds
formaterade ... [1468]
tog bort: Atmosphere
formaterade ... [1469]
formaterade ... [1470]
tog bort: Characterization
formaterade ... [1471]
Formaterat ... [1472]
formaterade ... [1473]
tog bort: Mercury
formaterade ... [1474]
tog bort: Natural Gas
formaterade ... [1475]
tog bort: Analysis
formaterade ... [1476]
tog bort: Mercury Removal Unit Catalysts
formaterade ... [1477]
formaterade ... [1478]
tog bort: Composition
formaterade ... [1479]
tog bort: Fogwaters
formaterade ... [1480]
tog bort: Coastal
formaterade ... [1481]
formaterade ... [1482]
Formaterat ... [1483]
tog bort: 2016
formaterade ... [1484]
tog bort: Measurements
formaterade ... [1485]
tog bort: Total Mercury
formaterade ... [1486]
tog bort: Monomethyl Mercury
formaterade ... [1487]
tog bort: Summertime Marine Stratus Cloudwater
formaterade ... [1488]
tog bort: Coastal
formaterade ... [1489]
tog bort: Degradation
formaterade ... [1490]
tog bort: Dimethylmercury
formaterade ... [1491]
tog bort: Natural Waters
formaterade ... [1492]
tog bort: Stable Isotope Signatures
formaterade ... [1493]
tog bort: Tracers
formaterade ... [1494]
tog bort: Environmental Geochemistry
formaterade ... [1495]
formaterade ... [1496]
tog bort: Mercury Isotope Fractionation
formaterade ... [1497]
tog bort: Dissolved

Wolfe, N. L., Zepp, R. G., Gordon, J. A., and Baughman, G. L.: Chemistry of methylmercurials in aqueous solution, Chemosphere, 2, 147-152, 1973.

Won, A. Y., Kim, M. K., and Zoh, K. D.: Characteristics of total and methyl mercury in precipitation in Seoul, Korea, Atmospheric Pollution Research, 10, 493-500, 10.1016/j.apr.2018.10.001, 2019.

Wright, L. P., Zhang, L., and Marsik, F. J.: Overview of mercury dry deposition, litterfall, and throughfall studies, Atmospheric Chemistry and Physics, 16, 13399-13416, 10.5194/acp-16-13399-2016, 2016.

Wu, L., Mao, H., Ye, Z., Dibble, T. S., Saiz-Lopez, A., and Zhang, Y.: Improving simulation of gas-particle partitioning of atmospheric mercury using CMAQ-newHg-Br v2, Journal of Advances in Modeling Earth Systems, 16, e2023MS003823, 10.1029/2023MS003823, 2024a.

Wu, P., Song, Z., Zhang, P., Huang, S., Yuan, T., and Zhang, Y.: Atmospheric monomethylmercury: Inferred sources constrained by observations and implications for human exposure, Environment International, 193, 109-127, 10.1016/j.envint.2024.109127, 2024b.

Wu, Q., Wang, S., Li, G., Liang, S., Lin, C.-J., Wang, Y., Cai, S., Liu, K., and Hao, J.: Temporal trend and spatial distribution of speciated atmospheric mercury emissions in China during 1978–2014, Environmental Science & Technology, 50, 13428-13435, 10.1021/acs.est.6b04308, 2016.

Wu, R., Wang, C., and Dibble, T. S.: First experimental kinetic study of the atmospherically important reaction of BrHg + NO_2, Chemical Physics Letters, 759, 137928, 10.1016/j.cplett.2020.137928, 2020.

Wu, R. R., Castro, P. J., Gaito, C., Beiter, K., Dibble, T. S., and Wang, C. J.: Combined experimental and computational kinetics studies for the atmospherically important BrHg radical reacting with NO and O_2, Journal of Physical Chemistry A, 126, 3914-3925, 10.1021/acs.jpca.2c02531, 2022.

Wu, X., Fu, X. W., Zhang, H., Tang, K. H., Wang, X., Zhang, H., Deng, Q. W., Zhang, L. M., Liu, K. Y., Wu, Q. R., Wang, S. X., and Feng, X. B.: Changes in atmospheric gaseous elemental mercury concentrations and isotopic compositions at Mt. Changbai during 2015-2021 and Mt. Ailao during 2017-2021 in China, Journal of Geophysical Research-Atmospheres, 128, 10.1029/2022jd037749, 2023a.

Wu, Y. R., Mao, Y. X., Liu, G. L., Li, Y. B., Guo, Y. Y., Liu, Y. W., Yin, Y. G., Cai, Y., and Jiang, G. B.: Analytical methods, occurrence, fate, and toxicity of ethylmercury in the environment: Review and outlook, Reviews of Environmental Contamination and Toxicology, 261, 10.1007/s44169-023-00037-x, 2023b.

Wängberg, I., Munthe, J., Pirrone, N., Iverfeldt, Å., Bahlman, E., Costa, P., Ebinghaus, R., Feng, X., Ferrara, R., Gårdfeldt, K., Kock, H., Lanzillotta, E., Mamane, Y., Mas, F., Melamed, E., Osnat, Y., Prestbo, E., Sommar, J., Schmolke, S., Spain, G., Sprovieri, F., and Tuncel, G.: Atmospheric mercury distribution in Northern Europe and in the Mediterranean region, Atmospheric Environment, 35, 3019-3025, 2001.

Xiao, Z., Munthe, J., Strömberg, D., and Lindqvist, O.: Photochemical behaviour of inorganic mercury compounds in aqueous solution, in: Mercury pollution: Integration and synthesis, edited by: Watras, C. J., and Huckabee, J. W., Lewis Publishers, 581-594, 1994.

Xiao, Z., Sommar, J., Wei, S., and Lindqvist, O.: Sampling and determination of gas phase divalent mercury in the air using a KCl coated denuder, Fresenius Journal of Analytical Chemistry, 358, 386-391, 1997.

Xie, Z. Q., Sander, R., Pöschl, U., and Slemr, F.: Simulation of atmospheric mercury depletion events (AMDEs) during polar springtime using the MECCA box model, Atmospheric Chemistry and Physics, 8, 7165 - 7180, 2008.

Yamakawa, A., Moriya, K., and Yoshinaga, J.: Determination of isotopic composition of atmospheric mercury in urban-industrial and coastal regions of Chiba, Japan, using cold vapor multicollector inductively coupled plasma–mass spectrometry, Chemical Geology, 448, 84-92, 10.1016/j.chemgeo.2016.11.010, 2017.

Yamakawa, A., Luke, W., Kelley, P., Ren, X., and Iaukea-Lum, M.: Unraveling atmospheric mercury dynamics at Mauna Loa through the isotopic analysis of total gaseous mercury, Ecotoxicology and Environmental Safety, 284, 116993, 10.1016/j.ecoenv.2024.116993, 2024.

Yang, J., Kim, J., Soerensen, A. L., Lee, W., and Han, S.: The role of fluorescent dissolved organic matter on mercury photoreduction rates: A case study of three temperate lakes, Geochimica et Cosmochimica Acta, 277, 192-205, 2020a.

Yang, M., Rasche, B., and Compton, R. G.: Acoustic cavitation generates molecular mercury(II) hydroxide, Hg(OH)2, from biphasic water/mercury mixtures, Chemical Science, 11, 556-560, 10.1039/C9SC04743C, 2020b.

Yang, S. and Liu, Y.: Nuclear volume effects in equilibrium stable isotope fractionations of mercury, thallium and lead, Scientific Reports, 5, 12626, 10.1038/srep12626, 2015.

Yang, X., Jiskra, M., and Sonke, J. E.: Experimental rainwater divalent mercury speciation and photoreduction rates in the presence of halides and organic carbon, Science of the Total Environment, 697, 133821, 10.1016/j.scitotenv.2019.133821, 2019.

tog bort: Simulation
formaterade ... [1510]
tog bort: Gas-Particle Partitioning
formaterade ... [1511]
tog bort: Atmospheric Mercury Using
formaterade ... [1512]
formaterade ... [1513]
formaterade ... [1514]
Formaterat ... [1515]
formaterade ... [1516]
tog bort: Experimental
formaterade ... [1517]
tog bort: Computational Kinetics Studies
formaterade ... [1518]
tog bort: Atmospherically Important
formaterade ... [1519]
tog bort: Radical Reacting
formaterade ... [1520]
formaterade ... [1521]
tog bort: Atmospheric Gaseous Elemental Mercury Concentrations
formaterade ... [1522]
tog bort: Isotopic Compositions
formaterade ... [1523]
tog bort: During
formaterade ... [1524]
tog bort: During
formaterade ... [1525]
formaterade ... [1526]
tog bort: Methods, Occurrence, Fate
formaterade ... [1527]
tog bort: Toxicity
formaterade ... [1528]
tog bort: Ethylmercury
formaterade ... [1529]
tog bort: Environment
formaterade ... [1530]
tog bort: Outlook
formaterade ... [1531]
tog bort: A
formaterade ... [1532]
tog bort: Gardfeldt
formaterade ... [1533]
formaterade ... [1534]
formaterade ... [1535]
tog bort:
formaterade ... [1536]
formaterade ... [1537]
formaterade ... [1538]
tog bort: Et
formaterade ... [1539]
formaterade ... [1540]
formaterade ... [1541]
tog bort: The
formaterade ... [1542]

Yin, Y., Chen, B., Mao, Y., Wang, T., Liu, J., Cai, Y., and Jiang, G.: Possible alkylation of inorganic Hg(II) by photochemical processes in the environment, Chemosphere, 88, 8-16, 2012.

Young, E. D., Galy, A., and Nagahara, H.: Kinetic and equilibrium mass-dependent isotope fractionation laws in nature and their geochemical and cosmochemical significance, Geochimica et Cosmochimica Acta, 66, 1095-1104, 10.1016/S0016-7037(01)00832-8, 2002.

Yu, B., Yang, L., Liu, H., Yang, R., Fu, J., Wang, P., Li, Y., Xiao, C., Liang, Y., Hu, L., Zhang, Q., Yin, Y., Shi, J., and Jiang, G.: Katabatic wind and sea-ice dynamics drive isotopic variations of total gaseous mercury on the Antarctic coast, Environmental Science & Technology, 55, 6449-6458, 10.1021/acs.est.0c07474, 2021.

Yuan, S., Chen, J., Hintelmann, H., Cai, H., Yuan, W., He, S., Zhang, K., Zhang, Y., and Liu, Y.: Event-based atmospheric precipitation uncovers significant even and odd Hg isotope anomalies associated with the circumpolar vortex, Environmental Science & Technology, 56, 12713-12722, 10.1021/acs.est.2c02613, 2022.

Yuan, S., Zhang, Y., Chen, J., Kang, S., Zhang, J., Feng, X., Cai, H., Wang, Z., Wang, Z., and Huang, Q.: Large variation of mercury isotope composition during a single precipitation event at Lhasa City, Tibetan Plateau, China, Procedia Earth and Planetary Science, 13, 282-286, 10.1016/j.proeps.2015.07.066, 2015.

Yuan, T. F., Zhang, P., Song, Z. C., Huang, S. J., Wang, X., and Zhang, Y. X.: Buffering effect of global vegetation on the air–land exchange of mercury: Insights from a novel terrestrial mercury model based on CESM2-CLM5, Environment International, 174, 10.1016/j.envint.2023.107904, 2023a.

Yuan, W., Wang, X., Lin, C.-J., Sommar, J., Lu, Z., and Feng, X.: Process factors driving dynamic exchange of elemental mercury vapor over soil in broadleaf forest ecosystems, Atmospheric Environment, 219, 117047, 10.1016/j.atmosenv.2019.117047, 2019a.

Yuan, W., Wang, X., Lin, C.-J., Sommar, J. O., Wang, B., Lu, Z., and Feng, X.: Quantification of atmospheric mercury deposition to and legacy re-emission from a subtropical forest floor by mercury isotopes, Environmental Science & Technology, 55, 12352-12361, 10.1021/acs.est.1c02744, 2021.

Yuan, W., Wang, X., Lin, C.-J., Song, Q., Zhang, H., Wu, F., Liu, N., Lu, H., and Feng, X.: Deposition and re-emission of atmospheric elemental mercury over the tropical forest floor, Environmental Science & Technology, 57, 10686-10695, 10.1021/acs.est.3c01222, 2023b.

Yuan, W., Wang, X., Lin, C.-J., Wu, C., Zhang, L., Wang, B., Sommar, J., Lu, Z., and Feng, X.: Stable mercury isotope transition during postdepositional decomposition of biomass in a forest ecosystem over five centuries, Environmental Science & Technology, 54, 8739-8749, 10.1021/acs.est.0c00950, 2020.

Yuan, W., Sommar, J., Lin, C.-J., Wang, X., Li, K., Liu, Y., Zhang, H., Lu, Z., Wu, C., and Feng, X.: Stable isotope evidence shows re-emission of elemental mercury vapor occurring after reductive loss from foliage, Environmental Science & Technology, 53, 651-660, 10.1021/acs.est.8b04865, 2019b.

Zacharewski, T. R. and Cherniak, E. A.: FTIR investigation of the heterogeneous reaction of HgO (s) with SO_2(g) at ambient temperature, Atmospheric Environment, 21, 2327-2332, 1987.

Zerkle, A. L., Yin, R., Chen, C., Li, X., Izon, G. J., and Grasby, S. E.: Anomalous fractionation of mercury isotopes in the Late Archean atmosphere, Nature Communications, 11, 1709, 2020.

Zhang, H.: Photochemical redox reactions of mercury, in: Structure and Bonding 120, Atwood, D. A. (ed.), Springer, Berlin Heidelberg, 37-79, 10.1007/430_015, 2006.

Zhang, H., Fu, X. W., Wang, X., and Feng, X. B.: Measurements and distribution of atmospheric particulate-bound mercury: A review, Bulletin of Environmental Contamination and Toxicology, 103, 48-54, 10.1007/s00128-019-02663-5, 2019c.

Zhang, H., Fu, X., Wu, X., Deng, Q., Tang, K., Zhang, L., Sommar, J., Sun, G., and Feng, X.: Using mercury stable isotopes to quantify bidirectional water–atmosphere Hg(0) exchange fluxes and explore controlling factors, Environmental Science & Technology, 10.1021/acs.est.3c01273, 2023a.

Zhang, H., Tan, Q., Zhang, L., Fu, X., and Feng, X.: A laboratory study on the isotopic composition of Hg(0) emitted from Hg-enriched soils in Wanshan Hg mining area, Journal of Geophysical Research: Atmospheres, 125, 10.1029/2020JD032572, 2020.

Zhang, H., Wang, Z. W., and Zhang, X. S.: Methylmercury concentrations and potential sources in atmospheric fine particles in Beijing, China, Science of the Total Environment, 681, 183-190, 10.1016/j.scitotenv.2019.05.128, 2019a.

Zhang, H., Wu, X., Deng, Q., Zhang, L., Fu, X., and Feng, X.: Extraction of ultratrace dissolved gaseous mercury and reactive mercury in natural freshwater for stable isotope analysis, Journal of Analytical Atomic Spectrometry, 36, 1921-1932,

formaterade ... [1543]
formaterade ... [1544]
tog bort: Wind
formaterade ... [1545]
tog bort: Sea-Ice Dynamics Drive Isotopic Variations
formaterade ... [1546]
tog bort: Total Gaseous Mercury
formaterade ... [1547]
tog bort: Coast
formaterade ... [1548]
tog bort: Based Atmospheric Precipitation Uncovers Si ... [1549]
formaterade ... [1550]
tog bort: Odd
formaterade ... [1551]
tog bort: Isotope Anomalies Associated
formaterade ... [1552]
tog bort: Circumpolar Vortex
formaterade ... [1553]
tog bort: Variation of Mercury Isotope Composition Du ... [1554]
formaterade ... [1555]
tog bort: -
formaterade ... [1556]
tog bort: Atmospheric Mercury Deposition
formaterade ... [1557]
tog bort: Legacy Re
formaterade ... [1558]
tog bort: Subtropical Forest Floor
formaterade ... [1559]
tog bort: Mercury Isotopes
formaterade ... [1560]
tog bort: Re-Emission
formaterade ... [1561]
tog bort: Atmospheric Elemental Mercury
formaterade ... [1562]
tog bort: Tropical Forest Floor
formaterade ... [1563]
tog bort: Mercury Isotope Transition
formaterade ... [1564]
tog bort: Postdepositional Decomposition
formaterade ... [1565]
tog bort: Biomass
formaterade ... [1566]
tog bort: Forest Ecosystem
formaterade ... [1567]
tog bort: Five Centuries
formaterade ... [1568]
tog bort: Isotope Evidence Shows Re
formaterade ... [1569]
tog bort: Elemental Mercury Vapor Occurring
formaterade ... [1570]
tog bort: Reductive Loss
formaterade ... [1571]
tog bort: Foliage
formaterade ... [1572]
flyttade (infogning) [19]
formaterade ... [1573]
Formaterat ... [1574]
formaterade ... [1575]
tog bort: Tan, Q., Zhang, L., Fu, X., and Feng, X.: A La ... [1576]
formaterade ... [1577]

10.1039/D1JA00212K, 2021a.

Zhang, H., Yin, R. S., Feng, X. B., Sommar, J., Anderson, C. W. N., Sapkota, A., Fu, X. W., and Larssen, T.: Atmospheric mercury inputs in montane soils increase with elevation: Evidence from mercury isotope signatures, Scientific Reports, 3, 3322, 2013.

Zhang, K., Pu, Q., Liu, J., Hao, Z., Zhang, L., Zhang, L., Fu, X., Meng, B., and Feng, X.: Using mercury stable isotopes to quantify directional soil–atmosphere Hg(0) exchanges in rice paddy ecosystems: Implications for Hg(0) emissions to the atmosphere from land surfaces, Environmental Science & Technology, 58, 11053-11062, 10.1021/acs.est.4c02143, 2024.

Zhang, K., Zheng, W., Sun, R., He, S., Shuai, W., Fan, X., Yuan, S., Fu, P., Deng, J., Li, X., Wang, S., and Chen, J.: Stable isotopes reveal photoreduction of particle-bound mercury driven by water-soluble organic carbon during severe haze, Environmental Science & Technology, 56, 10619-10628, 10.1021/acs.est.2c01933, 2022.

Zhang, L., Wright, L. P., and Blanchard, P.: A review of current knowledge concerning dry deposition of atmospheric mercury, Atmospheric Environment, 43, 5853-5864, 2009.

Zhang, L., Wang, S., Wu, Q., Wang, F., Lin, C. J., Zhang, L., Hui, M., Yang, M., Su, H., and Hao, J.: Mercury transformation and speciation in flue gases from anthropogenic emission sources: A critical review, Atmospheric Chemistry & Physics, 16, 2417-2433, 10.5194/acp-16-2417-2016, 2016.

Zhang, L., Lyman, S., Mao, H., Lin, C.-J., Gay, D. A., Wang, S., Gustin, M. S., Feng, X., and Wania, F.: A synthesis of research needs for improving the understanding of atmospheric mercury cycling, Atmospheric Chemistry and Physics, 17, 9133-9144, 10.5194/acp-17-9133-2017, 2017.

Zhang, P. and Zhang, Y. X.: Earth system modeling of mercury using CESM2-Part 1: Atmospheric model CAM6-Chem/Hg v1.0, Geoscientific Model Development, 15, 3587-3601, 10.5194/gmd-15-3587-2022, 2022.

Zhang, T. and Hsu-Kim, H.: Photolytic degradation of methylmercury enhanced by binding to natural organic ligands, Nature Geoscience, 3, 473-476, 10.1038/ngeo892, 2010.

Zhang, Y., Horowitz, H., Wang, J., Xie, Z., Kuss, J., and Soerensen, A. L.: A coupled global atmosphere-ocean model for air-sea exchange of mercury: Insights into wet deposition and atmospheric redox chemistry, Environmental Science & Technology, 10.1021/acs.est.8b06205, 2019b.

Zhang, Y., Song, Z., Huang, S., Zhang, P., Peng, Y., Wu, P., Gu, J., Dutkiewicz, S., Zhang, H., Wu, S., Wang, F., Chen, L., Wang, S., and Li, P.: Global health effects of future atmospheric mercury emissions, Nature Communications, 12, 3035, 10.1038/s41467-021-23391-7, 2021b.

Zhang, Y., Xu, Z., Han, G., Chu, Z., Zhou, Q., Chen, Q., Wu, G., Shi, G., Wang, X., and Chen, L.: Improved mechanistic modeling on reproducing particle-bound mercury in the marine atmosphere, Environmental Science & Technology, 59, 2611-2622, 10.1021/acs.est.4c09481, 2025.

Zhang, Y., Zhang, L., Cao, S., Liu, X., Jin, J., and Zhao, Y.: Improved aanthropogenic mercury emission inventories for China from 1980 to 2020: Toward more accurate effectiveness evaluation for the Minamata convention, Environmental Science & Technology, 57, 8660-8670, 10.1021/acs.est.3c01065, 2023a.

Zhang, Y., X., Zhang, P., Song, Z. C., Huang, S. J., Yuan, T. F., Wu, P. P., Shah, V. R., Liu, M. D., Chen, L., Wang, X. J., Zhou, J., and Agnan, Y.: An updated global mercury budget from a coupled atmosphere–land-ocean model: 40% more re-emissions buffer the effect of primary emission reductions, One Earth, 6, 316-325, 10.1016/j.oneear.2023.02.004, 2023b.

Zhao, H., Meng, B., Sun, G., Lin, C.-J., Feng, X., and Sommar, J.: Chemistry and isotope fractionation of divalent mercury during aqueous reduction mediated by selected oxygenated organic ligands, Environmental Science & Technology, 55, 13376-13386, 2021.

Zhao, Y., Hallar, A. G., and Mazzoleni, L. R.: Atmospheric organic matter in clouds: exact masses and molecular formula identification using ultrahigh-resolution FT-ICR mass spectrometry, Atmospheric Chemistry and Physics, 13, 12343-12362, 10.5194/acp-13-12343-2013, 2013.

Zhen, J., Li, T., Cai, H., Nie, X., He, S., Meng, M., Wang, Y., and Chen, J.: Photoreduction and origin of dissolved and particulate mercury in cloud water: Insights from stable mercury isotopes, Journal of Hazardous Materials, 474, 134654, 10.1016/j.jhazmat.2024.134654, 2024.

Zhen, J., Li, T., Xu, X., Du, P., Song, Y., Nie, X., Liu, X., Liu, H., Bi, Y., Wang, X., Xue, L., and Wang, Y.: Changed mercury speciation in clouds driven by changing cloud water chemistry and impacts on photoreduction: Field evidence at Mt. Tai in eastern China, Water Research, 244, 120402, 10.1016/j.watres.2023.120402, 2023.

Zheng, W. and Hintelmann, H.: Mercury isotope fractionation during photoreduction in natural water is controlled by its Hg/DOC

formaterade ... [1578]
tog bort: H., Fu, X., Wu, X., Deng, Q.,
formaterade ... [1579]
flyttade upp [19]: Tang, K., Zhang, L., Sommar, J., Sun, G., and
tog bort: Quantify Directional Soil–Atmosphere
formaterade ... [1580]
tog bort: Mercury Stable Isotopes to Quantify Bidirecti ... [1581]
tog bort: Mercury Stable Isotopes
formaterade ... [1582]
formaterade ... [1583]
formaterade ... [1587]
tog bort: Atmosphere
formaterade ... [1584]
tog bort: Exchanges
tog bort: Emissions
formaterade ... [1585]
tog bort: Rice Paddy Ecosystems
formaterade ... [1586]
formaterade ... [1588]
tog bort: Land Surfaces
formaterade ... [1589]
formaterade ... [1590]
tog bort: Isotopes Reveal Photoreduction of Particle-Bo ... [1591]
formaterade ... [1592]
formaterade ... [1593]
Formaterat ... [1594]
formaterade ... [1595]
tog bort: Coupled Global Atmosphere-Ocean Model
formaterade ... [1596]
tog bort: Air-Sea Exchange
tog bort: Mercury
formaterade ... [1598]
tog bort: Wet Deposition
formaterade ... [1599]
tog bort: Atmospheric Redox Chemistry
formaterade ... [1597]
formaterade ... [1600]
Formaterat ... [1601]
formaterade ... [1602]
tog bort: -
formaterade ... [1603]
tog bort: Isotope Fractionation
formaterade ... [1604]
tog bort: Divalent Mercury
formaterade ... [1605]
tog bort: Aqueous Reduction Mediated
formaterade ... [1606]
tog bort: Selected Oxygenated Organic Ligands
formaterade ... [1607]
formaterade ... [1608]
formaterade ... [1609]
formaterade ... [1610]

ratio, Geochimica et Cosmochimica Acta, 73, 6704-6715, 2009.

Zheng, W. and Hintelmann, H.: Nuclear field shift effect in isotope fractionation of mercury during abiotic reduction in the absence of light, Journal of Physical Chemistry A, 114, 4238-4245, 10.1021/jp910353y, 2010a.

Zheng, W. and Hintelmann, H.: Isotope fractionation of mercury during its photochemical reduction by low-molecular-weight organic compounds, Journal of Physical Chemistry A, 114, 4246-4253, 2010b.

Zheng, W., Foucher, D., and Hintelmann, H.: Mercury isotope fractionation during volatilization of Hg(0) from solution into the gas phase, Journal of Analytical Atomic Spectrometry, 22, 1097-1104, 10.1039/B705677j, 2007.

Zheng, W., Liang, L. Y., and Gu, B. H.: Mercury reduction and oxidation by reduced natural organic matter in anoxic environments, Environmental Science & Technology, 46, 292-299, 2012.

Zheng, W., Obrist, D., Weis, D., and Bergquist, B. A.: Mercury isotope compositions across North American forests, Global Biogeochemical Cycles, 30, 2015GB005323, 10.1002/2015GB005323, 2016.

Zheng, W., Lin, H., Mann, B. F., Liang, L., and Gu, B.: Oxidation of dissolved elemental mercury by thiol compounds under anoxic conditions, Environmental Science & Technology, 47, 12827-12834, 10.1021/es402697u, 2013.

Zheng, W., Demers, J. D., Lu, X., Bergquist, B. A., Anbar, A. D., Blum, J. D., and Gu, B. H.: Mercury stable isotope fractionation during abiotic dark oxidation in the presence of thiols and natural organic matter, Environmental Science & Technology, 53, 1853-1862, 10.1021/acs.est.8b05047, 2019.

Zheng, W., Chandan, P., Steffen, A., Stupple, G., de Vera, J., Mitchell, C., Wania, F., and Bergquist, B.: Mercury stable isotopes reveal the sources and transformations of atmospheric Hg in the high Arctic, Applied Geochemistry, 131, 10.1016/j.apgeochem.2021.105002, 2021.

Zhou, J. and Obrist, D.: Global mercury assimilation by vegetation, Environmental Science & Technology, 55, 14245-14257, 10.1021/acs.est.1c03530, 2021.

Zhou, J., Obrist, D., Dastoor, A., Jiskra, M., and Ryjkov, A.: Vegetation uptake of mercury and impacts on global cycling, Nature Reviews Earth & Environment, 2, 269-284, 10.1038/s43017-021-00146-y, 2021.

Zhu, W., Lin, C. J., Wang, X., Sommar, J., Fu, X. W., and Feng, X. B.: Global observations and modeling of atmosphere-surface exchange of elemental mercury: a critical review, Atmospheric Chemistry and Physics, 16, 4451-4480, 10.5194/acp-16-4451-2016, 2016.

Zhu, W., Fu, X., Zhang, H., Liu, C., Skyllberg, U., Sommar, J., Yu, B., and Feng, X.: Mercury isotope fractionation during the exchange of Hg(0) between the atmosphere and land surfaces: Implications for Hg(0) exchange processes and controls, Environmental Science & Technology, 56, 1445-1457, 10.1021/acs.est.1c05602, 2022.

Zhu, W., Li, Z., Li, P., Sommar, J., Fu, X., Feng, X., Yu, B., Zhang, W., Reis, A. T., and Pereira, E.: Legacy mercury re-emission and subsurface migration at contaminated sites constrained by Hg isotopes and chemical speciation, Environmental Science & Technology, 58, 5336-5346, 10.1021/acs.est.3c07276, 2024.

tog bort: Field Shift Effect
formaterade ... [1611]
tog bort: Isotope Fractionation
formaterade ... [1612]
tog bort: Mercury
tog bort: Absence
formaterade ... [1613]
tog bort: Abiotic Reduction
formaterade ... [1614]
formaterade ... [1615]
tog bort: Light
formaterade ... [1616]
tog bort: Fractionation
formaterade ... [1617]
tog bort: Mercury
formaterade ... [1618]
tog bort: Its Photochemical Reduction
tog bort: Low-Molecular-Weight Organic Compounds
formaterade ... [1619]
formaterade ... [1620]
formaterade ... [1621]
tog bort: Reduction
formaterade ... [1622]
tog bort: Oxidation
formaterade ... [1623]
tog bort: Reduced Natural Organic Matter
formaterade ... [1624]
tog bort: Anoxic Environments
formaterade ... [1625]
tog bort: Dissolved Elemental Mercury
tog bort: Thiol Compounds
formaterade ... [1626]
formaterade ... [1627]
tog bort: Anoxic Conditions
formaterade ... [1628]
tog bort: Stable Isotope Fractionation
formaterade ... [1629]
tog bort: Abiotic Dark Oxidation
formaterade ... [1630]
tog bort: Presence
formaterade ... [1631]
tog bort: Thiols
formaterade ... [1632]
tog bort: Natural Organic Matter
formaterade ... [1633]
formaterade ... [1634]
tog bort: De
formaterade ... [1635]
formaterade ... [1636]
tog bort: Mercury Assimilation
formaterade ... [1637]
tog bort: Vegetation
formaterade ... [1638]
Formaterat ... [1639]
formaterade ... [1640]
tog bort: Isotope Fractionation
formaterade ... [1641]
tog bort: Exchange
formaterade ... [1642]
tog bort: Atmosphere
formaterade ... [1643]
tog bort: Land Surfaces
tog bort: Exchange Processes
formaterade ... [1645]
tog bort: Controls
formaterade ... [1644]
formaterade ... [1646]
tog bort: Mercury Re

Appendix

List of symbols and acronyms

Symbol	Quantity	Unit etc.
α	mass accommodation coefficient	dimensionless
$\alpha^{xxx/198}$	fractionation factor of the Hg isotope with mass number xxx (relative to 198)	
α_{A-B}	$\equiv \alpha^{xxx}_{A-B}$, isotope fractionation factor between any two parts (chemicals, phases etc.) of a system	
β^{xxx}	$\equiv \beta^{xxx/198}$, scaling factor for an isotope effect acting on the Hg isotope with mass number xxx.	
β_{NFS}	$\equiv \beta^{xxx/198}_{NFS}$, scaling factor for NFS acting on the Hg isotope with mass number xxx.	
$\beta_{EIE-MDF}$	$\equiv \beta^{xxx/198}_{EIE-MDF}$, scaling factor for equilibrium MDF acting on the Hg isotope with mass number xxx.	
$\beta_{KIE-MDF}$	$\equiv \beta^{xxx/198}_{KIE-MDF}$, scaling factor for kinetic MDF acting on the Hg isotope with mass number xxx.	
β_{qr}	cumulative stability coefficient for a complex of the type $\{HgL_q(OH)_r\}^{(2-r)+}$	miscellaneous
γ	uptake coefficient (probability)	dimensionless
γ^0_{net}	initial net uptake coefficient (probability)	
γ^∞_{net}	steady-state net uptake coefficient (probability)	
$\delta^{xxx}Hg$	δ-notation for the ^{xxx}Hg isotopic composition in a sample relative to that of the NIST3133 standard.	dimensionless (‰)
$\delta^{202}Hg$	δ-notation to describe total mass-dependent fractionation	
δ_A, δ_B	δ-notation for an isotope in reservoir A and B, respectively	
δ_0	$\equiv(\delta^{xxx}Hg)_0$, initial $\delta^{xxx}Hg$ of a process	
$\Delta^{xxx}Hg$	Δ-notation, deviation from mass dependence ($\delta^{202}Hg$) of the Hg isotope with mass number xxx.	
$\varepsilon^{xxx}Hg$	enrichment factor for a Hg isotope with mass number xxx.	
ε^{xxx}_{A-B}	$\equiv \varepsilon^{xxx}Hg_{A-B}$, enrichment factor for an isotope between two reservoirs A and B.	
$E^{xxx}Hg$	enrichment factor for a Hg isotope of mass number xxx for the mass-independent part of a process.	
E^{xxx}_{A-B}	$\equiv E^{xxx}Hg_{A-B}$, MIF enrichment factor for an isotope between two reservoirs A and B	
Γ_g	conductance (= 1/resistance) of diffusion of a gas to the surface in a resistance model of gas-droplet interaction.	dimensionless
Γ_{rxn}	conductance (= 1/resistance) of reaction in the liquid phase in a resistance model of gas-droplet interaction.	
Γ_{sol}	conductance (= 1/resistance) of solubility and diffusion in the liquid phase in a resistance model of gas-droplet interaction.	
λ	wavelength of light	nm
σ	absorption cross section	cm^2 $molecule^{-1}$
τ	atmospheric lifetime	year
$\tau_{troposphere}$	overall tropospheric lifetime	
τ_{rxn}	lifetime in the troposphere due to net oxidation	
τ_{ocean}	lifetime in the troposphere due to oceanic net uptake	
τ_{land}	lifetime in the troposphere due to terrestrial net uptake	
τ_{wash}	lifetime in the troposphere due to tropospheric wash-out	
$\tau_{stratosphere}$	lifetime in the troposphere due to net transfer to the tropopause/stratosphere	
υ_X	mean thermal velocity of a gas X	$m\ s^{-1}$
Φ	photolysis quantum yield	dimensionless
a	parameter for T dependence of K_{gp}	dimensionless
b	parameter for T dependence of K_{gp}	
c	$\equiv c^{Hg^0}$, $c^{Hg^0}_{index}$, gas-phase mass concentration normalized to standard temperature (0 °C) and pressure (101.325 kPa).	ng m^{-3}
D_g	gas-phase diffusion coefficient	$m^2\ s^{-1}$
D_l	liquid-phase diffusion coefficient	$m^2\ s^{-1}$
E^0	standard electrode potential	V
E	electrode potential	
E_a	activation energy	J mol^{-1}
f	fraction (isotope mixing)	dimensionless

f_R	fraction of reactant remaining	
F	Faraday constant	96485 C mol^{-1}
F_c	form factor describing the transition region of a gas-phase reaction, typically ~0.7	dimensionless
F(λ)	photon flux	photons cm^2 s^{-1}
ΔG_R	Gibbs free energy of reaction	J mol^{-1}
ΔG^0	standard Gibbs free energy	
ΔH_f	enthalpy of formation	
ΔH_R	enthalpy of reaction	
ΔH^0_{abs}	standard enthalpy of adsorption	
J_X	net flux of the gas X into the condensed phase	mol m^{-2} s^{-1}
k, k(T)	rate coefficient	miscellaneous
k_0	$\equiv k_0^T$, low-pressure limit gas-phase rate coefficient	cm^6 $molecule^{-2}$ s^{-1}
k_∞	$\equiv k_\infty^T$, high-pressure limit gas-phase rate coefficient	cm^3 $molecule^{-1}$ s^{-1}
k_f	forward rate coefficient	miscellaneous
k_r	reverse rate coefficient	
k_H^{cc}	Henry's law coefficient	dimensionless
k_H^{cp}	Henry's law coefficient	mol L^{-1} atm^{-1}
k_{ads}	adsorption rate coefficient	miscellaneous
k_{des}	desorption rate coefficient	
k_{het}	heterogeneous rate coefficient	
k_{obs}	effective first-order rate constant	s^{-1}
k_{gas}	bimolecular rate coefficient of the gas phase part of a partially heterogeneous reaction	cm^3 $molecule^{-1}$ s^{-1}
k_{surf}	surface bimolecular rate coefficient (normalized by reactor surface-volume ratio)	cm^4 $molecule^{-1}$ s^{-1}
K_a	acid constant ($HA \rightleftarrows H^+ + A^-$)	mol L^{-1}
K_{gp}	coefficient for absorptive partitioning of GOM onto existing aerosol	m^3 μg^{-1}
K_q	stepwise stability coefficient for a $HgL_{q-1} + L \rightleftarrows HgL_q$ type equilibrium	L mol^{-1}
[M]	third body concentration	molecule cm^{-3}
m	empirically fitted exponent	dimensionless
m_{xxx}	mass of the isotope ^{xxx}Hg	amu
n	number of electrons transferred in a red-ox reaction	mol
ΔN/Δlogr	particle number concentration in the size range Δlogr (log-normal distributed polydisperse aerosol)	m^{-3}
pK	−logK	dimensionless
pK_a	$-\log(K_a)$	
PM	particulate matter	μg m^{-3}
r	radius (droplet or tubular reactor)	m
$\langle r^2_{xxx} \rangle$	mean-square nuclear charge radius	fm^2
R	gas constant	8.314 J mol^{-1} K^{-1}
$R^{xxx/198}$	$\equiv R^{xxx}$, ratio of isotope xxx to isotope 198	dimensionless
ΔS^0_{abs}	enthropy of adsorption	J mol^{-1} K^{-1}
T	absolute temperature	K
V	volume	m^3
$[X]_{g,\infty}$	background (bulk) gas-phase concentration of species X	mol m^{-3}
$[X]_{surf}$	$[X]_g$ at the surface of a droplet	
$[X]_g$	gas-phase concentration of species X	
$[X]_p$	particle-phase concentration of species X	

Acronym	**Plain text**
AAS	atomic absorption spectroscopy
AMDE	atmospheric mercury depletion event
AOM	atmospheric organic matter
AQ	anthraquinone
CFPP	coal-fired power plant
CI-MS	chemical ionization mass spectrometry
CV-AFS	cold vapor atomic fluorescence spectroscopy

DFC	dynamic flux chamber
DMHg	dimethylmercury
DOM	dissolved organic matter
EIE	equilibrium isotope effect
EIE-MDF	equilibrium MDF
even-MIF	mass-independent fractionation of even Hg isotope (^{200}Hg,^{204}Hg)
FEP	polymeric fluorinated ethylene propylene
FF	fast flow reactor, chemical reactor designed for rapid mixing and reaction of gases or liquids
FF-ID-CI-MS	fast flow ion-drift chemical ionization mass spectrometry
FT-IR	Fourier Transform Infrared
GOM	≡ Hg^{II}(g), gaseous oxidized mercury
HMDE	hanging mercury drop electrode
HFC	hyperfine coupling
KIE	kinetic isotope effect
KIE-MDF	kinetic MDF
LIDAR	light detection and ranging
LMCT	ligand to metal charge transfer
LMWO	low molecular weight organics
LOD	limit of detection
MDF	mass-dependent fractionation
MgIE	magnetic isotope effect (acting on ^{199}Hg, ^{201}Hg)
MIF	mass-independent fractionation
$MMHg^+$	species containing a methyl mercuric cation and an unspecified counteranion.
m/m	mass-to-mass ratio
M/M	mol-to-mol (stoichiometric) ratio
MRB	metal-reducing bacteria
MS	mass spectrometry
NFS	nuclear field shift, synonym for NVE
NVE	nuclear volume effect, synonym for NFS
odd-MIF	mass-independent fractionation of odd Hg isotope (^{199}Hg, ^{201}Hg)
PBM	≡ Hg^{II}(p), particle-bound mercury
PLP-LIF	pulsed laser photolysis-laser induced fluorescence
PM	particulate matter, synonym for TSP
$PM_{2.5}$	particulate matter ≤ 2.5 µm
PM_{10}	particulate matter ≤ 10 µm
POA	primary organic aerosol
PTR-MS	proton transfer reaction mass spectrometry
RH	relative humidity (% of absolute humidity)
RKKM	Rice-Ramsperger-Kassel-Markus (theory)
RM	reactive mercury (GOM + PBM)
RR	determination of rate constant by a relative rate method, opposite to an absolute determination
Rxn	abbreviation for reaction, representing a chemical reaction
SOA	secondary organic aerosols
STP	standard temperature and pressure (one atmosphere, 101.325 kPa and 0 °C)
TAM	total atmospheric mercury (Hg^0 + GOM + PBM)
TGM	total gaseous mercury (Hg^0 + GOM), in practice not quantitative for GOM
TSP	total suspended particles, all particle sizes suspended in the air
TS	transition state
TST	transition state theory
UV-A	ultraviolet A, 315 – 400 nm
UV-B	ultraviolet B, 280 – 315 nm
UV-C	ultraviolet C, 100 – 280 nm, also called deep UV
UV–VIS	ultraviolet (A + B) + visible light (400 – 700 nm)

formaterade: Teckenfärg: Blå